**Title**
Biophysical Characterization Studies of the Mercury Resistance Proteins MerT and MerA



**Author**
Harwood, Ian Matthew

**Publication Date**
2012

Peer reviewed|Thesis/dissertation

# Biophysical Characterization Studies of the Mercury Resistance Proteins MerT and MerA

by

Ian M. Harwood

DISSERTATION

Submitted in partial satisfaction of the requirements for the degree of

DOCTOR OF PHILOSOPHY

in

Biophysics

in the

GRADUATE DIVISION

of the

UNIVERSITY OF CALIFORNIA, SAN FRANCISCO

[redacted]

**Acknowledgements**

I am grateful to the following people for their support throughout my graduate studies:

Research Advisors
Susan M. Miller
Robert M. Stroud

Dissertation Committee
Robert M. Stroud, chair
Susan M. Miller
Robert J. Fletterick

Qualifying Exam Committee
Robert J. Fletterick, chair
Robert H. Edwards
Jane Gitschier
Lily Y. Jan

Biophysics Graduate Program
Matthew P. Jacobson, director
David A. Agard, director emeritus
Rebecca Brown, administrator
Julie Ransom, administrator

My Family & Friends
Mom and Dad
Megan and Adam
BARS

UCSF Friends & Colleagues
P. Therese Lang
Franz Gruswitz
Adrian Barker
Rachel E. Nauss
Alex Johs
The Miller Lab
The Stroud Lab
The Molecular Structure Group
The Biophysics Entering Class of 2004
All My Biophysics Program Colleagues
The Brass at UCSF

Prior Mentors, Professors, & Teachers
Ravi Basavappa
Jack A. Kampmeier
Peter E. Kane
Dan O'Leary
Victor Britton
Glen Vining
Sharon Hicks
Deborah Breger

…and everyone who helped and inspired me to complete this dissertation work.
Thank you.

# Biophysical Characterization Studies of the Mercury Resistance Proteins MerT and MerA

**Ian M. Harwood**

**Abstract**: Unlike other bacterial metal ion resistance systems, which either actively transport metal ions out of the cytosol or utilize soluble proteins to sequester metal ions in the periplasm or outside the cell, proteins of prokaryotic mercury resistance (*mer*) loci confer resistance to inorganic mercury ($Hg^{2+}$) by facilitating its uptake and reduction to elemental mercury ($Hg^{0}$). The expression of both a membrane transporter and mercuric reductase (MerA) defines the minimal set of proteins needed to confer inorganic mercury resistance in prokaryotes. The efficacy of the *mer* system and of other metal ion resistance pathways is dependent on the specificity, thermodynamics, kinetics and dynamics of the proteins that comprise each system. This dissertation examines some of these properties of the *mer* proteins and protein domains of MerA and of MerT, the most prevalent membrane transporters in *mer* isolates. First, we describe work aimed at expressing and purifying MerT for X-ray crystallography studies. By understanding the structure of MerT, we aimed to elucidate the mechanism by which $Hg^{2+}$ is transported into the cell and made available to MerA. Second, we present a novel method for the expression and purification of intact MerA and models fit to small-angle X-ray and neutron scattering observations of MerA in the absence of $Hg^{2+}$ and of an intermediate model of $Hg^{2+}$-handoff from the N-terminal domain (NmerA) and to the catalytic core (Core) of MerA. These are the first structural studies of the linker regions that tethers

NmerA to Core. Third, we examine the steady-state kinetics of intact MerA. Here we show that NmerA tethered to Core provides a kinetic advantage in reducing $Hg^{2+}$ when it is associated with either proteinaceous or low molecular-weight ligands. Finally, we introduce evidence that the linker region which tethers NmerA to Core also serves a secondary purpose of localizing MerA to the cell membrane absent of $Hg^{2+}$ and/or MerT.

# Table of Contents

# List of Tables

## Chapter 2



## Chapter 3

# List of Figures

## Introduction



## Chapter 1



## Chapter 2

**Chapter 3**

**Chapter 4**

# INTRODUCTION

## Overview

Controlled trafficking of metal ions in cellular environments is vital to avoiding detrimental metal-ligand interactions (Barkay et al. 2003; Barkay et al. 2010). To avoid toxicity from such undesirable or non-specific interactions, biological systems have evolved multi-protein trafficking pathways to chaperone (Vallee and Ulmer 1972; Finney and O'Halloran 2003) and/or detoxify (Silver and Phung 1996) specific metal ions. In these systems proteins traffic metal ions by forming transient, state-dependent complexes that last only until the metal ion is "handed off" from the protein-ion complex to the binding site in a specific downstream target. The efficacy of these pathways is dependent on the specificity, thermodynamics, kinetics and dynamics of these transfers. Even as the mechanism(s) of transfer may differ, in every pathway proteins coordinate the handoff of their metal ions using a series of inter- and/or intramolecular transfers between high affinity binding sites. Significant insights into transfer mechanisms between individual proteins (Rosenzweig and O'Halloran 2000; Finney and O'Halloran 2003; Banci et al. 2010) and between metal binding sites on domains within individual proteins, including membrane proteins (Wu et al. 2008; Su et al. 2011), have been gained for some pathways.

The focus of my dissertation research has aimed to address how the structure and dynamics of proteins in prokaryotic inorganic mercury ($Hg^{2+}$) resistance pathways, namely mercuric reductase (MerA) and the membrane protein MerT, affect metal ion trafficking efficiency and specificity, both between metal ion binding sites on a single protein domain, as well as between sites on separate domains of a single protein.

## Mercury: Legacy and Use in California

When selecting a model system to study I, considered pathways that traffic biologically essential metal ions (e.g., $Cu^{2/1+}$, $Fe^{2/3+}$, $Zn^{2+}$) which, when defective or inhibited, lead to various human diseases (Horvath et al. 2010; Bleackley and Macgillivray 2011; Jomova and Valko 2011; Torti and Torti 2011). Yet what most sparked my interest were systems relevant to environmental restoration and bioremediation. Having grown up on the Hudson River in New York State, I have personally experienced the devastation that industrial pollutants have on an ecosystem and exposed persons.

At UCSF I felt compelled to turn my attention to my new home, the San Francisco Bay Area and California, where mercury usage and pollution has a long history. Prior to the discovery of gold in the Sierra Nevada mountains and subsequent California gold rush from 1848-1855, mercury was mined from Coastal Range deposits rich in mercury near San Francisco, Lake Berryessa, and Clear Lake of California from the 1840s, and continuing through the 1960s. Following 1848, millions of pounds of California mercury were used in hydraulic gold mining through the 1950s. It is estimated that ten to thirty percent of all mercury used was lost into the Sierra Nevada environment, including the Bear-Yuba, Dutch Flat, and Trinity watersheds. Mercury from agricultural pesticides and fungicides and chloralkali process facilities (producing chlorine and sodium hydroxide from saline) additionally contributed to the still-present pollution throughout the Central Valley, Sacramento and San Joaquin Rivers and Delta, and San Francisco Bay (May et al. 1999; Flegal et al. 2005; Conaway et al. 2008).

Although no longer used in mining and farming, mercury is continually released into the environment in California and throughout the United States from coal burning, dental amalgams, sewage treatment, paper milling, and incineration of consumer wastes, including electronic “e-waste” and fluorescent lamps (Clarkson 2002; Barkay et al. 2003; Clarkson et al. 2003; Conaway et al. 2008). Outside the United States, mercury is still used in batteries, cleansers, medicines, and consumer beauty products ("Mineral commodity summaries 2007: Mercury"  2007). Mercury continues to be indispensable to industrial processes for the production of technology goods (and the many companies which utilize it in Silicon Valley).

## Mercury: Toxicity to Biological Systems

Despite being vital to many human applications, mercury is toxic to biological systems. Once in the environment, mercury becomes bioavailable as inorganic mercury chloride ($HgCl_2$), which can permeate lipid bilayer membranes (Gutknecht 1981). Inorganic mercurials can be taken up by sulfur-reducing bacteria and converted into lipid-soluble methylmercury ($H_3CHg^+$), which fish and other wildlife accumulate through diet (Gutknecht 1983; Bienvenue et al. 1984; Barkay et al. 2003). Such organomercurials ($R_3C$-Hg) are especially toxic to developing nervous tissue and have affected water fowl populations in the San Francisco Bay, Great Lakes, and Everglades (*Mercury in the Environment* 2000). Human exposure to bioamplified methylmercury from fish consumption may lead to paresthesia (feelings of numbness or "pins and needles"), cerebellar ataxia (loss of balance and coordination), dysarthria (speech impediments), loss of vision and hearing, and possibly cardiovascular disease (Clarkson 2002).

Lesions arising from organomercurial poisoning are irreversible and treatment is difficult as low-level chronic contact is often detected after extended periods of exposure (Robinson and Tuovinen 1984). A limited number of thiol-containing chelation therapies are used to promote organomercurial elimination from the body upon short-term exposure to methylmercury and other short-chain organmercurials, which are most difficult to mobilize from the body (Sanfeliu et al. 2003). Example treamtments include oral administration of penicillamine and N-acetyl-penicillamine, intramuscular injection of 2,3-dimercaptopropane-1-sulfonate, and N-acetyl-cysteine (Lund et al. 1984). Dietary selenium has also been shown to mitigate methymercury toxicity (Heath et al. 2010). To

limit exposure to methyl mercury in fish, California has issued consumption advisories due to mercury pollution in over twelve locations, and about forty other states have done the same in mercury-affected areas (*Mercury in the Environment* 2000; *Methylmercury in sport fish: Information for fish consumers* 2003).

At the molecular scale, $Hg^{2+}$ causes oxidative stress by binding thiol groups (–SH), including glutathione (GSH), the cell's primary redox buffer. $Hg^{2+}$ has a high affinity for thiols [$K_{form}$ for $Hg(SR)_2$ reported as high as $10^{40}$ $M^{-2}$ (Stricks and Kolthoff 1953)], thus posing a lethal threat to protein cysteines involved in various enzymatic processes and oligomeric organization (Williams et al. 2000; Clarkson 2002). When bound to a thiol, $Hg^{2+}$ can rapidly exchange onto other thiols (Cheesman 1988). The affinity of $Hg^{2+}$ for a thiol pair, and that of any liganded or chelated metal, is determined by how well the protein structure accommodates and coordinates the metal ion.

## Prokaryotic Mercury Resistance: the *mer* Operon

Chaperone, membrane transport, lyase, and reductase proteins have evolved in various Gram-negative and Gram-positive bacteria in response to both organic and inorganic mercurial exposure. *Mer* loci have been isolated from various transposable elements, such the Tn*21* transposon of plasmid NR1 (also known as R100) from *Shigella flexneri* (Nakahara et al. 1979; Johs et al. 2011), the Tn*501* transposon of plasmid pVS1 from *Pseudomonas aeruginosa* (Stanisich 1974; Stanisich et al. 1977; Fox and Walsh 1983; Distefano et al. 1989; Miller et al. 1989; Moore and Walsh 1989; Distefano et al. 1990; Engst and Miller 1999; Ledwidge et al. 2005a; Ledwidge et al. 2005b; Hong et al. 2010; Ledwidge et al. 2010), and plasmid pDU1358 from *Serratia marcescens* (Griffin et al. 1987). Bacterial mercury resistance is not universal and the resistance loci can be lost in the absence of selection pressure.

Expression of *mer* operon gene products is controlled by the encoded regulator protein MerR (Summers 1986; Barkay et al. 2003). Prior to $Hg^{2+}$ exposure the homodimeric MerR binds to an 18 bp hyphenated dyad *mer* operator, termed MerO, and recruits RNA polymerase to form a stable pre-initiation complex (Heltzel et al. 1990). *mer* RNA transcription is inhibited by MerR bending the DNA away from the polymerase. Binding of $Hg^{2+}$ to MerR leads to an allosteric change in MerR which remains bound to the DNA and causes unwinding of the operator region to improve RNA polymerase's access to the transcription start site. Summers' "ready to rock" model highlights the *mer* system's effectiveness in instantaneously responding to cytosolic exposure to $Hg^{2+}$ (Heltzel et al. 1990; Kulkarni and Summers 1999). Extensive reviews

of operon isolates and various *mer* proteins have been published (Silver 1996; Silver and Phung 1996; Miller 1999; Barkay et al. 2003).

Once expressed, *mer* proteins import $Hg^{2+}$ into the cell (Figure 1). If present, the periplasmic chaperone protein MerP binds mercury and directs it to the expressed membrane proteins, the ubiquitous MerT and the less common MerC (Steele and Opella 1997). Although there have been no experiments that directly show MerP can donate $Hg^{2+}$ to either transporter, it is unlikely that MerP only binds $Hg^{2+}$ just to protect the periplasmic space, as extracellular sequestration is less carbon efficient than mercury reduction. Once bound to the dithiol on either the first transmembrane helix of MerT or MerC, which are predicted to be accessible to the periplasmic environment, $Hg^{2+}$ is directed into the cytoplasm by an unknown mechanism. Both MerT and MerC are functional in the absence of MerP, and MerC is not essential to survival if MerT is expressed (Morby et al. 1995). The expression of MerP nonetheless is advantageous, as shown in $Hg^{2+}$-resistance efficiency of plating assays (Hamlett et al. 1992).

Unlike other prokaryotic metal resistance systems that work by extracellular sequestration or dedicated membrane transport proteins that actively pump out toxic metal ions, both carbon- and energy-intensive processes (Barkay et al. 2003), *mer* loci code for dedicated membrane transport proteins, MerT and/or MerC, which facilitate $Hg^{2+}$ transport across the plasma membrane. No other known metal resistance system facilitates the uptake of heavy metal toxin. *In vivo* experiments have shown that expression of either MerT or MerC is essential for prokaryotic $Hg^{2+}$ resistance. Although

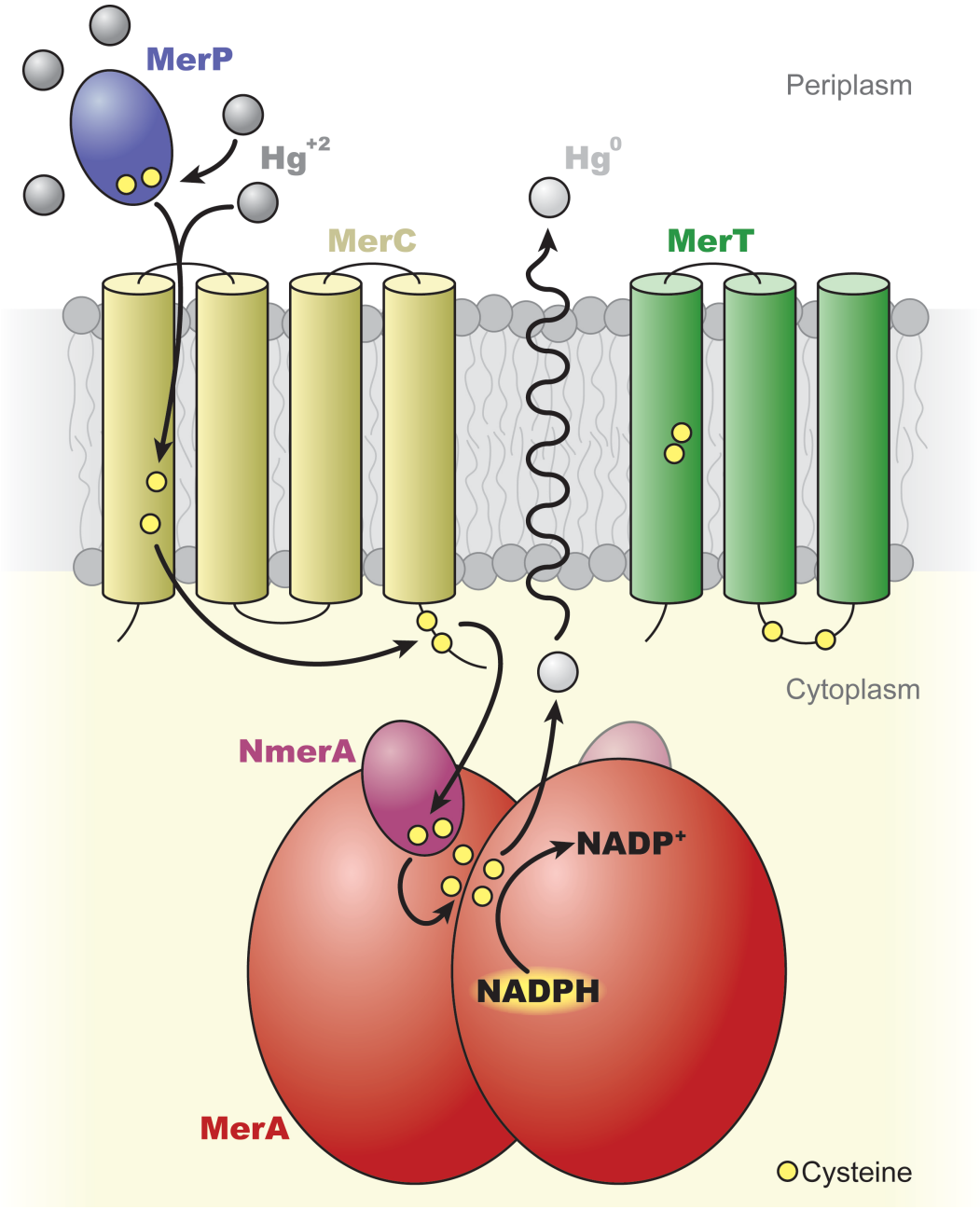


**Figure 1.** *Mer* proteins responsible for $Hg^{2+}$ sequestration, intake, and reduction. The membrane proteins MerC (yellow) and MerT (green) can acquire $Hg^{2+}$ (dark gray) from the periplasm as well as from the metallochaperone MerP (blue) to each respective protein's first pair of thiols, believed to be on the first transmembrane helix. Though the exact mechanism is unknown, it is proposed that $Hg^{2+}$ then exchanges to a pair of cytosolic cysteines, at which point it is handed off to NmerA (purple), the N-terminal domain of mercuric reductase, MerA. NmerA then delivers $Hg^{2+}$ to the Core (red) for reduction to $Hg^{0}$ (light gray). Both MerA and a membrane uptake protein (most commonly MerT) are required for $Hg^{2+}$ resistance.

$Hg^{2+}$ is able to permeate the cell membrane in the membrane in the absence of MerT or MerC (Gutknecht 1983), the lack of a functional transporter gene in cells exposed to $Hg^{2+}$ expressing MerA reduces resistance up to $10^6$ fold, rendering cells as sensitive to $Hg^{2+}$ as cells lacking a *mer* locus (Hamlett et al. 1992). Initial experiments with Tn*21* and Tn*501* *mer* operons led to the hypothesis that these proteins import $Hg^{2+}$ into the cytoplasm to be detoxified by reduction by MerA (Dempsey et al. 1978; Barkay et al. 2003). This theory is also supported by experiments that show radioactive $^{203}Hg^{2+}$ can bind to MerT and MerC and be moved into the cell, where it is reduced and volatilizes (Robinson and Tuovinen 1984). These *in vivo* assays showed that mercury transporters could bind extracellular mercury and transport it down a concentration gradient. Cells become hypersensitive to $Hg^{2+}$ when expressing intact MerT but lack a functional MerA, as shown with zone of inhibition (Foster et al. 1979), minimal inhibitory concentration (MIC) (Morby et al. 1995), and liquid culture density studies (Nakahara et al. 1979) with cells containing Tn*21* insertion and deletion mutants of MerA. $Hg^{2+}$ is bound by MerT in the absence of MerA and, by means of the membrane protein, becomes more readily available to cytosolic thiols. Although there had been no biophysical characterization of MerT and MerC prior to my studies, hydropathy plots suggest that MerT has three and MerC has four transmembrane-spanning helices (Morby et al. 1995; Brown et al. 2002). Fragments of MerC fused with PhoA, which is targeted to the periplasm, support this prediction (Sasaki et al. 2005). MerT and MerC are not homologous to any solved membrane protein structures. It is not known how the structures of these transporters define transport specificity, thiol affinity, or interaction interfaces. Past mutagenesis studies have examined cysteine pairs in MerT and MerC (Morby et al. 1995; Sahlman et

al. 1999). These have clearly established that the first cysteine pair in each transporter is essential for resistance while the second pair is not. The essential first cysteine pair of MerC is able to acquire $Hg^{2+}$ in the absence of MerP (Sahlman et al. 1997). MIC experiments have shown that mutating the second set of MerT cysteines to serines in cells lacking MerA results in hypersensitivity to $HgCl_2$. Interestingly, expression of MerP helps rescue the resistance phenotype, suggesting MerP may influence the roles of the cytoplasmic cysteines by binding to the periplasmic face of the membrane protein (Morby et al. 1995). When MerT's Gly38, which is proposed to reside in the periplasmic linker between the first and second transmembrane helices, is mutated to Asp, cells expressing MerP exhibit a phenotype similar to MerP deletion mutants, which further suggests the two proteins interact. In both MerC and MerT, conserved prolines one (MerC) or two (MerT) residues downstream of the first cysteine pair, as well as charged residues proximal to proline residues postulated to lie in the second transmembrane helix of each protein, have also been suggested to be involved in the $Hg^{2+}$ transport mechanism (Wilson et al. 2000).

Once across the cell membrane, $Hg^{2+}$ must next be directed to mercuric reductase (MerA) for reduction to $Hg^0$, the last stage in the resistance pathway. It has been proposed that $Hg^{2+}$ is presented to the N-terminal domain of MerA (NmerA) by MerT's C-terminal dithiol and/or MerC's corresponding dithiol predicted to be in a cytosolic loop between the third and fourth transmembrane helix (Brown 1985; Ledwidge et al. 2005a). NmerA is homologous to other βαββαβ ferredoxin-fold heavy metal-associated trafficking proteins and scavenging domains, including MerP and the copper chaperones

Atx1 and Ccc2a (Rosenzweig and O'Halloran 2000; Arnesano et al. 2001; Arnesano et al. 2002; Ledwidge et al. 2005a), and is tethered to the MerA catalytic core (Core) by a ~30 residue unstructured linker (Johs et al. 2011). Although not essential for resistance, it has been shown that expression of NmerA is advantageous under oxidative and electrophilic stress, including conditions of lowered GSH concentration, the primary cellular redox buffer in proteobacteria (Ledwidge et al. 2005a). The Miller group has previously proposed that this stress is lessened by NmerA specifically transferring $Hg^{2+}$ from MerT or MerC to Core, thus preventing undesirable $Hg^{2+}$ binding to cellular thiols (Ledwidge et al. 2005a). Previous publications both challenge and support this hypothesis. Interactions between fragments of MerC's C-terminus, which included MerC's intracellular dithiol, and MerA could not be detected in yeast two-hybrid setups (Sasaki et al. 2005). However, bacterial two-hybrid studies suggest that MerT interacts with NmerA but not Core (Schue et al. 2008). Although no region of MerA has been shown to localize it to the membrane, MerA sediments in membrane preparations from transporter-expressing cells, suggesting an association between the reductase and membrane proteins (Jackson and Summers 1982; Hamlett et al. 1992). NmerA is able to chaperone and deliver $Hg^{2+}$ to the Core's C-terminal cysteine pair (Scheme 1) (Ledwidge et al. 2005b). This action leads to a significant kinetic advantage in mercury reduction both when $Hg^{2+}$ is bound to small thiol-containing compounds, such as GSH, or larger proteins, such as thioredoxin.

Upon receiving $Hg^{2+}$, the functionally essential Core C-terminal cysteines on each monomer direct $Hg^{2+}$ into one of the Core's two active sites (Moore and Walsh 1989; Moore et al. 1992), which are symmetrically formed at the obligate homodimeric

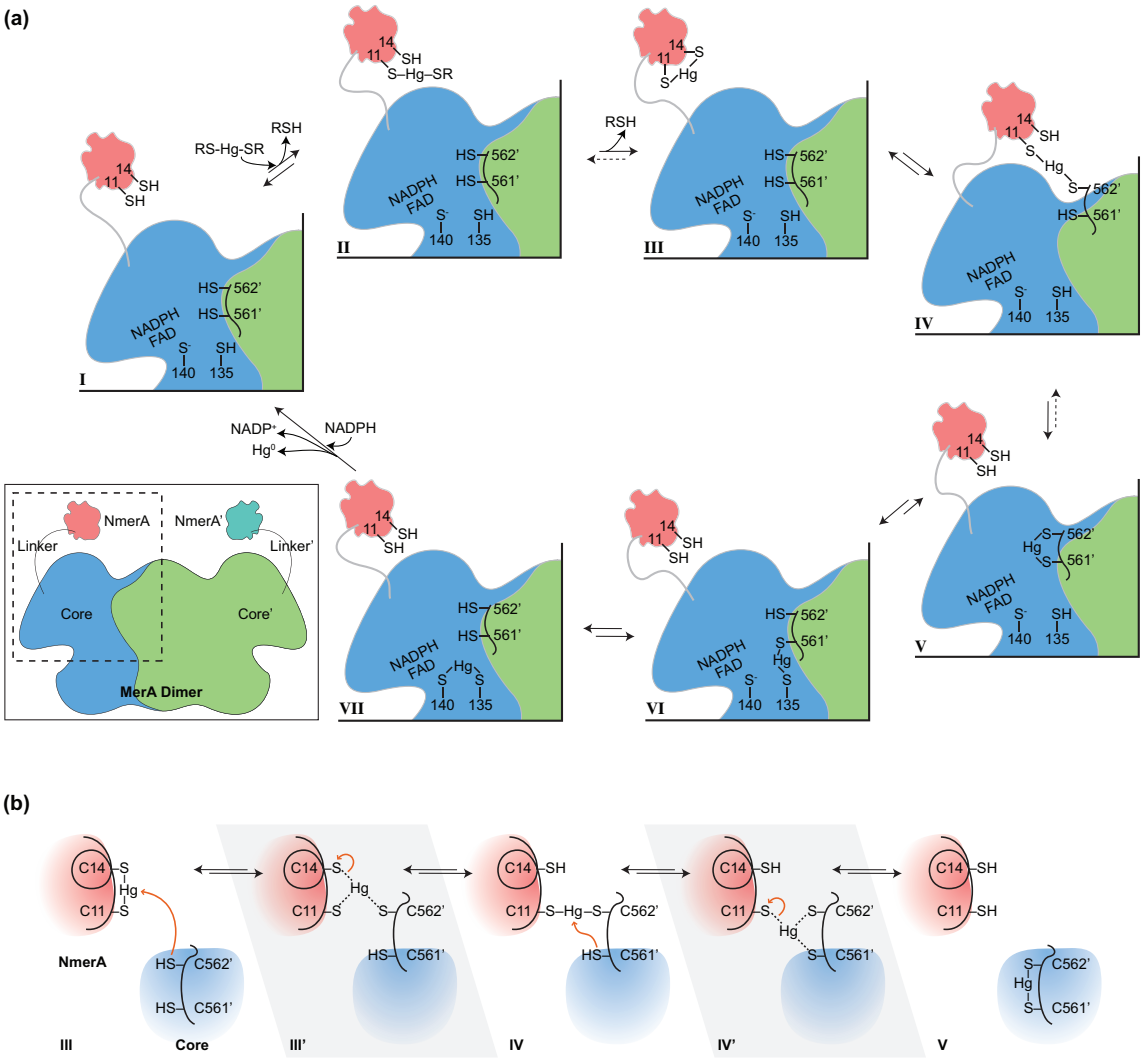


**Scheme 1.** Pathway for $Hg^{2+}$-ligand exchange and reduction in MerA. (a) Cysteine residues of NmerA (red), the active site of one monomer (blue), and the C-terminus of the complementing monomer (green) involved in $Hg^{2+}$ exchange and reduction to $Hg^0$ at one of the MerA dimer active sites are shown. (b) Detailed mechanism for $Hg^{2+}$-ligand exchange between NmerA (red) and MerA catalytic core (blue). The transient $[Hg(SR)_3]^-$ intermediate steps are grayed (from Johs et al. 2011).

Interface. Genetic complementation experiments, in which a Core mutant that lacked C-terminal thiols (C561 and C562 in Tn*21* MerA) (CCAA) was co-expressed with Core mutant that lacked internal thiols (C135 and C140) (AACC), exhibited $Hg^{2+}$ resistance, whereas cells expressing either one of these mutant variations was as sensitive to $Hg^{2+}$ as cells lacking *merA* (Distefano et al. 1990). Purification and catalytic characterization of the coexpressed protein mixture exhibited ~25% of the MerA activity of cells expressing the wild-type reductase, which is statistically anticipated for a CCAA-AACC heterodimeric/homodimeric mixture with only one functional active site per heterodimer. Crystallographic studies have also shown the necessity of two Core monomers in forming functional active sites (Schiering et al. 1991; Ledwidge et al. 2005a). $Hg^{2+}$ is reduced to $Hg^0$ at a MerA active site through an FAD-mediated transfer of electrons from NADPH (Scheme 1) (Miller et al. 1986). MerA is the only pyridine nucleotide disulfide oxidoreductase known to reduce $Hg^{2+}$ (Miller 1999; Barkay et al. 2003). Due to its low aqueous solubility, little affinity for ligands, and uncharged state, $Hg^0$ passively diffuses across the plasma membrane and partitions outside the cell, no longer threatening intra- and extracellular thiols (Barkay et al. 2003).

## Research Focus: MerT and MerA

This dissertation examines *mer* proteins and protein domains that transport and traffic inorganic mercury ($Hg^{2+}$). In particular, I have focused on MerT, the most prevalent membrane transporters in *mer* isolates, and on mercuric reductase MerA. The expression of both a membrane transporter (MerT and/or MerC) and the reductase (MerA) defines the minimal set of proteins needed to confer inorganic mercury resistance in prokaryotes (Barkay et al. 2003).

The past fifty years of MerT and MerA research has only begun to address questions relating to *inter*molecular exchange of $Hg^{2+}$ between *mer* MerT and MerA, and intramolecular $Hg^{2+}$ trafficking between the two thiol pairs of MerT, as well as from NmerA to Core. These studies have been mostly macroscopic, examining protein expression and interactions on resistance phenotype (Hamlett et al. 1992; Sasaki et al. 2006). In the last two decades studies have begun to investigate *mer* protein structure at atomic resolution (Schiering et al. 1991; Steele and Opella 1997; Qian et al. 1998; Ledwidge et al. 2005a; Ledwidge et al. 2010) and the kinetics and mechanisms of $Hg^{2+}$ exchange (Ledwidge et al. 2005a; Ledwidge et al. 2005b; Hong et al. 2010; Ledwidge et al. 2010).

Atomic resolution information about protein structure can prove immensely helpful in developing testable mechanistic hypotheses for explaining macroscopically observed biochemical and biophysical phenomena. Unlike MerP and Core, the structures of which have been solved, there is only conjecture as to the fold of MerT (and MerC)

(Steele and Opella 1997; Ledwidge et al. 2005a). In **Chapter 1** I present work aimed at expressing and purifying MerT for X-ray crystallography studies. By understanding the structure of MerT, I aimed to elucidate the mechanism by which $Hg^{2+}$ is transported and exchanges from its periplasm-facing thiols to the two cytosolic cysteines believed to be accessible to NmerA. The chapter includes studies of MerT expression in *E. coli*, detergent solubilization, purification, and crystal trials.

Although Core has been biochemically and kinetically characterized and its structure determined by X-ray crystallography, there have been few structural and kinetic studies on the full-length protein (i.e. the native protein with NmerA tethered to Core by the ~30 amino acid linker region). This lack of characterization resulted from difficulties expressing full-length protein without proteolytic cleavage of the linker region *in vivo* and during protein purification (Fox and Walsh 1982; Moore and Walsh 1989). In **Chapter 2** we present a novel method for the expression and purification of intact MerA and models fit to small-angle X-ray (SAXS) and neutron (SANS) scattering observations of MerA in the absence of $Hg^{2+}$ and in an intermediate state of $Hg^{2+}$-handoff from NmerA to the Core. Here, we examine the structure of the linker region that tethers NmerA to Core and identify the site of interaction between Core and NmerA during handoff using biophysical approaches for the first time. This work was published in the *Journal of Molecular Biology* (Johs et al. 2011).

The majority of previous NmerA studies have examined this region as a separate protein rather than as a domain of full-length MerA due to the difficulties in purifying

intact protein. *In vitro* studies that utilized NmerA and Core expressed as separate proteins showed that $Hg^{2+}$ can exchange between both proteins and has greater affinity for NmerA than for the Core C-terminal thiols when the inner cysteines are present as a disulfide (Ledwidge et al. 2005b). Although it was suggested that the Core's active site thiol pair provides the driving force to partition $Hg^{2+}$ forward for reduction, it was uncertain if NmerA negatively affected the catalytic efficiency of MerA when reducing $Hg^{2+}$ liganded to small thiol-containing compounds, such as GSH. Conversely, as NmerA is adept at acquiring $Hg^{2+}$ that is liganded to other proteins, such as organomercurial lyase (MerB) (Hong et al. 2010) and thioredoxin (Ledwidge et al. 2005a), we sought to understand how the tethering of NmerA to Core affects the kinetics of $Hg^{2+}$ reduction. In **Chapter 3** we present stopped flow mixing experiments of pure, intact MerA that show tethered NmerA first acquires $Hg^{2+}$ associated with low molecular-weight thiol ligands and then delivers $Hg^{2+}$ to the Core's C-terminal cysteines. We also report the steady state kinetics of $Hg^{2+}$ reduction using both a small molecule-Hg and an "in-pathway" protein-Hg substrate and show NmerA enhances the catalytic efficiency of turnover, even though its involvement adds steps to the reaction mechanism.

The ~30 residue linker that tethers NmerA to Core is the least understood of MerA's regions. The lack of studies of this region are mostly due to the previously observed proteolytic degradation of NmerA and the linker when MerA is expressed at 32 to 37 °C. In addition to its primary role in tethering NmerA to Core, observations from a bacterial two-hybrid interaction screen suggested the linker may assist in a proposed $Hg^{2+}$-independent association of MerT and NmerA (Schue et al. 2008). In **Chapter 4** we

present evidence for an alternative and novel model in which the linker serves a secondary purpose of localizing MerA to the cell membrane, providing benefit to cell viability in the absence of a MerT-NmerA interaction. Here we use chromatographic- and kinetics-based techniques to determine the presence of MerA in washed cell membranes when expressed in the presence and absence of MerT.

## References


Arnesano F, Banci L, Bertini I, Ciofi-Baffoni S, Molteni E, Huffman DL, O'Halloran TV (2002) "Metallochaperones and metal-transporting ATPases: a comparative analysis of sequences and structures." *Genome Res* 12:255-271.

Arnesano F, Banci L, Bertini I, Huffman DL, O'Halloran TV (2001) "Solution structure of the Cu(I) and apo forms of the yeast metallochaperone, Atx1." *Biochemistry* 40:1528-1539.

Banci L, Bertini I, McGreevy KS, Rosato A (2010) "Molecular recognition in copper trafficking." *Nat Prod Rep* 27:695-710.

Barkay T, Kritee K, Boyd E, Geesey G (2010) "A thermophilic bacterial origin and subsequent constraints by redox, light and salinity on the evolution of the microbial mercuric reductase." *Environ Microbiol* 12:2904-2917.

Barkay T, Miller SM, Summers AO (2003) "Bacterial mercury resistance from atoms to ecosystems." *FEMS Microbiol Rev* 27:355-384.

Bienvenue E, Boudou A, Desmazes JP, Gavach C, Georgescauld D, Sandeaux J, Seta P (1984) "Transport of mercury compounds across bimolecular lipid membranes: effect of lipid composition, pH and chloride concentration." *Chem Biol Interact* 48:91-101.

Bleackley MR, Macgillivray RT (2011) "Transition metal homeostasis: from yeast to human disease." *Biometals* 24:785-809.

Brown NL (1985) "Bacterial resistance to mercury — reductio ad absurdum?" *Trends Biochem Sci* 10:400-403.

Brown NL, Shih YC, Leang C, Glendinning KJ, Hobman JL, Wilson JR (2002) "Mercury transport and resistance." *Biochem Soc Trans* 30:715-718.

Cheesman BV, Arnold, A. P., Rabenstein, D. L. (1988) "Nuclear magnetic resonance studies of the solution chemistry of metal complexes. 25. Hg(thiol)3 complexes and Hg(II)-thiol ligand exchange kinetics." *J Am Chem Soc* 110:6359-6364.

Clarkson TW (2002) "The three modern faces of mercury." *Environ Health Perspect* 110 Suppl 1:11-23.

Clarkson TW, Magos L, Myers GJ (2003) "The toxicology of mercury--current exposures and clinical manifestations." *N Engl J Med* 349:1731-1737.

Conaway CH, Black FJ, Grieb TM, Roy S, Flegal AR (2008) "Mercury in the San Francisco Estuary." *Rev Environ Contam Toxicol* 194:29-54.

Dempsey WB, McIntire SA, Willetts N, Schottel J, Kinscherf TG, Silver S, Shannon WA, Jr. (1978) "Properties of lambda transducing bacteriophages carrying R100 plasmid DNA: mercury resistance genes." *J Bacteriol* 136:1084-1093.

Distefano MD, Au KG, Walsh CT (1989) "Mutagenesis of the redox-active disulfide in mercuric ion reductase: catalysis by mutant enzymes restricted to flavin redox chemistry." *Biochemistry* 28:1168-1183.

Distefano MD, Moore MJ, Walsh CT (1990) "Active site of mercuric reductase resides at the subunit interface and requires Cys135 and Cys140 from one subunit and Cys558 and Cys559 from the adjacent subunit: evidence from in vivo and in vitro heterodimer formation." *Biochemistry* 29:2703-2713.

Engst S, Miller SM (1999) "Alternative routes for entry of HgX2 into the active site of mercuric ion reductase depend on the nature of the X ligands." *Biochemistry* 38:3519-3529.

Finney LA, O'Halloran TV (2003) "Transition metal speciation in the cell: insights from the chemistry of metal ion receptors." *Science* 300:931-936.

Flegal AR, Conaway CH, Scelfo GM, Hibdon SA, Sanudo-Wilhelmy SA (2005) "A review of factors influencing measurements of decadal variations in metal contamination in San Francisco Bay, California." *Ecotoxicology* 14:645-660.

Foster TJ, Nakahara H, Weiss AA, Silver S (1979) "Transposon A-generated mutations in the mercuric resistance genes of plasmid R100-1." *J Bacteriol* 140:167-181.

Fox B, Walsh CT (1982) "Mercuric reductase. Purification and characterization of a transposon-encoded flavoprotein containing an oxidation-reduction-active disulfide." *J Biol Chem* 257:2498-2503.

Fox BS, Walsh CT (1983) "Mercuric reductase: homology to glutathione reductase and lipoamide dehydrogenase. Iodoacetamide alkylation and sequence of the active site peptide." *Biochemistry* 22:4082-4088.

Griffin HG, Foster TJ, Silver S, Misra TK (1987) "Cloning and DNA sequence of the mercuric- and organomercurial-resistance determinants of plasmid pDU1358." *Proc Natl Acad Sci USA* 84:3112-3116.

Gutknecht J (1981) "Inorganic mercury (Hg2+) transport through lipid bilayer membranes." *J Membrane Bio* 61:61-66.

Gutknecht J (1983) "Cadmium and thallous ion permeabilities through lipid bilayer membranes." *Biochim Biophys Acta* 735:185-188.

Hamlett NV, Landale EC, Davis BH, Summers AO (1992) "Roles of the Tn21 merT, merP, and merC gene products in mercury resistance and mercury binding." *J Bacteriol* 174:6377-6385.

Heath JC, Banna KM, Reed MN, Pesek EF, Cole N, Li J, Newland MC (2010) "Dietary selenium protects against selected signs of aging and methylmercury exposure." *Neurotoxicology* 31:169-179.

Heltzel A, Lee IW, Totis PA, Summers AO (1990) "Activator-dependent preinduction binding of sigma-70 RNA polymerase at the metal-regulated mer promoter." *Biochemistry* 29:9572-9584.

Hong B, Nauss R, Harwood IM, Miller SM (2010) "Direct measurement of mercury(II) removal from organomercurial lyase (MerB) by tryptophan fluorescence: NmerA domain of coevolved gamma-proteobacterial mercuric ion reductase (MerA) is more efficient than MerA catalytic core or glutathione." *Biochemistry* 49:8187-8196.

Horvath J, Beris P, Giostra E, Martin PY, Burkhard PR (2010) "Zinc-induced copper deficiency in Wilson disease." *J Neurol Neurosurg Psychiatry* 81:1410-1411.

Jackson WJ, Summers AO (1982) "Biochemical characterization of HgCl2-inducible polypeptides encoded by the mer operon of plasmid R100." *J Bacteriol* 151:962-970.

Johs A, Harwood IM, Parks JM, Nauss RE, Smith JC, Liang L, Miller SM (2011) "Structural characterization of intramolecular Hg(2+) transfer between flexibly linked domains of mercuric ion reductase." *J Mol Biol* 413:639-656.

Jomova K, Valko M (2011) "Advances in metal-induced oxidative stress and human disease." *Toxicology* 283:65-87.

Kulkarni RD, Summers AO (1999) "MerR cross-links to the alpha, beta, and sigma 70 subunits of RNA polymerase in the preinitiation complex at the merTPCAD promoter." *Biochemistry* 38:3362-3368.

Ledwidge R, Hong B, Dötsch V, Miller SM (2010) "NmerA of Tn501 mercuric ion reductase: structural modulation of the pKa values of the metal binding cysteine thiols." *Biochemistry* 49:8988-8998.

Ledwidge R, Patel B, Dong A, Fiedler D, Falkowski M, Zelikova J, Summers AO, Pai EF, Miller SM (2005a) "NmerA, the metal binding domain of mercuric ion reductase, removes Hg2+ from proteins, delivers it to the catalytic core, and protects cells under glutathione-depleted conditions." *Biochemistry* 44:11402-11416.

Ledwidge R, Soinski R, Miller SM (2005b) "Direct monitoring of metal ion transfer between two trafficking proteins." *J Am Chem Soc* 127:10842-10843.

Lund ME, Banner W, Jr., Clarkson TW, Berlin M (1984) "Treatment of acute methylmercury ingestion by hemodialysis with N-acetylcysteine (Mucomyst) infusion and 2,3-dimercaptopropane sulfonate." *J Toxicol Clin Toxicol* 22:31-49.

May JT, Hothem RL, Alpers CN, Law MA (1999) "Mercury Bioaccumulation in Fish in a Region Affected by Historic Gold Mining: The South Yuba River, Deer Creek, and Bear River Watersheds, California, 1999." *US Geological Survey* 95819:6129.

*Mercury in the Environment* (2000) Published by the US Geological Survey. Accessed January 28, 2008. http://www.usgs.gov/themes/factsheet/146-00/

*Methylmercury in sport fish: Information for fish consumers* (2003) Published by the Califonia Office of Envionrmental Health Hazard Assessment. Accessed January 28, 2008. http://www.oehha.org/fish/hg/index.html

Miller SM (1999) "Bacterial detoxification of Hg(II) and organomercurials." *Essays Biochem* 34:17-30.

Miller SM, Ballou DP, Massey V, Williams CH, Jr., Walsh CT (1986) "Two-electron reduced mercuric reductase binds Hg(II) to the active site dithiol but does not catalyze Hg(II) reduction." *J Biol Chem* 261:8081-8084.

Miller SM, Moore MJ, Massey V, Williams CH, Jr., Distefano MD, Ballou DP, Walsh CT (1989) "Evidence for the participation of Cys558 and Cys559 at the active site of mercuric reductase." *Biochemistry* 28:1194-1205.

"Mineral commodity summaries 2007: Mercury." (2007) *US Geological Survey* 104–105.

Moore MJ, Miller SM, Walsh CT (1992) "C-terminal cysteines of Tn501 mercuric ion reductase." *Biochemistry* 31:1677-1685.

Moore MJ, Walsh CT (1989) "Mutagenesis of the N- and C-terminal cysteine pairs of Tn501 mercuric ion reductase: consequences for bacterial detoxification of mercurials." *Biochemistry* 28:1183-1194.

Morby AP, Hobman JL, Brown NL (1995) "The role of cysteine residues in the transport of mercuric ions by the Tn501 MerT and MerP mercury-resistance proteins." *Mol Microbiol* 17:25-35.

Nakahara H, Silver S, Miki T, Rownd RH (1979) "Hypersensitivity to Hg2+ and hyperbinding activity associated with cloned fragments of the mercurial resistance operon of plasmid NR1." *J Bacteriol* 140:161-166.

Qian H, Sahlman L, Eriksson PO, Hambraeus C, Edlund U, Sethson I (1998) "NMR solution structure of the oxidized form of MerP, a mercuric ion binding protein involved in bacterial mercuric ion resistance." *Biochemistry* 37:9316-9322.

Robinson JB, Tuovinen OH (1984) "Mechanisms of microbial resistance and detoxification of mercury and organomercury compounds: physiological, biochemical, and genetic analyses." *Microbiol Rev* 48:95-124.

Rosenzweig AC, O'Halloran TV (2000) "Structure and chemistry of the copper chaperone proteins." *Curr Opin Chem Biol* 4:140-147.

Sahlman L, Hagglof EM, Powlowski J (1999) "Roles of the four cysteine residues in the function of the integral inner membrane Hg2+-binding protein, MerC." *Biochem Biophys Res Commun* 255:307-311.

Sahlman L, Wong W, Powlowski J (1997) "A mercuric ion uptake role for the integral inner membrane protein, MerC, involved in bacterial mercuric ion resistance." *J Biol Chem* 272:29518-29526.

Sanfeliu C, Sebastia J, Cristofol R, Rodriguez-Farre E (2003) "Neurotoxicity of organomercurial compounds." *Neurotox Research* 5:283-305.

Sasaki Y, Hayakawa T, Inoue C, Miyazaki A, Silver S, Kusano T (2006) "Generation of mercury-hyperaccumulating plants through transgenic expression of the bacterial mercury membrane transport protein MerC." *Transgenic Res* 15:615-625.

Sasaki Y, Minakawa T, Miyazaki A, Silver S, Kusano T (2005) "Functional dissection of a mercuric ion transporter, MerC, from Acidithiobacillus ferrooxidans." *Biosci Biotechnol Biochem* 69:1394-1402.

Schiering N, Kabsch W, Moore MJ, Distefano MD, Walsh CT, Pai EF (1991) "Structure of the detoxification catalyst mercuric ion reductase from Bacillus sp. strain RC607." *Nature* 352:168-172.

Schue M, Glendinning KJ, Hobman JL, Brown NL (2008) "Evidence for direct interactions between the mercuric ion transporter (MerT) and mercuric reductase (MerA) from the Tn501 mer operon." *Biometals* 21:107-116.

Silver S (1996) "Bacterial resistances to toxic metal ions--a review." *Gene* 179:9-19.

Silver S, Phung LT (1996) "Bacterial heavy metal resistance: new surprises." *Annu Rev Microbiol* 50:753-789.

Stanisich VA (1974) "Interaction between an R factor and an element conferring resistance to mercuric ions in Pseudomonas aeruginosa." *Molec Gen Genet* 128:201-212.

Stanisich VA, Bennett PM, Richmond MH (1977) "Characterization of a translocation unit encoding resistance to mercuric ions that occurs on a nonconjugative plasmid in Pseudomonas aeruginosa." *J Bacteriol* 129:1227-1233.

Steele RA, Opella SJ (1997) "Structures of the reduced and mercury-bound forms of MerP, the periplasmic protein from the bacterial mercury detoxification system." *Biochemistry* 36:6885-6895.

Stricks W, Kolthoff IM (1953) "Reactions between mercuric mercury and cysteine and glutathione. Apparent dissociation constants, heats and entropies of formation of various forms of mercuric mercapto-cysteine and -glutathione." *J Am Chem Soc* 75:5673-5681.

Su CC, Long F, Zimmermann MT, Rajashankar KR, Jernigan RL, Yu EW (2011) "Crystal structure of the CusBA heavy-metal efflux complex of Escherichia coli." *Nature* 470:558-562.

Summers AO (1986) "Organization, expression, and evolution of genes for mercury resistance." *Annu Rev Microbiol* 40:607-634.

Torti SV, Torti FM (2011) "Ironing out cancer." *Cancer Res* 71:1511-1514.

Vallee BL, Ulmer DD (1972) "Biochemical effects of mercury, cadmium, and lead." *Annu Rev Biochem* 41:91-128.

Williams LE, Pittman JK, Hall JL (2000) "Emerging mechanisms for heavy metal transport in plants." *Biochim Biophys Acta* 1465:104-126.

Wilson JR, Leang C, Morby AP, Hobman JL, Brown NL (2000) "MerF is a mercury transport protein: different structures but a common mechanism for mercuric ion transporters?" *FEBS Lett* 472:78-82.

Wu CC, Rice WJ, Stokes DL (2008) "Structure of a copper pump suggests a regulatory role for its metal-binding domain." *Structure* 16:976-985.

# CHAPTER 1

## Expression, Purification, and Crystallization trials of Tn*21* MerT, a prokaryotic *mer* operon membrane protein involved in $Hg^{2+}$ uptake and resistance

This chapter includes unpublished results. Robert M. Stroud was this project's principal investigator. Susan M. Miller collaboratively advised over the course of this project's work. I am grateful to Larry J. Miercke and Andrew Sandstrom for their assistance with protein purification, Franz Gruswitz for his helpful conversations and encouragement, and members of the Stroud Group for their insights.

## Abbreviations

βME: 2-Mercaptoethanol

CMC: critical micelle concentration

DM: n-Decyl-β-D-maltoside ($C_{10}$ alkyl chain, maltose headgroup)

DDM: n-Dodecyl-β-D-maltoside ($C_{12}$ alkyl chain, maltose headgroup)

DTT: dithiothreitol

EDTA: Ethylenediaminetetraacetic acid

FC-14: Fos-choline 14 ($C_{14}$ alkyl chain, phosphocholine headgroup; phospholipid analog also known as n-Tetradecylphosphocholine)

IEX: ion-exchange chromatography

IMAC: immobilized metal ion affinity chromatography

IPTG: isopropyl ß-D-thiogalactoside

LDAO: Lauryldimethylamine-N-Oxide ($C_{12}$ alkyl chain, N-Dimethylamine-N-Oxide headgroup; also known as n-Dodecyl-N,N-Dimethylamine-N-Oxide)

LIC: ligation-independent cloning

MBP: maltose binding protein

Mistic: membrane-integrating sequence for translation of integral membrane constructs (Roosild et al. 2005)

NG: n-Nonyl-β-D-glucoside ($C_9$ alkyl chain, glucose headgroup)

OG: n-Octyl-β-D-glucoside ($C_8$ alkyl chain, glucose headgroup)

OM: n-Octyl-β-D-maltoside ($C_8$ alkyl chain, maltose headgroup)

SDS: sodium dodecyl sulfate

SEC: size exclusion chromatography

TEV: tobacco etch virus

## Introduction

Unlike other bacterial metal ion resistance systems, which rely on either dedicated membrane proteins to actively transport metal ions out of the cytosol or soluble proteins that sequester metal ions in the periplasm or outside the cell, membrane proteins of prokaryotic mercury resistance (*mer*) loci facilitate inorganic mercury ($Hg^{2+}$) uptake. Once inside the cell, $Hg^{2+}$ is reduced by mercuric reductase (MerA) to $Hg^0$, which due to its uncharged state, low aqueous solubility, and little affinity for ligands, can passively diffuse across the cell membrane and partition outside the cell (Barkay et al. 2003). Reduction of $Hg^{2+}$ to a volatile monoatomic gas ultimately demands less carbon and energy resources of the cell than the aforementioned mechanisms of other metal ion resistance pathways.

The most common *mer* transport protein is MerT (Figure 1), which has been reviewed extensively (Brown et al. 1991; Hobman and Brown 1997; Brown et al. 2002; Barkay et al. 2003). Expression of MerT, or of the less-prevalent mercury transporter MerC (Sahlman et al. 1997; Sahlman et al. 1999), is required for resistance to inorganic mercurials ($Hg^{2+}$) (Lund and Brown 1987). Studies of this membrane protein have focused on the macroscopic observation of resistance phenotypes. Zone of inhibition (Foster et al. 1979) and liquid culture density assays (Nakahara et al. 1979) have shown that cells expressing MerT alongside insertion and deletion mutants of MerA, which in turn inhibits expression of functional reductase, are hypersensitive to $HgCl_2$. This observation suggests that, in the absence of MerA, MerT enhances $Hg^{2+}$ access to the cell's interior. $^{203}Hg^{2+}$ binding and volatilization assays have confirmed that MerT can

acquire extracellular mercury and facilitate its entry into the cytosplasm (Robinson and Tuovinen 1984). Studies of the ability of MerT to facilitate movement of other metal ions across the membrane have not been reported. However, it may be expected to exhibit specificity for $Hg^{2+}$ since facilitation of influx of a broad range of metal ions, especially other heavy metal ions of no known biological benefit, would be detrimental to cells without accompanying coping mechanisms. We are not aware of any hypothesis as to how the structure of MerT determines $Hg^{2+}$ transport specificity.

MerT's 116-amino acids are predicted to form three canonical transmembrane helices (TMH), an ~8 residue cytosolic N-terminal leader, a ~10 residue periplasmically-accessible loop that links TMH1 and TMH2, and a ~25 residue cytoplasmic loop that links TMH2 and THM3 (Figure 1) (Brown et al. 1991; Morby et al. 1995; Brown et al. 2002). The assignment of the TMHs is based on hydropathy analysis and has yet to be tested experimentally (Misra et al. 1984). All *mer* proteins are thought to bind $Hg^{2+}$ exclusively to pairs of cysteines, of which MerT has two. Although $Hg^{2+}$ tightly associates with thiols [$K_{form}$ for $Hg(SR)_2$ reported as high as $10^{40}$ $M^{-2}$] it can rapidly exchange with other thiols (Stricks and Kolthoff 1953). Once bound to a thiol, it can only exchange to another thiol (Cheesman et al. 1988). The affinity of $Hg^{2+}$ for a thiol pair is determined by how well the protein structure accommodates and coordinates the ion. The first set of cysteines (Cys24 and Cys25) is hypothesized to lie near the periplasmic vestibule of the protein within the membrane spanning region of TMH1 (Figure 1).

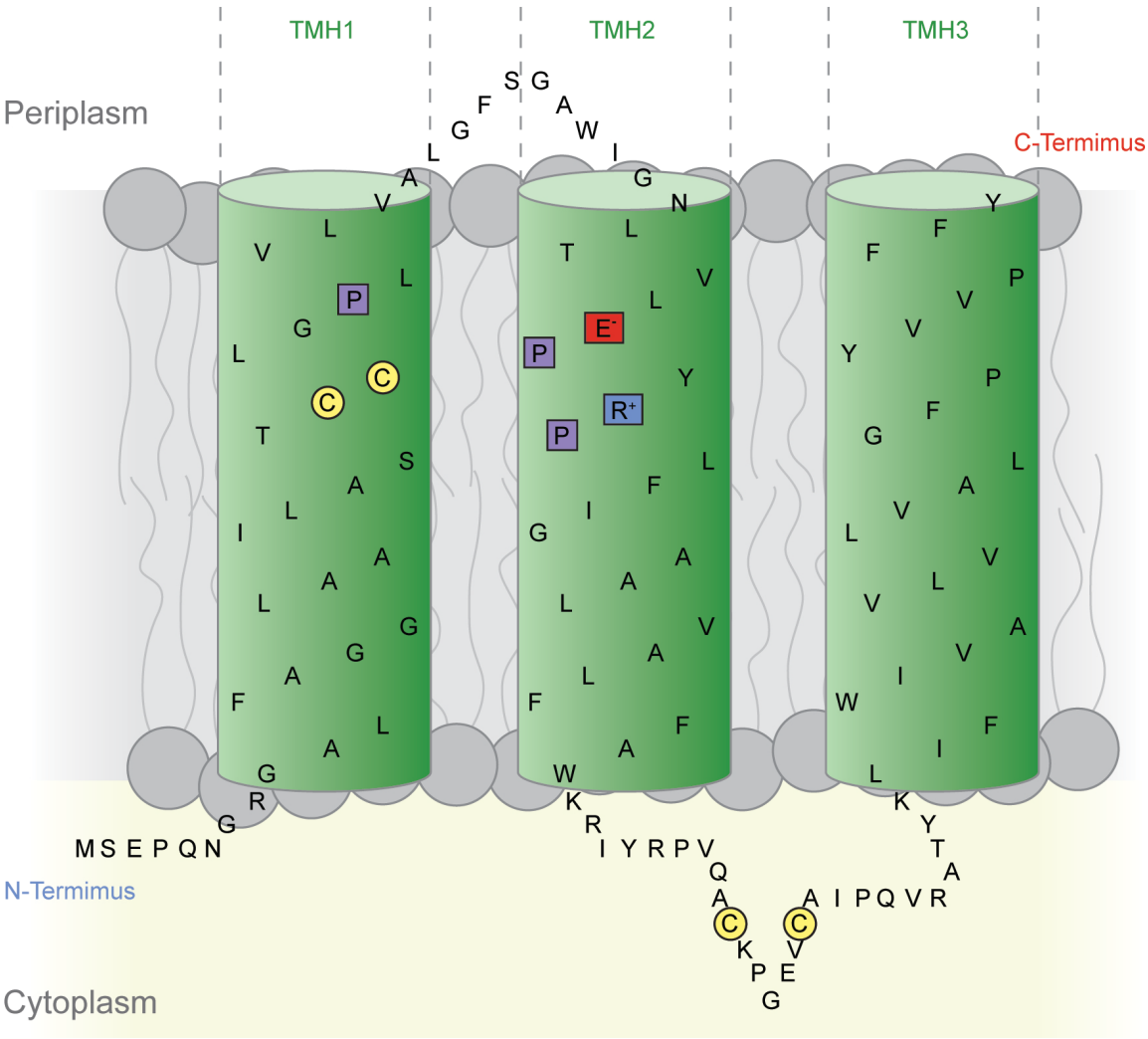


**Figure 1.** Sequence and predicted topology of Tn*21* MerT, based on the predicted topology of Tn*501* MerT (Brown et al. 1991). The three predicted transmembrane helices (TMH) are in green (Brown et al. 1991; Brown et al. 2002). The N-terminal leader prior to TMH1 and loop between TMH2 and TMH3 are believed to be cytosolically accessible. The short linker between TMH1 and TMH2 is believed to reside in the periplasm. The four cysteine residues, believed to be structurally isolated as one pair within the membrane-spanning region of TMH1 and as a second pair on the cytoplasmic loop, are highlighted in yellow circles. It has been suggested that each thiol pair, a canonical motif found in other *mer* proteins, binds $Hg^{2+}$. Other conserved residues, including prolines (purple squares) and charged residues proximal to the first thiol pair (positive in blue rectangles; negative in red rectangles), are highlighted (Wilson et al. 2000).

Mutagenesis studies have established that this first thiol pair is crucial for resistance and $Hg^{2+}$ transport, while the second cysteine pair (Cys75 and Cys81), which putatively resides on a cytosolic accessible loop that links TMH2 and TMH3, appears not to be essential (Figure 1) (Morby et al. 1995). Additionally, Pro28, two residues downstream of the first cysteine pair, and an ER*X*RP motif postulated to lie in MerT's second transmembrane helix may be involved in the translocation of $Hg^{2+}$ (Figure 1). Sequence alignments show that this proline and the ER*X*RP sequence are conserved across various MerT isolates (Morby et al. 1995), and that MerC and a third *mer* transporter, MerF, also conserve the first TMH proline (Wilson et al. 2000).

There is no evidence suggesting particular environmental conditions or metabolites are required for MerT-facilitated movement of $Hg^{2+}$ across the membrane. To evaluate the role of additional substrates in transport, cells expressing functional *mer* operons have been subjected to different environmental conditions, including varied pH and sodium chloride concentrations (Selifonova and Barkay 1994; Sahlman et al. 1997). However, it is impossible to deconvolute the effects of these perturbations on transport, reduction, and other cellular phenomena *in vivo*. Additionally, the media used in these assays contained NaCl which can facilitate the permeation of $HgCl_2$ used as the substrate in these experiments (Gutknecht 1981). Mercury resistance is observed in many disparate environments that only share the presence of mercury in common. Sequence analysis and similarity searches do not suggest that any regions of MerT from various *mer* isolates are homologous to any known metabolite binding regions. Transport is unlikely to be driven by or rely on coupling to additional cargo that may not be present,

such as is the case with the proton/$Cd^{2+}$ and $Zn^{2+}$ antiporter CzcA (Silver and Phung 1996; Goldberg et al. 1999), the proton/$Ag^{+}$ antiporter SilCBA (Silver 2003), and the P-type ATPase CadA efflux pumps (Silver and Phung 2005).

Other *mer* proteins interact with and traffic $Hg^{2+}$ to and from MerT. Minimal inhibitory concentration experiments have shown that expression of MerP alongside mutated MerT, in which the cytosolic thiol pair has been substituted by serines, in cells lacking MerA renders cells only as sensitive to $Hg^{2+}$ as those not expressing the membrane protein, while in the absence of MerP, cells expressing this mutant MerT or wild-type MerT are hypersensitive to $Hg^{2+}$ (Morby et al. 1995). Studies have shown that expression of MerP alongside mutant MerT, in which Cys76 or Cys82 have been mutated to serine, restores the observed resistance phenotype which is otherwise reduced by these mutatons (Morby et al. 1995). This suggests that MerP may interact with periplasmic residues of MerT and allosterically affect the transporter's second thiol pair, though expression of MerP is not required for $Hg^{2+}$ transport. When MerT's Gly38, which is proposed to reside in the periplasmic linker between the first and second transmembrane helices, is mutated to Asp, cells expressing MerP exhibit a phenotype similar to MerP deletion mutants which further suggests the two proteins interact (Morby et al. 1995). MerP increases mercury resistance in plating assays (Hamlett et al. 1992), but there have been no experiments that directly show MerP delivers $Hg^{2+}$ to MerT's first cysteine pair. Nonetheless, it is unlikely that MerP only binds $Hg^{2+}$ just to protect the periplasmic space, as extracellular sequestration is less carbon efficient than reduction.

After traversing the membrane, $Hg^{2+}$ must be acquired by MerA for reduction to $Hg^0$. It has been hypothesized that $Hg^{2+}$, upon binding to MerT's C-terminal dithiol, exchanges onto NmerA to be routed to the MerA catalytic core (Core) (Brown 1985; Ledwidge et al. 2005). It is unknown if Core's C-terminal thiols or NmerA can directly acquire $Hg^{2+}$ from MerT. Bacterial two-hybrid studies have suggested that MerT interacts with NmerA but not with the Core (Schue et al. 2007). In addition, a fraction of MerA was bound to sediments in membrane preparations from transporter-expressing cells (Jackson and Summers 1982; Hamlett et al. 1992). $Hg^{2+}$ bound to a peptide corresponding to the intracellular region of MerT can be passed to NmerA (Rossy et al. 2004), but it is neither surprising nor informative that a peptide with two cysteines can bind $Hg^{2+}$. Better experiments are needed to resolve whether MerP and the domains of MerA can form complexes with MerT independent of $Hg^{2+}$ and/or deliver or acquire $Hg^{2+}$ from either of MerT's cysteine pairs.

No atomic-resolution models of MerT have been determined by X-ray crystallography or NMR, and MerT is not homologous to any protein of known structure. Understanding of MerT's structure at atomic level detail would both provide insight useful for developing testable mechanistic hypotheses, as well as complement our general understanding of membrane protein architecture; of the 394 unique membrane protein structures known, only 13 are of proteins with three membrane-spanning helices (Kang and Li 2011; Nietlispach and Gautier 2011). It is not known how the structure of MerT defines transport specificity, thiol affinity, or interaction interfaces. Atomic resolution information obtained from x-ray crystallographic studies of membrane proteins, such as

the voltage-gated potassium channels, have illuminated the finest mechanistic details of these cellular "gatekeepers" and explained macroscopic phenomena (Spencer and Rees 2002). Structures of mutants exhibiting aberrant transport mechanisms would also provide insights into the mechanism of metal specificity, $Hg^{2+}$ transport, and transporter interactions with MerP and MerA domains. Atomic resolution structural information of a heavy metal transporting membrane protein would be archetypal for understanding the mechanism of how these metals are moved across cell membranes. This information would greatly complement decades of research and let us draw a complete picture of the *mer* resistance system inside and out.

Previous attempts to express MerT for *in vitro* study has required the protein be solubilized from inclusion body preparations using Triton X-100 (Hobman and Brown 1996; Senthil and Gautam 2010). Here we present our approach for expressing the Tn*21* MerT isolate in the cell membranes, solubilizing it with various detergents, and purifying the protein for crystallization trials. In doing so we explore a wide range of variables, including affinity tag usage and benefits, as well as chromatographic separation and assessment methods, for preparing pure, homogeneous, stable protein for hanging-drop vapor diffusion crystallization experiments. The strategies and tactics we describe, developed specifically for MerT, have been derived from our experience in membrane protein crystallography (Savage et al. 2003; Khademi et al. 2004; Savage and Stroud 2007; Hays et al. 2009; Newby et al. 2009; Gruswitz et al. 2010) and studies of membrane channel transport kinetics (Stroud et al. 2003; Khademi et al. 2004; Lee et al. 2004).

## Cloning and Construct Design

Plasmid pDG106, which codes for the Tn*21* mer operon originally isolated from *Shigella flexneri*, was a generous gift from Dr. Anne O. Summers (Gambill and Summers 1985; Ross et al. 1989; Hamlett et al. 1992; Park et al. 1992; Liebert et al. 1999). Standard molecular biology protocols were used for PCR amplification, restriction digest, ligation, and transformation. Chemically-competent Top10 *Escherichia coli* (Invitrogen, Carlsbad, CA) were transformed with the vectors following insertion of *merT* and selected on LB/kanamycin (30 μg/mL) or LB/carbenicillin (50 μg/mL) plates, as appropriate. In each construct, the MerT gene sequence and orientation were verified by DNA sequencing.

pLIC-CH:$His_8$-TEV_MerT and pMIS2.1mv:$His_8$-Mistic-TEV_MerT vectors: The 348 bp coding sequence of Tn*21 merT* from plasmid pDG106 was PCR-amplified using forward (5' TACTTCCAATCCAATGCATCTGAACCACAAAACGGC 3') and reverse (5' TTATCCACTTCCAATGTTATTAATAGAAAAATGGAACGACATAGG 3') primers. The PCR product was inserted into ligation-independent cloning (LIC) vectors as previously described (Aslanidis and de Jong 1990). The use of LIC allows for rapid gene insertion into a variety of vectors without complications from undesired restriction enzyme digestion. We inserted *merT* into pLIC-CH (PSI clone EvNO00292961), which codes for an N-terminal $His_8$ affinity purification tag followed by a tobacco etch virus (TEV) protease cleavage site, as well as into pMIS2.1mv (PSI clone EvNO00304415), which codes for a tandem N-terminal $His_8$ affinity purification tag and the membrane-

integrating sequence for translation of integral membrane constructs (Mistic) (Roosild et al. 2005) followed by a tobacco etch virus (TEV) protease cleavage site. Gene expression in both vectors is controlled by the *lac*/T7 strategy employed in pET vectors (Rosenberg et al. 1987; Studier et al. 1990). After TEV cleavage, this strategy leaves three protease recognition site residues (SNA) upstream of the native Tn*21* MerT sequence, which begins at Ser2, for both the resulting pLIC-CH:$His_8$-TEV_MerT and pMIS2.1mv:$His_8$-Mistic-TEV_MerT vectors.

pET47sl:$His_6$-3C_MerT: Tn*21 merT* was PCR-amplified from pLIC-CH:$His_8$-TEV_MerT using forward (5′ CGCGCG**GGATCC**TCTGAACCACCAAACGGC 3′) and reverse (5′ GGCGG**CCTCGA**GttattaATAGAAAAATGGAACGACATAG 3′) primers designed to introduce a BamH1 and XhoI at the beginning and end of the gene (in bold), respectively, and two stop codons at the end of the gene (lower case). The PCR product was ligated in between the BamHI and XhoI restriction sites of the kanamycin-resistant pET47sl vector, a modified pET47b(+) vector (Novagen, Madison, WI) that codes for an N-terminal $His_6$ affinity purification tag followed by a 3C protease cleavage site (Alexandrov et al. 2001). After 3C cleavage, this strategy leaves only three protease recognition site residues (GPG) upstream of the native Tn*21* MerT sequence, which begins at Ser2.

pMAL-c2Xa:$His_6$-MPB-3C_MerT: The *merT* gene was PCR-amplified from pET47sl:$His_6$-3C_MerT using forward (5′ CCGCGG**GAATTC**CTTGAAGTCCTCTTTCAGGG 3′) and reverse (5′

GCGGCG**TCTAGA**ttattaATAGAAAAATGGAACGACATAG 3′) primers designed to introduce a BamH1 and XbaI at the beginning and end of the gene (in bold), respectively, and two stop codons at the end of the gene (lower case). The PCR product was ligated in between the BamHI and XbaI restriction sites of the ampicillin-resistant pMAL-c2Xa vector, a modified pMAL-c2X vector (New England Biolabs, Ipswich, MA) that codes for tandem N-terminal $His_6$ and maltose binding protein (MBP) affinity purification tags followed by a 3C protease cleavage site. After 3C cleavage, this strategy leaves only three protease recognition site residues (GPG) upstream of the native Tn*21* MerT sequence, which begins at Ser2.

No difficulties were encountered cloning *merT* from pDG106 or any of the subsequently created vectors. pLIC-CH:$His_8$-TEV_MerT and pMIS2.1mv:$His_8$-Mistic-TEV_MerT were constructed for initial expression testing but were not intended for scale-up usage.

Affinity tag and cleavage site design: We considered several affinity purification approaches to engineer the above constructs. We have previously had success using $His_6$-tags to purify several prokaryotic membrane proteins (Savage et al. 2003; Gruswitz et al. 2007; Newby et al. 2009) As we discovered in working with MerT, the protein is less likely to aggregate in the presence of a reducing agent, which precludes use of antibody-affinity tags. However, we have been able to capture $His_6$-tagged membrane proteins using low concentrations of reducing agents (e.g. 0.5 mM DTT, 4 βME) when working with Ni-NTA matrices. The MBP affility tag has also been used in membrane protein

purification in cases where the solubilizing detergent does not feature a maltoside headgroup (e.g. OM, DM, DDM). In the presence of these detergents, MBP preferentially binds to the detergent's maltoside headgroup over amylose resin. Nonetheless, MBP can provide benefit by enhancing protein expression even when it can not be used for affinity purification (Hu et al. 2011). We strongly prefer to remove affinity purification tags prior to crystallization, and have had the greater success in doing so with 3C protease than with TEV protease.

Cleavage site linker design: For all constructs we minimized the number of downstream cleavage sequence residues that would remain after targeted proteolysis (the "sl" in pET47sl indicates "short linker"). We did not examine the effects of longer linker regions between the protease recognition sequence and MerT Ser2. We were unable to cleave MBP from MerT expressed using pMAL-c2Xa:$His_6$-MPB-3C_MerT. Additional linker residues may be required to increase access to the protease cleavage site and minimize steric occlusion of $His_6$-MBP-3C_MerT from 3C protease.

## Protein Expression & Membrane Preparation

MerT expression and membrane preparation protocol: *E. coli* C43 cells were transformed and plated on LB agar with either carbenicillin (50 μg/mL) or kanamycin (30 μg/mL), depending on the vector used, and grown over night (~16 hr) at 37 °C. A single colony was used to inoculate LB with the appropriate antibiotic and the culture was grown at 37 °C and shaken at 280 rpm (for growths in Fernbach flasks) or stirred at 300 rpm (for fermentor vessel growths) until $OD_{600}$ ~0.4. The time from inoculation to $OD_{600}$ ~0.4 was ~3.5 hr for 1 L shaken growths, and ~6 hr for 10 L or 70 L fermentation vessel growths. At $OD_{600}$ ~0.4 the temperature was reduced to 17 °C, and expression was induced with 1 mM IPTG at $OD_{600}$ ~0.6. After overnight (16-18 hours) expression, cells were harvested by centrifugation at 6000 × g for 10 min. Harvested pellets, corresponding to ~6 g per 1 L culture, were resuspended in a lysis buffer and frozen for storage at -20 °C.

All purification procedures were performed at 4 °C unless noted. Frozen cells were thawed and incubated with one or more complete ULTRA EDTA-free protease inhibitor cocktail tablets (Roche Applied Science, Indianapolis, IN), 100 μM PMSF, and 4 mM DTT or 20 mM ßME. Suspended cells were homogenized and lysed by six passes through an Emulsiflex-C3 homogenizer (Avestin, Ottawa, Canada). To remove insoluble debris, lysates were centrifuged at 20,000 × g for 1 h. The soluble and membrane fractions of the lysates were separated by centriguation at 70,000 × g for 2 h. The supernatant was discarded and each gram of membrane pellet was resuspended into 2 mL purification buffer, which depended on the chromatographic purification to follow.

Resuspensions were homogenized using a Polytron PT 1200 E with a microgenerator (Kinematica, Switzerland), to minimize sample aeration, and were aliquoted into 1.5 mL microcentrifuge tubes. Samples were flash frozen in liquid nitrogen and stored at -80 °C for later use.

Expression variables: The aforementioned MerT vectors were transformed into *Escherichia coli* C43(DE3) cells for protein expression (Miroux and Walker 1996), which we have found to give high expression of a variety of prokaryotic membrane proteins (Savage et al. 2003; Savage and Stroud 2007). To maximize protein expression, we varied expression media, temperature, and inoculant. Expression levels of each construct were similar whether in LB medium upon addition of 1 mM IPTG, or in ZYM-5052 auto induction medium (Studier 2005). As it is less expensive to prepare, LB medium was preferred and used for preparative work. When using either LB or ZYM-5052, induction of protein expression at low temperature (14-17 °C) produced the most protein. We also observed that growths inoculated with 2-3 colonies from transformants plated 16 to 18 hours prior produced larger quantities of MerT than growths inoculated with cells from liquid overnight (~16) cultures (which adds ~24 hours time between transformation and growth compared to the colony-to-culture protocol). The use of 10 L and 70 L fermentation vessels as growth chambers allowed for large quantities of protein to be uniformly produced in a temperature-controlled environment. Freezing of resuspended cell pellets and membrane pellets did not adversely affect the quantity or stability of MerT recovered during downstream purification.

## Mobile Phases Assessment and Design

Mobile phase design and assessment: Over the course of our experiments, we considered several factors when designing the non-detergent constituents of buffers to be used in MerT purification and crystallization. We were most concerned with maintaining MerT stability and solubility throughout tested purification pathways (Scheme 1), which like any membrane protein is also affected by detergents. We examined gel filtration elution profiles of MerT in all experimental mobile phases to assess protein homogeneity, stability, and purity. We consider a mobile phase and protein preparation suitable for crystallization trials when the protein is >98% pure, >95% homogeneous and >95% stable, as determined by the sample's gel filtration elution profile, and when stored unconcentrated at 4 °C for 2 weeks or when stored concentrated (i.e., the concentration used for crystallization experiments) at 4 °C for 1 week (Newby et al. 2009).

Reducing agents: As all *mer* proteins contain solvent-accessible cysteines critical to binding $Hg^{2+}$, we sought to maintain a reducing environment to minimize thiol oxidation. Buffers used prior to and for IMAC, specifically $Ni^{2+}$-NTA agarose (Qiagen, Valencia, CA) and $Co^{2+}$-charged TALON resins (Clontech, Mountain View, CA), contained minimal concentrations of reducing agent, at most 0.5 mM DTT or 4 mM βME as recommended by the manufacturer, and no EDTA. All other buffers contained 4-10 mM DTT and 20 mM βME. Gel elution profiles suggested that these concentrations of reducing agents were sufficient to prevent cysteine oxidation.

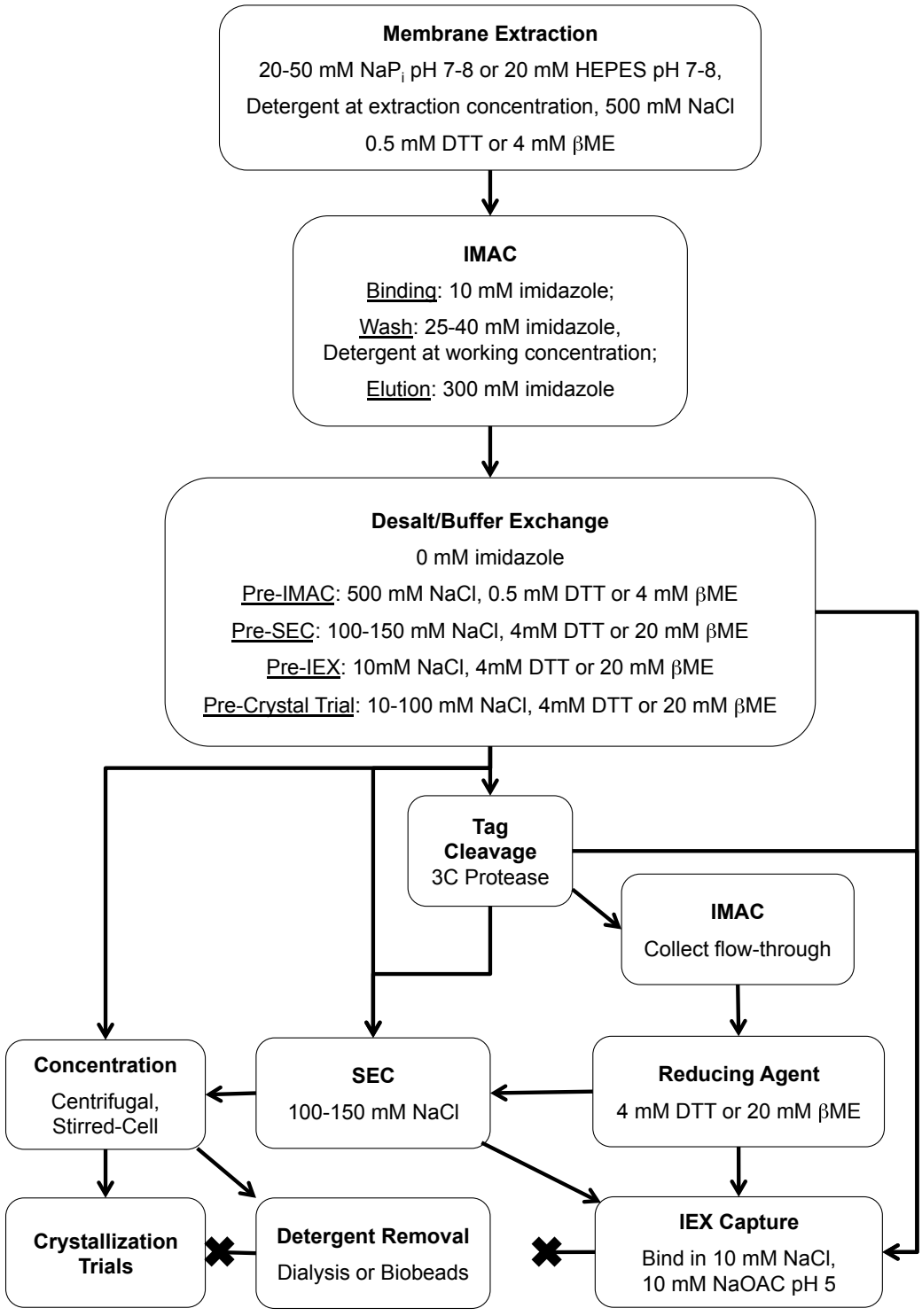


**Scheme 1.** MerT purification trials and mobile phase variables. Modifications of mobile phase variables used at each point in a protocol from previous steps are noted. X's denote ends to purification tactics for which the associated step did not benefit purification for crystal trials.

Buffer and pH: We sought to develop buffers that maintained a pH of 7-8 to allow study of MerT liganded to $Hg^{2+}$ with MerA, which is most catalytically efficient at pH 7.3. We found MerT is compatible with 20 mM HEPES pH 7-8, 20 mM MES pH 6.5, 10 mM NaOAc pH 5, and 20-50 mM $NaP_i$ pH 7-8. 20 mM $NaP_i$ pH 8 buffers were preferred for their compatibility with IMAC resigns and as an analogue to $KP_i$, the standard buffering agent used in MerA kinetic assays. Although phosphate buffers have a propensity to form phosphate salt crystals in spare-matrix crystallization experiments, we were not deterred from its use because of our access to a UV microscope (Korima, Carson, CA) which allows for the detection of tryptophan fluorescence in protein crystals (Tn*21* MerT contains three tryptophan residues). We avoided using amine buffers, such as TRIS, due to the potential formation of mercury-amine complexes.

Ionic Strength: Gel elution profiles did not suggest MerT stability is affected by concentration of 10 to 500 mM NaCl. For buffers used prior to and during IMAC we utilized 500 mM NaCl to minimize non-specific binding. Following IMAC, samples were desalted using a NAP-5 or NAP-10 column (GE Healthcare, Piscataway, NJ), or Econopak 10DG column (Bio-Rad Laboratories, Hercules, CA) into 10-500 mM NaCl. Desalting removes imidazole following IMAC, which is incompatible with 3C protease (Alexandrov et al. 2001), and allows the ionic strength of the mobile phase to be lowered. The critical micelle concentration (CMC) of detergents, the point at which micelles spontaneously form, is commonly lowered with increased ionic strength, which can result in undesirable phase separation in crystallization trials.

## Detergent Solubilization and Selection

Membrane extraction: Detergent solubilization trials for each MerT construct were conducted as previously described (Figure 2) (Newby et al. 2009). We observed that neither the construct design nor the afore mentioned mobile phase variables affected the ability of any detergent to solubilize MerT. We were able to solubilize MerT by treating membrane preparations for one hour at 4 °C with either 200 mM OM, 100 mM DM, 40 mM DDM, 20 mM MMPC, 20 mM FC-14, 200 mM LDAO, or 2% v/v Triton X-100 (TX100). 200 mM OG was able to solubilize only a fraction of MerT expressed under these conditions (Figure 2). Following OG treatment and centrifugation, a large white pellet of unsolubilized material was observed. SDS-PAGE and α-His6 western blot of pellet resuspensions confirmed the presence of significant amounts of MerT in addition to other insoluble proteins. MerT was unable to be extracted from the membrane under the same conditions with 150 mM NG or 150 mM NM.

Selection of detergents for purification and crystallization trials: Maltoside and glucoside headgroup detergents, especially DDM and OG respectively, have been used most frequently in membrane protein crystallization (Raman et al. 2006; Newstead et al. 2008). Our experience has followed this trend especially in using OG. It has been suggested that protein-detergent complexes that are more compact from use of short chain ($C_{12}$ and under) detergents are more amenable to crystallization (Newby et al. 2009). Thus, we attempted to purify MerT in mobile phases containing 40 mM OG, 40 mM OM, 10 mM DM or 0.5 mM DDM. We did not attempt to purify or crystallize MerT in mixed detergent or with addition of lipids.

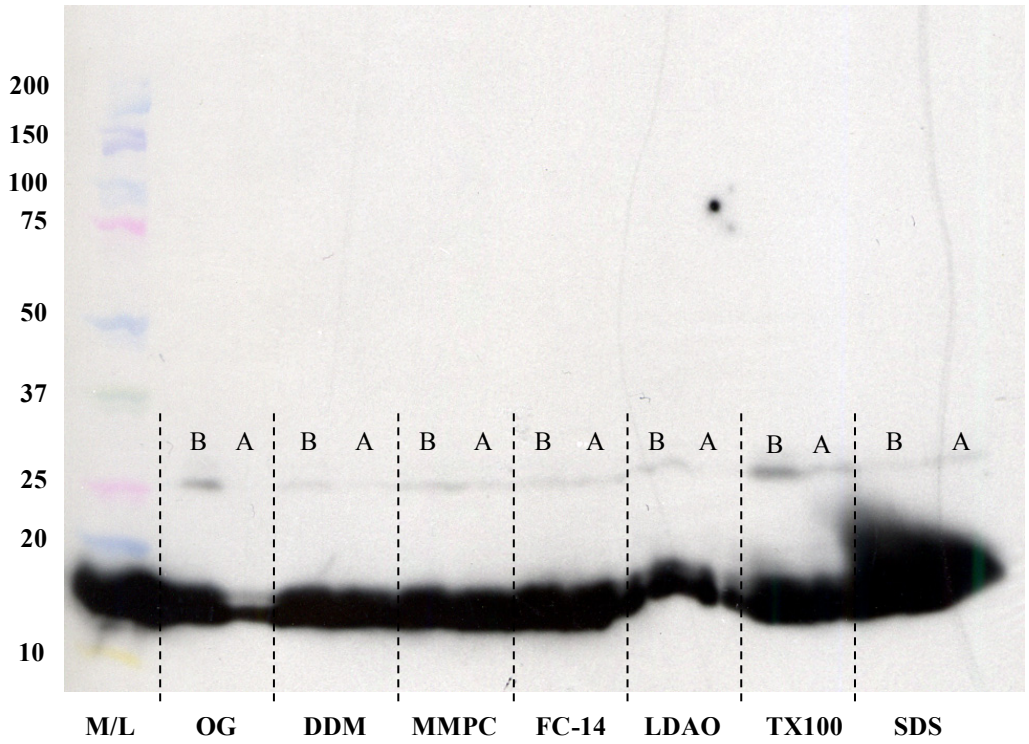


**Figure 2.** $His_6$-3C_MerT solubilization trials. Membrane preparations were exposed to each detergent at concentrations described below for 1 hr at 4 °C and samples were taken immediately prior (B) and after (A) centrifugation. Samples were separated by SDS-PAGE and detected by western blot as previously described (Newby et al. 2009) using His-Probe (H-3), a monoclonal $\alpha$-$His_6$ conjugated to horseradish peroxidase (HRP) (Santa Cruz Biotech, Santa Cruz, CA). M: Precision Plus Protein™ Standards Kaleidoscope™ molecular mass standards (Bio-Rad) with masses in kDa, and resuspended membrane preparation added immediately prior to gel run. Final detergent concentrations used in solubilization were: 200 mM OG, 40 mM DDM, 20 mM MMPC, 20 mM FC-14, 200 mM LDAO (detergent causes the observed rippling in SDS-PAGE gels), and 2% TX100. Protein solubilized in 2% SDS for 1 hr at room temperature was used as a positive control.

## MerT Stability in Glucoside and Maltoside Headgroup Detergents

OG-containing mobile phases: In addition to the aforementioned difficulty of extracting MerT from membrane preparations using 200 mM OG ($C_8$ alkyl chain) (Figure 2), use of OG as a mobile phase solubilizing agent resulted in MerT instability. Following elution from IMAC resins, MerT precipitates in mobile phases above pH 6.5 in the presence of 40 mM OG. To maintain protein solubility after IMAC, we immediately exchanged MerT in OG into 20 mM MES pH 6.5 and 10 mM NaCl. However, we were unable to cleave the $His_6$ affinity purification tag using 3C protease under these low pH conditions. We pursued crystallization of $His_6$-3C-MerT but were unable to devise mobile phase conditions that retain protein solubility for one week at 4 °C (Figure 3). As we were unable to extract MerT from membrane preparations using 150 mM NG ($C_9$ alkyl chain), we did not pursue exchanging or purifying MerT in NG or other glucoside headgroup detergents.

Maltoside headgroup detergent mobile phases: Unlike results with the glucoside headgroup detergents OG and NG, we were able to extract MerT from membrane preparations using maltoside headgroup detergents OM ($C_8$ alkyl chain), DM ($C_{10}$ alkyl chain), and DDM ($C_{10}$ alkyl chain). We found MerT to be soluble in our preferred working concentrations of 40 mM OM, 10 mM DM, or 0.5 mM DDM (Lorber et al. 1990) in post-solubilization mobile phases containing 20 mM HEPES pH 7-8, 20 mM MES pH 6.5, or 20-50 mM $NaP_i$ pH 7-8, 10-500 mM NaCl, and 0.5-4 mM DTT or 2-20 mM βME. We suggest that the maltoside headgroup plays a greater role in maintaining

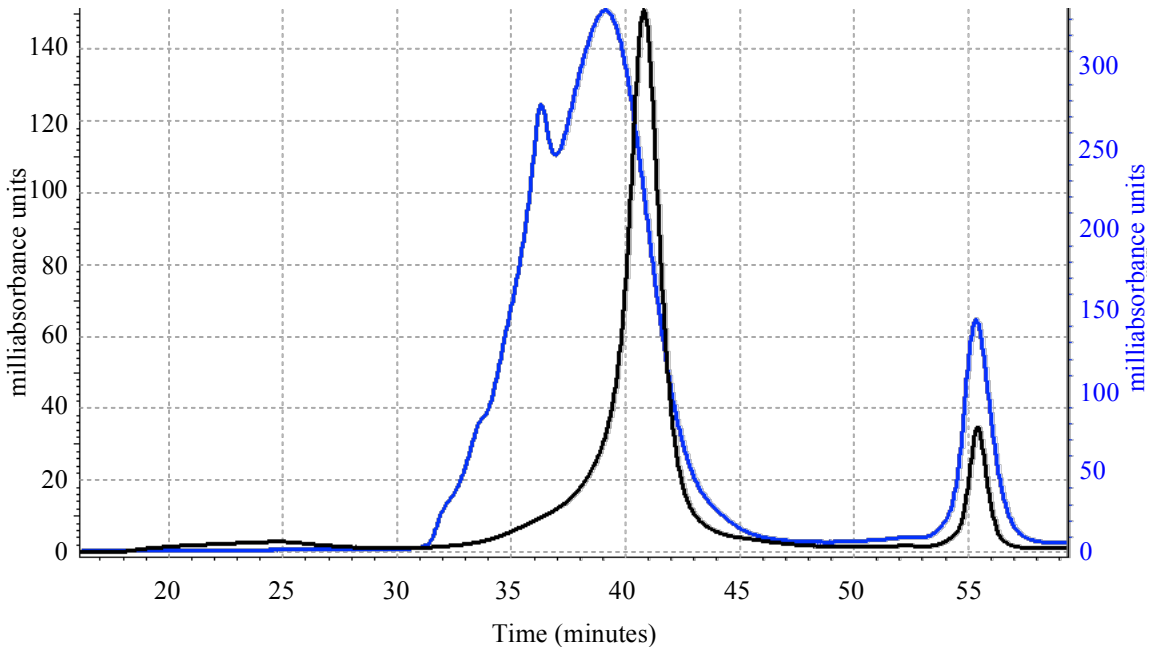


**Figure 3.** SEC elution profile of MerT in OG. Normalized elution profiles of MerT after IMAC elution (black; left axis scale) and storage at 4 °C for 4 days (blue; right scale). Sample was run in 20 mM Hepes pH 6, 100 mM NaCl, 40 mM OG, and 4 mM DTT.

MerT stability than glucoside headgroups or the length of the alkyl "tail" in either class of detergents.

Maltoside headgroup detergents compatibility with MBP affinity purification: We were unable to successfully bind $His_6$-MBP3C_MerT to amylose resin in any maltoside detergent. It is likely that the MBP tag becomes saturated with the maltose headgroup of these detergents. Future expression and purification strategies may utilize MBP to enhance protein expression or to act as an IEX tag.

Detergent choice for crystallization: With crystallization in mind we focused efforts to purify MerT in OM given the detergent's short alkyl tail of identical size to OG, the favorite detergent of the group. It has been suggested that protein-detergent complexes that are more compact, which is affected by the length of the detergent's alkyl chain, are more likely to form stable crystal lattices.

## Affinity Purification and Tag Removal with 3C Protease

Immobilized metal affinity chromatography (IMAC): Following MerT solubilization, we utilized IMAC for the first step in purifying $His_6$-3C_MerT and $His_6$-MBP-3C_MerT as described (Newby et. al 2009, protocol steps 22-36) with minimal modifications. Both constructs were captured by Ni-NTA resin (Qiagen) in the presence of 10 mM imidazole most effectively by 2 hr of batch binding at 4 °C. Following binding, the Ni-NTA matrix was washed with three column volumes of mobile phase containing either 20 mM HEPES pH 8 or 20 mM $NaP_i$ pH 8, 500 mM NaCl, 25-40 mM imidazole, detergent, and either 0.5 mM DTT or 4 mM βME. Higher imidazole concentrations and additional wash volumes resulted in premature leaching of MerT.

Protein was eluted using 300 mM imidazole and immediately desalted to remove imidazole and exchange MerT into a concentration of NaCl appropriate for the next step. For treatment with 3C protease to cleave the affinity tag(s), eluted MerT in mobile phase containing imidazole and 500 mM NaCl and was exchanged into the same mobile phase containing no imidazole and 10 mM NaCl preceding IEX, 100-150 mM NaCl preceding SEC, or 500 mM NaCl preceding a secondary IMAC step. Removal of imidazole is required for 3C protease activity (Alexandrov et al. 2001). In protocols that cleaved the $His_6$ tag from MerT using a $His_6$-MBP-tagged 3C protease and then utilized a secondary IMAC step to capture the cleaved tag and protease, reducing agent concentrations were kept constant (0.5 mM DTT or 4 mM βME). If IMAC was not to be used again, DTT or βME concentration was increased during the desalt step to 4 mM or 20 mM, respectively. For crystallization trials of IMAC purified (and uncleaved) $His_6$-3C_MerT, protein eluted

from the Ni-NTA matrix was exchanged into a mobile phase containing 10-100 mM NaCl and no imidazole. We recovered ~4 mg of MerT per L growth by IMAC.

Maltose-binding protein (MBP)/amylose affinity chromatography: We also attempted to capture $His_6$-MBP-3C_MerT onto amylose resin for initial purification following solubilization. Unlike IMAC this approach allows for higher working concentrations of reducing agents and, from our experience, is significantly more effective at minimizing contamination. However we were unable to capture this construct on the resin in any of the afore mentioned mobile phases. We believe that MBP has a greater affinity for the maltose headgroups of OM, DM and DDM, just as it does for free maltose used as the elutant, than to the amylose resin. Future purification approaches may include MBP/amylose capture in the presence of a non-maltoside (and, from our experience as previously described, glucoside) headgroup detergent, followed by possible detergent exchange into a maltoside detergent. An MBP-tag may also be useful for IEX.

Tag cleavage with 3C protease: Following IMAC and removal of imidazole, we were successful at cleaving the affinity tag from $His_6$-3C_MerT in the previously described chromatographic buffers lacking imidazole using $His_6$-MBP-3C protease at 4 °C for 1 hr in the presence of maltose detergents and 4 mM DTT or 20 mM βME, or for 3 hrs with 0.5 mM DTT or 4 mM βME. We were unable to cleave the tags from $His_6$-MBP-3C_MerT using either $His_6$-MBP-3C Protease or $His_6$-3C Protease. The inability to cleave the tag may be due to steric occlusion by MerT's MBP tag and require a longer linker between the two proteins to increase protease access to the cleavage site. We were

unable to the cleave tags of either MerT construct in presence of OG, or from $His_6$-3C_MerT when bound to Ni-NTA resin prior to imidazole elution.

Post-cleavage removal of 3C protease: We utilized IMAC and SEC to separate $His_6$-MBP-3C Protease and the $His_6$ affinity tag following cleavage from MerT. Due to overlapping elution profiles from Superdex 200 10/300 GL (GE Healthcare) and TSKgel (Tosoh Biosciences, King of Prussia, PA) SEC columns, we were only able to separate $His_6$-3C Protease from MerT using IMAC with Ni-NTA and Talon $Co^{2+}$ resins. We were unable to separate MerT from either $His_6$- or $His_6$-MBP tagged 3C protease using anion or cation IEX.

## Secondary Chromatography Steps and Protein Concentration

Size exclusion chromatography (SEC): Following IMAC and affinity tag cleavage by 3C protease, we used gel filtration chromatography to further remove contaminants, including $His_6$-MBP-3C protease, cleavage products, and other solubilized membrane components, as well as to exchange mobile phases and remove imidazole. Samples were run in mobile phases containing 100-150 mM NaCl to minimize electrostatic interactions with the chromatographic matrix. MerT and $His_6$-3C Protease co-elute from Superdex 200 10/300 GL and TSKgel SEC columns. Thus an IMAC purification step was required prior to SEC when using $His_6$-3C Protease to cleave tags from $His_6$-3C_MerT. We assessed MerT purity, stability, and homogeneity using SEC elution profiles from various matrices (Figure 4), as well as by SDS-PAGE and western analysis (Figure 5) (Newby et al. 2009).

MerT has an apparent chromatographic mass ($MM_{apparent}$) of ~80 kDa, estimated using molecular mass standards (Bio-Rad) (Figure 4). The observed mass, which is more than six-fold greater than the 12.9 kDa sequence calculated mass, may be due to the detergent of the protein-detergent micelle complex, as well as oligomerization. While we successfully employed SEC to remove protein contaminants, MerT in maltoside detergents co-elutes with excess free micelles, which we determined using in-line refractive index and light scattering detectors (Viscotek/Malvern, Worcestershire, UK) (Figure 6). Preparative SEC resulted in MerT dilution, which required us to concentrate the protein (and, inadvertently, the detergent) prior to crystallization trials.

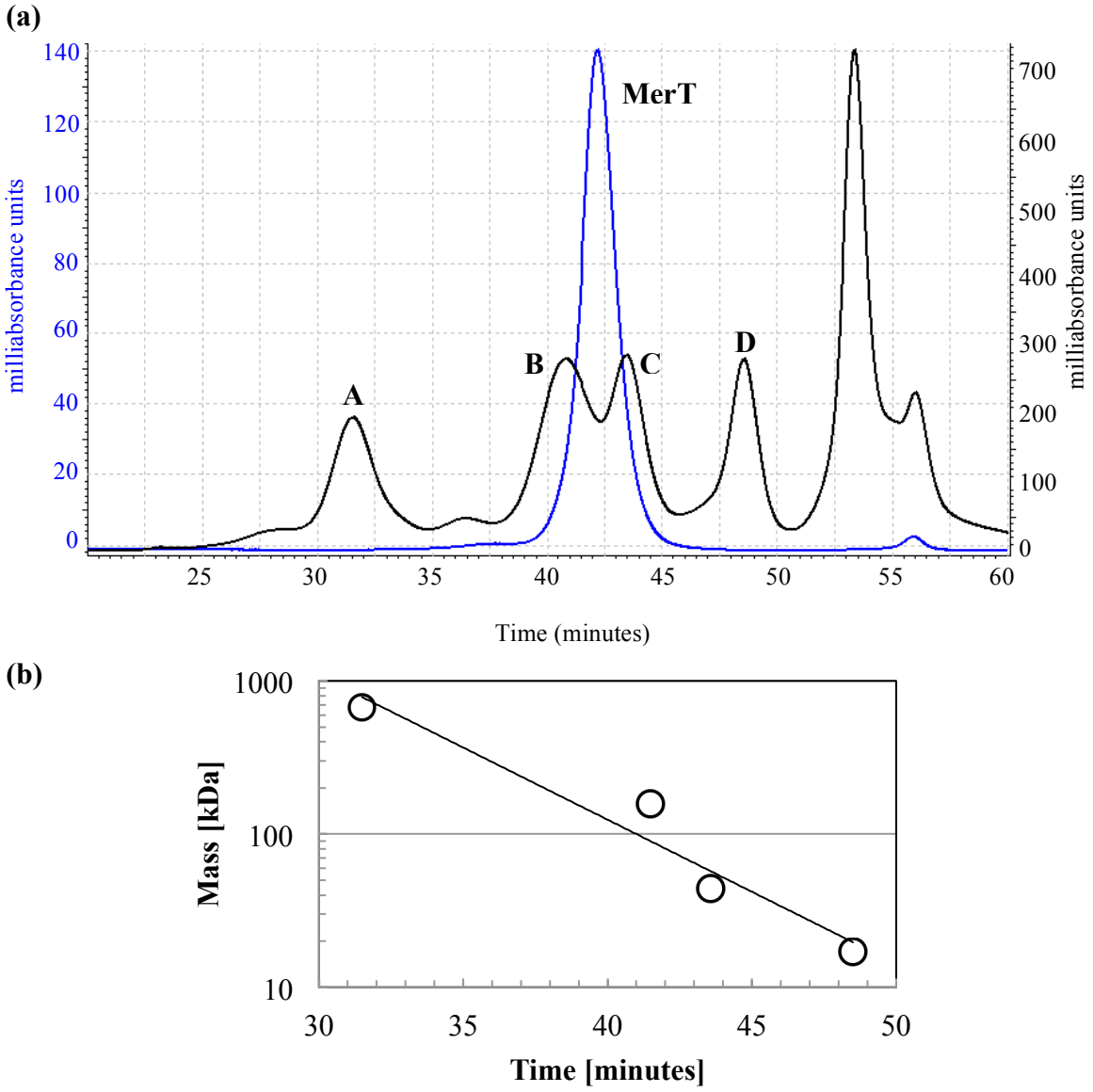


**Figure 4.** SEC Characterization of MerT and $MM_{apparent}$ estimation. (a) Normalized elution profiles of MerT (blue; left axis scale) and a mixture of gel filtration standards (black; right axis scale) observed at 280 nm on a TSKgel 4000 SEC column. Both samples were run in 20 mM Hepes pH 7, 100 mM NaCl, 0.5 mM DDM, and 4 mM DTT. This MerT elution profile and $MM_{apparent}$ of ~80 kDa is typical of observations of MerT in a variety of maltoside-containing mobile phases and profiles from Superdex 200 10/300 GL column elutions. (b) Molecular mass versus elution volume of gel filtration standards corresponding to thyroglobulin (A: 31.5 minutes; 670 kDa), bovine γ-globulin (B: 41.5 minutes; 158 kDa), chicken ovalbumin (C: 43.75 minutes; 44 kDa) and equine myoglobin (D: 48.5 mL; 17 kDa) versus known molecular mass. The logarithmic fit of these standards, mass (kDa) = 723,441× $e^{-0.217[\text{time (minutes)}]}$, was used to estimate $MM_{apparent}$.

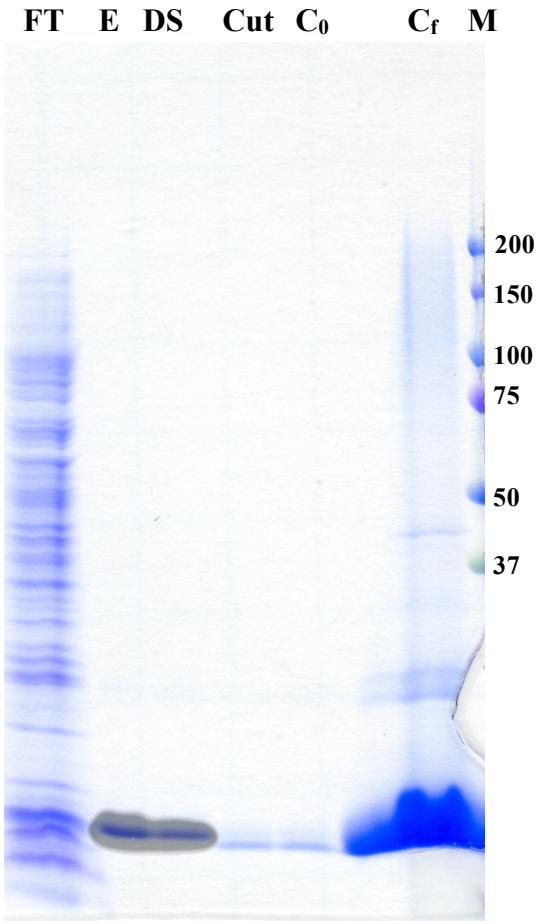


**Figure 5.** Merged results of coomassie and western SDS-PAGE characterization of $His_6$-3C_MerT Purification in OM. His-Probe (H-3), a monoclonal α-$His_6$ conjugated to horseradish peroxidase (HRP) (Santa Cruz Biotech), was used for western detection. FT: flow-through of Ni-NTA column showing capture of $His_6$-3C-MerT, as no western signal is detected with this sample. E: Ni-NTA elution. DS: Desalt and buffer exchange. MerT was exchanged into 20 mM $NaP_i$ pH 7.3, 40 mM OM, 100 mM NaCl, and 4 mM DTT. Cut: MerT following $His_6$-MBP-3C protease treatment and removal by SEC. The gel shift, as well as lack of His-Probe signal, indicates cleavage of the $His_6$-tag from MerT. The lack of a coomassie band and western signal at ~65 kDa indicates removal of the MBP-tagged protease. $C_0$: MerT immediately prior to concentration in a stirred cell with a 50 kDa molecular weight cut-off membrane. $C_f$: MerT following concentration to 25 mg/mL. MerT concentration was computed using a calculated $\varepsilon_{280}$ = 23.95 $mM^{-1}$ $cm^{-1}$ (Gasteiger et al. 2005). The shape of the coomassie band is distorted due to the co-concentration of OM. M: Precision Plus Protein™ Standards Kaleidoscope™ molecular mass standards (Bio-Rad) with masses in kDa.

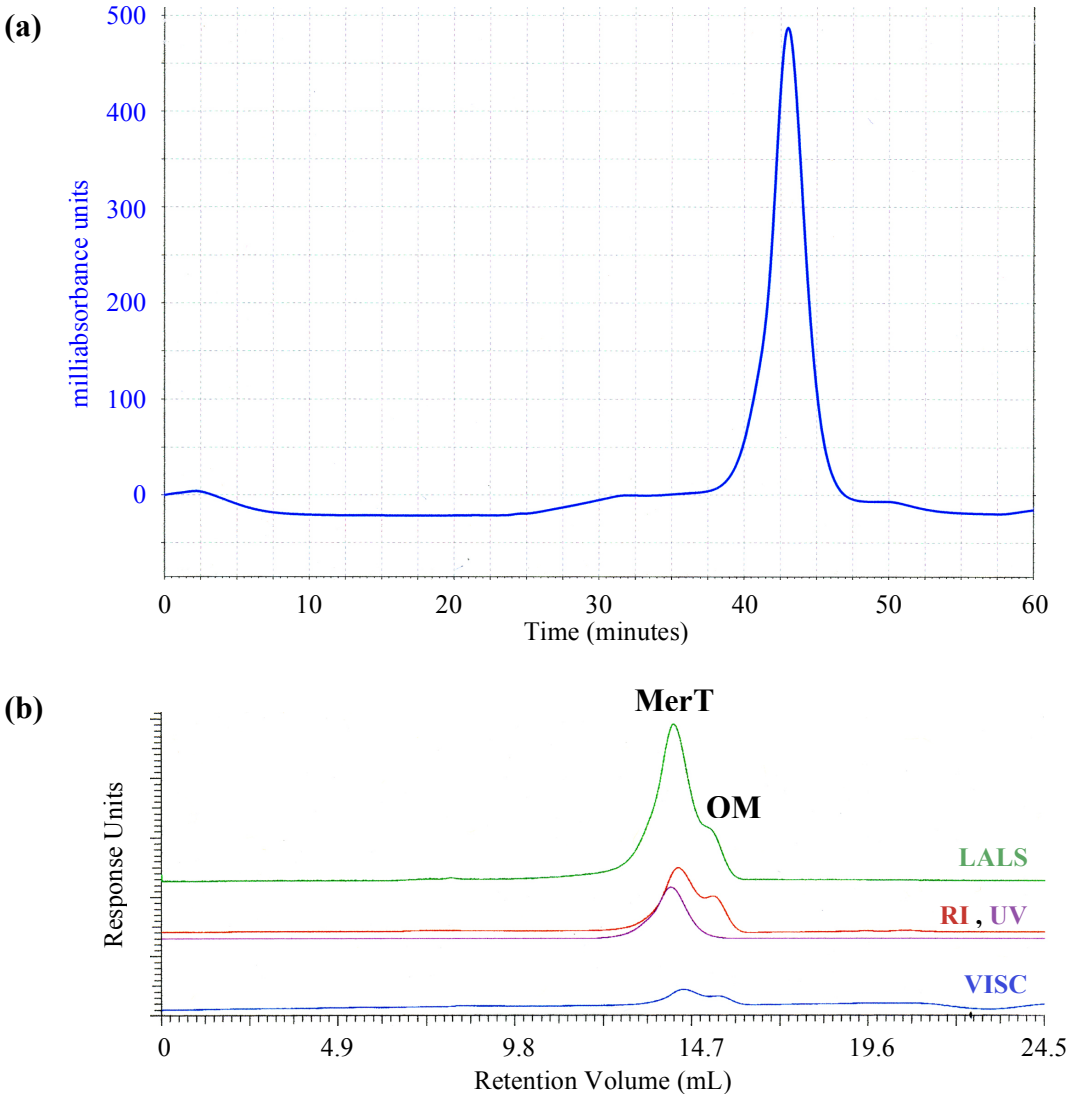


**Figure 6.** SEC Characterization of MerT in OM. (a) Elution profile from a Superdex 200 10/300 GL column (GE Healthcare) of MerT in 20 mM $NaP_i$ pH 7.3, 40 mM OM, 100 mM NaCl, and 4 mM DTT, following removal of $His_6$-MBP_3C Protease by IMAC. (b) Elution profile from the same column of MerT (primary peak) and excess OM (secondary peak) following stirred-cell concentration, monitored using in-line low-angle light scattering (LALS, green), refractive index (RI, red), UV (purple), and viscosity (VISC, blue) detectors. Spectroscopic intensity is shown in response units. Unlike proteins, most detergents do not absorb 280 nm light so their presence and excess relative to baseline can be detected. Here, the secondary shoulder present in all traces other than the UV is due to excess OM. DM, DDM (not shown), and OM concentrate alongside MerT, resulting in extensive phase separation in crystal screens.

Ion Exchange Chromatography: As an alternative to SEC to minimize protein dilution, we pursued capturing MerT onto ion exchange chromatography resins as a secondary purification step to both purify and concentrate the protein. Unlike centrifugal or stirred-cell concentration methods, detergent does not co-concentrate with the captured protein. We were unable to bind MerT or $His_6$-MerT using anion or cation matrices (specifically Q and S Sepharoses, respectively) in the afore mentioned post-Ni-NTA mobile phase conditions containing 10 mM NaCl at pHs between 6.5 and 8, appropriate to the matrix. Although we were able to capture MerT in 10 mM NaOAc pH 5 on S Sepharose, it was prone to precipitation immediately following elution with 750 mM to 1 M NaCl.

Protein Concentration: As we were unable to concentrate MerT using ion exchange, which our group prefers to minimize co-concentration of the mobile phase detergent, we utilized centrifugal or stirred-cell concentrators. MerT could be concentrated in these devices with 50 kDa molecular weight cut-off or smaller membranes. The final MerT concentration was estimated using a calculated $\varepsilon_{280}$ = 23.95 $mM^{-1}$ $cm^{-1}$ assuming all four protein cysteines are reduced (Gasteiger et al. 2005). The redox state of the protein thiols must be considered when calculating the spectroscopic extension coefficient as cystine, unlike cysteine, absorbs appreciably at wavelengths above 260 nm. MerT was concentrated to ~8 to ~30 mg/mL for crystallization trials.

## Crystallization Screening and Removal of Excess Detergent

MerT: Using the aforementioned techniques and mobile phase combinations, we were unable to crystallize MerT or $His_6$-3C_MerT. We screened preparations and concentrations of MerT using commercially prepared sparse-matrix screens by hanging-drop vapor diffusion on both 1-2 μL and 200-300 nL scales, as previously described (Newby et al. 2009).

Phase Separation and Detergent Removal: All crystal trials were hampered by extensive phase separation (≥ ~50% of screened conditions) due to the presence of excess detergent (Figure 7). As MerT co-elutes with maltoside headgroup detergent free micelles from gel filtration matrices, and cannot be separated from excess detergent using ion exchange chromatography, we sought other ways to remove detergent after purification. Attempts to absorb detergent onto hydrophobic BioBeads (Bio-Rad) resulted in MerT precipitation. Dialysis using 10-50 kDa molecular weight cut-off membranes consistently resulted in protein loss and dilution. Due to these difficulties, we were conscious to minimize detergent concentration during purification, but to no avail.

MerT and MerA: Crystallization of MerT may be inhibited by the limited solvent accessible surface predicted to lie outside the membrane spanning regions, and thus beyond the detergent micelle, at its cytosolic and perisplasmic/extracellular vestibules. To increase surfaces available for crystal lattice formation, we attempted to co-crystallize MerT with full-length mercuric reductase (MerA) and MerA catalytic core (Core),

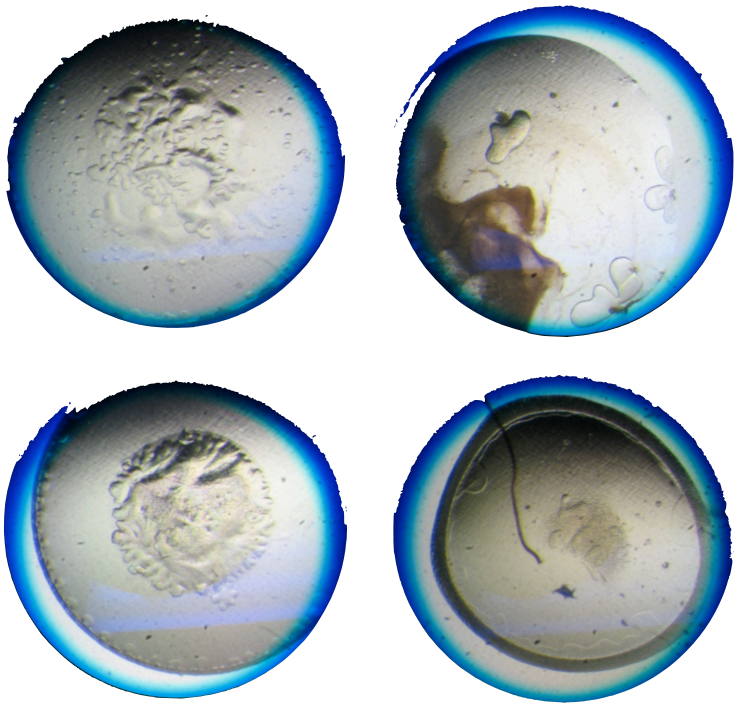

**Figure 7.** Examples of phase separation observed in MerT 2 µL hanging drop crystallization trials. Upon equilibration, the drop separates into aqueous and detergent-rich phases.

prepared as previously described (Ledwidge et al. 2005; Johs et al. 2011). It has been suggested that both proteins interact *in vivo* in the absence of $Hg^{2+}$ (Schue et al. 2007). The addition of MerA or Core did not aid in producing crystals or lessening phase separation.

$Hg^{2+}$ and MerT: We also attempted to exchange MerT into mobile phases free of reducing agent and add two equivalents of $Hg^{2+}$ (to bind to each of MerT's two thiol pairs), based on the spectroscopically-estimated protein concentration, prior to crystallization. Removal of reducing agent resulted in protein aggregation, as assessed by SEC, which was further exasperated upon addition of $HgCl_2$.

## Future Directions

Activity Assays: Previous studies of MerT have relied on purifying and refolding the protein from inclusion bodies (Senthil and Gautam 2010). Here we report a method for expressing MerT that localizes to the plasma membrane, and can be extracted using a variety of detergents. Yet the effectiveness of maintaining MerT's fold and activity has yet to be assayed for protein produced by either means, as no such assay has been designed or attempted. It may be possible to reconstitute purified MerT into lipids and form proteoliposomes that contain a $Hg^{2+}$-sensitive "molecular beacon" (Xu et al. 2011), a DNA strand which adopts a stable stem–loop structure to which a reporter dye acting as a fluorophore is attached to one arm of the stem and a quencher is attached to the other, and spectroscopically measure $Hg^{2+}$ translocation across MerT-loaded versus control liposomes (Scheme 2). This approach is analgous to measurement techniques our group has used to assay aquaporin and glycerol channel activity (Savage and Stroud 2007). It may also be possible to form black lipid membranes (Morales et al. 1993; Kleivdal et al. 1995) that contain MerT. With such a proteolipid bilayer it would be possible load $Hg(SG)_2$ or $HgCys_2$ on one side of the membrane and, on the other side, assay NADPH oxidized upon reduction of $Hg^{2+}$ to $Hg^0$ by full-length MerA or the Core alone. As the orientation of MerT can not be specified or determined or protein concentration accurately measured in any of these reconstitution assays, this approach is not appropriate for determining the kinetics of $Hg^{2+}$ flux across a membrane resulting from the presence of MerT, but would nonetheless suggest MerT activity and therefore structural integrity. We believe determining solubilized MerT is properly folded and functional is critical prior to future attempts to crystallize the protein.

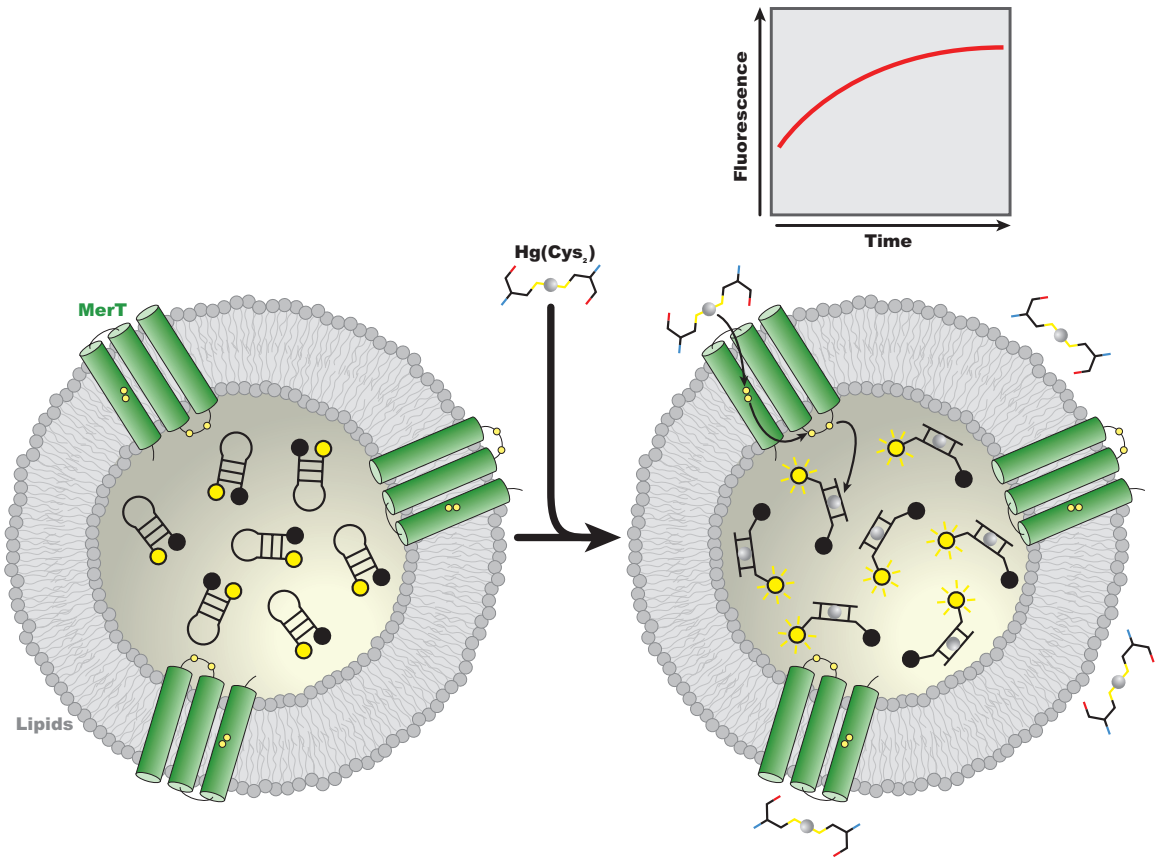


**Scheme 2.** Proposed MerT proteoliposome reconstitution for measurement of $Hg^{2+}$ flux across a lipid bilayer. Liposomes (gray) containing molecular beacons affixed to a quencher (black) and a fluorophore (yellow), and reconstituted MerT (green) are exposed to liganded $Hg^{2+}$, here as $HgCys_2$, to minimize autonomous mercury flux across the membrane (Gutknecht 1981). $Hg^{2+}$ entering the proteoliposome would bind to the molecular beacons and separate the quencher from the fluorophore, resulting in an increase in fluorescence signal.

Purification and Structure Determination: We have described methods for purifying MerT in maltoside detergents and our attempts to crystallize it. The field and technologies available for determination of membrane protein structure are rapidly advancing and, given its ability to be readily expressed, solubilized in a variety of detergents, and remain stable across many mobile phases, we believe MerT is a viable candidate for continued structural investigation. The use of other detergents, lipids, and combinations thereof may aid in overcoming phase separation during crystallization trials, which we feel was the most significant challenge to our studies. Crystal nucleation may be stimulated by the use of antibodies or by conjugating MerT to a small protein (preferably one previously crystallized) to enhance the solvent accessible surface area available to form crystal contacts. A scaffold protein of known structure may also aid in determination of phases by molecular replacement. Phase separation may also be overcome by crystallizing MerT in a lipidic cubic phase.

The 13 kDa MerT is an excellent candidate for structure determination by NMR. Of the thirteen unique 10-15 kDa membrane protein structures that have been determined, X-ray crystallography has been employed in the solution of the NaK channel structure (PDB 2AHY) (Alam and Jiang 2009). NMR has been used for the determination of at least 11 proteins with two to four transmembrane helices (Kang and Li 2011; Nietlispach and Gautier 2011). Solution-based approaches may be critical for the determination of sub-15 kDa membrane proteins due to their inherently limited solvent-accessible surface area available for the formation of crystal contacts in the presence of detergent.

## References


Alam A, Jiang Y (2009) "High-resolution structure of the open NaK channel." *Nat Struct Mol Biol* 16:30-34.

Alexandrov A, Dutta K, Pascal SM (2001) "MBP fusion protein with a viral protease cleavage site: one-step cleavage/purification of insoluble proteins." *Biotechniques* 30:1194-1198.

Aslanidis C, de Jong PJ (1990) "Ligation-independent cloning of PCR products (LIC-PCR)." *Nucleic Acids Res* 18:6069-6074.

Barkay T, Miller SM, Summers AO (2003) "Bacterial mercury resistance from atoms to ecosystems." *FEMS Microbiol Rev* 27:355-384.

Brown NL (1985) "Bacterial resistance to mercury — reductio ad absurdum?" *Trends Biochem Sci* 10:400-403.

Brown NL, Camakaris J, Lee BT, Williams T, Morby AP, Parkhill J, Rouch DA (1991) "Bacterial resistances to mercury and copper." *J Cell Biochem* 46:106-114.

Brown NL, Shih YC, Leang C, Glendinning KJ, Hobman JL, Wilson JR (2002) "Mercury transport and resistance." *Biochem Soc Trans* 30:715-718.

Cheesman BV, Arnold AP, Rabenstein DL (1988) "Nuclear Magnetic-Resonance Studies of the Solution Chemistry of Metal-Complexes .25. Hg(Thiol)3 Complexes and Hg(Ii)-Thiol Ligand-Exchange Kinetics." *J Am Chem Soc* 110:6359-6364.

Foster TJ, Nakahara H, Weiss AA, Silver S (1979) "Transposon A-generated mutations in the mercuric resistance genes of plasmid R100-1." *J Bacteriol* 140:167-181.

Gambill BD, Summers AO (1985) "Versatile mercury-resistant cloning and expression vectors." *Gene* 39:293-297.

Gasteiger E, Hoogland C, Gattiker A, Duvaud S, Wilkins MR, Appel RD, Bairoch A (2005) Protein Identification and Analysis Tools on the ExPASy Server. In: The Proteomics Protocols Handbook(Walker, J. E., ed) Hatfield, UK: Humana Press.

Goldberg M, Pribyl T, Juhnke S, Nies DH (1999) "Energetics and topology of CzcA, a cation/proton antiporter of the resistance-nodulation-cell division protein family." *J Biol Chem* 274:26065-26070.

Gruswitz F, Chaudhary S, Ho JD, Schlessinger A, Pezeshki B, Ho CM, Sali A, Westhoff CM, Stroud RM (2010) "Function of human Rh based on structure of RhCG at 2.1 A." *Proc Natl Acad Sci USA* 107:9638-9643.

Gruswitz F, O'Connell J, 3rd, Stroud RM (2007) "Inhibitory complex of the transmembrane ammonia channel, AmtB, and the cytosolic regulatory protein, GlnK, at 1.96 A." *Proc Natl Acad Sci USA* 104:42-47.

Gutknecht J (1981) "Inorganic mercury (Hg2+) transport through lipid bilayer membranes." *J Membrane Bio* 61:61-66.

Hamlett NV, Landale EC, Davis BH, Summers AO (1992) "Roles of the Tn21 merT, merP, and merC gene products in mercury resistance and mercury binding." *J Bacteriol* 174:6377-6385.

Hays FA, Roe-Zurz Z, Li M, Kelly L, Gruswitz F, Sali A, Stroud RM (2009) "Ratiocinative screen of eukaryotic integral membrane protein expression and solubilization for structure determination." *J Struct Funct Genomics* 10:9-16.

Hobman JL, Brown NL (1996) "Overexpression of MerT, the mercuric ion transport protein of transposon Tn501, and genetic selection of mercury hypersensitivity mutations." *Mol Gen Genet* 250:129-134.

Hobman JL, Brown NL (1997) "Bacterial mercury-resistance genes." *Met Ions Biol Syst* 34:527-568.

Hu J, Qin H, Gao FP, Cross TA (2011) "A systematic assessment of mature MBP in membrane protein production: overexpression, membrane targeting and purification." *Protein Expr Purif* 80:34-40.

Jackson WJ, Summers AO (1982) "Biochemical characterization of HgCl2-inducible polypeptides encoded by the mer operon of plasmid R100." *J Bacteriol* 151:962-970.

Johs A, Harwood IM, Parks JM, Nauss RE, Smith JC, Liang L, Miller SM (2011) "Structural characterization of intramolecular Hg(2+) transfer between flexibly linked domains of mercuric ion reductase." *J Mol Biol* 413:639-656.

Kang C, Li Q (2011) "Solution NMR study of integral membrane proteins." *Curr Opin Chem Biol* 15:560-569.

Khademi S, O'Connell J, 3rd, Remis J, Robles-Colmenares Y, Miercke LJ, Stroud RM (2004) "Mechanism of ammonia transport by Amt/MEP/Rh: structure of AmtB at 1.35 A." *Science (New York, NY* 305:1587-1594.

Kleivdal H, Benz R, Jensen HB (1995) "The Fusobacterium nucleatum major outer-membrane protein (FomA) forms trimeric, water-filled channels in lipid bilayer membranes." *Eur J Biochem* 233:310-316.

Ledwidge R, Patel B, Dong A, Fiedler D, Falkowski M, Zelikova J, Summers AO, Pai EF, Miller SM (2005) "NmerA, the metal binding domain of mercuric ion reductase,

removes Hg2+ from proteins, delivers it to the catalytic core, and protects cells under glutathione-depleted conditions." *Biochemistry* 44:11402-11416.

Lee JK, Khademi S, Harries W, Savage D, Miercke L, Stroud RM (2004) "Water and glycerol permeation through the glycerol channel GlpF and the aquaporin family." *J Synchrotron Radiat* 11:86-88.

Liebert CA, Hall RM, Summers AO (1999) "Transposon Tn21, flagship of the floating genome." *Microbiol Mol Biol Rev* 63:507-522.

Lorber B, Bishop JB, DeLucas LJ (1990) "Purification of octyl beta-D-glucopyranoside and re-estimation of its micellar size." *Biochim Biophys Acta* 1023:254-265.

Lund PA, Brown NL (1987) "Role of the merT and merP gene products of transposon Tn501 in the induction and expression of resistance to mercuric ions." *Gene* 52:207-214.

Miroux B, Walker JE (1996) "Over-production of proteins in Escherichia coli: mutant hosts that allow synthesis of some membrane proteins and globular proteins at high levels." *J Mol Biol* 260:289-298.

Misra TK, Brown NL, Fritzinger DC, Pridmore RD, Barnes WM, Haberstroh L, Silver S (1984) "Mercuric ion-resistance operons of plasmid R100 and transposon Tn501: the beginning of the operon including the regulatory region and the first two structural genes." *Proc Natl Acad Sci USA* 81:5975-5979.

Morales E, de la Torre L, Moy GW, Vacquier VD, Darszon A (1993) "Anion channels in the sea urchin sperm plasma membrane." *Mol Reprod Dev* 36:174-182.

Morby AP, Hobman JL, Brown NL (1995) "The role of cysteine residues in the transport of mercuric ions by the Tn501 MerT and MerP mercury-resistance proteins." *Mol Microbiol* 17:25-35.

Nakahara H, Silver S, Miki T, Rownd RH (1979) "Hypersensitivity to Hg2+ and hyperbinding activity associated with cloned fragments of the mercurial resistance operon of plasmid NR1." *J Bacteriol* 140:161-166.

Newby ZER, O'Connell JD, Gruswitz F, Hays FA, Harries WEC, Harwood IM, Ho JD, Lee JK, Savage DF, Miercke LJW, Stroud RM (2009) "A general protocol for the crystallization of membrane proteins for X-ray structural investigation." *Nat Protocols* 4:619-637.

Newstead S, Ferrandon S, Iwata S (2008) "Rationalizing alpha-helical membrane protein crystallization." *Protein Sci* 17:466-472.

Nietlispach D, Gautier A (2011) "Solution NMR studies of polytopic alpha-helical membrane proteins." *Curr Opin Struct Biol* 21:497-508.

Park SJ, Wireman J, Summers AO (1992) "Genetic analysis of the Tn21 mer operator-promoter." *J Bacteriol* 174:2160-2171.

Raman P, Cherezov V, Caffrey M (2006) "The Membrane Protein Data Bank." *Cell Mol Life Sci* 63:36-51.

Robinson JB, Tuovinen OH (1984) "Mechanisms of microbial resistance and detoxification of mercury and organomercury compounds: physiological, biochemical, and genetic analyses." *Microbiol Rev* 48:95-124.

Roosild TP, Greenwald J, Vega M, Castronovo S, Riek R, Choe S (2005) "NMR structure of Mistic, a membrane-integrating protein for membrane protein expression." *Science (New York, NY* 307:1317-1321.

Rosenberg AH, Lade BN, Chui DS, Lin SW, Dunn JJ, Studier FW (1987) "Vectors for selective expression of cloned DNAs by T7 RNA polymerase." *Gene* 56:125-135.

Ross W, Park SJ, Summers AO (1989) "Genetic analysis of transcriptional activation and repression in the Tn21 mer operon." *J Bacteriol* 171:4009-4018.

Rossy E, Seneque O, Lascoux D, Lemaire D, Crouzy S, Delangle P, Coves J (2004) "Is the cytoplasmic loop of MerT, the mercuric ion transport protein, involved in mercury transfer to the mercuric reductase?" *FEBS Lett* 575:86-90.

Sahlman L, Hagglof EM, Powlowski J (1999) "Roles of the four cysteine residues in the function of the integral inner membrane Hg2+-binding protein, MerC." *Biochem Biophys Res Commun* 255:307-311.

Sahlman L, Wong W, Powlowski J (1997) "A mercuric ion uptake role for the integral inner membrane protein, MerC, involved in bacterial mercuric ion resistance." *J Biol Chem* 272:29518-29526.

Savage DF, Egea PF, Robles-Colmenares Y, O'Connell JD, 3rd, Stroud RM (2003) "Architecture and selectivity in aquaporins: 2.5 Å X-ray structure of aquaporin Z." *PLoS Biol* 1:E72.

Savage DF, Stroud RM (2007) "Structural basis of aquaporin inhibition by mercury." *J Mol Biol* 368:607-617.

Schue M, Glendinning KJ, Hobman JL, Brown NL (2007) "Evidence for direct interactions between the mercuric ion transporter (MerT) and mercuric reductase (MerA) from the Tn501 mer operon." *Biometals* 21:107-116.

Selifonova OV, Barkay T (1994) "Role of Na+ in transport of Hg2+ and induction of the Tn21 mer operon." *Appl Environ Microbiol* 60:3503-3507.

Senthil K, Gautam P (2010) "Expression and single-step purification of mercury transporter (merT) from *Cupriavidus metallidurans* in *E. coli*." *Biotech Lett* 32:1663-1666.

Silver S (2003) "Bacterial silver resistance: molecular biology and uses and misuses of silver compounds." *FEMS Microbiol Rev* 27:341-353.

Silver S, Phung LT (1996) "Bacterial heavy metal resistance: new surprises." *Annu Rev Microbiol* 50:753-789.

Silver S, Phung LT (2005) "A bacterial view of the periodic table: genes and proteins for toxic inorganic ions." *J Ind Microbiol Biotechnol* 32:587-605.

Spencer RH, Rees DC (2002) "The alpha-helix and the organization and gating of channels." *Annu Rev Biophys Biomol Struct* 31:207-233.

Stricks W, Kolthoff IM (1953) "Reactions between mercuric mercury and cysteine and glutathione. Apparent dissociation constants, heats and entropies of formation of various forms of mercuric mercapto-cysteine and -glutathione." *J Am Chem Soc* 75:5673-5681.

Stroud RM, Savage D, Miercke LJ, Lee JK, Khademi S, Harries W (2003) "Selectivity and conductance among the glycerol and water conducting aquaporin family of channels." *FEBS Lett* 555:79-84.

Studier FW (2005) "Protein production by auto-induction in high density shaking cultures." *Protein Expr Purif* 41:207-234.

Studier FW, Rosenberg AH, Dunn JJ, Dubendorff JW (1990) "Use of T7 RNA polymerase to direct expression of cloned genes." *Methods Enzymol* 185:60-89.

Wilson JR, Leang C, Morby AP, Hobman JL, Brown NL (2000) "MerF is a mercury transport protein: different structures but a common mechanism for mercuric ion transporters?" *FEBS Lett* 472:78-82.

Xu H, Zhu X, Ye H, Yu L, Liu X, Chen G (2011) "A simple "molecular beacon"-based fluorescent sensing strategy for sensitive and selective detection of mercury (II)." *Chem Commun (Camb)* 47:12158-12160.

# CHAPTER 2

# Structural Characterization of Intramolecular $Hg^{2+}$ Transfer Between Flexibly-linked Domains of Mercuric Ion Reductase

This chapter is the manuscript for the article of the same title, authored by Alexander Johs, Ian M. Harwood, Jerry M. Parks, Rachel E. Nauss, Jeremy C. Smith, Liyuan Liang, and Susan M. Miller, which was published in 2011 in the *Journal of Molecular Biology*, volume 413, issue 3, pages 639-656.

## Project Background and Author's Contributions

As crystallization of Tn*21* MerT (Chapter 1) was thought to have been inhibited by the limited solvent accessible surface predicted to lie outside the membrane spanning regions, I sought to co-crystallize MerT with mercuric reductase (MerA) catalytic core (Core) (Ledwidge et al. 2005a) and full-length MerA, as to increase the protein surface area available for crystal lattice formation. For each MerT co-crystallization experiment, MerA and Core, separately, would need to be expressed and purified. At that time, Core expression and purification protocols suitable for crystallization experiments had been well established. However, the then-existing MerA purification protocols (Fox and Walsh 1982; Rinderle et al. 1983; Moore and Walsh 1989) resulted in inhomogeneous

preparations of the full-length protein (Schottel 1978; Fox and Walsh 1982; Distefano et al. 1989). As these MerA mixtures were unsuitable for crystallization experiments, and as the Miller group did not have a Tn*21* MerA expression construct, I cloned *Tn21 mera* from plasmid pDG106, constructed the pMAL:H-MBP-3C_MerA expression vector described in this chapter, and developed the accompanying expression and purification protocols. I produced and used MerA for the aforementioned co-crystallization experiments, as well as for subsequent crystallization experiments of MerA alone. For these experiments, I screened preparations and concentrations of MerA using commercially prepared sparse-matrix screens by hanging-drop vapor diffusion on both 1-2 μL and 200-300 nL scales as previously described (Newby et al. 2009), but was unable to produce crystals of full-length MerA. I prepared MerA for all other experiments described in this chapter.

While developing the MerA purification protocol, Dr. Miller referenced Schottel's early SEC studies of MerA which suggested the full-length protein was a trimer (Schottel 1978). I thus examined and analyzed the hydrodynamic properties of MerA using the analytical SEC and MALS as described in this chapter. To study the hydrodynamic properties of the NmerA-$Hg^{2+}$-Core handoff intermediate using these approaches, I decided to design and construct the mutMerA mutant described in this chapter. For these and all other experiments described below, Rachel Nauss liganded the protein with $Hg^{2+}$, and I subsequently purified the resultant Hg-mutMerA.

As we were unable to crystallize MerA we decided to direct our research focus on the study of functionally relevant conformations of full-length MerA by small-angle X-ray scattering (SAXS) and molecular dynamics studies in collaboration with Dr. Alex Johs and Dr. Jerry Parks of the Mercury Science Focus Area (SFA) at Oak Ridge National Laboratory (ORNL). Dr. Liyuan Liang is the research manager for the ORNL Mercury SFA; the research on biomolecular mechanisms of mercury transformations is led by Dr. Jeremy Smith. Dr. Miller is a funded external collaborator of this project. I collected SAXS data for all protein preparations described in this work and was responsible for the initial data quality analysis and post-data collection processing.

Counter to my analytical SEC results, Dr. Johs and I observed that Hg-mutMerA tended to aggregate upon exposure to the X-ray beam (Dr. Johs had had previous difficulties studying other *mer* proteins in the presence of $Hg^{2+}$). Thus, I suggested attempting to crosslink NmerA to Core to simulate the NmerA-$Hg^{2+}$-Core handoff intermediate in the absence of mercury. Rachel Nauss cross-linked the two domains, and I subsequently purified the resultant SS-mutMerA, and collected SAXS data and performed the initial data analysis. Dr. Miller requested additional comparison of Hg-mutMerA and SS-mutMerA to confirm the former was a suitable analogue for the latter, and I therefore pursued fluorescence and analytical ultracentrifugation experiments. The results of my experiments were inconclusive. Simultaneously, Dr. Johs was successful in using small-angle neutron scattering (SANS) to directly compare both the molecular conformations of both mutMerA preparations and show that SS-mutMerA represented the global structure of MerA of $Hg^{2+}$ handoff from NmerA to Core.

For all MerA preparations, Dr. Johs was responsible for downstream SAXS/SANS analysis, and modeling. Dr. Parks assisted with MD-based conformational sampling and with modeling of NmerA docking to Core. While Drs. Johs and Parks and I wrote for our respective corresponding methods, results, discussions and figures of this chapter's publication, I additionally drafted the paper's introduction. Dr. Miller edited all sections of the manuscript. Over the course the experiments and manuscript preparation, Drs. Miller, Johs, Parks, Liang, Rachel Nauss, and I engaged in group conversations, and Dr. Johs and I had frequent independent discussions about the project's direction and experimental results. Dr. Johs and I were deemed to have contributed equally to this work and are listed as co-first authors.

Following this work and prior to departing UCSF, I assisted Rachel Nauss in the production of separate large-scale preparations of a MerA to determine the dynamic motions of Core and the flexibly linked NmerA domains experimentally by neutron spin-echo spectroscopy at ORNL. These MerA preparations have been used for data collection by this chapter's and additional authors, and a manuscript is currently in preparation.

—Ian Harwood, 2012

I, Dr. Alexander Johs, certify to the best of my knowledge that the above background and description of the chapter authors' contributions are accurate.

—Dr. Alexander Johs, 2012

[Reprinted from a communication to Dr. Miller on August 2, 2012]

# Structural characterization of intramolecular $Hg^{2+}$ transfer between flexibly-linked domains of mercuric ion reductase

A. Johs[1*], I. M. Harwood[2,3*], J. M. Parks[4], R. Nauss[3], J.C. Smith[4], L. Liang[1], S. M. Miller[2,3†]

[1]Environmental Sciences Division, Oak Ridge National Laboratory, Oak Ridge, TN 37831, USA

[2]Graduate Group in Biophysics, University of California San Francisco, 600 16th Street, San Francisco, California 94158-2517, USA

[3]Department of Pharmaceutical Chemistry, University of California San Francisco, 600 16th Street, San Francisco, California 94158-2517, USA

[4]UT/ORNL Center for Molecular Biophysics, Oak Ridge National Laboratory, 1 Bethel Valley Road, Oak Ridge, Tennessee 37831-6309, USA

* These authors contributed equally to this work.

† Corresponding author: e-mail: smiller@cgl.ucsf.edu, phone: +1 (415) 476-7155, fax: +1 (415) 502-8298

## Abstract

The enzyme mercuric ion reductase, MerA, is the central component of bacterial mercury resistance encoded by the *mer* operon. Many MerA proteins possess metallochaperone-like N-terminal domains, NmerA, that can transfer $Hg^{2+}$ to the catalytic core domain (Core) for reduction to $Hg^0$. These domains are tethered to the homodimeric Core by ~30-residue linkers that are susceptible to proteolysis, the latter of which has prevented characterization of the interactions of NmerA and Core in the full-length protein. Here, we report purification of homogeneous full-length MerA from the Tn*21* *mer* operon using a fusion protein construct and combine small-angle X-ray and neutron scattering with molecular dynamics simulation to characterize the structures of full-length wild-type and mutant MerA proteins that mimic the system before and during handoff of $Hg^{2+}$ from NmerA to the Core. The radii of gyration, distance distribution functions and Kratky plots derived from the small-angle X-ray scattering data are consistent with full-length MerA adopting elongated conformations as a result of flexibility in the linkers to the NmerA domains. The scattering profiles are best reproduced using an ensemble of linker conformations. This flexible attachment of NmerA may facilitate fast and efficient removal of $Hg^{2+}$ from diverse protein substrates. Using a specific mutant of MerA allowed formation of a metal-mediated interaction between NmerA and Core, and determination of the position and relative orientation of NmerA to the Core during $Hg^{2+}$ handoff.

## Keywords

mercury resistance, metal trafficking, SAXS, SANS, intramolecular metal ion transfer

## Abbreviations used:

MerA: full-length wild type homodimeric mercuric ion reductase with NmerA domains tethered to the catalytic core domains

Core: subcloned construct of just the catalytic core of MerA

mutMerA: full-length MerA with the cysteines at positions 14, 135, 140 and 561 mutated to alanines (C14A, C135A, C140A, C561A), also called CAAAAC-MerA

Hg-mutMerA: mutMerA with $Hg^{2+}$ complexed between C11 of NmerA of one monomer and C562' on the Core of the other monomer in the homodimer

SS-mutMerA: mutMerA with a disulfide link between C11 of NmerA of one monomer and C562' on the Core of the other monomer in the homodimer

SEC: size exclusion chromatography

MALS: multi-angle light scattering

SAXS: small-angle X-ray scattering

SANS: small-angle neutron scattering

NMR: nuclear magnetic resonance

MBP: maltose binding protein

DTT: dithiothreitol

GSH: glutathione

DTNB: 5,5'-dithio-*bis*-(2-nitrobenzoic acid)

$Hg(TNB)_2$: Hg-(2-nitro-5-thiobenzoate)$_2$

TNB: 2-nitro-5-thiobenzoate

FAD: flavin adenine dinucleotide

NADPH: reduced nicotinamide adenine dinucleotide phosphate

## Introduction

Accumulation of elevated levels of essential metal ions (e.g., $Cu^{+}/Cu^{2+}$, $Zn^{2+}$) or low levels of nonessential metal ions (e.g., $Hg^{2+}$, $Cd^{2+}$) can lead to nonspecific binding and catalytic reactions that result in cellular toxicity and/or cell death (Silver and Phung 1996; Barkay et al. 2003; Finney and O'Halloran 2003). To avoid these effects, organisms have evolved individual trafficking pathways to chaperone (Finney and O'Halloran 2003) and/or detoxify (Silver and Phung 1996) specific metal ions. Although overall mechanisms differ, all pathways control the movement of their metal ions by using a set of inter- and/or intramolecular transfers between high-affinity binding sites on two or more pathway proteins (Silver and Phung 1996; Barkay et al. 2003; Finney and O'Halloran 2003; Banci et al. 2010a; Robinson and Winge 2010). Thus, the efficacy of these pathways depends on the specificity, as well as the kinetics, thermodynamics and dynamics of the individual transfers. As these properties derive from the structural features of the interacting partners, characterizing the individual and interacting structures is critical for understanding the mechanisms of, and factors controlling, the metal ion transfers. Among the many structures that have been elucidated for individual proteins and cloned domains from soft, thiophilic metal ion pathways (Schiering et al. 1991; Steele and Opella 1997; Rosenzweig and O'Halloran 2000; Huffman and O'Halloran 2001; Lamb et al. 2001; Abajian et al. 2004; Ledwidge et al. 2005a; Loftin et al. 2005; Lafrance-Vanasse et al. 2009; Su et al. 2009; Ledwidge et al. 2010), one of the most common structural folds is a small (~70 residue) βαββαβ ferredoxin-type fold with a conserved XMXCXXC metal-binding motif that appears both in individual metallochaperone proteins (Steele and Opella 1997; Robinson and Winge 2010) and in

domains tethered to other proteins (Lamb et al. 2001; Arnesano et al. 2002; Banci et al. 2002; Barkay et al. 2003). Both inter- and intramolecular metal ion transfers have been demonstrated to occur between several of these proteins/domains and their cognate partners bearing either the same or a very different structure (Cobine et al. 2002; Ledwidge et al. 2005b; Banci et al. 2006; Gonzalez-Guerrero and Arguello 2008; Hong et al. 2010). To date, however, only a few metal-mediated complexes of interacting proteins have proven to be sufficiently stable to allow detailed structural characterization, and all have involved *intermolecular* interactions between two proteins both having this babbab fold (Banci et al. 2006; Banci et al. 2009a; Banci et al. 2009b). Here, we characterize the structural interactions involved in the *intramolecular* transfer of $Hg^{2+}$ between the tethered metallochaperone-like NmerA domain and the C-terminal vicinal cysteine pair in the large catalytic Core of a mercuric ion reductase enzyme (MerA).

MerA is the central protein of mercury resistance encoded by *mer* loci, which are widely distributed among aerobic bacteria (Barkay et al. 2003; Barkay et al. 2010). Although the exact complement of genes/proteins varies in these loci, their expression is always controlled by a $Hg^{2+}$-sensing transcriptional regulator located in the cytosol, and all utilize an integral membrane protein (e.g., MerT) to facilitate uptake of $Hg^{2+}$ into the cytosol where MerA acquires and reduces it to elemental mercury ($Hg^0$) (Barkay et al. 2003). In some pathways, an organomercurial lyase (MerB) is present and confers resistance to organomercurials ($[RHg(II)]^+$) by cleaving Hg-C bonds to form a hydrocarbon product and $Hg^{2+}$ that is then passed to MerA for reduction (Barkay et al. 2003). $Hg^{2+}$ and $[RHg(II)]^+$ have exceptionally high affinities for thiols [$K_{form}$ for

$Hg(SR)_2$ ~$10^{35}$ - $10^{40}$ $M^{-2}$ (Stricks and Kolthoff 1953)], but can also exchange rapidly between thiols (Cheesman et al. 1988). As a result, *mer* pathway proteins must possess features that enable them not only to acquire any $Hg^{2+}$ or $[RHg(II)]^{+}$ associated with cellular protein thiols before the *mer* proteins are synthesized, but also prevent dispersion of the imported and MerB-generated $Hg^{2+}$ prior to reduction.

Sequences of isolated MerA proteins share a conserved catalytic Core structure, but show variation in their N-termini with zero (Sedlmeier and Altenbuchner 1992), one (Brown et al. 1983; Summers 1986) or two (Wang et al. 1989) tandem repeats of a βαββαβ metallochaperone-like NmerA domain (Scheme 1) (Barkay et al. 2003). Recent phylogenetic analysis suggests this variation may be associated with differences in the bacterial cellular physiology, especially the type and level of small-molecule thiol buffer used by the organism (Barkay et al. 2010), and may also be associated with structural variations in other *mer* pathway proteins (Hong et al. 2010). Sequences with a single NmerA domain represent more than half those identified in GenBank (Barkay et al. 2010) and include the most extensively characterized MerA proteins from the *mer* loci carried by transposons Tn*21* and Tn*501* (Fox and Walsh 1983; Distefano et al. 1989; Miller et al. 1989; Moore and Walsh 1989; Distefano et al. 1990; Engst and Miller 1999; Ledwidge et al. 2005a; Ledwidge et al. 2005b; Hong et al. 2010; Ledwidge et al. 2010), which are the focus of the study here. These operons were originally isolated on plasmid NR1 from *Shigella flexneri* (Nakaya et al. 1960), and plasmid pVS1 from *Pseudomonas aeruginosa* PAT (Stanisich 1974; Stanisich et al. 1977), respectively.

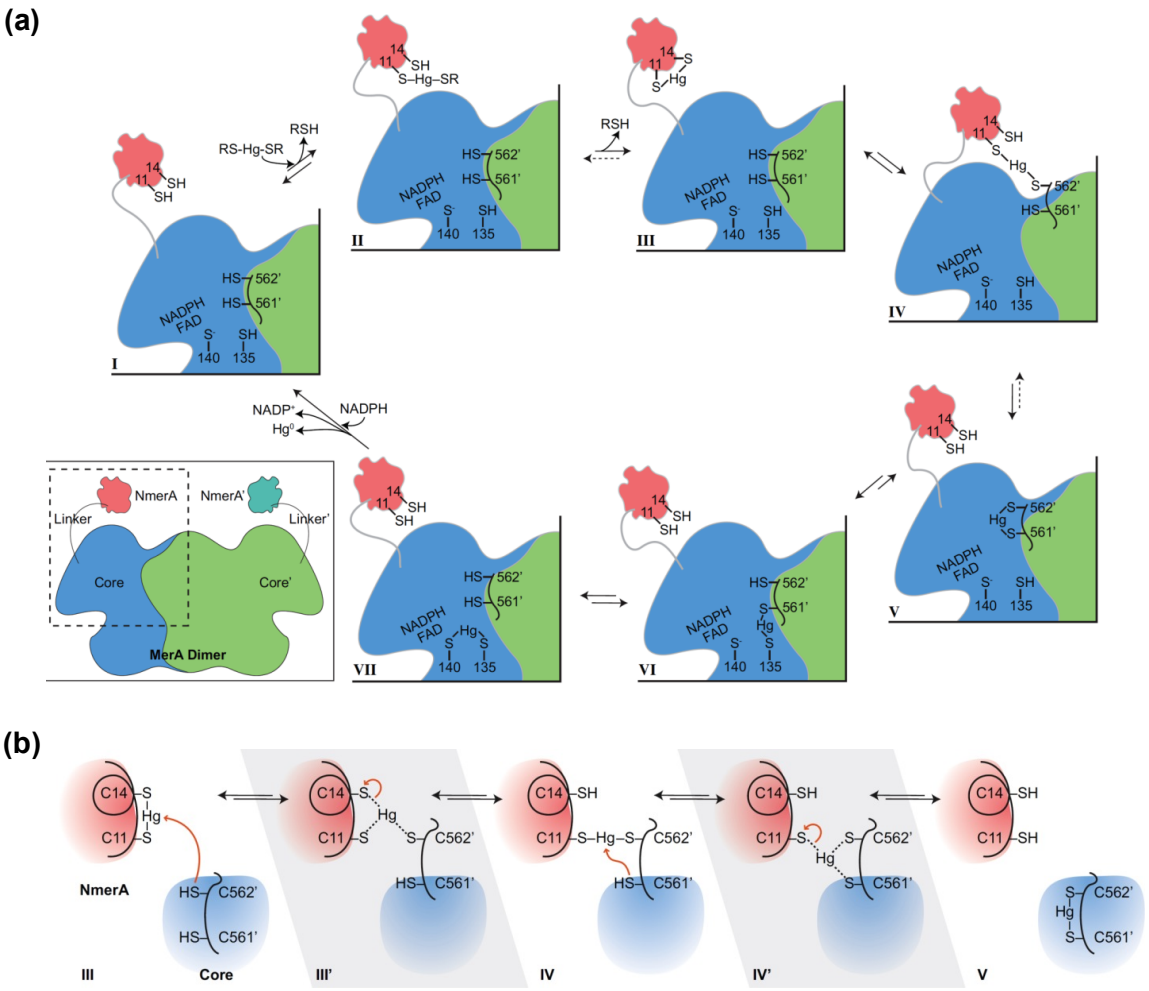


**Scheme 1** (a) Pathway for $Hg^{2+}$-ligand exchange and reduction in MerA. Cysteine residues of NmerA (red), the active site of one monomer (blue), and the C-terminus of the complementing monomer (green) involved in $Hg^{2+}$ exchange and reduction to $Hg^0$ at one of the MerA dimer active sites are shown. (b) Detailed mechanism for $Hg^{2+}$-ligand exchange between NmerA (red) and MerA catalytic core (blue). The transient $[Hg(SR)_3]^-$ intermediate steps are grayed.

As illustrated in Scheme 1, the MerA catalytic Core is an obligate homodimer bearing homology with members of the pyridine nucleotide disulfide oxidoreductase family, with two active sites symmetrically positioned at the interface of the two ~50 kDa monomers (Distefano et al. 1990; Schiering et al. 1991; Ledwidge et al. 2005a). The vicinal C-terminal thiols in the catalytic core, C561' and C562', are partially buried, but receive $Hg^{2+}$ from $Hg(SR)_2$ substrates (Moore and Walsh 1989; Engst and Miller 1999) and deliver it to the solvent-inaccessible active-site thiols, C135 and C140 (Engst and Miller 1999), on the complementary monomer for reduction (Miller et al. 1989; Distefano et al. 1990) (Scheme 1). The N-terminal metallochaperone-like domain, NmerA is connected to the MerA catalytic core (Core), by a ~30 amino acid linker of unknown structure. Previous attempts to produce pure, intact MerA have been plagued by proteolytic cleavage in this linker region, which has limited structural and functional characterization of the full-length protein. However, *in vitro* studies using separately expressed constructs of the NmerA domain and the Core showed that the Core can acquire $Hg^{2+}$ from the XMXCXXC motif in NmerA (Ledwidge et al. 2005a) and further showed that NmerA provides a significant kinetic advantage in mercury reduction when $Hg^{2+}$ is bound to cellular proteins such as thioredoxin (Ledwidge et al. 2005a) or other *mer* proteins including the organomercurial lyase, MerB (Ledwidge et al. 2005a; Hong et al. 2010). In addition, *in vivo* studies comparing the effect of co-expressing the NmerA domain with Core versus Core alone in cells lacking their normal cellular thiol redox buffer glutathione showed that the presence of NmerA significantly enhanced cell survival (Ledwidge et al. 2005a). Taken together, these studies strongly suggest that NmerA plays a key role in mediating $Hg^{2+}$ transfers from other proteins to the Core.

Structural features of NmerA are likely to enhance its ability to form a transient $Hg^{2+}$ handoff complex and specifically orchestrate the release of $Hg^{2+}$ from the NmerA pair of cysteines (C11 and C14) to the vicinal C-terminal thiols of the Core (C561' and C562') (Scheme 1b). However, there are no atomic-resolution structural details of the interaction of NmerA with Core prior to $Hg^{2+}$ binding or during $Hg^{2+}$ handoff from NmerA to the Core. Attempts to crystallize full-length MerA have resulted in crystals unsuitable for structure determination. Secondary structure predictions and the tendency of full-length MerA to be readily proteolyzed in the linker suggest that this region is unstructured, which may also explain the inability of full-length MerA to form well-diffracting crystals.

Flexibly linked domains have been increasingly recognized to play important functional roles in cellular processes, as flexibility allows such domains to sample large volumes to interact with distal targets while maintaining proximity to important functional domains. Examples of proteins with flexibly-linked domains include DNA repair proteins (Hammel et al. 2010), kinases (Bernado et al. 2008), the cellulosome (Hammel et al. 2005) and replication protein A (Pretto et al. 2010). As noted above, flexibility of the linker connecting NmerA and the MerA Core may be essential for allowing NmerA the freedom to acquire $Hg^{2+}$ from other proteins, including the upstream *mer* proteins MerT or MerB, while keeping it localized to the MerA Core for trafficking efficiency.

Characterization of the structure and dynamics of domains with flexible linkers is a challenge. High-field nuclear magnetic resonance (NMR) has been used to study flexible systems at atomic resolution where the use of residual dipolar couplings and paramagnetic relaxation enhancement have become important tools for characterizing conformational properties of partially folded and intrinsically disordered proteins (Palmer 1997; Chaudhury and Gray 2008; Clore and Iwahara 2009; Jensen et al. 2009). Alternatively, recent advances coupling small-angle X-ray scattering (SAXS) and molecular dynamics (MD) simulations have been applied successfully to characterize macromolecules consisting of domains with existing crystallographic or NMR structures that are joined by flexible linkers (Bernado et al. 2007; Pelikan et al. 2009; Chen et al. 2010; Guo et al. 2010; Hammel et al. 2010; Jamros et al. 2010; Rozycki et al. 2011).

To our knowledge, no studies have investigated the structural or kinetic properties of intramolecular metal transfer between tethered domains of a single protein. Here this is made possible by a novel purification strategy that allows preparation of homogeneous full-length MerA for the first time. Preliminary characterization of the size and oligomerization state of MerA is performed using size-exclusion chromatography and multi-angle light scattering. Constructs of MerA are made that mimic the system before $Hg^{2+}$ acquisition and during transfer of $Hg^{2+}$ from NmerA to the catalytic core. The structure and conformations of these MerA constructs in solution are characterized using SAXS and MD-based conformational sampling. The results delineate the conformational distribution of MerA prior to $Hg^{2+}$ acquisition and define the orientation of NmerA with respect to the catalytic core of MerA during $Hg^{2+}$ transfer.

## Results and Discussion

### Purification of homogeneous full length Tn*21* MerA as a Maltose-Binding Protein (MBP) fusion

Previous MerA purification protocols, which rely on affinity resins that bind the pyridine nucleotide-binding site on the MerA catalytic core (Core) (Fox and Walsh 1982; Rinderle et al. 1983; Moore and Walsh 1989) and do not distinguish between protein with and without the NmerA domains, led to the observation that full-length MerA is susceptible to *in vivo* proteolysis in the linker that tethers NmerA to Core. Analysis of protein from these preparations on SDS-PAGE gels shows variable ratios of full-length and core monomers that may be present as a variable mixture of homodimers of full-length MerA, homodimers of Core, and heterodimers with one of each (Schottel 1978; Fox and Walsh 1982; Distefano et al. 1989). Rather than attempting to separate a potentially low and variable amount of full-length homodimers from these preparations for the present studies, we fused the full-length *merA* gene from the Tn*21 mer* operon[1] to the 3'-end of the sequence for a 3C-protease-cleavable, dual $His_6$-maltose-binding-protein (MBP) affinity tag to focus the purification on protein retaining the NmerA domain (Figure S1a). The first purification step utilizes an amylose resin column to select for proteins retaining MBP, which should eliminate any proteolyzed homodimers of Core. SDS-PAGE analysis of the maltose elution fraction shows a band for full-length MerA

[1] Although the Tn*501* MerA has been more extensively studied, the Tn*21* protein is ~90% identical (see Figure S3) and was used here as it was required in conjunction with other ongoing studies.

but no band for Core (Figure S1b). After maltose elution, the MBP tag was cleaved specifically from MerA with 3C protease, and size-exclusion chromatography (SEC) easily separated the desired full-length MerA homodimers (119 kDa dimer) from uncleaved MerA dimers retaining the MBP tags (210 kDa dimer), 3C protease (65 kDa), and the $His_6$-MBP tag as shown by SDS-PAGE analysis (Figure S1b).

Although the amylose resin would also be expected to capture MerA heterodimers of full-length $His_6$-MBP-MerA and Core monomers, SDS-PAGE analysis of the amylose elution showed only the desired band for the $His_6$-MBP-MerA monomers but no bands either for Core monomers or for $His_6$-MBP-NmerA that would result from proteolytic cleavage in the linker (Figure S1b). In addition, SDS-PAGE (Figure S1b) and anti-MerA Core western blot analysis of the flow-through from the amylose column showed no evidence of over-expressed Core monomers. Thus, it appears that the $His_6$-MBP tag protects MerA from cytosolic proteolysis of the linker, possibly by steric occlusion.

Quantification of MerA thiols (Riddles et al. 1979) showed an average of ≥ 5.8 of the expected 6 thiols per MerA monomer. $K_{MHg}$, $k_{cat}$, and $k_{cat}/K_{MHg}$ for reduction of $Hg^{2+}$ using mercuric bis-glutathione [$Hg(SG)_2$] as substrate are comparable to values previously reported for Tn*501* MerA (Table S1) (Ledwidge et al. 2005a). Thiol titrations provide additional confirmation that Core resulting from proteolytic degradation of full-length MerA is not a contaminant since the lower total of only four available thiols (C237, C409, C561, and C562) in Core would decrease the average total thiol count to much less than six. Quantification of thiols in the CAAAAC-MerA mutant (mutMerA) described

later showed an average ≥ 3.9 of the expected 4 thiols per monomer. To our knowledge, this is the first reported strategy for purification of full-length MerA dimers without Core contamination.

## MerA occupies a hydrodynamic volume larger than expected for a compact dimer

SEC elution profiles of compact globular proteins, such as the Core, can be used to estimate the molecular mass of a protein (Grubisic et al. 1967). However, since the hydrodynamic radius of a protein also influences its elution profile, conformational states of a protein that differ significantly in shape may elute at different times. Such peak shifts arising from non-globularity can obfuscate mass calculations based only on molecular standards but may give insight into structural differences.

Although structural and biochemical studies have firmly established that the Core is a homodimer (Distefano et al. 1990; Schiering et al. 1991; Ledwidge et al. 2005a), early SEC studies suggested full-length MerA was a trimer (Schottel 1978). To obtain a qualitative assessment of the relative size of full-length MerA versus Core homodimers, we examined their behavior using analytical SEC (Figure 1). When compared with molecular mass standards (Figs. 1 and S2), the Tn*501* MerA catalytic core dimer[2] has an apparent mass on SEC of ~80 kDa (Table 1) even though the 48.5 kDa mass of the protein monomers was confirmed by electrospray mass spectrometry. Strikingly however, full-length Tn*21* MerA has an apparent mass on SEC of ~165 kDa, about 40% greater than the calculated dimeric mass of 119 kDa. Thus the presence of the two NmerA and linker regions (one per monomer), which accounts for only 19 kDa per dimer, significantly increases the MerA apparent mass when compared with the apparent mass

[2] Tn*501* Core was used in these studies as it was readily on hand from our previous work (Ledwidge et al. 2005a; Ledwidge et al. 2005b) and is 90% identical in sequence to the Tn*21* MerA catalytic core (Figure S3).

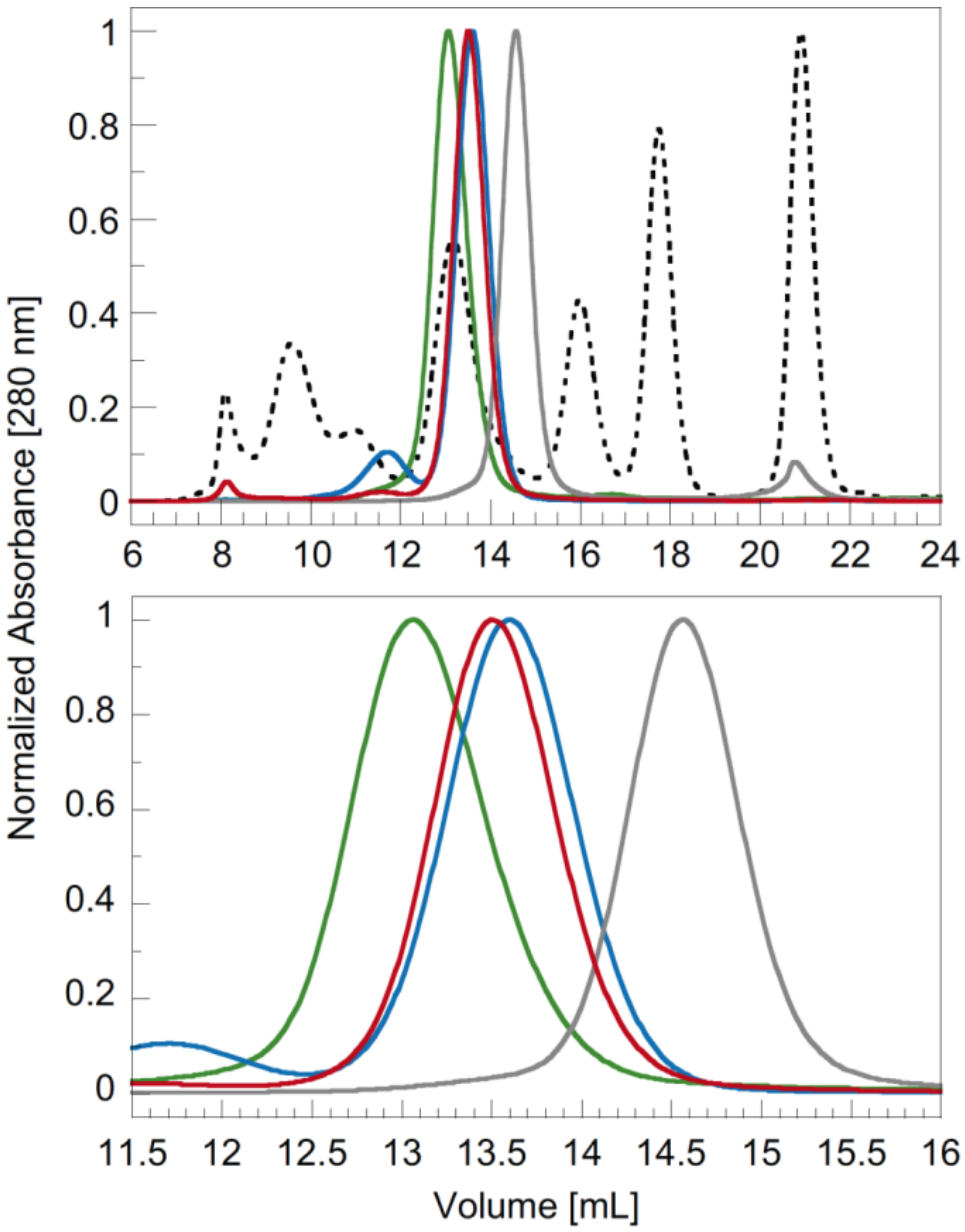


**Figure 1.** Analytical size-exclusion chromatography (SEC) comparisons of apparent molecular size. Elution profiles of purified MerA (green), Hg-mutMerA (red), SS-mutMerA (blue), and Core (gray) separated on a Superdex 200 10/300 GL. Peaks of well-separated gel filtration standard profiles (dotted line) correspond to bovine γ-globulin (13.1 mL; 158 kDa), chicken ovalbumin (15.9 mL; 44 kDa), equine myoglobin (17.7 mL; 17 kDa), and vitamin B12 (20.9 mL; 1.35 kDa).

**Table 1.** Experimentally Determined Parameters.

| | *Parameters* | *MerA* | *[a]MerA +2 $Hg^{2+}$* | *[b]MerA +4 $Hg^{2+}$* | *mutMerA* | *SS-mutMerA* | *Hg-mutMerA* | *Core* |
|---|---|---|---|---|---|---|---|---|
| *Sequence* | $MM_{calculated}$ [kDa][c] | 119.5 | 119.9 | 120.3 | 119.3 | 119.3 | 119.7 | 99.9 |
| *SEC* | $MM_{apparent}$ [kDa][d] | 165 | 168 | 167 | 164 | 127 | 133 | 80 |
| *MALS* | $MM_{calculated}$ [kDa] | 118.8 ± 0.5 | - | 115.1 ± 0.4 | 118.1 ± 0.3 | 118.1 ± 0.2 | 119.0 ± 0.3 | 97.9 ± 0.2 |
| *SAXS* | $R_G$ [Å][e] | - | - | - | 39.1 ± 2.1 | 36.4 ± 0.2 | - | 31.6 ± 0.1 |
| | $rsR_G$ [Å][f] | - | - | - | 39.8 | 36.1 | - | 31.6 |
| | $D_{max}$ [Å][f] | - | - | - | 135 | 120 | - | 98 |
| | $MM_{I(0)}$[g] [kDa] | - | - | - | 120 | 117 | - | 102 |
| | $V$ [Å$^3$][h] | - | - | - | $2.00 \cdot 10^5$ | $1.98 \cdot 10^5$ | - | $1.54 \cdot 10^5$ |
| *SANS* | $R_G$ [Å][e] | - | - | - | - | 36.5 ± 0.4 | 36.5 ± 0.3 | - |

[a] Full-length MerA titrated with 2 equivalents $Hg^{2+}$ per dimer.

[b] Full-length MerA titrated with 4 equivalents $Hg^{2+}$ per dimer.

[c] Sequence molecular masses were calculated using ProtParam (Wilkins et al. 1999) and include the mass of the two FAD cofactors (1.6 kDa each) per MerA dimer.

[d] SEC masses based on elution of BioRad molecular mass standards (see supplemental Figure S2).

[e] $R_G$ values obtained using the Guinier approximation.

[f] The real space $rsR_G$ and $D_{max}$ values were obtained from the distance distribution functions *P(r)*.

[g] Molecular weights estimated from zero angle intensity *I(0)*.

[h] Excluded particle volumes estimated using the Porod invariant.

of the Core alone under our SEC conditions.

The above observation is consistent with MerA existing as a trimer, but might instead arise from a change in the hydrodynamic radius of the full-length dimer versus the Core dimer. To differentiate between these two possibilities, multi-angle light scattering (MALS) was used to determine protein mass. The masses of both full-length MerA and the Core determined by MALS were those calculated for their respective dimers (Table 1). Thus, we conclude that full-length MerA is dimeric and occupies a larger hydrodynamic volume than expected for a compact (spherical) globular protein of similar mass.

## Binding of $Hg^{2+}$ to MerA does not alter its hydrodynamic volume

The large hydrodynamic radius of the full-length protein suggests that the NmerA domains are extended away from the catalytic core, consistent with their role in scavenging $Hg^{2+}$ from other cellular proteins. However, once they acquire $Hg^{2+}$, they must move very near the Core for transfer of $Hg^{2+}$ to the C-terminal pair of cysteines on each monomer. In this state, the hydrodynamic radius might be expected to be smaller. In an initial assessment, we again compared the SEC elution profiles of unbound MerA and MerA bound to two or four equivalents of $Hg^{2+}$ (one or two equivalents of $Hg^{2+}$ per MerA monomer). When MerA is separated from dithiothreitol (DTT) under aerobic conditions, the inner active site cysteines (C135 and C140) that bind $Hg^{2+}$ during reduction become oxidized (Fox and Walsh 1982; Fox and Walsh 1983; Miller et al. 1989) but both the NmerA pair of cysteines (C11 and C14) and the C-terminal pair of cysteines (C561 and C562) on each monomer remain reduced and available to bind $Hg^{2+}$, Scheme 1 (Miller et al. 1989). Titration of the protein with two equivalents of $Hg(TNB)_2$ per MerA monomer resulted in complete release of the TNB ligands indicating all four available pairs of cysteines in the MerA dimer can bind $Hg^{2+}$ as expected (Ledwidge et al. 2005a). SEC analysis of this complex showed no detectable difference in its elution profile when compared to MerA without bound $Hg^{2+}$, and MALS confirmed that binding of two $Hg^{2+}$ per monomer did not alter the oligomerization state of the protein (Table 1). This suggests that binding of $Hg^{2+}$ to the NmerA domains does not lead to significant compaction of the structure. However, the presence of $Hg^{2+}$ bound to both the NmerA and C-terminal binding sites at the same time prevents $Hg^{2+}$ transfer between the two sites and may also inhibit interaction between the NmerA domain and Core.

While our previous studies of $Hg^{2+}$ transfer between the sites in separately expressed NmerA and Core indicated very little accumulation of a complex between the separate proteins (Ledwidge et al. 2005b), stable handoff complexes between $Cu^{+}$ trafficking proteins have been observed by both NMR and X-ray crystallography (Rosenzweig and O'Halloran 2000; Arnesano et al. 2001; Banci et al. 2006; Banci et al. 2009a). Thus, we examined the effect of adding a single equivalent of $Hg(TNB)_2$ per MerA monomer (2 per dimer) with the goal of determining whether the formation of a stable NmerA-$Hg^{2+}$-Core handoff complex (IV in Scheme 1a) leads to a smaller hydrodynamic radius. Titration of full length MerA with one equivalent of $Hg(TNB)_2$ per monomer resulted in release of the expected amount of TNB. However, again there was no change in the SEC elution profile of the complex compared with unbound MerA (Table 1). The absence of a peak shift in the SEC profile suggests that the NmerA-$Hg^{2+}$-Core handoff complex occurs only transiently as $Hg^{2+}$ is passed between the dithiol chelating pairs in NmerA and the Core C-terminus (Scheme 1). However, one additional caveat in this experiment is the possibility that both equivalents of $Hg^{2+}$ added per dimer could end up bound to one set of interacting NmerA and C-terminal cysteines while the other set remains unbound. Since neither set could form the handoff complex in such a dimer, the hydrodynamic radius would remain the same as in the unbound and fully bound dimers. Thus, to eliminate the ambiguities and visualize the interaction between NmerA and the Core during handoff, we designed a mutant to stabilize the proposed transient NmerA-$Hg^{2+}$-Core dithiol handoff intermediate (IV in Scheme 1).

## Generation and SEC characterization of the $Hg^{2+}$ handoff intermediate complex

A working model for $Hg^{2+}$ transfer is given in Scheme 1a and b. In simple $Hg(SR)_2$ complexes, exchange of thiol ligands occurs by an association/dissociation mechanism with formation of transient $[Hg(SR)_3]^-$ intermediates (Cheesman et al. 1988). Thus, in Scheme 1 complete transfer from the NmerA C11/C14 pair to the C-terminal C561'/C562' pair requires two successive ligand exchange reactions with formation of a short-lived two-coordinate handoff intermediate between steps. The $Hg^{2+}$ ligands in the handoff intermediate will be the C-terminal cysteine that attacks the NmerA dithiol complex in the first step and the last NmerA cysteine to release in the overall transfer. In crystal structures of the Core, C562 on the mobile C-terminus is more solvent accessible than C561 (Schiering et al. 1991; Ledwidge et al. 2005a), suggesting C562 will initiate attack on the NmerA complex. Recent studies of Tn*501* NmerA showed the p$K_a$ of C14 (~6.5) to be lower than that of C11 (~9), suggesting C11 will be the latter of the two NmerA thiols to release $Hg^{2+}$ during exchange (Ledwidge et al. 2010). This is also consistent with NMR studies of the $Cu^+$ handoff complex between Atx1 and Ccc2a, two homologs of NmerA, which showed that the cysteines on both proteins that are homologous with C11 on NmerA are the first and last participants in the two successive Cu(trithiol) complexes formed during $Cu^+$ transfer (Banci et al. 2006). Based on the above arguments, we generated a MerA mutant (mutMerA, Figure 2a) retaining only C11 and C562 to selectively stabilize the two-coordinate $Hg^{2+}$-handoff complex. As expected, when titrated with one equivalent of $Hg(TNB)_2$ per monomer, full release of two equivalents of TNB indicates mutMerA binds only one $Hg^{2+}$ per monomer between

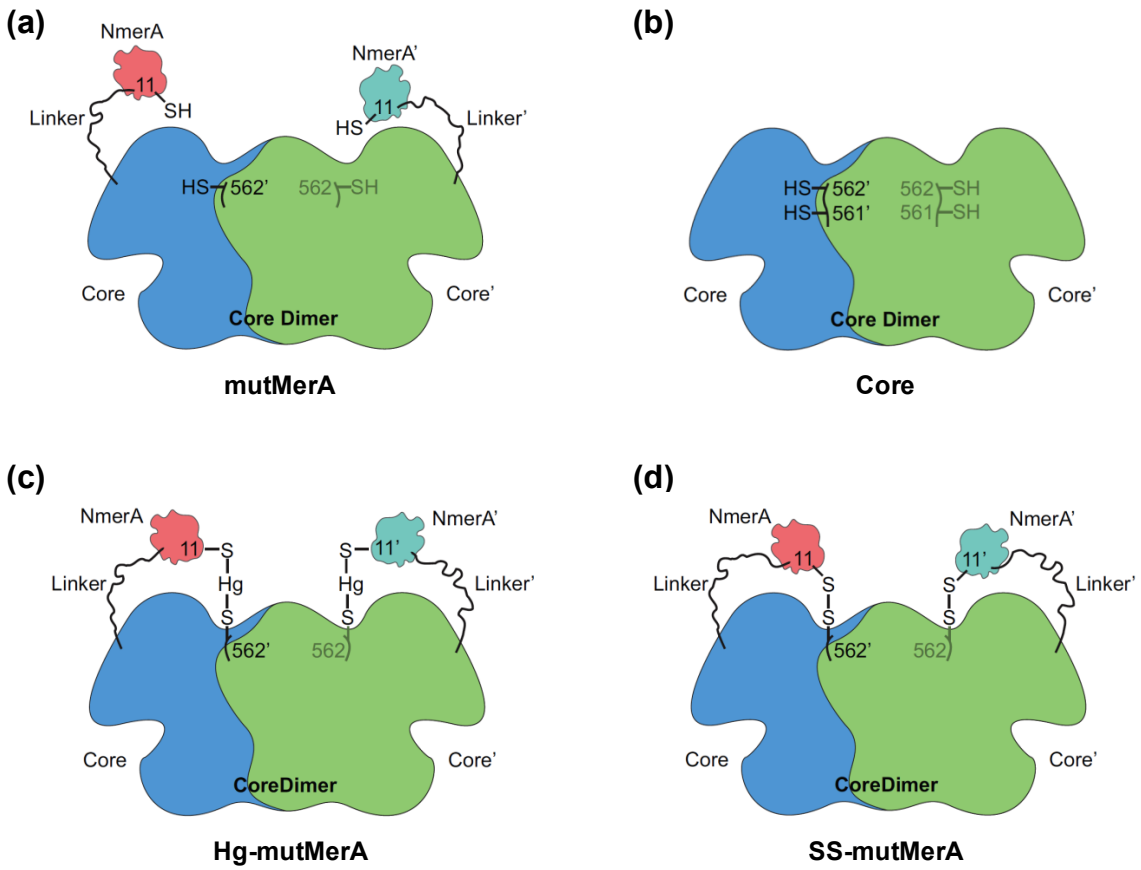


**Figure 2.** Schematic representation of MerA mutants used in this study. The figure illustrates proposed conformations of (a) mutMerA (or full-length MerA) prior to $Hg^{2+}$ binding, (b) MerA catalytic core without NmerA and the flexible linker (Core), (c) the $Hg^{2+}$ handoff complex (Hg-mutMerA) and (d) the disulfide-crosslinked handoff complex (SS-mutMerA). Cysteines involved in $Hg^{2+}$ transfer between NmerA and Core are: C11 and C562' (and C11' and C562).

NmerA and Core to form a mimic of the transient $Hg^{2+}$ handoff complex (Hg-mutMerA, Figure 2c).

In the absence of $Hg^{2+}$, mutMerA exhibits an identical SEC elution profile to that of wild-type MerA (Table 1). However, in contrast to the behavior described above for wild-type MerA when bound to one or two equivalents of $Hg^{2+}$ per monomer, Hg-mutMerA exhibits an SEC elution profile different from that of MerA (Figure 1). Compared with the SEC profiles of molecular mass standards (Figure S2), the apparent molecular mass of Hg-mutMerA is ~133 kDa, ~30 kDa less than mutMerA, but still significantly larger than Core (Table 1). The same behavior was observed when Hg-mutMerA was prepared using $HgBr_2$ or $Hg(TNB)_2$. Along with MALS mass determination, the SEC profile suggests that the complex is the expected dimeric species and the shift in elution time is due to a significant change in the hydrodynamic volume of the protein. As predicted, introducing a $Hg^{2+}$ crosslink between C11 in NmerA and C562' in the Core leads to a more compact conformation of the MerA dimer that should allow characterization of the protein-protein interactions during handoff.

For reasons noted below, we also made an alternative mimic of the handoff complex with a disulfide crosslink between the NmerA C11 and the Core C562' (SS-mutMerA, Figure 2d) by reaction of mutMerA with one equivalent of DTNB per monomer. The SEC elution profile for this preparation shows a peak shift similar to that of Hg-mutMerA (Figure 1) with an apparent mass of ~127 kDa (Table 1). This apparent mass, which was also corroborated by MALS measurements, indicated that DTNB

treatment preferentially forms the internal crosslink between NmerA and the Core, rather than resulting in the oligomerization of MerA dimers. The similar behavior of Hg-mutMerA and SS-mutMerA on SEC suggests that SS-mutMerA, while not a perfect mimic of the handoff complex, should provide insight into the site of interaction between NmerA and Core during the handoff.

## Model-independent analysis of SAXS/SANS data reveals differences in molecular dimensions and indicates partial disorder

In light of the above results, small-angle scattering studies of Core, mutMerA, Hg- and SS-mutMerA (Figure 2) in solution were performed to characterize the relative spatial orientations of NmerA and the Core. Additionally, the flexibility of the linker before acquisition of $Hg^{2+}$ and during the intramolecular $Hg^{2+}$ handoff in MerA was probed. SAXS data were collected for wild-type MerA, mutMerA, Core and SS-mutMerA. However, samples of wild-type MerA suffered from significant radiation damage resulting in aggregation of the protein (Kuwamoto et al. 2004). Therefore only SAXS data for mutMerA, Core and SS-mutMerA were used for further analysis (Figure 3a). The scattering intensities for all three proteins show no concentration dependence and follow the Guinier law in the low *q*-range, indicating a monodisperse distribution under the experimental conditions (Figure 3a and b). Molecular mass values obtained from *I*(0) in comparison with values for a set of protein standards (Mylonas and Svergun 2007) are consistent with dimers in solution for all protein samples in this study (Table 1). The experimentally determined $R_G$ for Tn*501* Core is 31.6 ± 0.1 Å, which is similar to the theoretical $R_G$ of 30.9 Å obtained from calculated scattering intensities for the biologically relevant homodimer generated from the Tn*501* Core crystal structure (PDB ID 1ZK7) using the program FoXS (Schneidman-Duhovny et al. 2010). The successively larger $R_G$ values for SS-mutMerA (36.4 ± 0.2 Å) and for mutMerA (39.1 ± 2.1 Å) (Figure 3b, Table 1) are consistent with the SEC data and indicate that SS-mutMerA has a more compact structure than mutMerA.

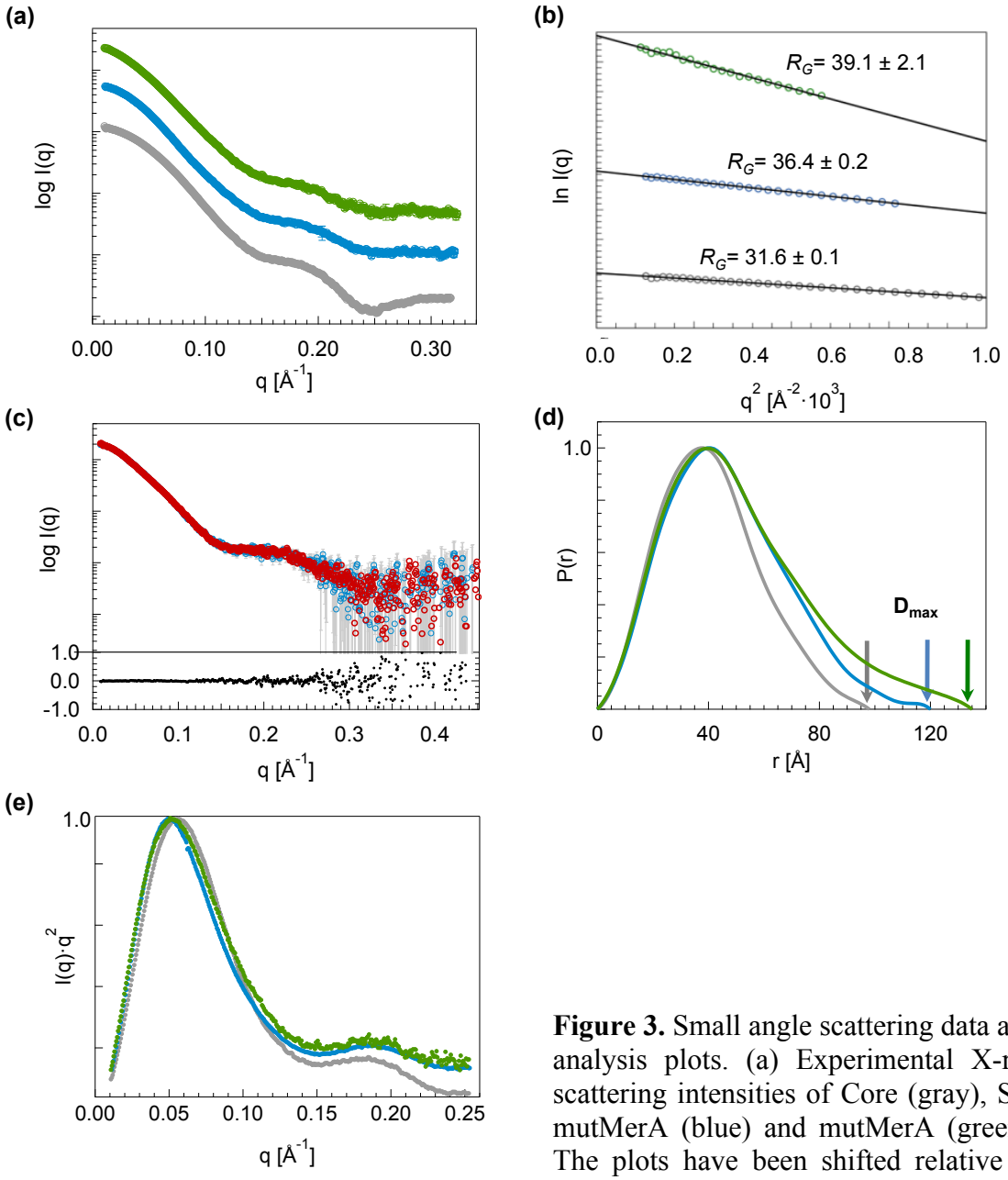


**Figure 3.** Small angle scattering data and analysis plots. (a) Experimental X-ray scattering intensities of Core (gray), SS-mutMerA (blue) and mutMerA (green). The plots have been shifted relative to each other for clarity. (b) Guinier plots with linear fits ($q \cdot R_G$ < 1.3) and extrapolation to determine *I(0)* and $R_G$. The plots have been shifted relative to each other for clarity. (c) Direct comparison of small-angle neutron scattering intensities of SS-mutMerA (blue) and Hg-mutMerA (red). Residuals after subtraction are shown as black dots at the bottom (see Figure S3 in supporting materials for Guinier plots). (d) Distance distribution functions P(r), $D_{max}$ and real space $R_G$ values obtained by indirect Fourier transformation. Core (gray), $rsR_G$ = 31.6 Å, $D_{max}$ = 98 Å, SS-mutMerA (blue), $rsR_G$ = 36.1 Å, $D_{max}$ = 120 Å and mutMerA (green), $rsR_G$ = 39.8 Å, $D_{max}$ = 135 Å. Plots are scaled to unity. (e) Kratky plots of Core, (gray) SS-mutMerA (blue) and mutMerA (green) scaled to unity.

SAXS data collection for Hg-mutMerA also was hampered by significant radiation damage (Kuwamoto et al. 2004), which led to use of SS-mutMerA as a model of the biologically relevant $Hg^{2+}$ handoff complex. However, with a shorter S-S interatomic distance of ~2.6 Å for a typical disulfide bond versus a linear S-Hg-S linkage, the disulfide bond in SS-mutMerA may alter the interaction of NmerA with the Core. To compare the global structures of SS-mutMerA and Hg-mutMerA directly, small-angle neutron scattering (SANS) profiles were collected for both, since, in contrast to X-rays, neutrons interact weakly with atomic nuclei and therefore do not damage biological samples. The superimposed SANS profiles of SS-mutMerA and Hg-mutMerA in $D_2O$ buffer after scaling to $I(0)$, and residuals after subtraction are shown in Figure 3c. There are no apparent differences between the two SANS profiles, and the associated $R_G$ values derived from Guinier plots were also identical, with $R_G$ = 36.5 ± 0.4 Å for SS-mutMerA and $R_G$ = 36.5 ± 0.3 Å for Hg-mutMerA (Figure S4). These results are consistent with the disulfide crosslinked form (SS-mutMerA) representing the global structure of MerA at the midpoint of transfer of Hg(II) from NmerA to the catalytic core domain (IV in Scheme 1).

Normalized pair distance distribution functions, $P(r)$, obtained by indirect Fourier transformation of the SAXS data (Svergun 1992), are shown for Core, mutMerA and SS-mutMerA in Figure 3d. Real space $R_G$ values extracted from the $P(r)$ function are in good agreement with the Guinier-derived $R_G$ values (Table 1). The *P(r)* functions exhibit a common maximum near r = 40 Å. The $P(r)$ distribution for the Core is nearly symmetric, indicating a compact shape with a maximum intraparticle distance $D_{max}$ of 98 Å,

consistent with maximal distances of ~100 Å measured in the homodimer structure of the Tn*501* Core (PDB ID 1ZK7). In contrast, the $P(r)$ distributions for mutMerA and SS-mutMerA show significant asymmetry and have longer $D_{max}$ values of 120 Å and 135 Å, respectively. Tailing $P(r)$ functions extending to longer distances are characteristic of multi-domain proteins with flexible linkers (Putnam et al. 2007) and suggest that even longer distances may be sampled at low frequency. The shape of the $P(r)$ distribution and the high $D_{max}$ for mutMerA strongly indicate that the tethered NmerA domains in this molecule populate elongated conformations in solution.

The presence of unfolded or disordered regions in proteins can be identified using a Kratky plot ($I(q)\cdot q^2$ vs $q$) (Glatter and Kratky 1982; Putnam et al. 2007). Figure 3e shows Kratky plots for Core, mutMerA and SS-mutMerA. For disordered polymers, such as proteins fully denatured in guanidinium chloride, $I(q)\cdot q^2$ is constant with $q$ beyond the Guinier regime (Calmettes et al. 1994). Whereas the Kratky plot for the Core in Figure 3e converges to zero at high $q$, the plots for mutMerA and SS-mutMerA are of higher intensity at values of $q > 0.12$ Å$^{-1}$ and do not converge to zero, indicating the presence of partial disorder in mutMerA and SS-mutMerA but not in the Core. The presence of this disorder-induced observable difference in the Kratky plot is striking, especially for SS-mutMerA, given the small fraction of the protein mass belonging to the linker region (~5%). Together with the relatively high $R_G$ and tailing $P(r)$, the Kratky plots for mutMerA and SS-mutMerA are consistent with these species having anisotropic shapes and with the presence of flexibility in their linkers.

## SAXS and MD-based conformational sampling

Although structures of the Tn*21* MerA used in this study are not available, structures with ~90% sequence identity (Figure S3) are available for the Tn*501* MerA Core (PDB ID 1ZK7) and NmerA domain (PDB ID 2KT2) and were used as templates to build models of the Tn*21* protein (see Methods). As noted above, both the $R_G$ and $D_{max}$ values for the Core are consistent with the dimensions of the homodimer generated from the crystal structure. In addition, the SAXS profile calculated for the Core structure fits the experimental data quite well indicating the Core retains this structure in solution (Figure S5).

To further characterize the conformational distribution of the full-length forms of MerA in solution, the experimental scattering results were combined with an MD-based conformational search using a model with the NmerA domains tethered to the Core by the linkers (see Methods). This approach allows further testing of the hypothesis that NmerA is flexibly attached to the Core and provides some quantification of the extent of conformational sampling in the two distinct functional states represented by mutMerA and SS-mutMerA.

The discrepancies, $\chi^2$, between the SAXS profiles calculated from individual MD conformations and the experimental SAXS data for mutMerA are plotted in Figure 4a as a function of the calculated $R_G$ for each conformation. As a result of the length of the linkers, the range of $R_G$ values obtained from the sampling procedure spans ~15 Å. The blue trace in Figure 4b shows the single best fit to the experimental data ($\chi^2$ = 1.96).

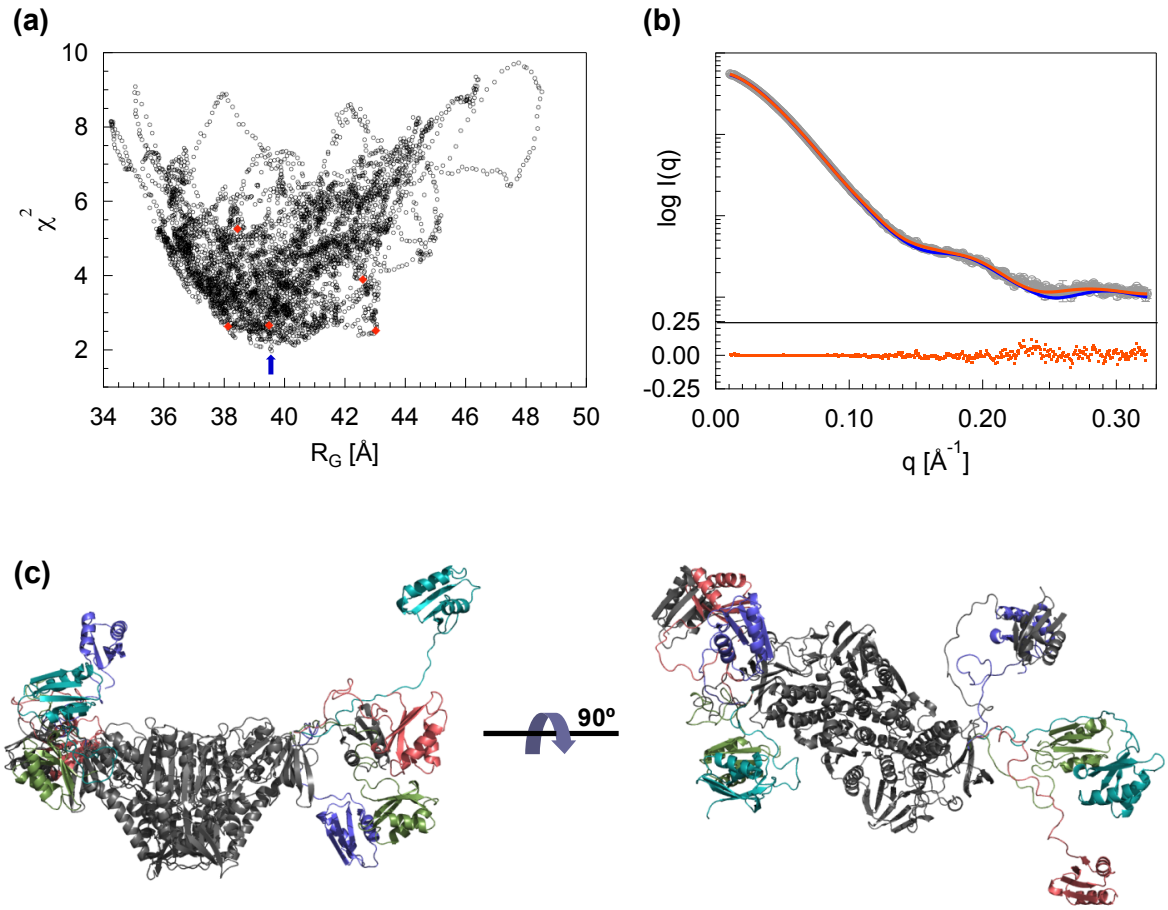


**Figure 4.** Comparison of experimental and calculated scattering profiles for mutMerA. (a) Plot of the discrepancy ($\chi^2$) between experimental data and calculated scattering profiles for 5000 models of MerA obtained from MD trajectories versus their respective calculated $R_G$ values spanning a range of 15 Å. The single best fit conformation with a $\chi^2$ of 1.96 is indicated by an arrow. The conformations identified by the minimal ensemble search (MES) are highlighted in the plot (orange diamonds). (b) Experimental SAXS data (grey circles), single best fit conformation to the experimental scattering profile with $\chi^2$ = 1.96 (blue line) and combined profile from five contributing conformations identified by MES (orange line) with $\chi^2$ = 1.39 with residuals in orange dots at the bottom. (c) Superposition of the five models identified by MES. The catalytic core domain is shown in gray, the linker and NmerA domains are depicted in a different color for each conformation. Weighting factors for the 5 conformations are 0.40 (pink), 0.29 (green), 0.16 (cyan), 0.08 (purple) and 0.07 (gray). The ensemble on the right is rotated by 90º about the x-axis relative to the ensemble on the left.

However, in a highly flexible system, multiple conformations will contribute to the population. Therefore, a minimal ensemble search (MES) was employed to identify one or more sets of conformations that better represent the SAXS data (Pelikan et al. 2009). In repeated searches, several different ensembles of five weighted mutMerA conformations gave similarly improved $\chi^2$ values. Expanding the search to more than five conformations did not statistically improve the fit. One such ensemble of five conformations highlighted by the orange diamonds in Figure 4a improved $\chi^2$ from 1.96 to 1.39 (orange line in Figure 4b). Superposition of these five conformations, Figure 4c, suggests that in solution NmerA samples a large volume including conformations with NmerA near the C-terminal cysteines at the Core dimer interface as well as conformations with the NmerA metal binding site extended up to ~80 Å from the C-terminal cysteines. These results suggest that, although the flexible linker limits the distances sampled between Core and NmerA, it possibly does not impose constraints on the orientation of NmerA with respect to the Core.

## SS-mutMerA reveals conformation during $Hg^{2+}$ handoff

In SS-mutMerA, the NmerA domains are additionally linked to the Core via disulfide bonds to the cysteines nearest the C-termini of the two Core monomers to model the MerA structure midway through $Hg^{2+}$ transfer between the NmerA and Core cysteine pairs (IV in Scheme 1b). In the two published structures of the Core (Schiering et al. 1991; Ledwidge et al. 2005a), the short C-terminal segment of ~12 residues is found in two different conformations with the C-terminal cysteine pair either buried near the active site[3] but visible from the same surface where NmerA is normally tethered (Schiering et al. 1991) or folded out to the side (Ledwidge et al. 2005a). These lead to the prediction that the Hg-NmerA complex will interact with the Core cysteines somewhere along the dimeric interface within an arc of ~90° from the tethered face of NmerA to the side (Figure S6). Since both NmerA domains are tethered to the same surface in the homodimer, their simultaneous interaction with the Core on that face will give a very different shape and scattering profile for SS-mutMerA from that with the two domains interacting on opposing sides of the Core. Application of the MD-based conformational search, starting from symmetric models with NmerA docked at several angles within this arc, showed that models with NmerA docked toward the top face give poor fits to the experimental scattering data (e.g., Figure S7), but those with NmerA toward the side fit much better (Figure 5). In the model in Figure 5, the NmerA domains interact with the C-termini of the complementary monomers (i.e., C11 bonded to C562'). We also tested the hypothesis that the NmerA domains could interact with their own C-termini (C11 bonded

[3] Coordinates of MerA from *Bacillus* sp. strain RC607 are not deposited in the PDB, but were made available by Dr. Emil Pai at the University of Toronto.

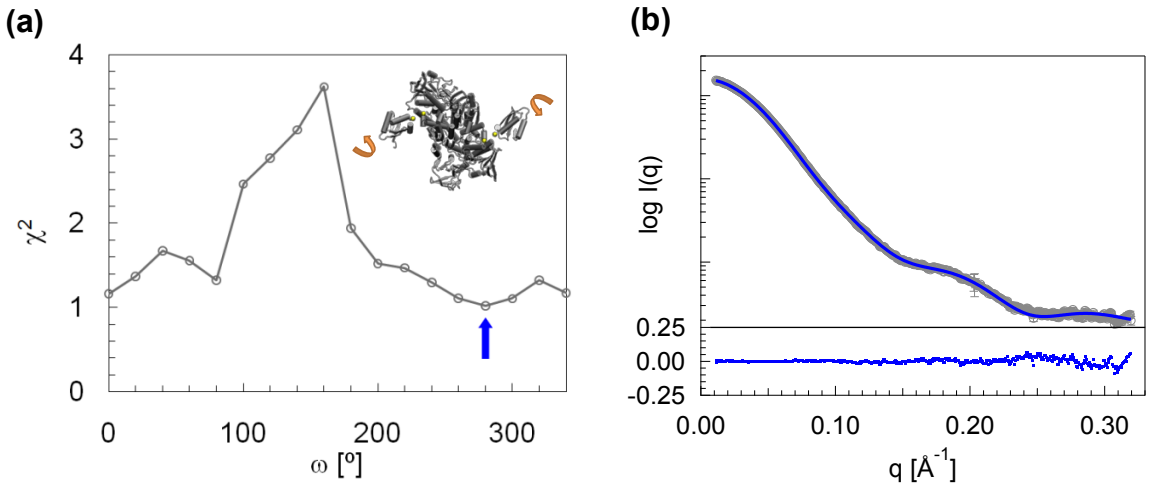


**Figure 5.** Model of SS-mutMerA. (a) Plot of $\chi^2$ as a function of NmerA rotation angle ω as indicated by arrows in the inset (see text for definition of ω). (b) Overlay of the experimental SAXS data (grey circles) and calculated scattering data for the single best-fit conformation to the experimental scattering profile with $\chi^2$ = 1.02 (blue line). Residuals between experimental data and best fit are shown as blue dots at the bottom.

to C562), which would significantly restrict the conformational flexibility of the linkers. This configuration also resulted in poor fits to the experimental data (Figure S8). Models with NmerA docked on opposite sides of Core significantly improved the fits (Figure 5). Further analysis of the rotational orientation of NmerA with respect to Core for the model in Figure 5 (see also Figure S9) gave a model with an overall best fit to the experimental scattering data of $\chi^2$ = 1.02 (Figure 5b). However, $\chi^2$ varies only slightly for models within a rotation arc of ~100° (Figure 5a), which may indicate the presence of rotational flexibility about the disulfide bond in SS-mutMerA or may be due to limitations in the resolution of the technique. The conformation giving the overall best fit to the experimental data (Figure 5b) is shown in Figure 6a. Since the model-independent analysis indicated the presence of partial disorder, we also performed MES on this best fitting model of SS-mutMerA, allowing only the interdomain linker to move. No ensemble of multiple linker conformations further improved $\chi^2$. However, the linker conformation in the best-fitting model (Figure 6a) is consistent with the long $D_{max}$ value and the disorder indicated by the Kratky plot, both of which indicate that the linkers in SS-mutMerA are flexible and are not packed tightly against the catalytic core during handover of $Hg^{2+}$.

One of the goals of determining the site of interaction between NmerA and Core in SS-mutMerA was to identify residue and backbone interactions that may help orient the domains or facilitate ligand exchanges during the intramolecular $Hg^{2+}$ transfer. Although the current results identify the general site, the small size of NmerA precludes a reliable analysis of its rotational orientation relative to Core and the details of their

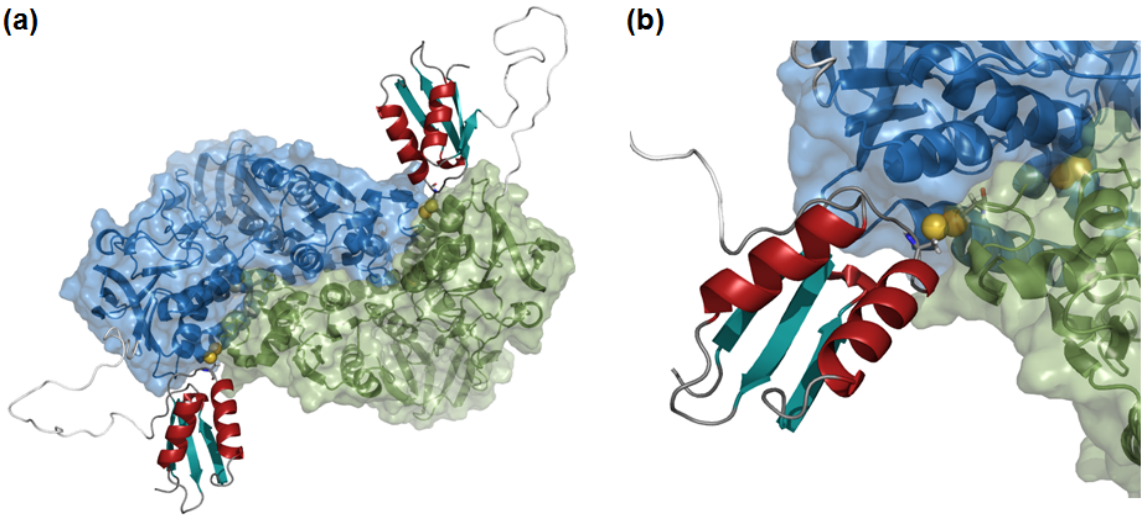


**Figure 6.** (a) Best-fitting model ($\chi^2$ = 1.02) of SS-mutMerA in which C11 of NmerA (ribbon representation) is disulfide-bonded to C562' of the core domain (surface representation). (b) Close-up of one of the two transient docking sites. Relevant thiol sulfurs on C11 and C562' are shown as yellow spheres. The orientations of the two separate NmerA domains with respect to a plane through the dimer interface in the single best fit model were determined at $\phi$ = 76.0º, $\psi$ = 56.3º and $\phi$ = 74.4º, $\psi$ = 47.4º, respectively (for a definition of angles see supplemental Figure S6).

interactions within the experimental resolution. Furthermore, the configuration represented by SS-mutMerA corresponds to only one specific intermediate (Scheme 1, IV) in the proposed ligand exchange mechanism. The initial step involves formation of a tri-coordinate $Hg^{2+}$ intermediate by attack of C562' on the C11-$Hg^{2+}$-C14 complex (Scheme 1b, III'), which may require a different orientation of NmerA with respect to Core. However, as can be seen in Figure 6b for the "best-fitting rotational conformation", the surface area buried upon docking of NmerA to Core is relatively small (~435 $Å^2$ for each NmerA and Core interface site), suggesting there are only a few interactions between residues on each domain in this or other rotational conformers. The size of the buried surfaces is similar to those observed in the more weakly interacting Cu-trafficking protein pairs (Banci et al. 2009a) and is consistent with a lack of significant interaction between NmerA and Core in the absence of the metal ion, as has been observed for other pairs of metal trafficking proteins (Banci et al. 2009a; Banci et al. 2010b). Although detailed interactions between domains cannot be identified conclusively because of limitations in the experimental resolution, determining the approximate interfacial sites enables testable hypotheses to be formed regarding the identities of specific residues involved in interdomain recognition, which we are currently pursuing.

The present results describe the conformations sampled by MerA before acquisition of and during the intramolecular transfer of $Hg^{2+}$ between domains. Unlike many other modular proteins, MerA does not switch between distinctly structured conformational states. Rather, the present work indicates that the NmerA domains, connected to the Core by ~30 residue linkers, function as flexibly tethered

metallochaperones that independently sample large volumes in proximity to the catalytic Core. This topology allows them to interact with other proteins up to ~8 nm from the Core. The flexible attachment of NmerA may facilitate fast and efficient removal of $Hg^{2+}$ from diverse protein substrates, enabling the small tethered NmerA domain to reach and acquire $Hg^{2+}$ independent of the topology of the target proteins. As such, it may represent a fundamental rescue mechanism for cellular proteins compromised by heavy metals.

## Materials and Methods

Cloning and Mutagenesis: Plasmid pDG106, which codes for the Tn*21 mer* operon originally isolated from *Shigella flexneri*, was a generous gift from Dr. Anne O. Summers (Gambill and Summers 1985). Standard molecular biology protocols were used for PCR amplification, restriction digest, ligation, and transformation. The 1,692 bp coding sequence corresponding to the 564-residue MerA was PCR-amplified using forward (5′ GGG**GGATCC**ACTCTCAAAATCACCGGCATGACTTG 3′) and reverse (5′ CCC**GGATCC**ttattaCCCGGCGCAGCAG 3′) primers designed to introduce BamH1 sites at the beginning and end of the gene (in bold) and two stop codons at the end of the gene (lower case). The PCR product was ligated at the BamHI restriction site of H-MBP-3C, a modified pMAL-c2X vector (New England Biolabs, Ipswich, MA) that codes for tandem N-terminal $His_6$ and maltose binding protein (MBP) affinity purification tags followed by a 3C protease cleavage site, Figure S1a (Alexandrov et al. 2001). After 3C cleavage, this strategy leaves only three protease recognition site residues (GPG) upstream of the native Tn*21* MerA sequence, which begins at Ser2, Figure S3. Chemically-competent Top10 *Escherichia coli* (Invitrogen, Carlsbad, CA) were transformed with the resulting pMAL:H-MBP-3C_MerA vector and selected on LB/carbenicillin (50 μg/mL) plates. The MerA gene sequence and orientation were verified by DNA sequencing.

Based on p$K_a$ values obtained from NMR titration experiments and kinetic data (Ledwidge et al. 2010), C11 is expected to be the last residue to release $Hg^{2+}$ from NmerA and C562' is the first residue to attack $Hg^{2+}$. To study the specific $Hg^{2+}$ handoff

between NmerA and the MerA catalytic core, we used site-directed mutagenesis to generate the following mutations all in the same construct, H-MBP-3C_mutMerA: C14A (NmerA), C135A and C140A (Core active site), C561A (Core C-terminus). Only C11 (NmerA) and C562 (Core C-terminus) were retained. Mutations were verified by DNA sequencing.

Protein Expression and Purification: For expression, *Escherichia coli* C43 cells (Miroux and Walker 1996), which we have found to give high expression of MBP-fusion proteins, were transformed with pMAL:H-MBP-3C_MerA and plated on LB/carbenicillin (50 μg/mL) agar. A single colony was used to inoculate 1 L of LB/carbenicillin (50 mg/L) media, which was then shaken at 37 °C and 280 rpm for ~16 h. 50 mL of this starter culture was centrifuged at 3000 × g for 10 min and decanted. The cell pellet was resuspended in fresh 50 ml of LB/carbenicillin (50 mg/L) media and used to inoculate 6 × 1 L of LB/carbenicillin (50 mg/L) media in 2.8 L non-baffled Fernbach flasks. Inoculants were shaken at 37 °C and 280 rpm and grown to $OD_{600}$ ~0.4, at which point the temperature was reduced to 17 °C. At $OD_{600}$ ~0.6, expression was induced with 0.3 mM isopropyl ß-D-thiogalactoside (IPTG) and growth continued overnight (~16 hrs). Cells were harvested by centrifugation at 6000 × g for 10 min. Harvested pellets, corresponding to ~6 g per 1 L growth, were resuspended in 12 mL lysis buffer [50 mM $KP_i$ pH 7.3, 100 mM NaCl, 1 mM EDTA, 10 mM 1,4-dithiothreitol (DTT)], and frozen for storage at -20 °C.

All purification procedures were performed at 4 °C unless noted. Frozen cells from 2 L growth were thawed and incubated with one complete ULTRA protease inhibitor cocktail tablet (Roche Applied Science, Indianapolis, IN), 100 μM PMSF, and 100 μM FAD. Suspended cells were lysed by four passes through an Emulsiflex-C3 homogenizer (Avestin, Ottawa, Canada) and centrifuged at 42,000 × g for 2 h. The supernatant was diluted 10-fold to ~700 mL with lysis buffer, and loaded onto 60 mL of pre-equilibrated amylose resin (New England Biolabs, Ipswich, MA) in a 5.0 × 20 cm Econo-Column glass gravity flow chromatography column. Following a 700 mL wash with lysis buffer, protein was eluted with ~60 mL of the lysis buffer containing 10 mM maltose. Elution fractions exhibiting yellow color were pooled and concentrated to ~2 mL in an Amicon Ultra centrifugal filter (100,000 MWCO). To cleave the $His_6$-MBP affinity purification tags from MerA, 3C protease was added at a 1:50 ratio (3C:MerA) by weight and incubated for 1 hr. Cleaved MerA was separated from 3C protease and $His_6$-MBP on a Superdex 200 10/300 GL size-exclusion chromatography (SEC) column (GE Healthcare, Piscataway, NJ) and equilibrated with SEC buffer [50 mM $KP_i$ pH 7.3, 10 mM DTT] or SAXS buffer [SEC buffer with 10% glycerol]. Column elution was monitored using an HPLC workstation (Shimadzu, Columbia, MD) with an in-line photodiode array detector. Elution fractions from the predominant peak, which exhibited absorbance at both 280 and 456 nm (arising from one FAD bound to each MerA catalytic core monomer), were pooled and aliquoted for SAXS or analytical chromatography, or flash frozen in liquid nitrogen and stored at -80 °C for later use. Full-length mutMerA was purified following the same protocol after expression from the pMAL:H-MBP-

3C_mutMerA vector. Tn*501* Core-MerA was purified as previously described (Ledwidge et al. 2005a).

Preparation of Hg-mutMerA: Purified mutMerA was treated with fresh 5 mM DTT for 30 min at room temperature and was then buffer-exchanged into 50 mM $KP_i$ pH 7.3 using an Econo-Pac® 10-DG column (Bio-Rad Laboratories) to remove DTT. Protein concentrations were determined from the absorbance at 450 nm ($\varepsilon_{450}$ = 11.5 $mM^{-1}$ $cm^{-1}$ per FAD with one FAD bound to each monomer) and protein thiols were quantified in either 50 mM $KP_i$ pH 7.3 or 6 M guanidine hydrochloride using 5,5'-dithio-*bis*-(2-nitrobenzoic acid) (DTNB) (Riddles et al. 1979). To determine the stoichiometry of $Hg^{2+}$ binding, Hg-(2-nitro-5-thiobenzoate)$_2$ ($Hg(TNB)_2$) in 50 mM $KP_i$ pH 7.3 was titrated into a sample of 5 μM dimer and the increase in absorbance at 450 nm arising from the generation of TNB was measured on a diode array spectrophotometer (Hewlett Packard 8452A) at room temperature. The final TNB concentration was calculated using $\varepsilon_{450}$ = 7.36 $mM^{-1}$ $cm^{-1}$. Alternatively, to prepare quantities of Hg-mutMerA for biophysical studies, one equivalent of $HgBr_2$ in 50 mM $KP_i$ pH 7.3 was titrated into the buffer-exchanged mutMerA (~5 mM dimers) at room temperature following thiol titration as described above. All samples for SAXS studies were purified using a Superdex 200 10/300 GL SEC column equilibrated with 50 mM $KP_i$ pH 7.3.

Preparation of SS-mutMerA: A solution of ~5 mM mutMerA dimers, reduced and quantified as described above, was mixed with one molar equivalent of DTNB per subunit and allowed to react until the generation of TNB reached completion, as

monitored spectroscopically at 450 nm against a protein-only reference using a dual-beam Uvikon XL spectrophotometer (Kontron) at 25 °C.

To remove excess $HgBr_2$ from Hg-mutMerA and DTNB and TNB from SS-mutMerA preparations, protein was concentrated to ~2 mL in an Amicon Ultra centrifugal filter (100,000 MWCO) and purified by SEC as described above. Elution fractions from the predominant peak, which exhibited absorbance at both 280 nm and 456 nm, were pooled and aliquoted for SAXS or analytical chromatography.

Analytical SEC and SEC-multi-angle light scattering (MALS): The apparent molecular size of the Core, MerA, mutMerA, and SS- and Hg-mutMerA preparations were determined by analytical SEC using a Superdex 200 10/300 GL SEC column equilibrated with 50 mM $KP_i$ pH 7.3. Protein samples (50 µL) were prepared at 125 µM monomer (62.5 µM dimer), based on absorbance at 456 nm with $\varepsilon_{456}$ = 11.3 $mM^{-1}$ $cm^{-1}$ per FAD for Core and MerA, and at 450 nm as described above for mutMerA and Hg- and SS-mutMerA. Gel filtration standards (Bio-Rad Laboratories, Hercules, CA) were analyzed at the same time.

Multi-angle light scattering (MALS) was used to evaluate the protein molecular mass independent of chromatographic behavior. Protein samples (50 µL at 25 µM, prepared as described above) were injected onto a KW-803 SEC column (Shodex) equilibrated with 50 mM $KP_i$ at pH 7.3 on an Ettan LC workstation (GE Healthcare, Piscataway, NJ). The light scattering and refractive index of column eluents were

measured using inline DAWN® HELEOS and Optilab rEX detectors (Wyatt Technologies Corp., Santa Barbara, CA), respectively. Molecular weight (MW) calculations were performed with ASTRA software (Wyatt Technologies Corp., Santa Barbara, CA) using a specific refractive index increment d*n*/d*c* value of 0.185 ml/g, where *n* is the refractive index, and *c* is the molecular concentration.

Scattering data collection: SAXS data were collected at beamline 12.3.1 at the Advanced Light Source, Lawrence Berkeley National Laboratory, CA. The wavelength *l* of the incident X-ray beam was 1.000 Å. The distance between the sample and a MarCCD 165 X-ray detector system was 150 cm. This configuration resulted in an accessible *q*-range of 0.01 to 0.32 $Å^{-1}$. The scattering vector is defined as $q = (4p/l)\cdot\sin q$, where 2*q* is the scattering angle.

Aliquots of the various MerA constructs were dialyzed at 4 ºC into a buffer of 50 mM $KP_i$ pH 7.3 and 10% (v/v) glycerol. Immediately before data collection, all samples were centrifuged at 17000 × g to remove any residual particles. The temperature during data collection was 20 ºC and the sample volume was 15 µL. SAXS data were collected for mutMerA at concentrations of 1.9, 3.8 and 7.6 mg/mL, for SS-mutMerA at 2.6, 5.5 and 8.6 mg/mL and for Core at 2.3, 4.5, 9.0 and 18.1 mg/mL. The data were processed as described previously (Johs et al. 2010).

SANS data were collected for SS-mutMerA and Hg-mutMerA on the EQ-SANS instrument at the Spallation Neutron Source, Oak Ridge National Laboratory, TN. The

concentration of the samples used for neutron scattering was 5.3 mg/mL in a buffer of 50 mM $KP_i$ in $D_2O$ (pD = 7.3).

X-ray scattering profiles were processed with PRIMUS from the ATSAS 2.3 software package (Konarev et al. 2003; Konarev et al. 2006). The radius of gyration $R_G$ was derived using the Guinier approximation (Guinier and Fournet 1955) from scattering data in the low-$q$ region ($q \cdot R_G < 1.3$). Extrapolation of the scattering intensity to zero angle $I(0)$ allowed estimation of the relative molecular mass after comparison with a set of protein standards (Mylonas and Svergun 2007). The following commercially available proteins (Hampton Research, Aliso Viejo, CA, U.S.A.) were used as molecular mass reference standards: lysozyme (14.3 kDa, 6.1 mg/mL), xylanase (21 kDa, 6.4 mg/mL), bovine serum albumin (66 kDa, 4.4 mg/mL) and glucose isomerase (173 kDa, 2.1 mg/mL) in PBS buffer (137 mM NaCl, 2.7 mM KCl, 10 mM $Na_2HPO_4$, 1.8 mM $KH_2PO_4$, pH =7.4) with 10% glycerol and stored as a frozen stock. The excluded particle volume was obtained from the Porod invariant (Glatter and Kratky 1982). SAXS data were subjected to indirect Fourier transformation using the program GNOM (Svergun 1992) to obtain the pair distance distribution function $P(r)$ and the maximum intraparticle distance $D_{max}$.

Homology modeling: The program MODELLER (Sali and Blundell 1993; Eswar et al. 2006) was used to construct models of full-length Tn*21* MerA. Sequence alignment of Tn*21* and Tn*501* MerA performed using ClustalW2 (Larkin et al. 2007) revealed 87% identity for NmerA and 90% for Core (Figure S3). An NMR structure of Tn*501* NmerA

(PDB ID 2KT2) and a 1.6 Å resolution crystal structure of Tn*501* Core (PDB ID 1ZK7) were used as templates. To be consistent with the protein construct used in the experiments, C14, C135, C140 and C561 were mutated to Ala in the models. Models for SS-mutMerA were obtained by introducing interdomain crosslinks between C11 (chain A) and C562' (chain B) and C11' with C562 (Figure 2). Both FAD molecules present in the crystal structure of Tn*501* MerA were included in the construction of the Tn*21* model. A total of 50 protein models were generated, and a single best model was chosen based on DOPE scores(Shen and Sali 2006). An initial random conformation was assigned to residues 68-99.

MD-based conformational sampling: An adapted version of the BILBO-MD protocol (Pelikan et al. 2009), was used to generate and screen macromolecular conformations. Briefly, BILBO-MD proceeds as follows: structured domains of a macromolecule are modeled as rigid bodies (i.e. with no internal motion), but the flexible linker regions are allowed to move freely; high-temperature MD simulations are performed in the gas phase, enabling extensive and efficient conformational sampling. To reduce computational cost and increase sampling of conformation space, electrostatic interactions are set to zero and a group-based scheme is used for van der Waals terms. In the present simulations no constraints were imposed on $R_G$. BILBO-MD uses the program CHARMM (in our case, version c35b2) to perform the MD simulations (Brooks et al. 1983). Theoretical SAXS profiles were computed for a total of 5000 MD conformations for mutMerA and SS-mutMerA using FoXS (Schneidman-Duhovny et al. 2010). Error-weighted least-squares fits ($\chi^2$) to the experimental scattering data were

calculated for all computed scattering profiles. A minimal ensemble search (MES) was used to select a limited number of conformations that represent the experimental data better than a single conformation (Pelikan et al. 2009).

Hg(II) handoff from NmerA to Core: For SS-mutMerA, several near-approach conformations were identified from the mutMerA simulations. Initial conformations were chosen such that NmerA from one protomer was near the C-terminus of the other protomer in the Core homodimer, resulting in several initial orientations (Figure S6). Symmetric homodimers were generated and C11 (NmerA) and C562' (Core) were covalently linked by a disulfide bond, followed by energy minimization and MD-based conformational sampling. Once an orientation was identified that yielded a minimal $\chi^2$ value, the orientations of the two NmerA domains underwent further optimization. NmerA was rotated in 20º increments about an axis defined by the center of mass (COM) of NmerA, SG(C11), SG(C562') and CA(Q412) (Figure S9a). For NmerA, a plane was defined to include SG (Cys11), the center of mass (COM) of residues 1-68, and CB (Leu22). Similarly, a plane was defined for the core to include SG (Cys562'), CA (Gln412), and CB (Ala191'). The angle of rotation ω was defined as the angle between the plane of NmerA and that of the core (Figure S9b). For each rotamer, a symmetric homodimer was generated and the sampling procedure described above was used to identify the conformation with the lowest $\chi^2$ (Figure 5a). The buried surface areas for NmerA/Core interaction sites were estimated using PyMOL (DeLano 2002) by calculating solvent accessible surface areas with a probe radius of 1.4 Å.

## Acknowledgements

We thank Wei Yang and Guobin Luo for providing CHARMM force field parameters for FAD, Jinkui Zhao and Carrie Gao for assistance with the EQ-SANS instrument at the Spallation Neutron Source at ORNL, Elaine Kirschke and Daniel Southworth for assistance with the MALS instrument. A portion of this research at Oak Ridge National Laboratory's Spallation Neutron Source was sponsored by the Scientific User Facilities Division, Office of Basic Energy Sciences, U.S. Department of Energy. The SIBYLS beamline (BL12.3.1) at the Advanced Light Source of Lawrence Berkeley National Laboratory is supported by the U.S. Department of Energy under contract number DE-AC02-05CH11231. This research was supported by the Office of Biological and Environmental Research, U.S. Department of Energy (DOE), in part by the Mercury Science Focus Area Program at Oak Ridge National Laboratory (ORNL) and in part by grant ER64984 to SMM. ORNL is managed by UT-Battelle, LLC, for DOE under Contract No. DE-AC05-00OR22725.

## Supplementary Information

**Table S1.** Steady-state rate constants of Tn*21* and Tn*501* full-length MerA for reduction of $Hg^{2+}$ using mercuric bis-glutathione [$Hg(SG)_2$] as substrate.

| | GSH (mM) | $K_{MHg}$ (μM) | $k_{cat}$ ($s^{-1}$) | $k_{cat}/K_{MHg}$ ($M^{-1}$ $s^{-1}$) |
|---|---|---|---|---|
| Tn*21* MerA[a] | 1.0 | 14.6 | 8.8 | $6.0 \times 10^5$ |
| Tn*501* MerA[b] | 1.0 | 10.7 | 9.4 | $8.8 \times 10^5$ |

[a]This work. [b]From Ledwidge et al. 2005a.

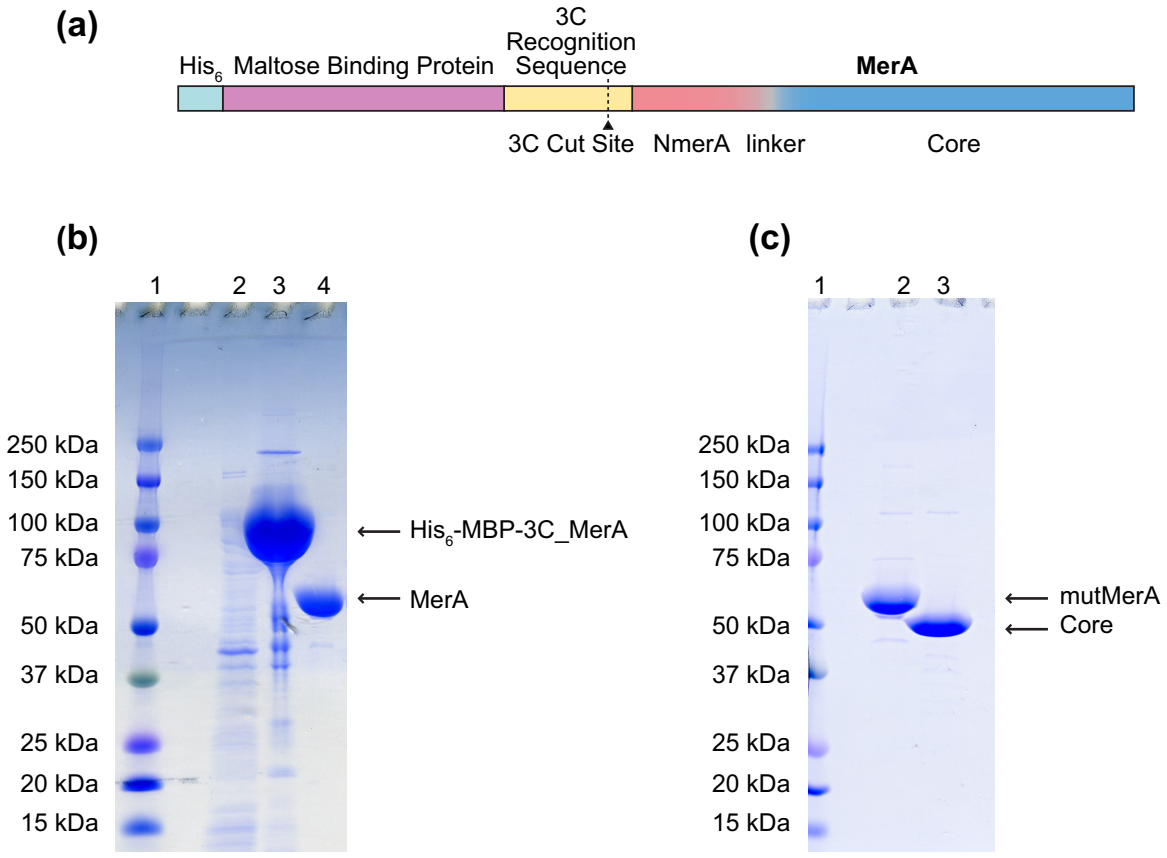


**Figure S1.** Characterization of MerA purification and mass by SDS-PAGE. (a) Schematic of the MerA construct. (b) Stages of MerA purification revealed by Coomassie Blue staining on a Novex® 4-20% tris-glycine SDS-PAGE gel (Invitrogen). Lane 1: Precision Plus Protein™ Standards Kaleidoscope™ molecular mass standards (Bio-Rad Laboratories); Lane 2: Amylose column flow-through; Lane 3: Amylose column maltose elution of $His_6$-MBP-3C_MerA concentrated prior to 3C protease treatment; Lane 4: Pooled SEC fractions of MerA following 3C treatment and separation. The shift in apparent mass from 100 kDa prior to 3C treatment to 55 kDa corresponds to the cleavage and separation of $His_6$-MBP-3C (45 kDa). (c) Comparison of purified mutMerA and Core. Lane 1: Molecular mass standards; Lane 2: Purified mutMerA; Lane 3: Purified Core.

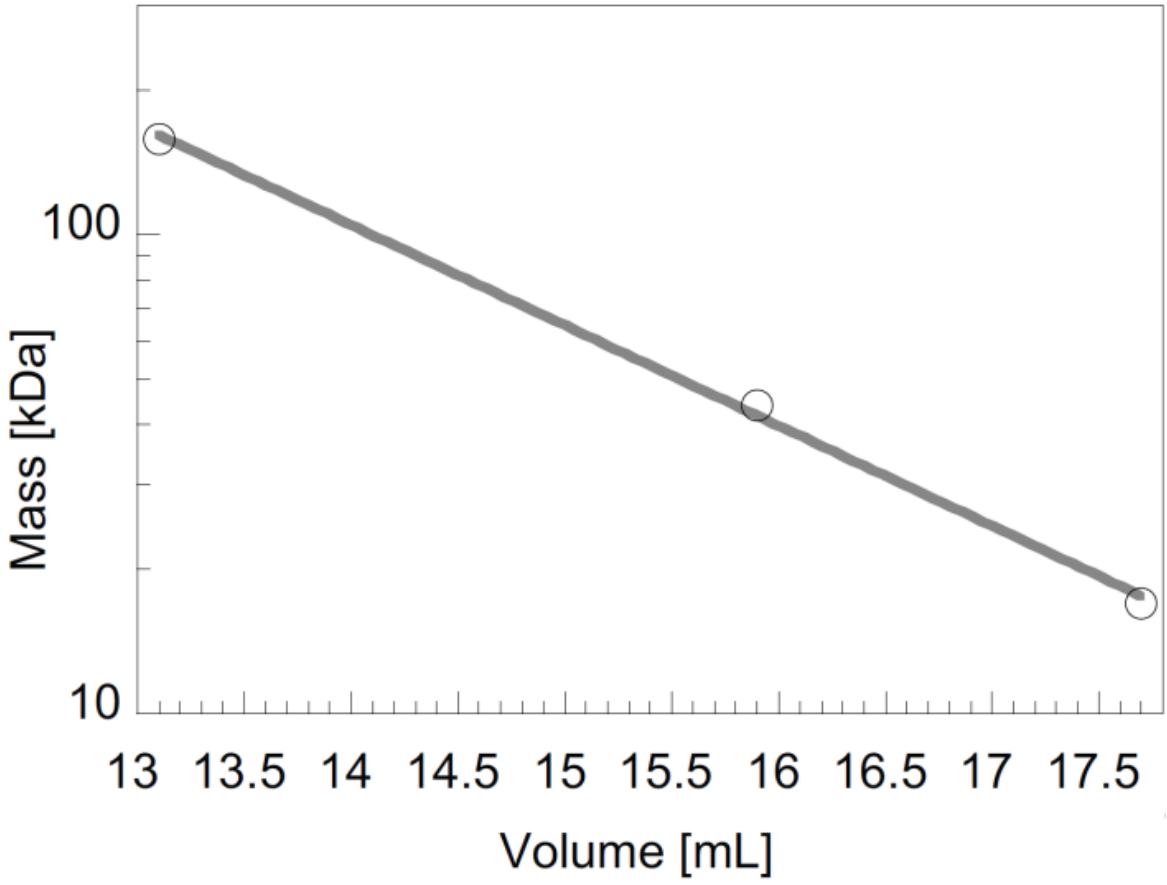


**Figure S2.** Molecular mass versus elution volume of gel filtration standards corresponding to bovine γ-globulin (13.1 mL; 158 kDa), chicken ovalbumin (15.9 mL; 44 kDa) and equine myoglobin (17.7 mL; 17 kDa) versus known molecular mass. The logarithmic fit of these standards, mass (kDa) = 89,298 × $e^{-0.482[\text{elution volume (mL)}]}$, was used to calculate $MM_{apparent}$ in Table 1.

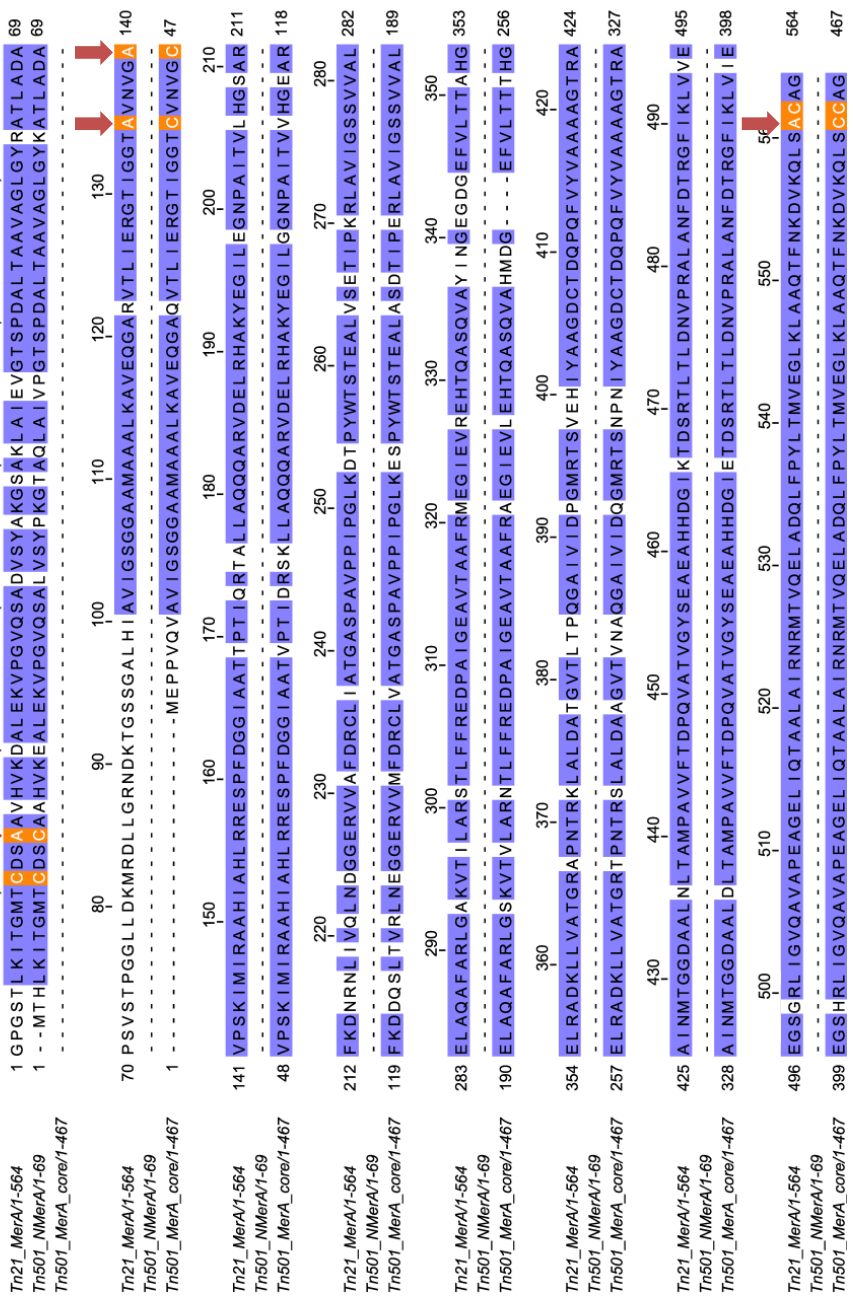


**Figure S3.** Alignment of MerA Tn*21* sequence for homology modeling. Structural templates included an NMR structure of NmerA (PDB ID 2KT2) and the crystal structure of oxidized Tn*501* MerA core (PDB ID 1ZK7). Relevant cysteines are shown in orange. Note the four mutations (C14A, C135A, C140A, C561A) introduced into the sequence of Tn*21* MerA (red arrows). The third G in the Tn*21* sequence shown here corresponds to the position of Met1 in the actual MerA sequence, the GPG here is left after cleavage of the MBP-fusion tag. The residues are numbered according to the actual sequence with the initial GP assigned -2, -1.

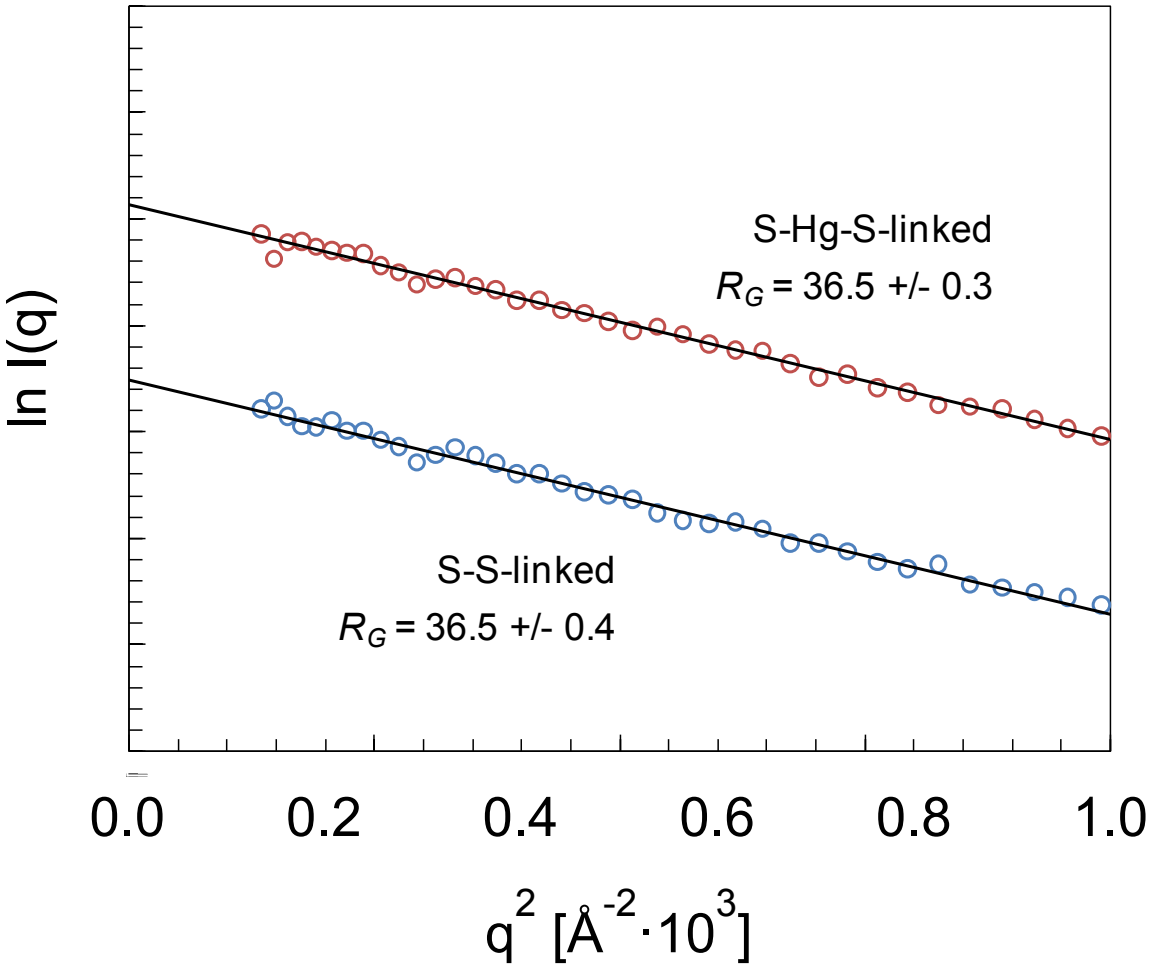


**Figure S4.** Guinier plots and experimental $R_G$ values obtained from SANS profiles of Hg-mutMerA (red) and SS-mutMerA (blue). The plots have been shifted relative to each other for clarity.

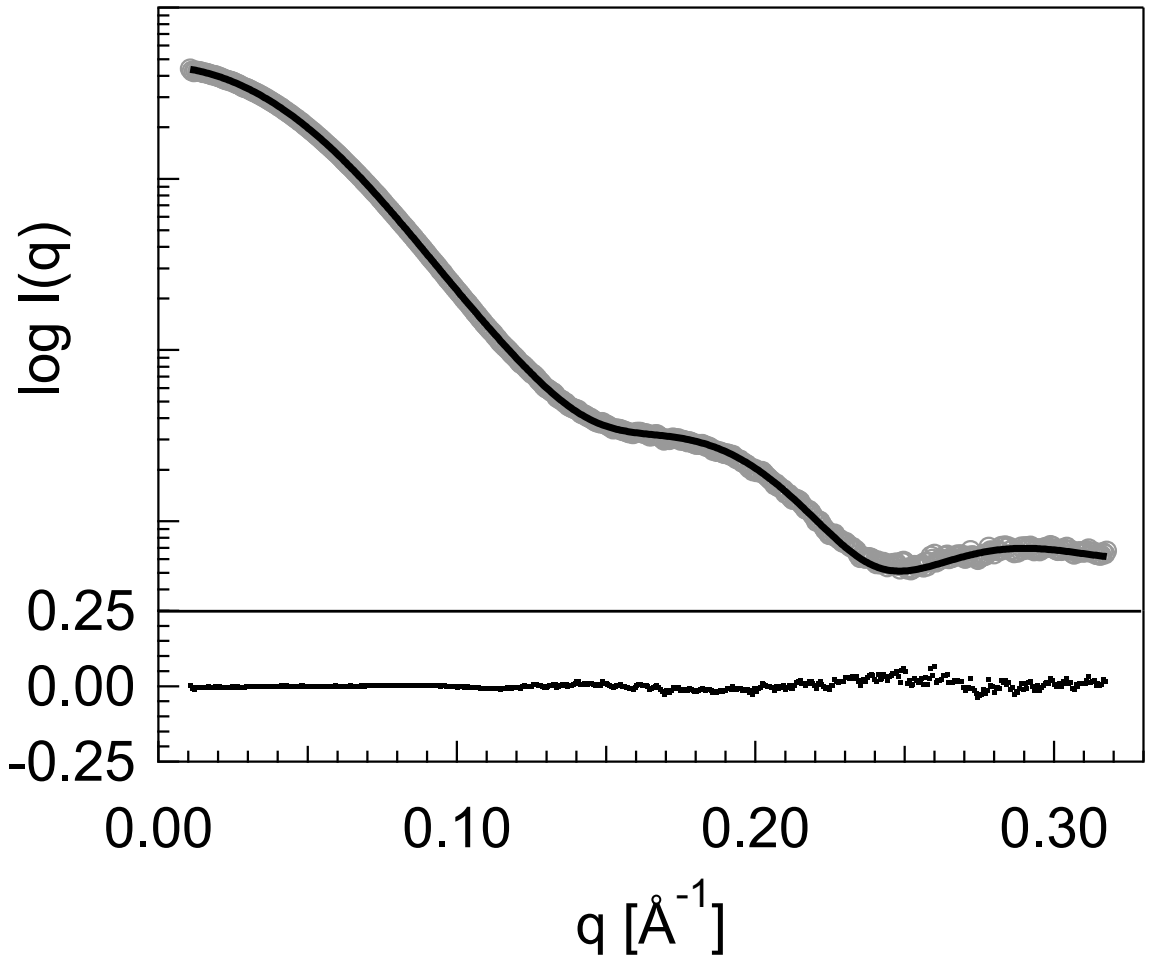


**Figure S5.** Experimental SAXS data (grey circles) of Tn*501* Core and calculated scattering profile (black line) of a homodimer generated from the Tn*501* crystal structure (PDB ID 1ZK7) with $\chi^2$ = 1.77. Residuals between experimental and calculated intensities are shown as black dots at the bottom.

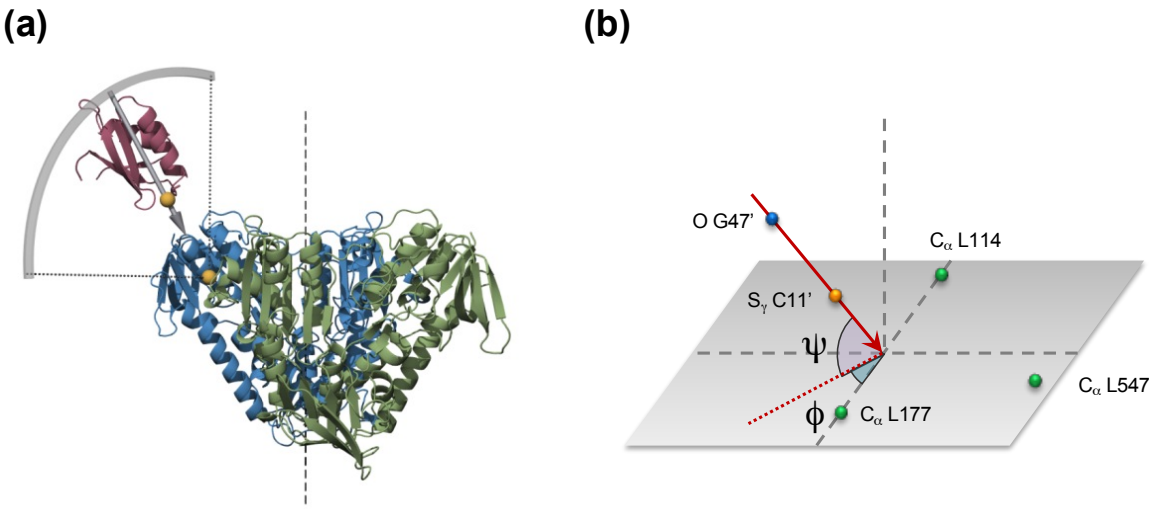


**Figure S6.** (a) Schematic illustration of NmerA position with respect to the catalytic core domain. Sulfur atoms of C11' and C562 are shown as yellow spheres. The dashed line indicates the axis of rotational symmetry for the homodimeric Core domain. Initial models for the MD conformational search were generated with NmerA placed at variable angles with respect to the Core within the grey arc. (b) The orientation of NmerA relative to the core is defined by two angles ($\phi$, $\psi$) between a vector defined by O (G47') and $S_\gamma$ (C11') and a plane approximating the protomer interface defined by $C_\alpha$ (L114), $C_\alpha$ (L177) and $C_\alpha$ (L547). $\phi$ is the azimuth angle measured from an axis connecting $C_\alpha$ of L114 and $C_\alpha$ of L177. $\psi$ is the inclination angle between the vector and the plane.

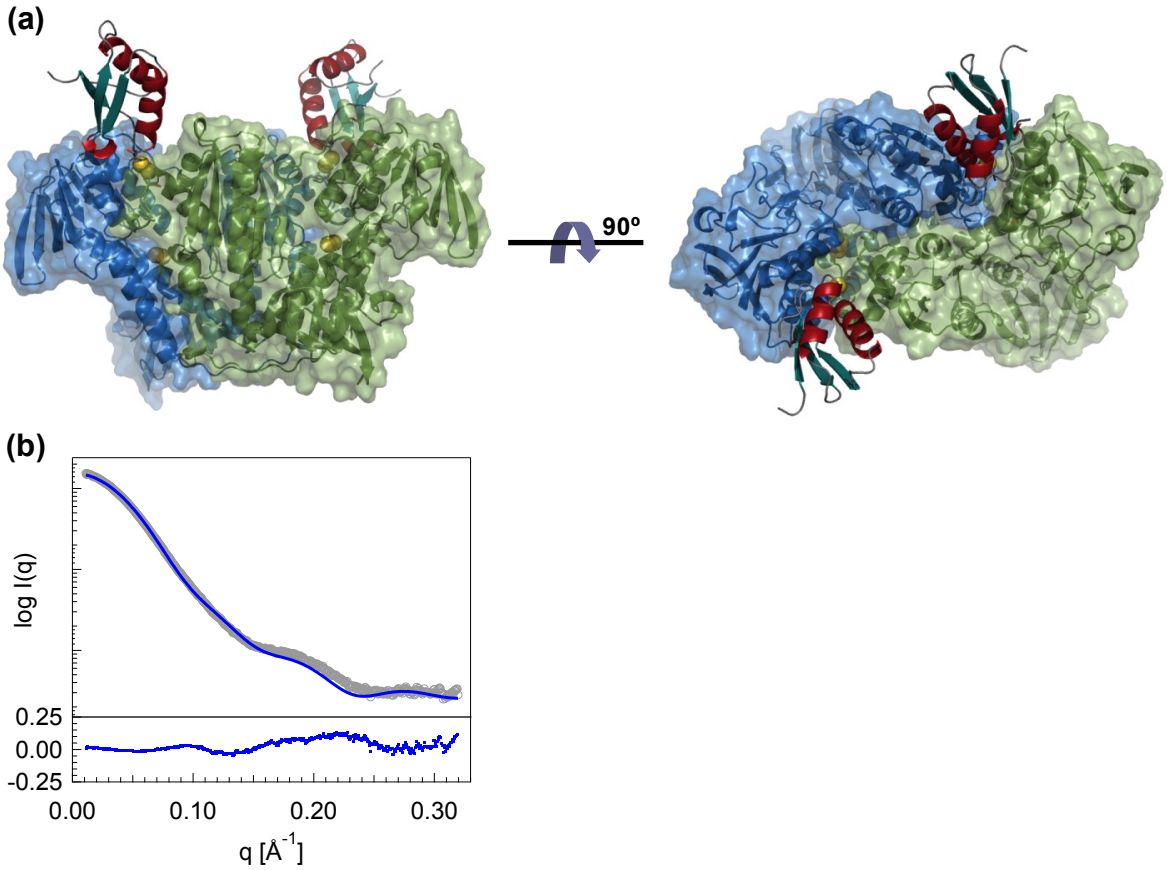


**Figure S7.** (a) Model of SS-mutMerA with NmerA in a position similar to a previously proposed alternative docking orientation (Ledwidge et al., 2005b). (b) Experimental SAXS data (grey circles) and single best-fit conformation to the experimental scattering profile with $\chi^2$ = 3.89 (blue line). Residuals between experimental data and best fit are shown as blue dots at the bottom.

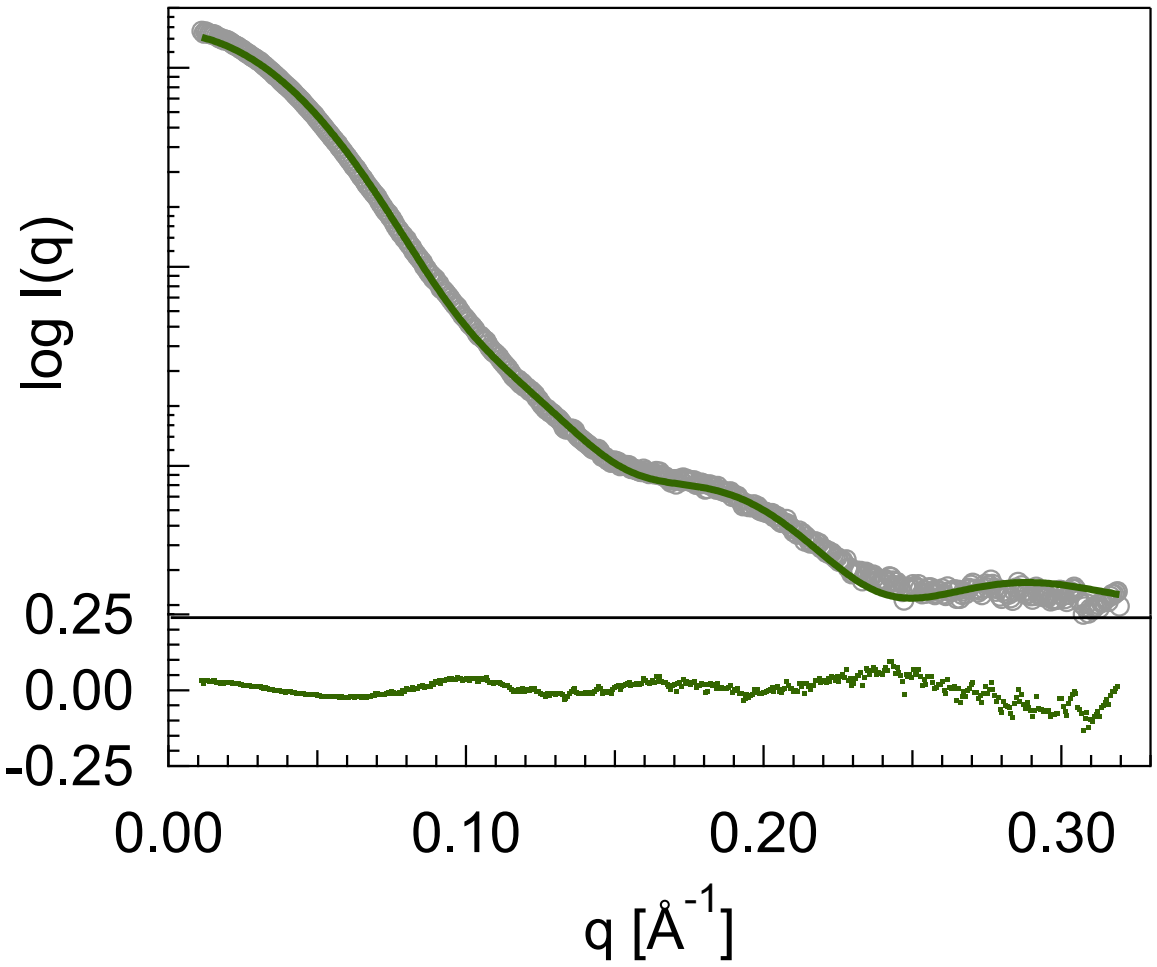


**Figure S8.** Best fit of the calculated to the experimental scattering data for a model of SS-mutMerA with each NmerA Cys11 bonded to the Core Cys562 of the same monomer with $\chi^2$ = 4.08 (green line). Residuals between experimental data and best fit are shown as green dots at the bottom.

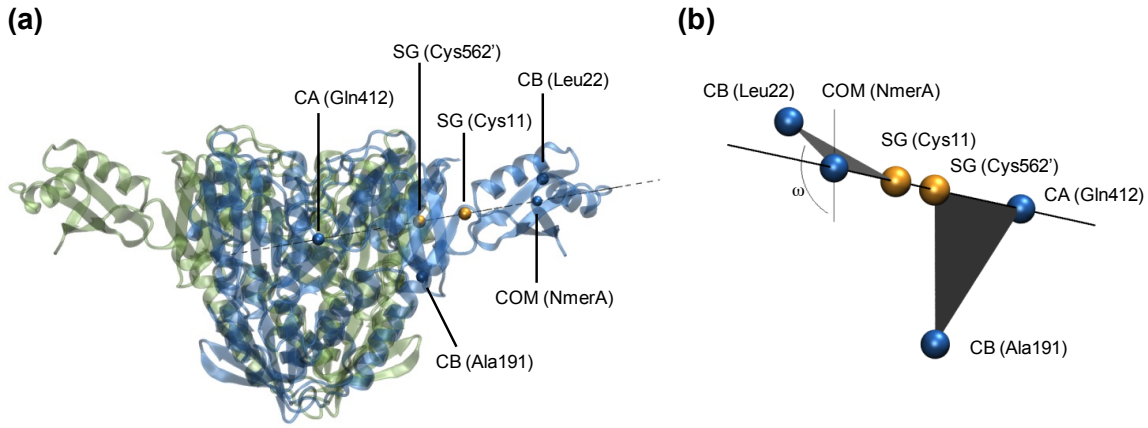


**Figure S9.** Rotation of NmerA with respect to Core. (a) For NmerA, a plane was defined to include SG (Cys11), the center of mass (COM) of residues 1-68, and CB (Leu22). Similarly, a plane was defined for the Core to include SG (Cys562'), CA (Gln412), and CB (Ala191'). (b) As CA (Gln412), SG (Cys562'), SG (Cys11) and COM were collinear, a rotation angle ω about this axis was defined as the angle between the plane of NmerA and that of the Core. ω was rotated about the collinear axis in 20º steps to generate initial structures for further refinement of the orientation of NmerA with respect to the Core.

## References


Abajian C, Yatsunyk LA, Ramirez BE, Rosenzweig AC (2004) "Yeast cox17 solution structure and Copper(I) binding." *Journal of Biological Chemistry* 279:53584-53592.

Alexandrov A, Dutta K, Pascal SM (2001) "MBP fusion protein with a viral protease cleavage site: one-step cleavage/purification of insoluble proteins." *Biotechniques* 30:1194-1198.

Arnesano F, Banci L, Bertini I, Cantini F, Ciofi-Baffoni S, Huffman DL, O'Halloran TV (2001) "Characterization of the binding interface between the copper chaperone Atx1 and the first cytosolic domain of Ccc2 ATPase." *J Biol Chem* 276:41365-41376.

Arnesano F, Banci L, Bertini I, Ciofi-Baffoni S, Molteni E, Huffman DL, O'Halloran TV (2002) "Metallochaperones and metal-transporting ATPases: a comparative analysis of sequences and structures." *Genome Res* 12:255-271.

Banci L, Bertini I, Calderone V, Della-Malva N, Felli IC, Neri S, Pavelkova A, Rosato A (2009a) "Copper(I)-mediated protein-protein interactions result from suboptimal interaction surfaces." *Biochem J* 422:37-42.

Banci L, Bertini I, Cantini F, Felli IC, Gonnelli L, Hadjiliadis N, Pierattelli R, Rosato A, Voulgaris P (2006) "The Atx1-Ccc2 complex is a metal-mediated protein-protein interaction." *Nat Chem Biol* 2:367-368.

Banci L, Bertini I, Cantini F, Massagni C, Migliardi M, Rosato A (2009b) "An NMR study of the interaction of the N-terminal cytoplasmic tail of the Wilson disease protein with copper(I)-HAH1." *Journal of Biological Chemistry* 284:9354-9360.

Banci L, Bertini I, Ciofi-Baffoni S, Finney LA, Outten CE, O'Halloran TV (2002) "A new zinc-protein coordination site in intracellular metal trafficking: solution structure of the Apo and Zn(II) forms of ZntA(46-118)." *J Mol Biol* 323:883-897.

Banci L, Bertini I, Ciofi-Baffoni S, Kozyreva T, Zovo K, Palumaa P (2010a) "Affinity gradients drive copper to cellular destinations." *Nature* 465:645-648.

Banci L, Bertini I, McGreevy KS, Rosato A (2010b) "Molecular recognition in copper trafficking." *Nat Prod Rep* 27:695-710.

Barkay T, Kritee K, Boyd E, Geesey G (2010) "A thermophilic bacterial origin and subsequent constraints by redox, light and salinity on the evolution of the microbial mercuric reductase." *Environ Microbiol* 12:2904-2917.

Barkay T, Miller SM, Summers AO (2003) "Bacterial mercury resistance from atoms to ecosystems." *FEMS microbiology reviews* 27:355-384.

Bernado P, Mylonas E, Petoukhov MV, Blackledge M, Svergun DI (2007) "Structural characterization of flexible proteins using small-angle X-ray scattering." *J Am Chem Soc* 129:5656-5664.

Bernado P, Perez Y, Svergun DI, Pons M (2008) "Structural characterization of the active and inactive states of Src kinase in solution by small-angle X-ray scattering." *J Mol Biol* 376:492-505.

Brooks BR, Bruccoleri RE, Olafson BD, States DJ, Swaminathan S, Karplus M (1983) "Charmm - a Program for Macromolecular Energy, Minimization, and Dynamics Calculations." *J Comp Chem* 4:187-217.

Brown NL, Ford SJ, Pridmore RD, Fritzinger DC (1983) "Nucleotide sequence of a gene from the Pseudomonas transposon Tn501 encoding mercuric reductase." *Biochemistry* 22:4089-4095.

Calmettes P, Durand D, Desmadril M, Minard P, Receveur V, Smith JC (1994) "How random is a highly denatured protein?" *Biophys Chem* 53:105-113.

Chaudhury S, Gray JJ (2008) "Conformer selection and induced fit in flexible backbone protein-protein docking using computational and NMR ensembles." *J Mol Biol* 381:1068-1087.

Cheesman BV, Arnold AP, Rabenstein DL (1988) "Nuclear magnetic resonance studies of the solution chemistry of metal complexes. 25. Hg(thiol)3 complexes and Hg(II)-thiol ligand exchange kinetics." *J Am Chem Soc* 110:6359-6364.

Chen H, Ricklin D, Hammel M, Garcia BL, McWhorter WJ, Sfyroera G, Wu YQ, Tzekou A, Li S, Geisbrecht BV, Woods VL, Jr., Lambris JD (2010) "Allosteric inhibition of complement function by a staphylococcal immune evasion protein." *Proc Natl Acad Sci USA* 107:17621-17626.

Clore GM, Iwahara J (2009) "Theory, practice, and applications of paramagnetic relaxation enhancement for the characterization of transient low-population states of biological macromolecules and their complexes." *Chem Rev* 109:4108-4139.

Cobine PA, George GN, Jones CE, Wickramasinghe WA, Solioz M, Dameron CT (2002) "Copper transfer from the Cu(I) chaperone, CopZ, to the repressor, Zn(II)CopY: metal coordination environments and protein interactions." *Biochemistry* 41:5822-5829.

DeLano WL (2002) *The PYMOL Molecular Graphics System*. San Carlos, CA, U.S.A.: DeLano Scientific LLC.

Distefano MD, Au KG, Walsh CT (1989) "Mutagenesis of the redox-active disulfide in mercuric ion reductase: catalysis by mutant enzymes restricted to flavin redox chemistry." *Biochemistry* 28:1168-1183.

Distefano MD, Moore MJ, Walsh CT (1990) "Active site of mercuric reductase resides at the subunit interface and requires Cys135 and Cys140 from one subunit and Cys558 and Cys559 from the adjacent subunit: evidence from in vivo and in vitro heterodimer formation." *Biochemistry* 29:2703-2713.

Engst S, Miller SM (1999) "Alternative routes for entry of HgX2 into the active site of mercuric ion reductase depend on the nature of the X ligands." *Biochemistry* 38:3519-3529.

Eswar N, Webb B, Marti-Renom MA, Madhusudhan MS, Eramian D, Shen MY, Pieper U, Sali A (2006) "Comparative protein structure modeling using Modeller." *Curr Protoc Bioinformatics* Chapter 5:Unit 5 6.

Finney LA, O'Halloran TV (2003) "Transition metal speciation in the cell: insights from the chemistry of metal ion receptors." *Science* 300:931-936.

Fox B, Walsh CT (1982) "Mercuric reductase. Purification and characterization of a transposon-encoded flavoprotein containing an oxidation-reduction-active disulfide." *J Biol Chem* 257:2498-2503.

Fox BS, Walsh CT (1983) "Mercuric reductase: homology to glutathione reductase and lipoamide dehydrogenase. Iodoacetamide alkylation and sequence of the active site peptide." *Biochemistry* 22:4082-4088.

Gambill BD, Summers AO (1985) "Versatile mercury-resistant cloning and expression vectors." *Gene* 39:293-297.

Glatter O, Kratky O (1982) *Small angle X-ray scattering*: Academic Press London.

Gonzalez-Guerrero M, Arguello JM (2008) "Mechanism of Cu+-transporting ATPases: soluble Cu+ chaperones directly transfer Cu+ to transmembrane transport sites." *Proc Natl Acad Sci USA* 105:5992-5997.

Grubisic Z, Rempp P, Benoit H (1967) "A universal calibration for gel permeation chromatography." *J Polymer Sci* 5:753-759.

Guinier A, Fournet G (1955) *Small Angle Scattering of X-Rays*: Wiley, New York.

Guo HB, Johs A, Parks JM, Olliff L, Miller SM, Summers AO, Liang L, Smith JC (2010) "Structure and conformational dynamics of the metalloregulator MerR upon binding of Hg(II)." *J Mol Biol* 398:555-568.

Hammel M, Fierobe HP, Czjzek M, Kurkal V, Smith JC, Bayer EA, Finet S, Receveur-Brechot V (2005) "Structural basis of cellulosome efficiency explored by small angle X-ray scattering." *Journal of Biological Chemistry* 280:38562-38568.

Hammel M, Yu Y, Fang S, Lees-Miller SP, Tainer JA (2010) "XLF Regulates Filament Architecture of the XRCC4.Ligase IV Complex." *Structure* 18:1431-1442.

Hong B, Nauss R, Harwood IM, Miller SM (2010) "Direct measurement of mercury(II) removal from organomercurial lyase (MerB) by tryptophan fluorescence: NmerA domain of coevolved gamma-proteobacterial mercuric ion reductase (MerA) is more efficient than MerA catalytic core or glutathione." *Biochemistry* 49:8187-8196.

Huffman DL, O'Halloran TV (2001) "Function, structure, and mechanism of intracellular copper trafficking proteins." *Annu Rev Biochem* 70:677-701.

Jamros MA, Oliveira LC, Whitford PC, Onuchic JN, Adams JA, Blumenthal DK, Jennings PA (2010) "Proteins at Work: A Combined Small Angle X-Ray Scattering And Theoretical Determination Of The Multiple Structures Involved On The Protein Kinase Functional Landscape." *Journal of Biological Chemistry* 285:36121-36128.

Jensen MR, Markwick PR, Meier S, Griesinger C, Zweckstetter M, Grzesiek S, Bernado P, Blackledge M (2009) "Quantitative determination of the conformational properties of partially folded and intrinsically disordered proteins using NMR dipolar couplings." *Structure* 17:1169-1185.

Johs A, Shi L, Droubay T, Ankner JF, Liang L (2010) "Characterization of the decaheme c-type cytochrome OmcA in solution and on hematite surfaces by small angle x-ray scattering and neutron reflectometry." *Biophysical journal* 98:3035-3043.

Konarev PV, Petoukhov MV, Volkov VV, Svergun DI (2006) "ATSAS 2.1, a program package for small-angle scattering data analysis." *J Appl Cryst* 39:277-286.

Konarev PV, Volkov VV, Sokolova AV, Koch MHJ, Svergun DI (2003) "PRIMUS: a Windows PC-based system for small-angle scattering data analysis." *J Appl Cryst* 36:1277-1282.

Kuwamoto S, Akiyama S, Fujisawa T (2004) "Radiation damage to a protein solution, detected by synchrotron X-ray small-angle scattering: dose-related considerations and suppression by cryoprotectants." *J Synchrotron Radiat* 11:462-468.

Lafrance-Vanasse J, Lefebvre M, Di Lello P, Sygusch J, Omichinski JG (2009) "Crystal structures of the organomercurial lyase MerB in its free and mercury-bound forms: insights into the mechanism of methylmercury degradation." *Journal of Biological Chemistry* 284:938-944.

Lamb AL, Torres AS, O'Halloran TV, Rosenzweig AC (2001) "Heterodimeric structure of superoxide dismutase in complex with its metallochaperone." *Nat Struct Biol* 8:751-755.

Larkin MA, Blackshields G, Brown NP, Chenna R, McGettigan PA, McWilliam H, Valentin F, Wallace IM, Wilm A, Lopez R, Thompson JD, Gibson TJ, Higgins DG (2007) "Clustal W and Clustal X version 2.0." *Bioinformatics* 23:2947-2948.

Ledwidge R, Hong B, Dötsch V, Miller SM (2010) "NmerA of Tn501 mercuric ion reductase: structural modulation of the pKa values of the metal binding cysteine thiols." *Biochemistry* 49:8988-8998.

Ledwidge R, Patel B, Dong A, Fiedler D, Falkowski M, Zelikova J, Summers AO, Pai EF, Miller SM (2005a) "NmerA, the metal binding domain of mercuric ion reductase, removes Hg2+ from proteins, delivers it to the catalytic core, and protects cells under glutathione-depleted conditions." *Biochemistry* 44:11402-11416.

Ledwidge R, Soinski R, Miller SM (2005b) "Direct monitoring of metal ion transfer between two trafficking proteins." *J Am Chem Soc* 127:10842-10843.

Loftin IR, Franke S, Roberts SA, Weichsel A, Heroux A, Montfort WR, Rensing C, McEvoy MM (2005) "A novel copper-binding fold for the periplasmic copper resistance protein CusF." *Biochemistry* 44:10533-10540.

Miller SM, Moore MJ, Massey V, Williams CH, Jr., Distefano MD, Ballou DP, Walsh CT (1989) "Evidence for the participation of Cys558 and Cys559 at the active site of mercuric reductase." *Biochemistry* 28:1194-1205.

Miroux B, Walker JE (1996) "Over-production of proteins in Escherichia coli: mutant hosts that allow synthesis of some membrane proteins and globular proteins at high levels." *J Mol Biol* 260:289-298.

Moore MJ, Walsh CT (1989) "Mutagenesis of the N- and C-terminal cysteine pairs of Tn501 mercuric ion reductase: consequences for bacterial detoxification of mercurials." *Biochemistry* 28:1183-1194.

Mylonas E, Svergun DI (2007) "Accuracy of molecular mass determination of proteins in solution by small-angle X-ray scattering." *J Appl Cryst* 40:S245-S249.

Nakaya R, Nakamura A, Murata Y (1960) "Resistance transfer agents in Shigella." *Biochem Biophys Res Commun* 3:654-659.

Newby ZER, O'Connell JD, Gruswitz F, Hays FA, Harries WEC, Harwood IM, Ho JD, Lee JK, Savage DF, Miercke LJW, Stroud RM (2009) "A general protocol for the crystallization of membrane proteins for X-ray structural investigation." *Nat Protocols* 4:619-637.

Palmer AG, 3rd (1997) "Probing molecular motion by NMR." *Curr Opin Struct Biol* 7:732-737.

Pelikan M, Hura GL, Hammel M (2009) "Structure and flexibility within proteins as identified through small angle X-ray scattering." *Gen Physiol Biophys* 28:174-189.

Pretto DI, Tsutakawa S, Brosey CA, Castillo A, Chagot ME, Smith JA, Tainer JA, Chazin WJ (2010) "Structural dynamics and single-stranded DNA binding activity of the three N-terminal domains of the large subunit of replication protein A from small angle X-ray scattering." *Biochemistry* 49:2880-2889.

Putnam CD, Hammel M, Hura GL, Tainer JA (2007) "X-ray solution scattering (SAXS) combined with crystallography and computation: defining accurate macromolecular structures, conformations and assemblies in solution." *Q Rev Biophys* 40:191-285.

Riddles PW, Blakeley RL, Zerner B (1979) "Ellmans Reagent - 5,5'-Dithiobis(2-Nitrobenzoic Acid) - Re-Examination." *Anal Biochem* 94:75-81.

Rinderle SJ, Booth JE, Williams JW (1983) "Mercuric reductase from R-plasmid NR1: characterization and mechanistic study." *Biochemistry* 22:869-876.

Robinson NJ, Winge DR (2010) "Copper metallochaperones." *Annu Rev Biochem* 79:537-562.

Rosenzweig AC, O'Halloran TV (2000) "Structure and chemistry of the copper chaperone proteins." *Curr Opin Chem Biol* 4:140-147.

Rozycki B, Kim YC, Hummer G (2011) "SAXS ensemble refinement of ESCRT-III CHMP3 conformational transitions." *Structure* 19:109-116.

Sali A, Blundell TL (1993) "Comparative protein modelling by satisfaction of spatial restraints." *J Mol Biol* 234:779-815.

Schiering N, Kabsch W, Moore MJ, Distefano MD, Walsh CT, Pai EF (1991) "Structure of the detoxification catalyst mercuric ion reductase from Bacillus sp. strain RC607." *Nature* 352:168-172.

Schneidman-Duhovny D, Hammel M, Sali A (2010) "FoXS: a web server for rapid computation and fitting of SAXS profiles." *Nucleic Acids Res* 38 Suppl:W540-544.

Schottel JL (1978) "The mercuric and organomercurial detoxifying enzymes from a plasmid-bearing strain of Escherichia coli." *J Biol Chem* 253:4341-4349.

Sedlmeier R, Altenbuchner J (1992) "Cloning and DNA sequence analysis of the mercury resistance genes of Streptomyces lividans." *Molecular & general genetics : MGG* 236:76-85.

Shen MY, Sali A (2006) "Statistical potential for assessment and prediction of protein structures." *Protein Sci* 15:2507-2524.

Silver S, Phung LT (1996) "Bacterial heavy metal resistance: new surprises." *Annu Rev Microbiol* 50:753-789.

Stanisich VA (1974) "Interaction between an R factor and an element conferring resistance to mercuric ions in Pseudomonas aeruginosa." *Molec Gen Genet* 128:201-212.

Stanisich VA, Bennett PM, Richmond MH (1977) "Characterization of a translocation unit encoding resistance to mercuric ions that occurs on a nonconjugative plasmid in Pseudomonas aeruginosa." *J Bacteriol* 129:1227-1233.

Steele RA, Opella SJ (1997) "Structures of the reduced and mercury-bound forms of MerP, the periplasmic protein from the bacterial mercury detoxification system." *Biochemistry* 36:6885-6895.

Stricks W, Kolthoff IM (1953) "Reactions between mercuric mercury and cysteine and glutathione. Apparent dissociation constants, heats and entropies of formation of various forms of mercuric mercapto-cysteine and -glutathione." *J Am Chem Soc* 75:5673-5681.

Su CC, Yang F, Long F, Reyon D, Routh MD, Kuo DW, Mokhtari AK, Van Ornam JD, Rabe KL, Hoy JA, Lee YJ, Rajashankar KR, Yu EW (2009) "Crystal structure of the membrane fusion protein CusB from Escherichia coli." *J Mol Biol* 393:342-355.

Summers AO (1986) "Organization, expression, and evolution of genes for mercury resistance." *Annu Rev Microbiol* 40:607-634.

Svergun DI (1992) "Determination of the Regularization Parameter in Indirect-Transform Methods Using Perceptual Criteria." *J Appl Cryst* 25:495-503.

Wang Y, Moore M, Levinson HS, Silver S, Walsh C, Mahler I (1989) "Nucleotide sequence of a chromosomal mercury resistance determinant from a Bacillus sp. with broad-spectrum mercury resistance." *J Bacteriol* 171:83-92.

Wilkins MR, Gasteiger E, Bairoch A, Sanchez JC, Williams KL, Appel RD, Hochstrasser DF (1999) "Protein identification and analysis tools in the ExPASy server." *Methods Mol Biol* 112:531-552.

# CHAPTER 3

# The role of NmerA in acquisition and processing of $Hg^{2+}$ liganded to small-molecule and protein substrates

This chapter includes unpublished results that build upon my work and associated publications presented in previous thesis chapters. Rachel E. Nauss was responsible for the synthesis of mercuric bis(thionitrobenzoate) [$Hg(TNB)_2$]. Susan M. Miller was this work's principal investigator.

## Project Background and Author's Contributions

During my examinations of the hydrodynamic properties of MerA using SEC (Chapter 2), I proposed determining if my preparation of Tn*21* MerA could simultaneously bind one or two equivalents of $Hg^{2+}$ per monomer. To do this, I prepared MerA and Rachel Nauss titrated the protein with $Hg(TNB)_2$. As described in this chapter, Ms. Nauss monitored the amount of TNB released upon $Hg^{2+}$ binding and determined that MerA could bind two equivalents of $Hg^{2+}$ per monomer (Ledwidge et al. 2005a). At that time, as we did not expect MerA to be able to bind more than two $Hg^{2+}$ per monomer, the protein was not titrated with additional $Hg(TNB)_2$.

Next, I sought to determine if the binding of either one or two equivalents of $Hg^{2+}$ would affect the hydrodynamic radius of MerA. Prior to my work there had only been studies of the hydrodynamic properties of MerA in the absence of $Hg^{2+}$ (Schottel 1978) and no reports regarding the effect of $Hg^{2+}$ binding on the conformation of MerA. As biochemical and structural studies have firmly established that MerA is a homodimer (Distefano et al. 1990; Schiering et al. 1991; Ledwidge et al. 2005a), the work by Schottel, who had proposed that MerA was a homotrimer based on SEC elution profiles, suggested that MerA's larger than expected hydrodynamic radius was due to an extended and possibly disordered conformation. When titrated with one $Hg^{2+}$ equivalent per MerA monomer, it is possible for $Hg^{2+}$ to be coordinated as NmerA C11-$Hg^{2+}$-Core C562' (see Chapter 2 and this chapter's Scheme 1 aIV). As NmerA and Core would be cross-linked through $Hg^{2+}$ in this "$Hg^{2+}$-handoff" conformation, I proposed that, if one $Hg^{2+}$ equivalent were stably coordinated between NmerA and Core, $Hg_1$-MerA would occupy a smaller hydrodynamic volume and in turn exhibit an elution shift from a SEC column. However, as previous studies of NmerA and Core expressed as separate proteins showed that $Hg^{2+}$ favors binding to NmerA over Core (Ledwidge et al. 2005b), I did not expect the NmerA C11-$Hg^{2+}$-Core C562' to be stable and observed by SEC. I also hypothesized that no change would be observed upon binding two $Hg^{2+}$ per MerA monomer ($Hg_2$-MerA) as NmerA and Core would independently bind $Hg^{2+}$. After Ms. Nauss generated the $Hg_1$-MerA and $Hg_2$-MerA complexes as before, I independently examined and analyzed the hydrodynamic properties of these samples and MerA absent of $Hg^{2+}$ using analytical SEC (Figure i). By comparing the elution profiles of MerA, $Hg_1$-MerA, and

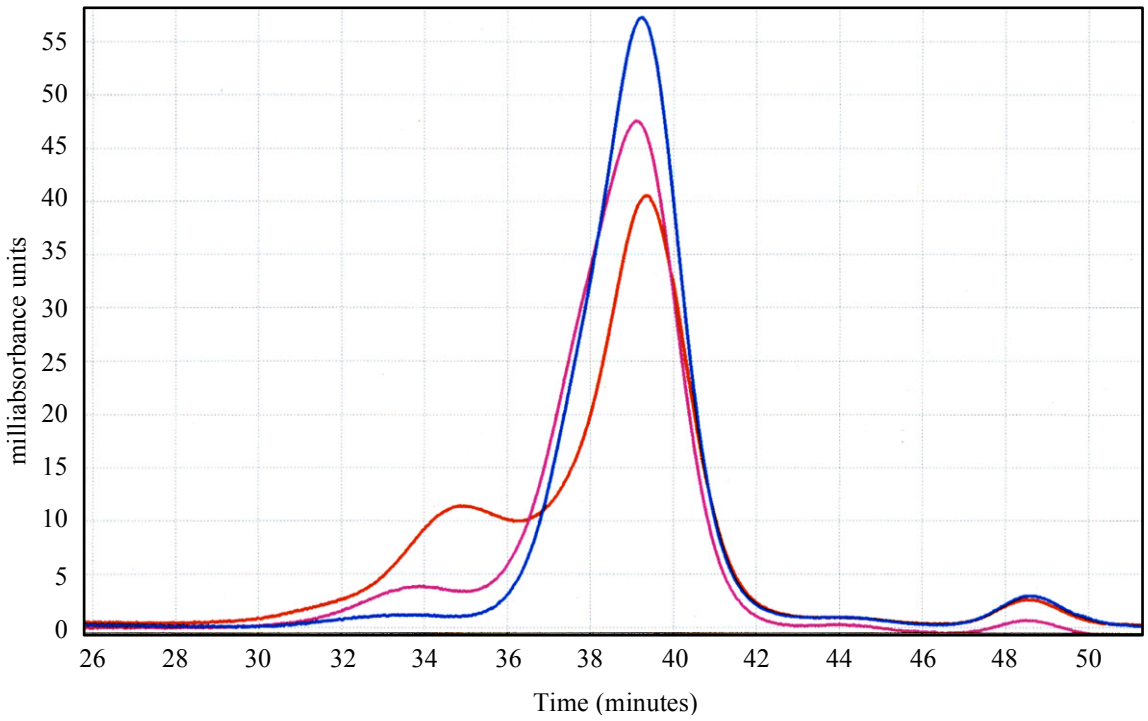


**Figure i**. Analytical size-exclusion chromatography (SEC) elution profiles of Tn*21* MerA (red), $Hg_1$-MerA (pink), and $Hg_2$-MerA (blue). 1.5 nmoles of each preparation in 50, 90, and 100 µL, respectively, were injected onto a Superdex 200 10/300 GL column equilibrated with 50 mM $KP_i$, pH 7.3, at 0.333 mL/min, as described in Chapter 2. Absorbance was monitored at 280 nm. The peaks in the MerA elution profile at ~35 min and in the $Hg_1$-MerA profile at ~33.5 min are dimers of the MerA homodimer. Cysteine residues of one MerA, when not coordinating $Hg^{2+}$, can form a disulfide bond with another MerA. Upon coordination of $Hg^{2+}$ cysteines are unable crosslink with other thiols. The $Hg_2$-MerA trace does not exhibit the formation of higher-order MerA oligomers as $Hg^{2+}$ is bound to all MerA cysteines, rendering them unable to become crosslinked.

$Hg_2$-MerA, I independently interpreted this data as not showing that there is a change in hydrodynamic radius of MerA upon binding one or two equivalents of $Hg^{2+}$ per monomer. I therefore concluded that $Hg_1$-MerA was not a stable coordination of $Hg^{2+}$ as NmerA C11-$Hg^{2+}$-Core C562'. This finding resulted in my deciding to design and construct the mutMerA mutant described for study in Chapter 2 to examine the conformation of NmerA and Core at the point of $Hg^{2+}$ exchange between these two regions when tethered in full length MerA.

The analytical SEC experiments above were the impetus for me deciding to pursue the $Hg^{2+}$ binding equilibrium and kinetics studies of Tn*21* MerA that I present in this chapter. Unlike the above SEC experiments, Ms. Nauss prepared $Hg(TNB)_2$ for this chapter's work but was not involved in any of the experiments. I independently generated all protein samples, executed the experiments, and analyzed and interpreted the Tn*21* MerA equilibrium data.

Over the course of ~2 days in January of 2011, Dr. Miller and I laid out a series of experiments to examine the kinetics of "in-pathway" inter- and intramolecular $Hg^{2+}$ transfers from MerB to NmerA to Core, and to investigate the driving force that ultimately directs $Hg^{2+}$ to Core's inner cysteine pair (C136 and C141 in pDU1358 MerA). It was at that time that I suggested generating the AACCCC MerA mutant described in this chapter to account for steric effects of NmerA in $Hg^{2+}$ acquisition and transfer. First, as I had characterized the aggregation of MerB upon treatment with $HgBr_2$ (Hong et al. 2010), I sought to determine if $Hg^{2+}$ could be liganded to the MerB mutant described in

this chapter's work, MerB C96S, without aggregating the protein. To do so, I used analytical SEC and submitted samples to the UCSF mass spectroscopy facility to examine protein stability and confirm $Hg^{2+}$ binding, respectively. In my independent analysis and interpretation of this data, I concluded that Hg-MerB C96S could be prepared without the protein aggregating by treating it with $Hg(SG)_2$. I used this method to prepare Hg-MerB C96S for the steady state kinetics experiments with pDU1358 MerA described in this chapter.

The next set of experiments in the aforementioned series of studies was to measure and compare the steady state reduction of $Hg^{2+}$ by pDU1358 MerA, AACCCC, and Core with the $Hg^{2+}$ substrates $Hg(SG)_2$ and Hg-MerB C96S. Ms. Nauss was not involved in these experiments, and I independently prepared all proteins and reagents, executed the experiments, and determined the rate constants and experimental errors presented in this chapter. Dr. Miller and I discussed the interpretation of this data.

Upon completion of these steady state experiments, it was my goal to repeat the previously published studies of $Hg^{2+}$ acquisition kinetics from Hg-MerB to pDU1358 NmerA and to Core's C-terminal cysteines (Hong et al. 2010). Unlike these studies, in which Hg-MerB samples were prepared with $HgBr_2$, I planned to use Hg-MerB C96S prepared with $Hg(SG)_2$ to avoid the aforementioned protein aggregation. I also sought to study $Hg^{2+}$ acquisition from Hg-MerB C96S to MerA's C-terminal thiols by using the AACCCC mutant, and to MerA's C-terminal thiols through NmerA by using wild-type MerA. To detect $Hg^{2+}$ binding to the Core C-terminal cysteines, I had planned to measure

the change in FAD absorbance of the appropriate MerA variant upon stopped flow mixing with Hg-MerB C96S, as I describe in this chapter's work for Tn*21* MerA upon mixing with $Hg(SG)_2$. The goal of these experiments as a whole is to understand the kinetics of the $Hg^{2+}$ transfers from MerB to NmerA to Core's C-terminal cysteines. I was unable to initiate these experiments prior to leaving UCSF, and the Miller group remains interested in the pursuit of these studies. Since my departure work has continued with MerB, including use of a maltose-binding protein-3C protease cleavage site (MBP-3C) tag for the preparation of MerB, which is a strategy that I introduced to the laboratory for the expression and purification of MerA and is described in Chapter 2.

Although the presentation of the content of this chapter was originally constructed in collaboration with Dr. Miller, I have independently (re)written this chapter without relying on any other contributors.

—Ian Harwood, 2012

I, Ms. Rachel Nauss, certify to the best of my knowledge, that the above background and description of the chapter authors' contributions are accurate.

—Ms. Rachel Nauss, 2012

[Reprinted from a communication to Dr. Miller on August 29, 2012]

## Introduction

Mercuric ion reductase (MerA) is the central protein of the bacterial *mer* mercury resistance pathway and is responsible for reducing $Hg^{2+}$ to $Hg^0$. Like other members of the class-I pyridine nucleotide-disulfide oxidoreductase protein family, which include glutathione reductase (GR) and the high $M_r$ (~55 kDa) thioredoxin reductases (TrxR) of higher eukaryotes, MerA is a homodimeric flavoprotein that noncovalently binds flavin adenine dinucleotide (FAD) (Williams et al. 2000; Argyrou and Blanchard 2004; "Reorganizing the protein space at the Universal Protein Resource (UniProt)" 2012). These flavoproteins reduce their substrate by utilizing one FAD per protein monomer to mediate the transfer of reducing equivalents from nicotinamide adenine dinucleotide phosphate (NADPH) to their substrate (GR reduces glutathione, a ~307 Da tripeptide which serves as the primary thiol buffer molecule in the cell, from its oxidized (GSSG) to reduced form (GSH); TR reduces thioredoxin (TRX), a ubiquitous ~12 kDa protein with two redox-active cysteines). The catalytic cores of these proteins are obligate homodimers composed of two ~50 kDa monomers, each with one (GR) or two (TrxR, MerA) thiol pairs that collectively form two symmetrically positioned active sites at the monomer interface (Scheme 1 inset) (Argyrou and Blanchard 2004; Ledwidge et al. 2005a).

While MerA catalytic core (Core) bears homology to GR, TrxRs, and other members of the protein family (Fox and Walsh 1982; Brown et al. 1983; Williams et al. 2000), the majority of MerAs identified in GenBank (Barkay et al. 2003) also feature a ~7 kDa βαββαβ ferredoxin-type fold heavy-metal-associated (HMA) N-terminal domain

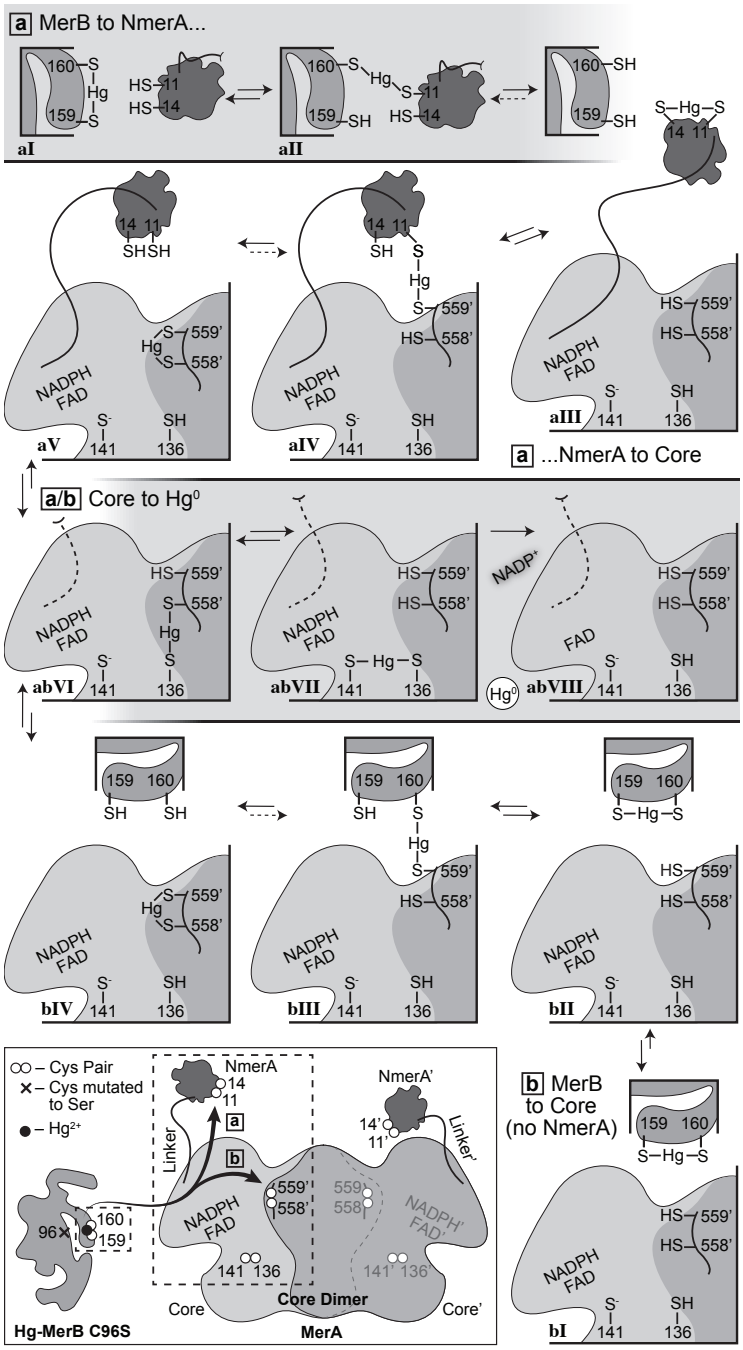


**Scheme 1**. $Hg^{2+}$-ligand exchange pathways for pDU1358 [a] full length MerA and [b] Core. The inset shows $Hg^{2+}$ (filled circle) bound to C159 and C160 of R831b MerB C96S, a mutant of the organomercurial lyase in which Cys96 has been mutated to Ser (×), and the full length MerA homodimer. Cysteines are represented as open circles. In this scheme, $Hg^{2+}$ from the Hg-MerB C96S substrate is acquired first by NmerA (aI-aIII) and the delivered to the Core's C-terminal thiols (aIII-aV) or directly by Core's C-terminal thiols (bI-bIV). MerA residue numbers also correspond to Tn*501* MerA; Tn*21*'s C-terminal thiols are C561 and C562, and inner cysteines are C135 and C140.

(Brown et al. 1983; Summers 1986; "Reorganizing the protein space at the Universal Protein Resource (UniProt)" 2012). This domain, termed NmerA, is tethered to the Core monomer by a ~30-amino-acid flexible linker (Scheme 1 inset) (Johs et al. 2011). MerAs with a single NmerA domain per monomer, the focus of our studies here, include the well-characterized MerA proteins originally obtained from *Serratia marcescens* (of the plasmid pDU1358) (Griffin et al. 1987), *Shigella flexneri* (carried by the Tn*21* transposon of the plasmid NR1) (Nakahara et al. 1979; Johs et al. 2011), and *Pseudomonas aeruginosa* (carried by the Tn*501* transposon of plasmid pVS1) (Stanisich 1974; Stanisich et al. 1977; Fox and Walsh 1983; Distefano et al. 1989; Miller et al. 1989; Moore and Walsh 1989; Distefano et al. 1990; Engst and Miller 1999; Ledwidge et al. 2005a; Ledwidge et al. 2005b; Hong et al. 2010; Ledwidge et al. 2010). The only two known exceptions to the NmerA-linker-Core paradigm include the MerA isolated from *Streptomyces lividans*, which does not contain an NmerA domain (Sedlmeier and Altenbuchner 1992), as well as the MerA obtained from *Bacillus* sp. strain RC607, which features two tandem NmerA domains per monomer (Wang et al. 1989). In addition to being the only known class-I pyridine nucleotide disulfide oxidoreductase to reduce $Hg^{2+}$ (Miller 1999; Barkay et al. 2003), MerA is also the only known protein family member to feature a flexibly tethered accessory domain. However, NmerA is not essential for resistance as shown by the *Streptomyces lividans* MerA which lacks the domain (Sedlmeier and Altenbuchner 1992). Furthermore, site-directed mutagenesis of Tn*501* NmerA's $Hg^{2+}$-binding thiols, C11 and C14 (Scheme 1), to alanines does not alter MerA function or $Hg^{2+}$ resistance (Moore and Walsh 1989). In the absence of NmerA, Core's essential C-terminal tail C558' and 559' (numbering refers to Tn*501* and pDU1358

MerA; C561' and C562' are the cognate C-terminal cysteines in Tn*21* MerA) receive $Hg^{2+}$ (Scheme 1, bII through bVI) and deliver it to C136 and C141 of the complementary monomer (Scheme 1, abVI though abVII) to be reduced to $Hg^0$ (Scheme 1, abVIIII) (Moore and Walsh 1989; Moore et al. 1992).

As the above evidence has shown that MerA Core and the *mer* resistance pathway is viable without expression of a functional NmerA, we are interested in determining the role of NmerA in the mercury resistance pathways of cells harboring *mer* loci that confer either narrow-spectrum resistance to $Hg^{2+}$-only, such as Tn*21* and Tn*501*, or broad-spectrum operons which resist $Hg^{2+}$ and organomercurials [RHg(I)], such as the *mer* loci of pDU1358 and of R831b (Begley et al. 1986a, b; Pitts and Summers 2002; Barkay et al. 2003; Di Lello et al. 2004). In comparing the effect of expressing NmerA with Core as separate proteins versus the Core alone in cells lacking GSH, it was determined *in vivo* that expression of NmerA significantly enhanced cell survival (Ledwidge et al. 2005a). This observation led to the proposal that NmerA lessens oxidative and electrophilic stress by preventing undesirable $Hg^{2+}$ binding to cellular thiols. Additionally, the Miller group has demonstrated *in vitro* that NmerA can acquire $Hg^{2+}$ liganded to GSH (Ledwidge et al. 2005a), non-*mer* proteins such as TRX, and to the broad-spectrum resistance pathway's organomercurial ligase MerB (Scheme 1 aI through aIII) (Hong et al. 2010). With each of these $Hg^{2+}$-substrates, NmerA provides a significant kinetic advantage in mercury reduction. Based on kinetics studies of the acquisition of $Hg^{2+}$ liganded to GSH (Ledwidge et al. 2005a) or MerB (Hong et al. 2010) by NmerA and Core expressed as separate (untethered) proteins, it has been hypothesized that, in full length MerA, $Hg^{2+}$ is

preferentially acquired by NmerA and then delivered by NmerA to the Core's C-terminal thiols for downstream reduction (Scheme 1a). However, it is not understood how NmerA provides this advantage, especially as acquisition of $Hg^{2+}$ by NmerA and the subsequent handoff of $Hg^{2+}$ to Core from Hg-NmerA (Scheme 1a) introduces additional steps in MerA's $Hg^{2+}$-ligand exchange pathway relative to that of Core alone (Scheme 1b).

The aforementioned *in vitro* studies that have examined the kinetics of $Hg^{2+}$ acquisition by NmerA and Core's C-terminal thiols and the steady state kinetics of $Hg^{2+}$ reduction have utilized both NmerA and Core as discrete (untethered) proteins and samples of 95% pure and intact full-length MerA (with NmerA and Core tethered). At the time of these studies the production of pure, intact MerA was difficult due to proteolytic cleavage in linker region (Ledwidge et al. 2005a). Recently we developed a method for producing pure, intact Tn*21* MerA (Johs et al. 2011) which allows us here to present three kinetics studies on $Hg^{2+}$ acquisition and reduction by the full length reductase to further understand the role NmerA plays in resistance to broad- and narrow-spectrum mercurials.

First, we examine the equilibrium of $Hg^{2+}$ binding between NmerA and Core's C-terminal thiols. Our previous studies using Tn*501* NmerA and Core showed that $Hg^{2+}$ has a strong affinity for NmerA over Core and, based on these results, we hypothesized the same would be true for both regions when tethered together (Ledwidge et al. 2005b). By measuring the generation of thionitrobenzoate (TNB) upon the release of $Hg^{2+}$ from mercuric bis(thionitrobenzoate) [$Hg(TNB)_2$] using absorption spectroscopy in

combination with the change in FAD fluorescence upon $Hg^{2+}$ binding to Core's C561, we determined where $Hg^{2+}$ binds when MerA is titrated with zero to three equivalents of $Hg^{2+}$ per monomer. However, by their nature, these equilibrium experiments could not inform us as to whether the Core's C-terminal thiols acquire $Hg^{2+}$ directly from $Hg(TNB)_2$ or if NmerA first acquires $Hg^{2+}$ from $Hg(TNB)_2$ and then delivers it to the Core. To address this question, we next studied the rates of $Hg^{2+}$ acquisition from $Hg(TNB)_2$ by NmerA and Core using a stopped-flow mixing apparatus again by monitoring TNB generation and FAD fluorescence.

Both of these above equilibrium and kinetics studies further our understanding of the role of NmerA in processing of $Hg^{2+}$ liganded to small molecules such as GSH. We have also been interested in NmerA's role in acquiring $Hg^{2+}$ liganded to proteins. Previously Miller and coworkers studied the kinetics of $Hg^{2+}$ reduction by the narrow-spectrum Tn*501* MerA using Hg-TRX as a substrate (Ledwidge et al. 2005a), as well as the rate at which the broad-spectrum pDU1358 NmerA can acquire $Hg^{2+}$ from MerB (Hong et al. 2010). In the final set of experiments presented in this chapter we report the first kinetic studies of $Hg^{2+}$ reduction utilizing pure pDU1358 MerA using both $Hg(SG)_2$ and Hg-MerB as substrates. Unlike the aforementioned studies of $Hg^{2+}$ turnover using Hg-TRX with MerA of the Tn*501 mer* locus (Ledwidge et al. 2005a), which does not code for an cytosolic $Hg^{2+}$-binding protein that is an in-pathway substrate for MerA, here we compare the reduction of $Hg^{2+}$ liganded to the upstream *mer* protein MerB by MerA from the broad-spectrum operon of pDU1358 and a variant of its Core to further understand the importance of NmerA in resistance to organomercurials. From these three

sets of experiments we conclude that NmerA provides a kinetic advantage to resistance of both broad- and narrow-spectrum mercurials present at physiologically-relevant concentrations.

## Results and Discussion

### Equilibrium of $Hg^{2+}$ binding between NmerA and Core in Tn*21* MerA

Full length MerA has two pairs of thiols per monomer that can receive $Hg^{2+}$ from a substrate. The first set is NmerA's C11 and C14, and both of these residues are exposed to the solvent prior to and upon binding to $Hg^{2+}$ (Scheme 1 aI-aIV) (Ledwidge et al. 2010). The second pair of cysteines reside in tandem at the 4- and 3-residue positions upstream of the Core's C-terminus (the residue number of these C-terminal thiols varies with each MerA isolate; see Scheme 1). Unlike NmerA's thiols, the Core's C-terminal cysteines alternate between being exposed to the solvent to acquire $Hg^{2+}$ and being buried within the Core (Scheme 1 aIII-aV; bI-bVI) to deliver $Hg^{2+}$ to the complementary MerA monomer's third set of thiols (Scheme 1 abVI-abVII), which are located near the bound FAD and bind $Hg^{2+}$ for reduction to $Hg^0$ (Scheme 1 abVIII) (Ledwidge et al. 2005a). This third pair of thiols is buried within the Core and cannot acquire directly $Hg^{2+}$ from a substrate, as demonstrated by the essential nature of the Core's C-terminal cysteines (Moore and Walsh 1989; Moore et al. 1992). As Core's C-terminal thiols are required for narrow-spectrum resistance but NmerA's cysteines, and the domain itself, are not (Fox and Walsh 1983; Moore and Walsh 1989), there have been various hypotheses as to the role of NmerA's and Core's cysteine pairs in the acquisition of $Hg^{2+}$. NmerA may first acquire $Hg^{2+}$ from a substrate and then deliver it to the Core's C-terminal thiols for processing. Alternately, $Hg^{2+}$ may preferentially bind to the Core's C-terminal cysteines, and NmerA's C11/C14 may serve as a "backup" $Hg^{2+}$ binding site.

To examine the relative affinity of $Hg^{2+}$ for NmerA and Core's C-terminal thiols, the kinetics of $Hg^{2+}$ transfer between Tn*501* MerA's NmerA and Core as separately expressed (untethered) proteins was studied by our group (Ledwidge et al. 2005b). In these experiments, stopped flow mixing was used to determine the rate at which $Hg^{2+}$ was transferred to and from Core by measuring the change in FAD fluorescence. When $Hg^{2+}$ is not bound to the Core's C-terminal thiols (C558 and C559 in Tn*501* MerA), the fluorescence of the bound FAD is quenched by the nearby C558 thiolate (Scheme 2). Upon coordination of $Hg^{2+}$ as C558-$Hg^{2+}$-C559, the resulting increase in fluorescence provides a direct measure of $Hg^{2+}$ binding to the C-terminal cysteines. In these experiments, the "forward" transfer of $Hg^{2+}$ from Hg-NmerA to Core was studied by measuring the increase in FAD fluorescence in a stopped-flow apparatus at various concentrations of Hg-NmerA to maintain pseudo-first order conditions. Likewise, decreases in FAD fluorescence upon the "reverse" transfer of $Hg^{2+}$ from Hg-Core to NmerA at varied concentrations of NmerA were also observed. At every concentration tested, $Hg^{2+}$ favored binding to NmerA over Core ($K_{formHgNmerA}$[1] > $K_{formHgCore}$). For each ratio of Hg-NmerA/Core and NmerA/Hg-Core mixed, the FAD fluorescence of the Core showed that 100% of $Hg^{2+}$ was transferred from Hg-Core to NmerA ("reverse" direction), but less than 100% of $Hg^{2+}$ was transferred from Hg-NmerA to Core ("forward" direction) (Ledwidge et al. 2005b). This was surprising as we had hypothesized that the affinity of $Hg^{2+}$ for each of MerA's thiol pairs would increase in the forward $Hg^{2+}$-ligand exchange pathway [NmerA cysteine pair (Scheme 1 aIII) < Core C-terminal cysteine pair (Scheme 1 aV) < Core inner cysteine pair (Scheme abVII)].

[1] $K_{form}$, formation constant; $k_{form}$, rate constant.

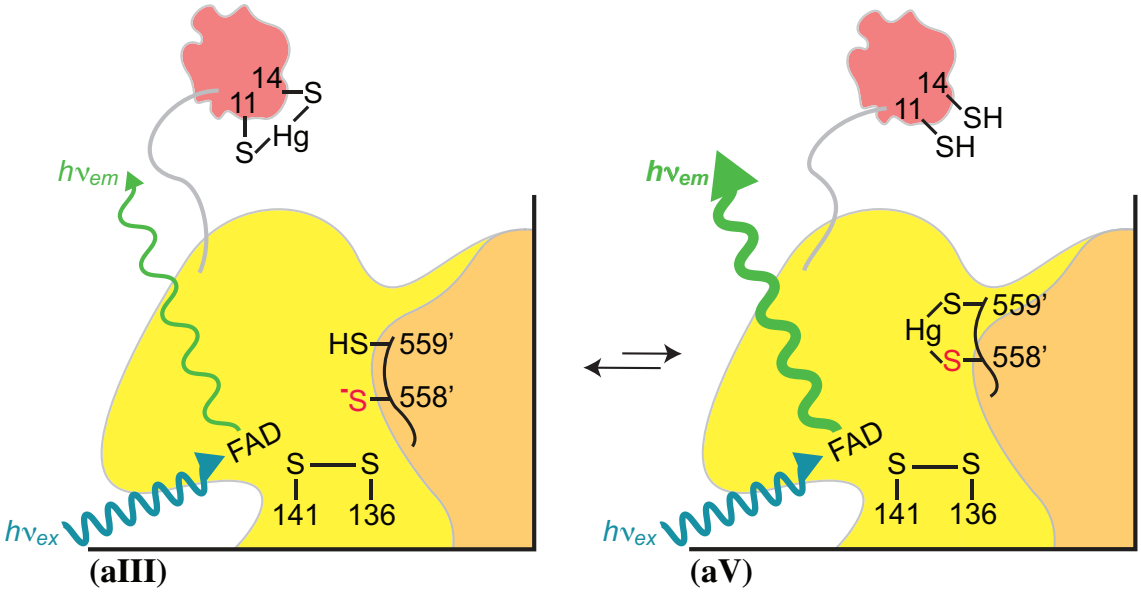


**Scheme 2.** FAD fluorescence quenching in the presence of the C558 thiolate (left) and emission upon coordination of $Hg^{2+}$ as C558-Hg-C559 (right) in full length MerA. Residue numbering refers to Tn*501* and pDU1358 MerA for consistency with Scheme 1, although Tn*21* was used in the equilibrium and kinetics studies presented in this chapter (Tn*501*'s and pDU1358's NmerA's C11/C14 and Core's C-terminal C558/C559 correspond to Tn*21* MerA's C11/C14 and C561/C562, respectively). In these experiments, the Core inner cysteines C136 and C141 (C135 and C140 in Tn*21* MerA) are oxidized and unable to bind $Hg^{2+}$. The C558 thiol (C561 in Tn*21* MerA) is highlighted in red. The "forward" transfer of $Hg^{2+}$ from Hg-NmerA to Core is represented from left to right, and "reverse" $Hg^{2+}$ transfer from right to left. The panel labels aIII and aV correspond to the panels of Scheme 1. Figure adapted from Ledwidge et al. 2005b.

Unlike the above experiments, which treated NmerA and Core as individual proteins, here the equilibrium of $Hg^{2+}$ binding between NmerA and Core when natively tethered together is examined, as is the case in full length Tn*21* MerA. Tn*21* MerA was used as it was readily available and is ~90% identical in sequence to Tn*501* MerA (Tn*21* NmerA's C11/C14 and Core's C-terminal C561/C562 correspond to Tn*501* MerA C11/C14 and C558/C559, respectively) (Johs et al. 2011). Unlike the above studies in which the concentration of NmerA could be varied relative to that of Core, the ratio of NmerA to Core in intact MerA is fixed at 1:1.

First we sought to determine the maximum number of $Hg^{2+}$ ions each MerA monomer can simultaneously bind. As there had been no evidence to suggest otherwise, each monomer of full length MerA was expected to bind a maximum two equivalents of $Hg^{2+}$, one to the NmerA's C11/C14 thiol pair, and the other to the Core C-terminal C561/C562 cysteine pair. In these experiments, the Core inner cysteines (C135 and C140) are oxidized and unable to bind $Hg^{2+}$. MerA was titrated with zero to 3.0 equivalents of mercuric bis(thionitrobenzoate) [$Hg(TNB)_2$] per MerA monomer and the increase in absorption at 450 nm arising from the generation of TNB upon $Hg^{2+}$ release was monitored (Ledwidge et al. 2005a). As expected, a maximum of four equivalents of TNB per MerA monomer were generated over the course of the titration, indicative of a maximum of two equivalents of $Hg^{2+}$ being acquired by each MerA monomer (Figure 1a, black). This result shows that, in full length MerA, binding of $Hg^{2+}$ to NmerA does not prevent Core from acquiring $Hg^{2+}$ under equilibrium conditions, or *vice versa*.

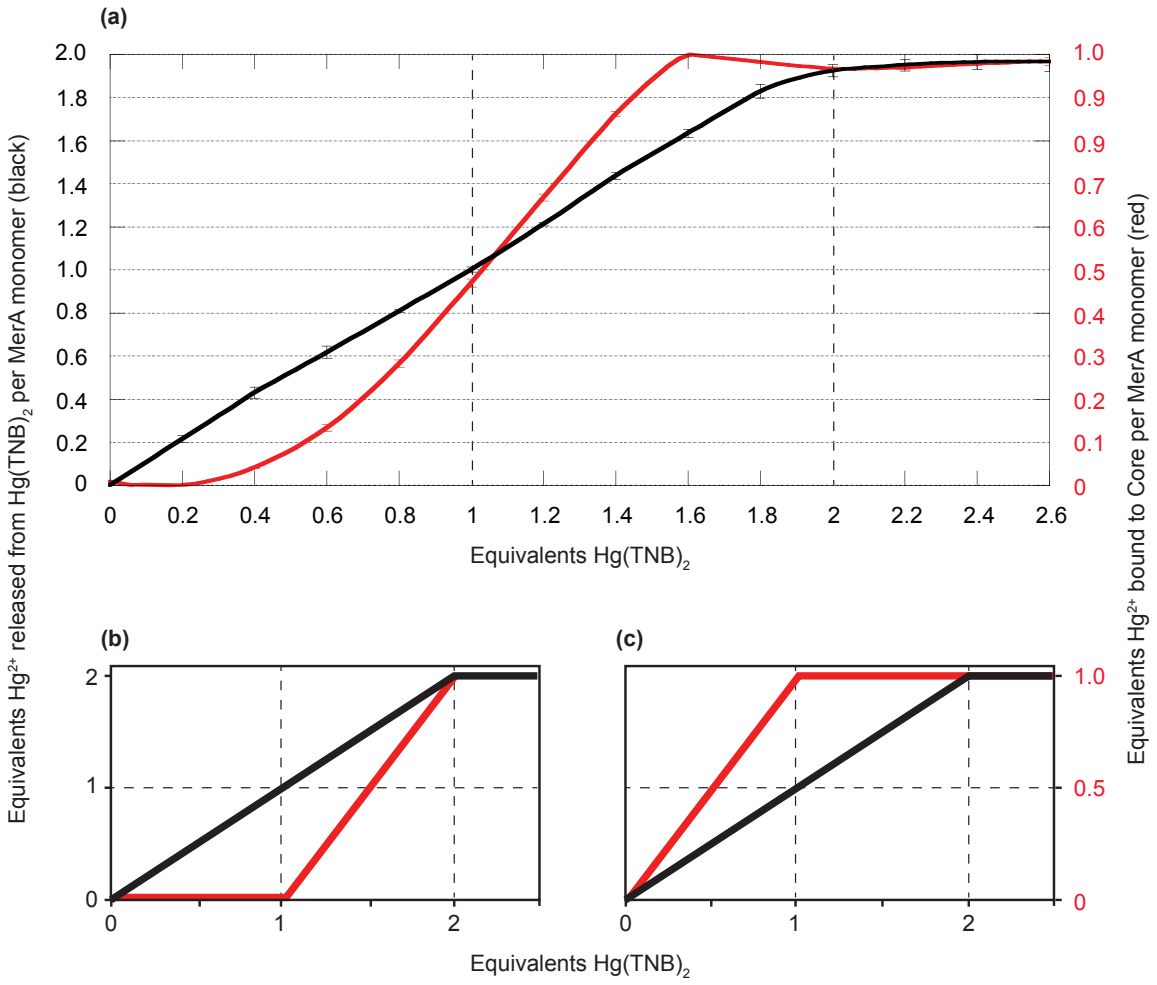


**Figure 1.** Titration of Tn*21* MerA with zero to 3.0 equivalents of $Hg(TNB)_2$ (up to 2.6 equivalents are shown, as no change was observed beyond this point). MerA prepared for these experiments is able to bind two equivalents of $Hg^{2+}$ per MerA monomer, one to the NmerA C11/C14 pair, and the other to the Core C561/C562 pair. (a) Equivalents per MerA monomer of $Hg^{2+}$ released from $Hg(TNB)_2$ as determined by TNB generation and absorbance at 450 nm (black, left axis), and of $Hg^{2+}$ bound to C561, measured by FAD fluorescence (red, right axis). Error bars represent standard error of triplicate measurements. The almost 1:1 ratio of $Hg(TNB)_2$ added to $Hg^{2+}$ released indicates all $Hg^{2+}$ binds to MerA upon addition of $Hg(TNB)_2$. As released $Hg^{2+}$ can bind only to either Core or NmerA, the difference in the total $Hg^{2+}$ equivalents released from the equivalents of $Hg^{2+}$ bound to Core equals the equivalents of $Hg^{2+}$ bound to NmerA. (b) Model of released $Hg^{2+}$ first saturating NmerA and then Core ($K_{formHgNmerA} >> K_{formHgCore}$), and (c) of $Hg^{2+}$ first saturating Core and then NmerA ($K_{formHgNmerA} << K_{formHgCore}$).

Although monitoring TNB generation allowed us to confirm MerA's ability to acquire two $Hg^{2+}$ per monomer, it did not differentiate as to where $Hg^{2+}$ was binding over the course of the titration. To detect $Hg^{2+}$ binding to the Core's C-terminal thiols across the titration, change in MerA FAD fluorescence was measured, as described above for the separate Hg-NmerA/Core and NmerA/Hg-Core mixing experiments (Ledwidge et al. 2005b). Inner filter effects were avoided by using excitation/emission wavelengths of 490/515 nm, as neither $Hg(TNB)_2$ or TNB absorbs light in this range. As our previous observations of $Hg^{2+}$ binding to separate NmerA and Core, discussed above, showed that $K_{\text{formHgNmerA}}$ is greater than $K_{\text{formHgCore}}$ (Ledwidge et al. 2005b), we hypothesized that no change in fluorescence would be observed until the addition of more than 1.0 equivalent of $Hg(TNB)_2$, as all $Hg^{2+}$ prior to this would first saturate NmerA (Figure 1b). However, a change in FAD fluorescence, indicative of $Hg^{2+}$ binding to Core, was observed beginning upon the addition of ~0.4 equivalents of $Hg(TNB)_2$ per MerA monomer (Figure 1a, red). The FAD fluorescence signal increased linearly from ~0.6 equivalents until ~1.6 equivalents of $Hg(TNB)_2$ added per monomer, at which point the fluorescence signal was at its maximum and the Core C-terminal thiols were saturated with $Hg^{2+}$ (Figure 1a).

As the intracellular concentration of $Hg^{2+}$ is unlikely to ever approach that of MerA (which has been reported to be as high as 6% of the total soluble protein (Fox and Walsh 1982)), since transcriptional induction of the repressed *mer* operon occurs within minutes of exposure to sub-micromolar concentrations of $Hg^{2+}$ (Condee and Summers 1992; Gambill and Summers 1992), the acquisition of $Hg^{2+}$ present at low concentrations

by MerA is of biological relevance. When presented with 0.2 or fewer equivalents of $Hg(TNB)_2$, the lack of a change in fluorescence indicates that MerA binds $Hg^{2+}$ at NmerA's C11/C14 but not at Core's C561/C562. Consistent with our previous observations of NmerA and Core expressed as separate proteins (Ledwidge et al. 2005b), this supports that $K_{formHgNmerA}$ is greater than the $K_{formHgCore}$ for full length MerA. As NmerA is able to more readily acquire $Hg^{2+}$ than Core, our findings suggest that NmerA is especially advantageous to resistance efficiency when intracellular concentrations of mercurials are low, such as after initial exposure to mercurials, and as mercurials are depleted from the intracellular space by reduction of $Hg^{2+}$ by MerA. While these experiments examine the equilibrium of $Hg^{2+}$ binding between NmerA and Core of full length MerA, they do not inform us as to whether the Core's C-terminal thiols acquire $Hg^{2+}$ directly from $Hg(TNB)_2$ when presented with more than 0.4 equivalents of $Hg(TNB)_2$. If the rate of $Hg^{2+}$ acquisition from $Hg(TNB)_2$ by NmerA ($k_{formHgNmerA}$) is far greater than that of Core ($k_{formHgCore}$), $Hg^{2+}$ may first be acquired from $Hg(TNB)_2$ by NmerA then trafficked to the Core as opposed to being directly acquired by the Core's C-terminal thiols. Thus, we examined the kinetics of $Hg^{2+}$ acquisition by NmerA and the Core's C-terminal cysteines, which we discuss below.

## Initial acquisition kinetics of $Hg^{2+}$ by Tn*21* NmerA and Core

In considering the $Hg^{2+}$ reduction pathway for full length MerA, the $k_{cat}$[2] of $Hg^{2+}$ reduction may be limited by all forward steps after the initial encounter of MerA and the Hg-substrate (Scheme I aII through abVIII), the first of which is loss of the second substrate ligand during the acquisition of $Hg^{2+}$ by NmerA (aII through aIII) and its subsequent transfer from NmerA to Core (aIII through aV). Although the acquisition of $Hg^{2+}$ by NmerA and the subsequent handoff of $Hg^{2+}$ to Core from Hg-NmerA (Scheme 1a) introduces additional steps in MerA's $Hg^{2+}$-ligand exchange pathway relative to that of Core alone (Scheme 1b), previous measurements of these steady state kinetic constants for Tn*501* MerA and Core show that these steps do not limit the rate of $Hg^{2+}$ reduction (Table 1). When presented with $Hg(SG)_2$, the $k_{cat}$ for Tn*501* MerA (9.4 ± 0.1 $s^{-1}$) is slightly faster than that for Core (8.7 ± 0.1 $s^{-1}$) under the same conditions (Ledwidge et al. 2005a).

Similarly, the $k_{cat}/K_{MHg}$ for MerA, which only includes steps from the initial encounter with $Hg^{2+}$ through the first irreversible step, will be primarily limited by the acquisition of $Hg^{2+}$ by NmerA (Scheme I aI through aIII) (and possibly the trafficking of $Hg^{2+}$ by NmerA to Core, Scheme 1 aIV). Previous steady state kinetic studies of $Hg^{2+}$ reduction showed that Tn*501* MerA has a ~2.2-fold lower $K_{MHg}$ (10.7 ± 0.6 μM) than Core (24.0 ± 1.0 μM) when $Hg(SG)_2$ was used as a substrate (Table 1) (Ledwidge et al. 2005a). We hypothesize that MerA's higher $k_{cat}/K_{MHg}$ and lower $K_{MHg}$ is due to higher $k_{onHg}$ for NmerA's C11/14 than to Core's C-terminal C558/559. Unlike MerA's

[2] See Scheme 3 for a minimalistic model of $Hg^{2+}$ acquisition and reduction to $Hg^0$.

$$A + Hg\text{-}X \underset{k_{off}}{\overset{k_{on}}{\rightleftharpoons}} Hg\text{-}A + X \xrightarrow{k_{cat}} A + Hg^0 + X$$

$$K_{MHg} = (k_{off} + k_{cat}) / k_{on}$$

**Scheme 3.** Minimalistic model of $Hg^{2+}$ acquisition and reduction to $Hg^0$. X represents the appropriate mercury ligand, and A represents the appropriate species of either MerA or Core. In discussing the acquisition of $Hg^{2+}$ by NmerA, A in the first half of this scheme can represent NmerA expressed as a separate protein but, as NmerA can not reduce $Hg^{2+}$ to $Hg^0$, the second half of the scheme is not applicable. When A represents the full length protein, $k_{cat}$ is inclusive of the transfer of $Hg^{2+}$ from the tethered NmerA to Core as shown in Scheme 1 aIII-aV.

**Table 1.** Comparison of steady-state values for Tn*501* MerA, Tn*501* Core, and Tn*21* MerA with $Hg(SG)_2$ as the $Hg^{2+}$ substrate[a]

| Enzyme | $k_{cat}$ ($s^{-1}$) | $K_{MHg}$ (μM) | $k_{cat}/K_{MHg}$ ($M^{-1}\ s^{-1} \times 10^{-5}$) |
|---|---|---|---|
| Tn*501* MerA[b] | 9.4 ± 0.1 | 10.7 ± 0.6 | 8.8 ± 0.5 |
| Tn*501* Core[b] | 8.7 ± 0.1 | 24.0 ± 1.0 | 3.6 ± 0.2 |
| Tn*21* MerA[c] | 8.8 | 14.6 | 6.0 |

[a] Conditions: 50 mM $KP_i$, pH 7.3, 50 μM NADPH, 25 nM enzyme, 25 °C, and 1 mM excess GSH. $Hg(SG)_2$ reactions contain 1 mM excess GSH in part to mimic the cellular environment where small molecular weight thiols are present at millimolar levels, and in part to avoid formation of a covalent adduct of $Hg^{2+}$ with NADPH (Marshall et al. 1984).

[b] From Ledwidge et al. 2005a.

[c] From Johs et al. 2011.

C-terminal tail, which can adopt buried conformation(s) and occlude its cysteines from the solvent (Ledwidge et al. 2005a), NMR studies of NmerA show that its C11 and C14 are constitutively exposed (Ledwidge et al. 2010). Additionally, our structural studies of MerA have shown that the NmerA-linker is able to adopt an ensemble of multiple conformations, positioning NmerA up to ~80 Å from Core (Johs et al. 2011). The ability of NmerA to sample a large volume of solvent as a result of the linker flexibility, along with to the accessibility of its two cysteines, may aid in NmerA acquiring $Hg^{2+}$ from substrates more rapidly than Core.

Here we sought to measure the kinetics of $Hg^{2+}$ acquisition by full length Tn*21* from $Hg(TNB)_2$ using a stopped-flow mixing apparatus. In these experiments, MerA was mixed with either 0.5, 1, and 2 equivalents of $Hg(TNB)_2$, respectively, and the increase in absorbance arising from the generation of TNB upon the release of $Hg^{2+}$ from $Hg(TNB)_2$ was monitored as a function of time (Figure 2 a and b). Prior to the addition of $Hg(TNB)_2$, the initial absorbance at 450 nm of 0.115 was due to the presence of the FAD in MerA. First, the increase in absorbance signal at 450 nm after mixing each concentration of $Hg(TNB)_2$ used with MerA was measured for 5 minutes and the FAD absorbance was subtracted to calculate the amount of TNB generated (data not shown). As expected, 1, 2, or 4 equivalents of TNB were generated, respectively, which is indicative of the release of 0.5, 1, and 2 equivalents of $Hg^{2+}$ per MerA monomer. To observe the initial release of $Hg^{2+}$ from $Hg(TNB)_2$, the change in absorbance upon TNB generation for 40 ms and 500 ms after mixing was measured (Figure 2 a and b, respectively). When MerA is mixed with 0.5 equivalents of $Hg(TNB)_2$, ~83% of the total change in absorbance signal due to

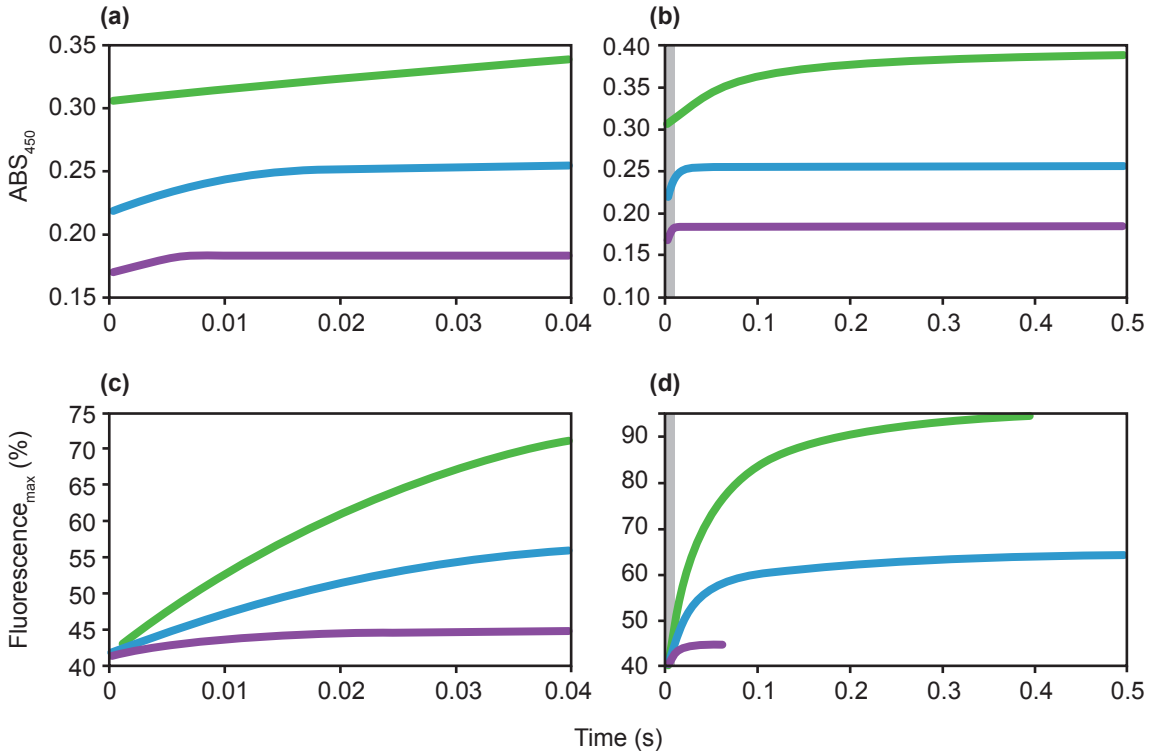


**Figure 2.** Stopped-flow measurements of Tn*21* MerA reacted with $Hg(TNB)_2$. 10 μM MerA (final concentration after mixing) was mixed with either 0.5 (purple), 1.0 (blue), or 2.0 (green) equivalents of $Hg(TNB)_2$ per MerA monomer at 25 °C. (a) 450 nm absorbance from 1.54 ms (dead time) to 40 ms due to release of TNB upon transfer of $Hg^{2+}$ from $Hg(TNB)_2$ to MerA cysteines. The initial absorbance at 450 nm was 0.115 due to the presence of the FAD in MerA. Upon mixing MerA with $Hg(TNB)_2$, ~83% of total TNB for the 0.5 equivalent reaction had been produced within the 1.54 ms dead time. (b) TNB generation from 1.54 ms to 0.5 seconds. The absorbance signal at the beginning of the reaction show in (a) is highlighted in the gray area. (c) MerA FAD fluorescence upon excitation at 490 nm resulting from $Hg^{2+}$ binding to the Core C561/C562 thiolate/thiol pair from 1.54 ms to 40 ms. The fluorescence of the protein was ~42% in the absence of $Hg(TNB)_2$ due to the presence of the FAD in MerA. Upon mixing MerA with $Hg(TNB)_2$, the fluorescence signal remained at ~42% for all reactions at 1.54 ms. (d) Fluorescence signal from 1.54 ms to 0.5 seconds. The fluorescence signal at the beginning of the reaction shown in (c) is highlighted in the gray area. The observation that ~83% of the $Hg(TNB)_2$ is consumed by the dead time without a corresponding increase in fluorescence supports that NmerA first acquires $Hg^{2+}$ and then traffics it to Core. We estimate $k_{\text{formHgNmerA}}$ to be > ~1100 $s^{-1}$, and $k_{\text{formHgCore}}$ to be > ~26 $s^{-1}$, ~42-fold slower than $k_{\text{formHgNmerA}}$.

the generation of TNB is observed within the first 1.54 ms after mixing, the dead time for the instrument. As the starting concentration of $Hg(TNB)_2$ ($C_0$) is known and the concentration of TNB at 1.54 ms can be determined from the absorbance signal at 450 nm, the concentration of $Hg(TNB)_2$ that remains at 1.54 ms ($C_t$) can be calculated as $C_t = C_0 - ½[TNB]_t$ (two TNB are generated per $Hg^{2+}$ released from $Hg(TNB)_2$). If the acquisition of $Hg^{2+}$ from $Hg(TNB)_2$ during the dead time of the instrument is modeled as a pseudo first-order reaction, the rate constant ($k$) for $Hg^{2+}$ acquisition can be calculated as $k = -\ln(C_t/C_0) \times t^{-1}$, which here we estimate to be at least ~1100 $s^{-1}$.

The increase in FAD fluorescence that resulted upon $Hg^{2+}$ binding to MerA's C-terminal C561 was also observed (Figure 2 c and d). Here the baseline fluorescence was set to zero prior to addition of MerA, and the maximum fluorescence signal was set to 100% after equilibration of MerA with 2.0 equivalents of $Hg(TNB)_2$ for 5 minutes. Prior to mixing with $Hg(TNB)_2$, MerA mixed with just buffer fluoresced at ~42% of the maximum observed signal. Unlike the absorbance signal, the observed fluorescence did not change within the dead time after mixing. Thus, the rate constant of at least ~1100 $s^{-1}$ estimated above from the absorbance data is attributed to the acquisition of $Hg^{2+}$ by NmerA ($k_{formHgNmerA}$). As no change in fluorescence is observed within the dead time of the measurement, during this period $Hg^{2+}$ is only acquired by NmerA and not by Core. The change in fluorescence was used to determine the fraction of MerA's C-terminal cysteines at 0.01 s that, upon mixing with 0.5 or 1.0 equivalents of $Hg(TNB)_2$, had not acquired $Hg^{2+}$, which in turn was used to fit the data to a single exponential. Here, we estimate the $k_{formHgCore}$ to be at least ~26 $s^{-1}$, about ~42-times slower than that of NmerA.

Upon mixing with 2.0 equivalents of $Hg(TNB)_2$, a small secondary reaction phase was observed in the fluorescence trace which, although we have not been able to satisfactorily model, is likely to be the result of Core directly acquiring $Hg^{2+}$ from $Hg(TNB)_2$. As the change in absorbance signal (but lack thereof in the fluorescence signal) supports that $Hg^{2+}$ is first acquired by NmerA and not by Core, we conclude that the dominant reaction phase observed in the fluorescence signal and, ignoring the contributions of the minor phase, the estimated $k_{formHgCore}$ is that of Core's C-terminal thiols acquiring $Hg^{2+}$ from Hg-NmerA.

The above stopped-flow observations support that $Hg^{2+}$, when not present at saturating concentrations as is expected *in vivo*, is first rapidly acquired by NmerA and then trafficked to the Core's C-terminal thiols, as opposed to being directly acquired by Core. As the steady state $k_{cat}$ for $Hg^{2+}$ reduction by Tn*21* MerA when using $Hg(SG)_2$ as a substrate is 8.8 $s^{-1}$ (Table 1) (Johs et al. 2011), which is ~3-fold slower than the estimated $k_{formHgCore}$, our results show that neither the 2$^{nd}$ step of NmerA's acquisition of $Hg^{2+}$, when liganded to small molecules such as glutathione, or its subsequent trafficking of $Hg^{2+}$ to Core is limiting to the rate of $Hg^{2+}$ reduction. *In vivo*, however, MerA must not only acquire $Hg^{2+}$ liganded to small molecules but also from Hg-protein complexes, the kinetics of which we discuss later in this chapter.

## Hypotheses for why NmerA does not decrease the MerA steady state $k_{cat}$

Given our understanding of the structure of MerA and kinetics of $Hg^{2+}$ turnover by the full length protein and by Core, we offer two possible explanations of how NmerA, after acquiring $Hg^{2+}$ from a small molecule substrate such as $Hg(SG)_2$ or $Hg(TNB)_2$, increases the $k_{cat}$ of $Hg^{2+}$ reduction even though its presence adds complexity and additional steps to the handoff mechanism. First, the binding of $Hg^{2+}$ to NmerA may allosterically induce a conformational change in the otherwise disordered linker region which serves to tether NmerA to Core. Such a change may restrict the conformations that NmerA may occupy to ones proximal to the catalytic core's C-terminus between the time NmerA acquires $Hg^{2+}$ and delivers it to Core (Schme I aIII to aIV). In comparison to a diffusion-limited mechanism, a positioned NmerA would be able to more readily present $Hg^{2+}$ to the C-terminus, therefore increasing the rate at which NmerA approaches a handoff-compatible conformation. There have been no studies to date that support or negate this hypothesis. Secondly, an interaction between Hg-NmerA and the catalytic core may stimulate the exposure of the C-terminal thiols from within the catalytic core (note that in Scheme I aIII, the C-terminus is buried within Core, whereas in aIV, C562 is accessible to the solvent). We have shown that the orientation of Tn*21* NmerA relative to that of the catalytic core is well-defined when handing off $Hg^{2+}$ to C562' (Scheme 1 aVI) (Johs et al. 2011). Secondary interactions between NmerA and the catalytic core may encourage more frequent delivery of $Hg^{2+}$ to the C-terminus. Either hypothesis or a combination of both may account for the observed increase in the apparent $k_{cat}$.

## Steady state kinetics of the broad-spectrum pDU1358 MerA with small molecule-Hg and protein-Hg substrates

Although our above studies have focused on MerA's ability to acquire $Hg^{2+}$ liganded to small molecules such as glutathione, we are also interested in the MerA's ability to acquire $Hg^{2+}$ liganded to proteins. For example, when intracellular glutathione concentrations of glutathione are diminished, $Hg^{2+}$ may become liganded to non-*mer* pathway proteins such as TRX. Previous studies of Tn*501* MerA showed that the steady state $k_{cat}$ using Hg-TRX as a substrate ($9.0 \pm 0.1\ s^{-1}$) is similar to the $k_{cat}$ observed using $Hg(SG)_2$ as a substrate ($9.4 \pm 0.1\ s^{-1}$)[3] (Table 2) (Ledwidge et al. 2005a). Thus, for these "off-pathway" substrates, the delivery of $Hg^{2+}$ by NmerA to Core is not limited by the nature of the substrate.

However, to prevent the non-specific dispersion of $Hg^{2+}$ to other cellular proteins and small molecule thiols such as GSH and TRX, *mer* pathway proteins themselves also serve as $Hg^{2+}$-substrates for MerA (Barkay et al. 2003; Ledwidge et al. 2005a; Hong et al. 2010; Johs et al. 2011). In cells harboring narrow-spectrum *mer* loci, such as Tn*21* and Tn*501*, the transmembrane $Hg^{2+}$-transporter MerT is believed to import $Hg^{2+}$ to its cytoplasmic cysteine pair, from where it is acquired by NmerA (Barkay et al. 2003; Rossy et al. 2004; Schue et al. 2008). Direct acquisition of $Hg^{2+}$ by NmerA from MerT has yet to be demonstrated, but bacterial two-hybrid studies have suggested some type of

[3] It should be noted that in reactions using $Hg(SG)_2$ as a substrate, 1 mM excess GSH was included in the reaction mixture in part to mimic the cellular environment where small molecular weight thiols are present at millimolar levels, and in part to avoid formation of a covalent adduct of $Hg^{2+}$ with NADPH. In the Hg-TRX reactions, no excess of GSH was used, as to prevent the formation of $Hg(SG)_2$ as a secondary substrate.

**Table 2.** Comparison of steady-state values for Tn*501* MerA with $Hg^{2+}$ liganded to a protein as the substrate (from Ledwidge et al. 2005a)[a]

| Substrate[b] | $k_{cat}$ ($s^{-1}$) | $K_{MHg}$ (μM) | $k_{cat}/K_{MHg}$ ($M^{-1}$ $s^{-1}$ × $10^{-5}$) |
|---|---|---|---|
| $Hg(SG)_2$ | 9.4 ± 0.1 | 10.7 ± 0.6 | 8.8 ± 0.5 |
| Hg(TRX) | 9.0 ± 1.0 | 297 ± 58 | 0.3 ± 0.07 |

[a] Conditions: 50 mM $KP_i$, pH 7.3, 50 μM NADPH, 25 nM enzyme, 25 °C.

[b] When $Hg(SG)_2$ was used as the substrate, 1 mM excess GSH was included in the reaction mixture in part to mimic the cellular environment where small molecular weight thiols are present at millimolar levels, and in part to avoid formation of a covalent adduct of $Hg^{2+}$ with NADPH. When Hg-TRX was used as a substrate, no excess of GSH was used, as to prevent the formation of $Hg(SG)_2$ as a secondary substrate.

protein-protein interaction between MerA and MerT (Schue et al. 2008). NmerA has also been shown to acquire $Hg^{2+}$ from a peptide based on MerT's intracellular loop that contains the aforementioned cysteine pair (Rossy et al. 2004). In cells harboring broad-spectrum *mer* loci, such as that of pDU1358, MerA acquires $Hg^{2+}$ from the organomercurial lyase MerB, which first generates $Hg^{2+}$ from organomercurials by catalyzing the cleavage of the C-Hg bond (Pitts and Summers 2002; Lafrance-Vanasse et al. 2009). Previously studies have qualitatively supported that $Hg^{2+}$ is transferred directly from MerB to MerA (Schottel 1978), and we have examined the abilities of pDU1358 NmerA and Core expressed as individual (untethered) proteins to acquire $Hg^{2+}$ liganded to R831b MerB, which differs from pDU1358 MerB by only one amino acid (L10R). In those studies, we showed that the apparent second order rate constant for $Hg^{2+}$ transfer from R831b MerB to pDU1358 NmerA (~$2.3 \pm 0.1 \times 10^4$ $M^{-1}s^{-1}$) is ~100-fold greater than that for pDU1358 Core ($1.2 \times 10^4$ $M^{-1}s^{-1}$) or GSH ($1.2 \pm 0.2 \times 10^2$ $M^{-1}s^{-1}$), establishing that NmerA is kinetically favored over Core to acquire $Hg^{2+}$ from MerB (Hong et al. 2010).

Here the steady state kinetics of $Hg^{2+}$ reduction by pDU1358 MerA was studied first using $Hg(SG)_2$ as the $Hg^{2+}$ substrate, and then using a mutant of MerB as an "in-pathway" $Hg^{2+}$-protein substrate. For both sets of experiments pDU1358 MerA and Core were used, paralleling the previous steady state kinetics studies of Tn*501* MerA and Core (Ledwidge et al. 2005a), but we also generated a new full length MerA mutant, termed AACCCC. In this mutant, the two NmerA cysteines have been mutated to alanine, in turn rendering NmerA unable to bind $Hg^{2+}$ while retaining the Core's C-terminal and active

site thiols. As the flexibility of the linker region allows NmerA to occupy a large volume of solvent around the Core (Johs et al. 2011), $Hg^{2+}$-substrates may be sterically occluded from Core's C-terminal cysteines by the presence of NmerA. This steric effect, along with Core's C-terminus being able to adopt solvent inaccessible conformations (Ledwidge et al. 2005a), may limit an Hg-substrate's access to pDU1358 MerA's C-terminal C5568 and C559 (which correspond to C558/C559 of Tn*501* MerA, and C561/C562 of Tn*21* MerA). The use of the AACCCC mutant allows us to study $Hg^{2+}$ acquisition by the Core's C-terminal thiols in the presence of NmerA (and any resulting steric effects) without NmerA being able to bind $Hg^{2+}$. As shown in Table 3, pDU1358 MerA, AACCCC, and Core exhibit similar $k_{cat}$ values for the reduction of $Hg^{2+}$ using $Hg(SG)_2$ as the substrate as have been previously reported for pDU1358 Core (Hong et al. 2010) and Tn*501* MerA and Core (Table 1) (Ledwidge et al. 2005a). For each concentration of $Hg(SG)_2$ used in the measurement, the $k_{obs}$ for $Hg^{2+}$ reduction by full length MerA is faster than that of the cognate $k_{obs}$ for Core and AACCCC (Figure 3). Also, the $K_{MHg}$ for AACCCC is ~20% larger than was measured for Core (Table 3). This increase in $K_{MHg}$ for AACCCC suggests that the physical presence of NmerA in AACCCC may impede direct access of $Hg(SG)_2$ to the C-terminus, decreasing the $k_{on}$ for $Hg^{2+}$ relative to that of Core alone. As no studies have suggested a disadvantage for $Hg^{2+}$ directly exchanging onto the MerA C-terminus, we do not believe this phenomenon is relevant to enzyme function.

Next, we sought to measure the steady state kinetics of $Hg^{2+}$ turnover by pDU1358 using $Hg^{2+}$-MerB as an "in-pathway" $Hg^{2+}$-protein substrate. In wild-type

**Table 3.** Comparison of steady-state values for pDU1358 MerA variants with $Hg(SG)_2$ as the $Hg^{2+}$ substrate[a]

| Enzyme | Enzyme Concentration (nM) | $k_{cat}$ ($s^{-1}$) | $K_{MHg}$ (μM) | $k_{cat}/K_{MHg}$ ($M^{-1}$ $s^{-1}$ × $10^{-5}$) |
|---|---|---|---|---|
| MerA | 15 | 9.6 ± 0.3 | 11.5 ± 1.5 | 8.3 ± 0.9 |
| AACCCC | 50 | 7.3 ± 0.3 | 41.8 ± 4.2 | 1.7 ± 0.1 |
| Core | 15 | 7.4 ± 0.2 | 33.5 ± 3.4 | 2.1 ± 0.2 |
| Core[b] | 50 | 7.7 ± 0.1 | 63.0 ± 3.2 | 1.2 ± 0.1 |

[a] Conditions: 50 mM $KP_i$, pH 7.3, 50 μM NADPH, 25 °C, and 1 mM excess GSH. $Hg(SG)_2$ reactions contain 1 mM excess GSH in part to mimic the cellular environment where small molecular weight thiols are present at millimolar levels, and in part to avoid formation of a covalent adduct of $Hg^{2+}$ with NADPH (Marshall et al. 1984).

[b] From Hong et al. 2010.

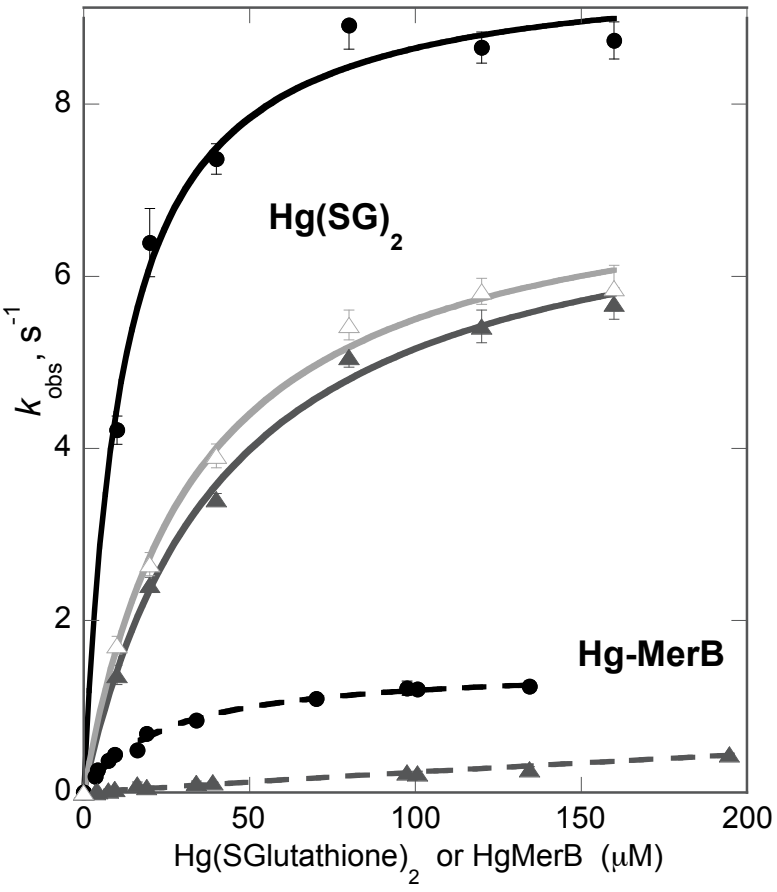


**Figure 3.** Comparison of steady-state $k_{obs}$ of pDU1358 MerA (filled black circles/lines), AACCCC MerA (filled dark gray triangles/lines), and Core (open light gray triangles/lines) with $Hg(SG)_2$ (solid lines) and Hg-MerB C96S (dashed lines) as substrates. Conditions as described in Tables 3 and 4.

MerB, $Hg^{2+}$ generated upon protonolytic cleavage of the mercury-carbon bond in organomercurial compounds equilibrates between MerB's three active site thiols (C96, C159, and C160). When $Hg^{2+}$ can be coordinated in part by C96, as is the case for wild-type MerB, the $k_{max}$ of $Hg^{2+}$ transfer from MerB to NmerA was determined to be $5.23 \pm 0.22$ $s^{-1}$ (Hong et al, 2010). C96 is buried within the protein and coordination of $Hg^{2+}$ in part by C96 makes $Hg^{2+}$ less accessible to the solvent, helping to avoid non-specific dispersion of the metal ion (Benison et al. 2004; Di Lello et al. 2004; Lafrance-Vanasse et al. 2009). However, unlike C96, C159 and C160 are located on a solvent-accessible flexible loop and a mutant of MerB in which Cys96 has been substituted with a Ser is only able to coordinate $Hg^{2+}$ as C159-Hg-C160. It was determined that the $k_{max}$ of $Hg^{2+}$ release from this MerB mutant, termed MerB C96S, to NmerA is $631.3 \pm 30.6$ $s^{-1}$, which is ~120-fold faster than release from wild-type MerB (unpublished data by Hong, Nauss, and Miller). For our work here we did not want the rate of $Hg^{2+}$ acquisition from MerB by NmerA (Scheme 1 aI-aIII) or by the Core's C-terminal thiols (Scheme 1 bII-bIV) to be limited by the above effects of C96, and thus we chose to use Hg-MerB C96S as the $Hg^{2+}$ substrate. In measuring the steady state kinetics of $Hg^{2+}$ reduction when Core's C-terminal C558 and C559 acquire $Hg^{2+}$ from MerB C96S, we chose to use AACCCC instead of Core. Since our experiments above showed that the presence of NmerA can occlude $Hg(SG)_2$ (~811 Da) from the Core's C-terminal thiols, the use of AACCCC allows us to compare $Hg^{2+}$ acquisition from the much larger MerB C96S (24 kDa) by NmerA and by the Core's C-terminal thiols considering this steric occlusion effect.

It was previously determined that $Hg^{2+}$ reduction by Tn*501* MerA using $Hg(SG)_2$ as the substrate (Table 4) is ~29-fold more catalytically efficient than using Hg-TRX (Table 1) (Ledwidge et al. 2010). The differences between these respective $k_{cat}/K_{MHg}$ values is predominantly due to an ~27-fold increase in $K_{MHg}$ from 10.7 ± 0.6 μM, when $Hg(SG)_2$ was used, to 287 ± 58 μM, when Hg-TRX was used as an "off-pathway" $Hg^{2+}$ substrate. As TRX and MerA did not co-evolve, the association of these two proteins for $Hg^{2+}$ transfer has not been evolutionarily optimized as would be expected for "in pathway" $Hg^{2+}$ exchanges, such as from MerB to MerA. Thus we propose that the higher $K_{MHg}$ of $Hg^{2+}$ reduction by Tn*501* MerA observed for Hg-TRX, compared to that of $Hg(SG)_2$, is due to a reduction in $k_{on}$ of $Hg^{2+}$ to NmerA.

Like Tn*501* MerA, pDU1358 MerA is also less efficient at reducing $Hg^{2+}$ when liganded to a protein, in our studies being MerB C96S, than to GSH. However, for pDU1358 MerA, the difference in $k_{cat}/K_{MHg}$ values for these $Hg^{2+}$ substrates is *not* due to a significant change in $K_{MHg}$ as it is with Tn*501* MerA. The $K_{MHg}$ for $Hg^{2+}$ reduction by pDU1358 MerA using Hg-MerB C96S as a substrate (24.4 ± 2.1 μM) is just over 2-fold larger than when $Hg(GS)_2$ is used as the substrate (11.5 ± 1.5 μM). Thus, the $k_{on}$ for $Hg^{2+}$ acquisition by NmerA is of the same magnitude for both substrates. For pDU1358 MerA, the decrease in $k_{cat}/K_{MHg}$ using Hg-MerB C96S as the substrate is predominantly due to the decrease in $k_{cat}$, which is ~6.5-times slower (1.48 ± 0.04 $s^{-1}$) than when $Hg(SG)_2$ is the substrate (9.6 ± 0.3 $s^{-1}$). We do not yet fully understand this reduction in $k_{cat}$, but it may be due to an interaction we have yet to demonstrate which slows the dissociation of NmerA and MerB (Scheme 1 bIII-bIV). As the buried C96 protects $Hg^{2+}$ from the solvent

**Table 4.** Comparison of steady-state values for Tn*501* MerA and pDU1358 MerA variants with $Hg^{2+}$ liganded to a protein as the substrate [a]

| Enzyme | [Enzyme] (nM) | Substrate | $k_{cat}$ ($s^{-1}$) | $K_{MHg}$ (μM) | $k_{cat}/K_{MHg}$ ($M^{-1}$ $s^{-1}$ × $10^{-5}$) |
|---|---|---|---|---|---|
| Tn*501* MerA[b] | 25 | Hg(TRX) | 9.0 ± 1.0 | 297 ± 58 | 0.3 ± 0.07 |
| Tn*501* Core[b] | 25 | Hg(TRX) | 7.0 ± 1.0 | 1177 ± 225 | 0.06 ± 0.01 |
| pDU1358 WT | 15 | Hg-MerB C96S | 1.48 ± 0.04 | 24.4 ± 2.1 | 0.60 ± 0.04 |
| pDU1358 AACCCC | 50 | Hg-MerB C96S | Not reliable | ≥ 1400 | 0.021 ± 0.002 |

[a] Conditions: 50 mM $KP_i$, pH 7.3, 50 μM NADPH, 25 °C. Unlike experiments utilizing $Hg(SG)_2$ as the substrate, in which a 1 mM excess GSH was present, no GSH or excess thiol of any kind was used in reactions with Hg-protein substrates.

[b] From Ledwidge et al. 2005a.

and limits the ability of $Hg^{2+}$ to scramble to other non-*mer* pathway thiols, a secondary protein-protein interaction between NmerA and MerB may stimulate the specific and desirable dissociation of $Hg^{2+}$ from MerB's C96 to MerA. We are interested in pursuing experiments using pDU1358 MerA variants to examine the rates of $Hg^{2+}$ acquisition from Hg-MerB variants by NmerA, and of the subsequent transfer of $Hg^{2+}$ from Hg-NmerA to the Core's C-terminal thiols, in part to examine this hypothesis.

The observation that $k_{cat}/K_{MHg}$ for pDU1358 MerA is more than 28-times greater than that of AACCCC when Hg-MerB C96S is the substrate further establishes NmerA's importance to *mer* pathway resistance against organomercurials (Table 4). Under physiological conditions, where the concentration of MerA will be much greater than Hg-MerB ([Hg-MerB]<<$K_{MHg}$), the difference in $k_{cat}/K_{MHg}$ between pDU1358 MerA and AACCCC is more important in describing the intrinsic efficiency of $Hg^{2+}$ reduction than the difference in $k_{cat}$. Although optimized for cleaving C-Hg bonds, the structure of MerB may not be conducive to directly "saddling up" against MerA's Core in a way that promotes the transfer of $Hg^{2+}$ from MerB, especially when partly coordinated by MerB C96 in the interior of the protein, to the Core's C-terminal thiols, which themselves can be buried within the Core. NmerA solves this problem by serving as an adaptor domain able to recover $Hg^{2+}$ from GSH or MerB faster than Core, in turn providing a kinetic advantage to both broad- and narrow-spectrum mercury resistance pathways.

## Conclusions

The combination of our above studies of the $Hg^{2+}$-binding equilibrium between the narrow-spectrum NmerA and Core's C-terminal thiols in full length Tn*21* MerA, the rates at which these two regions in this protein acquire $Hg^{2+}$ from $Hg(SG)_2$, and the comparison of the steady state kinetics of $Hg^{2+}$ reduction by the broad-spectrum pDU1358 MerA and Core when presented with $Hg^{2+}$ liganded to a MerB mutant further support that NmerA is kinetically favored over Core's C-terminal cysteines in acquiring $Hg^{2+}$ from small molecule and protein substrates. NmerA can adopt multiple conformations around MerA's Core because of the flexibility of its tether and inturn occludes substrate access to Core's C-terminal thiols, as demonstrated by the difference in $K_{MHg}$ for the reduction of $Hg(SG)_2$, but our equilibrium data shows that NmerA does not prohibit these Core cysteines from binding $Hg^{2+}$ in the presence of Hg-NmerA or *vice* versa. However, it is unlikely *in vivo* that Core ever directly acquires $Hg^{2+}$ when liganded to either a small molecule or protein. Our estimates of $k_{onHg}$ from $Hg(SG)_2$ for Tn*21* NmerA suggests that it acquires $Hg^{2+}$ at least 42-times faster than that of Core, and the ~50-fold larger $K_{MHg}$ for mercury reduction by pDU1358 Core relative to that of MerA with Hg-MerB C96S similarly suggests that the $k_{onHg}$ from Hg-MerB C96S to NmerA is much greater than to Core. It remains curious that the $k_{cat}$ of $Hg^{2+}$ reduction is ~6.5-times slower for Hg-MerB C96S than when $Hg(SG)_2$ is the substrate. Future structural and kinetics investigations may determine if this difference in $k_{cat}$ can be explained by a secondary protein-protein interaction between NmerA and MerB which may stimulate the release transfer of $Hg^{2+}$ from MerB's C96 but also may slow the dissociation of NmerA from MerB and, in turn, the delivery of $Hg^{2+}$ from Hg-NmerA to the Core's C-terminal

thiols. Nonetheless, as the $k_{cat}/K_{MHg}$ for mercury turnover by MerA when $Hg^{2+}$ is liganded to either small molecules or protein substrates is consistently greater than the $k_{cat}/K_{MHg}$ for turnover by Core alone, it is clear that NmerA plays a significant and beneficial role in the resistance pathways against both narrow- and broad-spectrum mercurials.

## Materials and Methods

Preparation of Tn*21* MerA and $Hg(TNB)_2$

Tn*21* MerA was prepared as previously described (Johs et al. 2011). Prior to use, purified MerA was incubated with 5 mM dithiothreitol (DTT) at room temperature for 30 min, and then separated from DTT and exchanged into 50 mM potassium phosphate ($KP_i$), pH 7.3, by gel filtration chromatography using an illustra NAP™-5 or -10 column for volumes under 0.5 mL and 1.0 mL, respectively (GE Healthcare). The concentration of MerA was calculated and thiol titrations were performed under denaturing conditions as previously described (Pitts and Summers 2002; Ledwidge et al. 2005a) to confirm 6 reduced thiols per MerA monomer (or all MerA variants discussed in this chapter, the two thiols adjacent to the FAD, C135 and C140 in Tn*21* MerA, remain as a disulfide) (Miller et al. 1989). $Hg(TNB)_2$ was prepared and quantitated as previously described (Ledwidge et al. 2005a).

Titration of Tn*21* MerA with $Hg(TNB)_2$ and assessment of $Hg^{2+}$-binding equilibrium

All reactions were performed in triplicate in 50 mM $KP_i$ buffer, pH 7.3, with temperature control at 25 °C. Concentrations of MerA and equivalents of $Hg(TNB)_2$ are given per MerA monomer. 10 μM Tn*21* MerA in 1 mL of buffer was titrated with 20 μL steps of 100 μM $Hg(TNB)_2$ (0.2 equivalents per MerA monomer per step) up to 3.0 equivalents of $Hg^{2+}$ per MerA monomer. Only 2.0 equivalents of $Hg^{2+}$ are expected to bind to MerA, one to NmerA's C11 and C14 cysteine pair, and the other to Core's C561 and 562 cysteine pair; preparation of MerA for these experiments renders the inner Core

cysteines, C135 and C140, oxidized as a disulfide and unable to bind $Hg^{2+}$. Nonetheless, a maximum of 3.0 equivalents of $Hg(TNB)_2$ were titrated to ensure complete saturation, and each reaction was allowed to equilibrate for 5 minutes prior to measurement. TNB generated over the titration course, indicative of $Hg^{2+}$ release from $Hg(TNB)_2$ and, in turn, $Hg^{2+}$ binding to MerA, was monitored by the increase in absorbance at 450 nm using an Uvikon XL spectrophotometer. The final TNB concentration was calculated using $\Delta\varepsilon_{450}$ = 7.36 $mM^{-1}$ $cm^{-1}$ (Riddles et al. 1979).

The measurement of $Hg^{2+}$ release from $Hg(TNB)_2$ alone does not allow for the differentiation of $Hg^{2+}$ binding to NmerA's C11 and C14 or to Core's C-terminal C561 and C562. $Hg^{2+}$ binding to NmerA cannot be detected using absorbance or fluorescence spectroscopy. However, as MerA's C-terminal C561 thiolate partially quenches the fluorescence of the enzyme-bound FAD, coordination of $Hg^{2+}$ as C561-$Hg^{2+}$-C562 can be detected as an increase in FAD fluorescence (Ledwidge et al. 2005b). Over the titration course the change of FAD fluorescence, resulting from $Hg^{2+}$ binding to MerA's C-terminal thiols, was measured using a Jobin Yvon fluorometer with excitation and emission monochromator slits both set to 2.4 nm, an integration time of 1 second, and excitation/emission wavelengths of 490/515 nm. Neither $Hg(TNB)_2$ or TNB absorbs at 490 nm, thereby avoiding inner filter effects. The TNB absorbance and FAD fluorescence emission signals from each experiment were corrected for dilution over the course of the titration and normalized. To calculate the number of $Hg^{2+}$ equivalents bound to NmerA at each titration step, the number of $Hg^{2+}$ equivalents bound to MerA's C-terminal thiols was subtracted from the total number of $Hg^{2+}$ equivalents released from $Hg(TNB)_2$.

Stopped-flow kinetics of initial $Hg^{2+}$ acquisition rates from $Hg(TNB)_2$ by Tn*21* MerA

To measure the initial rates of $Hg^{2+}$ release from $Hg(TNB)_2$ and binding to Tn*21* MerA's C-terminal thiols, stopped-flow kinetic experiments were conducted using a HiTech SF-61DX2 (TgK Scientific Ltd) instrument in single mixing mode using photomultiplier detection in dual beam mode with temperature control at 25 °C. 100 μL of 20 μM MerA in one syringe was mixed by the stopped-flow apparatus with 100 μL of 10, 20, or 40 μM $Hg(TNB)_2$ (0.5, 1, and 2 equivalents, respectively) in the second syringe. Upon mixing by the stopped-flow apparatus, the final concentration of MerA was 10 μM, and of $Hg(TNB)_2$ was 5, 10, or 20 μM, respectively. Prior to the addition of $Hg(TNB)_2$, the initial absorbance at 450 nm of 0.115 was due to the presence of the FAD in MerA. TNB production was monitored by absorbance at 450 nm, as above. FAD fluorescence was measured using excitation wavelength of 490 nm with a 500 nm cutoff filter. Baseline fluorescence was set to zero prior to addition of MerA. The maximum fluorescence signal was set to 100% after equilibration of MerA with 2.0 equivalents of $Hg(TNB)_2$ for 5 minutes. Prior to mixing with $Hg(TNB)_2$, MerA fluoresced at ~42% of the maximum observed signal (Figure 2).

Cloning and mutagenesis of full-length pDU1358 MerA

Standard molecular biology protocols were used for PCR amplification, restriction digest, ligation, and transformation. Plasmid pDU1358 was a generous gift from Dr. Anne Summers (Griffin et al. 1987). Forward (5' GGGAATTCCAT**GGATCC**CATCTAAAAATCACCGGC 3') and reverse (5' CGA**GGATCC**TGGGGCGAGCTTCATGGTTCCAT 3') primers were used for PCR-

amplification and to introduce a BamH1 site (bold) immediately upstream of pDU1358 MerA-residue His3 codon and downstream of the native stop codon. The PCR product was gel purified and ligated into pCR-Blunt II-TOPO vector using the Zero Blunt TOPO PCR Cloning Kit (Invitrogen). After verification by sequencing, the MerA insert was excised using BamHI, gel purified, and ligated at the BamHI restriction site of H-MBP-3C, a modified pMAL-c2X vector (New England Biolabs) that codes for tandem N-terminal His6 and maltose binding protein (MBP) affinity purification tags followed by a 3C protease cleavage site (Alexandrov et al. 2001). After 3C cleavage the final protein has only four residues (GPGS) from the protease recognition site and translation of the BamHI restriction site left upstream of His3 in the native pDU1358 MerA sequence. However, the Ser is chemically homologous to Thr2 of the native pDU1358 MerA sequence it replaces. Chemically competent Top10 *Escherichia coli* (Invitrogen) were transformed with the resulting pMAL:H-MBP-3C_MerA vector and selected on LB/carbenicillin (50 μg/mL) (LBC) plates. The MerA gene sequence and orientation were verified by DNA sequencing.

Standard site-directed mutagenesis protocols were used to generate the double mutant: H-MBP-3C_AACCCC MerA in which C11 and C14, located in NmerA, are mutated to alanines, while all catalytic Core active site (C136 and C141) and C-terminal (C558 and C559) thiols are retained. Mutations were verified by DNA sequencing.

Expression and Purification of pDU1358 MerA full-length variants and Core

pDU1358 MerA and AACCCC MerA were expressed, purified, and stored in aliquots at –80 °C in storage buffer [50 mM $KP_i$, pH 7.3, and 5 mM DTT] as previously described for Tn*21* MerA (Johs et al. 2011). pDU1358 MerA catalytic core (Core) was expressed and purified as previously described at 4 °C (Ledwidge et al. 2005a), except that the pooled, concentrated yellow eluent from the Orange 3 column was further purified by size-exclusion chromatography on a Superdex 200 10/300 GL column (GE Healthcare) equilibrated with storage buffer, then aliquoted, and stored at –80 °C (Figure 4).

Expression and purification of R831b MerB C96S

pET21b:H-MerB C96S, which encodes a mutant of the R831b MerB with C96 mutated to serine, was a generous gift from Dr. Anne Summers (Pitts and Summers, 2002). *E. coli* BL21(DE3) were transformed with pET21b:H-MerB C96S and plated on LBC agar. A single colony was used to inoculate 1 L of LBC media, which was then shaken at 37 °C and 280 rpm for ~ 16 h. Fifty milliliters of this starter culture were centrifuged at 3000***g*** for 10 min and decanted. The cell pellet was resuspended in 50 mL of LBC and used to inoculate 6 × 1 L of LBC in 2.8-L non-baffled Fernbach flasks. Cultures were shaken at 37 °C and 280 rpm and grown to an $OD_{600nm}$ of 0.6–0.8, at which point expression was induced with 0.4 mM IPTG and cell growth was continued for 4 h. Cells were harvested by centrifugation at 6000***g*** for 10 min. Harvested pellets, (~ 6 g of cells per 1 L of growth medium) were resuspended in 12 mL of lysis buffer [50 mM $KP_i$, pH 7.3, 500 mM NaCl] and frozen for storage at −20 °C.

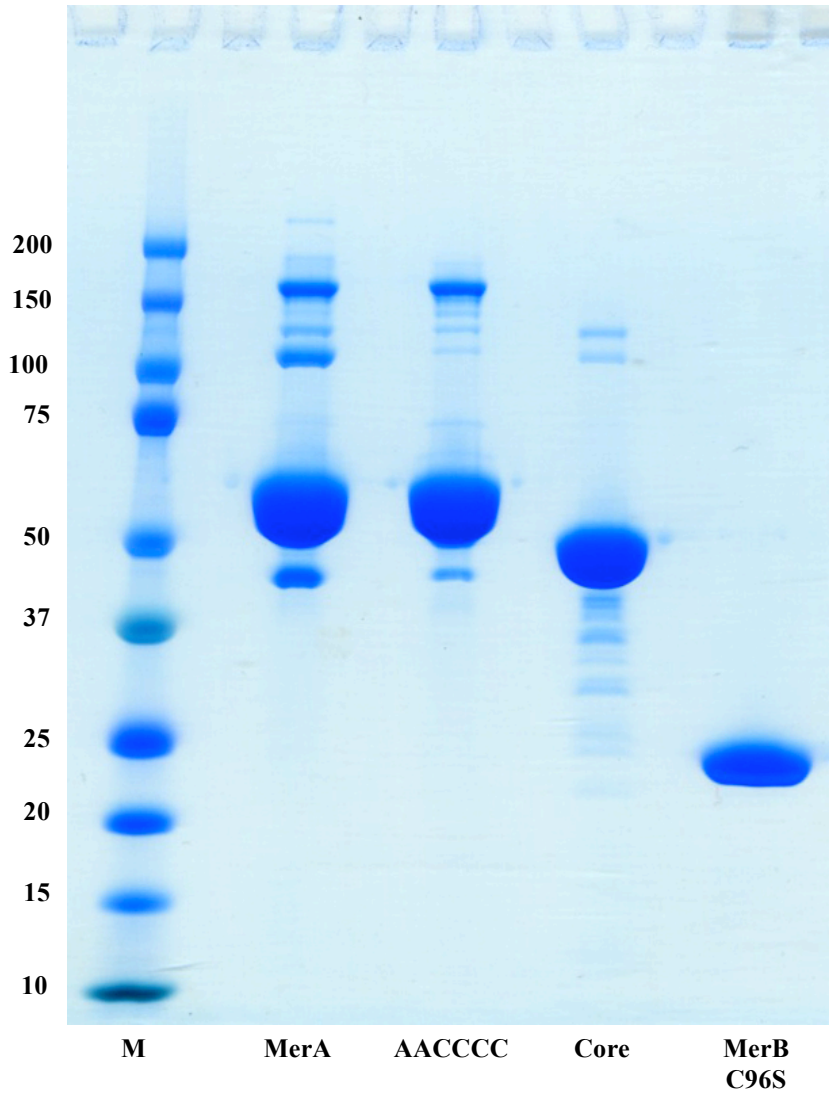


**Figure 4.** SDS-PAGE analysis of purified pDU1358 MerA variants and MerB C96S. M: Precision Plus Protein™ Standards Kaleidoscope™ molecular mass standards (Bio-Rad) with masses in kDa.

Frozen cells were thawed in the presence of one complete ULTRA protease inhibitor cocktail tablet (Roche) and 2 mM 2-mercaptoethanol (2ME). Suspended cells were lysed by four passes through an EmulsiFlex-C3 homogenizer (Avestin) and centrifuged at 42,000***g*** for 2 h. Imidazole (10 mM final) was added to the supernatant. For every 6 g of cells lysed, 15 mL of Ni-NTA agarose resin pre-equilibrated in binding buffer [lysis buffer with 10 mM imidazole and 2 mM 2ME] were added to the lysate and nutated for 2 hours at 4 °C. After binding, the resin was poured into a 5 cm × 20 cm glass gravity flow chromatography column and washed with 3 column volumes of binding buffer followed by 5 column volumes of wash buffer [binding buffer with 50 mM imidazole]. Protein was eluted with 300 mM imidazole in binding buffer and collected based on absorbance at 280 nm. DTT was added immediately to a final concentration of 10 mM, and the eluent was concentrated to ~ 2 mL in an Amicon Ultra centrifugal filter (10,000 molecular weight cutoff) (Millipore). Concentrated MerB C96S was separated from imidazole and 2ME on a Superdex 200 10/300 GL SEC equilibrated with storage buffer. Fractions from the predominant peak with absorbance at 280 nm were pooled, concentrated as before to at least 4× the concentration needed for kinetics experiments, flash frozen in liquid nitrogen, and stored at –80 °C. The protein was judged ≥95% pure by SDS–PAGE and the yield was ~4.5 μmoles of protein from 24 L of cell growth (Figure 4).

Preparation of pDU1358 MerA variants and of MerB C96S for Kinetics Assays

pDU1358 MerA full-length variants and Core were prepared for kinetic assays as described above for Tn*21* MerA (Ledwidge et al. 2005a; Johs et al. 2011). Prior to use,

MerB C96S was incubated with 10 mM DTT at room temperature for 30 min, and then was separated from DTT and exchanged into 50 mM $KP_i$, pH 7.3, as described above for Tn*21* MerA. Protein concentrations were calculated and thiol titrations were performed under denaturing conditions as previously described (Pitts and Summers 2002; Ledwidge et al. 2005a) to confirm the appropriate number of reduced thiols for each protein [3 for MerB C96S; 4 for Core and AACCCC MerA, and 6 for MerA (in all MerA variants, the two thiols adjacent to the FAD, C136 and C141, remain as a disulfide)] (Miller et al. 1989).

Preparation of $Hg(SG)_2$ and of Hg-MerB C96S

$Hg(SG)_2$ was prepared as previously described (Ledwidge et al. 2005a; Hong et al. 2010). Hg-MerB C96S was prepared by titration of MerB C96S with 1 equivalent of $Hg(GS)_2$. The desired 1:1 Hg:MerB C96S binding stoichiometry, resulting from the coordination of $Hg^{2+}$ as C159-$Hg^{2+}$-C160, was verified by thiol titration under denaturing conditions. The concentration of Hg-MerB C96S was quantified as previously (Pitts and Summers 2002).

Stopped-Flow Steady-State Kinetic Analysis of pDU1358 MerA variants

A HiTech SF-61DX2 stopped-flow apparatus, setup as described above, was used for all kinetic measurements. All reactions were performed in 50 mM $KP_i$, pH 7.3, with temperature control at 25 °C. Initial rates of $Hg^{2+}$ reduction were measured by monitoring the loss of absorbance at 340 nm due to NADPH oxidation ($\Delta\varepsilon_{340}$ = 6.2 $mM^{-1}$ $cm^{-1}$). 100 µL of a saturating concentration 100 µM of NADPH (Sigma, N-1630) and the substrate

(either 20–400 μM of $Hg(SG)_2$ in the presence of 2 mM unliganded GSH, or of 10–600 μM of Hg-MerB C96S) in one syringe was mixed by the stopped-flow apparatus with 100 μL of either 30 nM MerA, 30 nM MerA catalytic Core, or 100 nM AACCCC MerA (concentrations held constant throughout each experiment) in the second syringe. These reactants were diluted to half their starting concentration upon stopped-flow mixing. Initial velocity measurements were taken three to five times per substrate concentration. Data were fit to the Michaelis-Menten equation and errors in $k_{cat}$, $K_{MHg}$, and $k_{cat}/K_{MHg}$ were calculated as previously described (Hong et al. 2010).

## References


Alexandrov A, Dutta K, Pascal SM (2001) "MBP fusion protein with a viral protease cleavage site: one-step cleavage/purification of insoluble proteins." *Biotechniques* 30:1194-1198.

Argyrou A, Blanchard JS (2004) "Flavoprotein disulfide reductases: advances in chemistry and function." *Prog Nucleic Acid Res Mol Biol* 78:89-142.

Barkay T, Miller SM, Summers AO (2003) "Bacterial mercury resistance from atoms to ecosystems." *FEMS Microbiol Rev* 27:355-384.

Begley TP, Walts AE, Walsh CT (1986a) "Bacterial organomercurial lyase: overproduction, isolation, and characterization." *Biochemistry* 25:7186-7192.

Begley TP, Walts AE, Walsh CT (1986b) "Mechanistic studies of a protonolytic organomercurial cleaving enzyme: bacterial organomercurial lyase." *Biochemistry* 25:7192-7200.

Benison GC, Di Lello P, Shokes JE, Cosper NJ, Scott RA, Legault P, Omichinski JG (2004) "A stable mercury-containing complex of the organomercurial lyase MerB: catalysis, product release, and direct transfer to MerA." *Biochemistry* 43:8333-8345.

Brown NL, Ford SJ, Pridmore RD, Fritzinger DC (1983) "Nucleotide sequence of a gene from the Pseudomonas transposon Tn501 encoding mercuric reductase." *Biochemistry* 22:4089-4095.

Condee CW, Summers AO (1992) "A mer-lux transcriptional fusion for real-time examination of in vivo gene expression kinetics and promoter response to altered superhelicity." *J Bacteriol* 174:8094-8101.

Di Lello P, Benison GC, Valafar H, Pitts KE, Summers AO, Legault P, Omichinski JG (2004) "NMR structural studies reveal a novel protein fold for MerB, the organomercurial lyase involved in the bacterial mercury resistance system." *Biochemistry* 43:8322-8332.

Distefano MD, Au KG, Walsh CT (1989) "Mutagenesis of the redox-active disulfide in mercuric ion reductase: catalysis by mutant enzymes restricted to flavin redox chemistry." *Biochemistry* 28:1168-1183.

Distefano MD, Moore MJ, Walsh CT (1990) "Active site of mercuric reductase resides at the subunit interface and requires Cys135 and Cys140 from one subunit and Cys558 and Cys559 from the adjacent subunit: evidence from in vivo and in vitro heterodimer formation." *Biochemistry* 29:2703-2713.

Engst S, Miller SM (1999) "Alternative routes for entry of HgX2 into the active site of mercuric ion reductase depend on the nature of the X ligands." *Biochemistry* 38:3519-3529.

Fox B, Walsh CT (1982) "Mercuric reductase. Purification and characterization of a transposon-encoded flavoprotein containing an oxidation-reduction-active disulfide." *J Biol Chem* 257:2498-2503.

Fox BS, Walsh CT (1983) "Mercuric reductase: homology to glutathione reductase and lipoamide dehydrogenase. Iodoacetamide alkylation and sequence of the active site peptide." *Biochemistry* 22:4082-4088.

Gambill BD, Summers AO (1992) "Synthesis and degradation of the mRNA of the Tn21 mer operon." *J Mol Biol* 225:251-259.

Griffin HG, Foster TJ, Silver S, Misra TK (1987) "Cloning and DNA sequence of the mercuric- and organomercurial-resistance determinants of plasmid pDU1358." *Proc Natl Acad Sci USA* 84:3112-3116.

Hong B, Nauss R, Harwood IM, Miller SM (2010) "Direct measurement of mercury(II) removal from organomercurial lyase (MerB) by tryptophan fluorescence: NmerA domain of coevolved gamma-proteobacterial mercuric ion reductase (MerA) is more efficient than MerA catalytic core or glutathione." *Biochemistry* 49:8187-8196.

Johs A, Harwood IM, Parks JM, Nauss RE, Smith JC, Liang L, Miller SM (2011) "Structural characterization of intramolecular Hg(2+) transfer between flexibly linked domains of mercuric ion reductase." *J Mol Biol* 413:639-656.

Lafrance-Vanasse J, Lefebvre M, Di Lello P, Sygusch J, Omichinski JG (2009) "Crystal structures of the organomercurial lyase MerB in its free and mercury-bound forms: insights into the mechanism of methylmercury degradation." *J Biol Chem* 284:938-944.

Ledwidge R, Hong B, Dötsch V, Miller SM (2010) "NmerA of Tn501 mercuric ion reductase: structural modulation of the pKa values of the metal binding cysteine thiols." *Biochemistry* 49:8988-8998.

Ledwidge R, Patel B, Dong A, Fiedler D, Falkowski M, Zelikova J, Summers AO, Pai EF, Miller SM (2005a) "NmerA, the metal binding domain of mercuric ion reductase, removes Hg2+ from proteins, delivers it to the catalytic core, and protects cells under glutathione-depleted conditions." *Biochemistry* 44:11402-11416.

Ledwidge R, Soinski R, Miller SM (2005b) "Direct monitoring of metal ion transfer between two trafficking proteins." *J Am Chem Soc* 127:10842-10843.

Marshall JL, Booth JE, Williams JW (1984) "Characterization of the covalent mercury (II)-NADPH complex." *J Biol Chem* 259:3033-3036.

Miller SM (1999) "Bacterial detoxification of Hg(II) and organomercurials." *Essays Biochem* 34:17-30.

Miller SM, Moore MJ, Massey V, Williams CH, Jr., Distefano MD, Ballou DP, Walsh CT (1989) "Evidence for the participation of Cys558 and Cys559 at the active site of mercuric reductase." *Biochemistry* 28:1194-1205.

Moore MJ, Miller SM, Walsh CT (1992) "C-terminal cysteines of Tn501 mercuric ion reductase." *Biochemistry* 31:1677-1685.

Moore MJ, Walsh CT (1989) "Mutagenesis of the N- and C-terminal cysteine pairs of Tn501 mercuric ion reductase: consequences for bacterial detoxification of mercurials." *Biochemistry* 28:1183-1194.

Nakahara H, Silver S, Miki T, Rownd RH (1979) "Hypersensitivity to Hg2+ and hyperbinding activity associated with cloned fragments of the mercurial resistance operon of plasmid NR1." *J Bacteriol* 140:161-166.

Pitts KE, Summers AO (2002) "The roles of thiols in the bacterial organomercurial lyase (MerB)." *Biochemistry* 41:10287-10296.

"Reorganizing the protein space at the Universal Protein Resource (UniProt)." (2012) *Nucleic Acids Res* 40:D71-75.

Riddles PW, Blakeley RL, Zerner B (1979) "Ellmans Reagent - 5,5'-Dithiobis(2-Nitrobenzoic Acid) - Re-Examination." *Anal Biochem* 94:75-81.

Rossy E, Seneque O, Lascoux D, Lemaire D, Crouzy S, Delangle P, Coves J (2004) "Is the cytoplasmic loop of MerT, the mercuric ion transport protein, involved in mercury transfer to the mercuric reductase?" *FEBS Lett* 575:86-90.

Schiering N, Kabsch W, Moore MJ, Distefano MD, Walsh CT, Pai EF (1991) "Structure of the detoxification catalyst mercuric ion reductase from Bacillus sp. strain RC607." *Nature* 352:168-172.

Schottel JL (1978) "The mercuric and organomercurial detoxifying enzymes from a plasmid-bearing strain of Escherichia coli." *J Biol Chem* 253:4341-4349.

Schue M, Glendinning KJ, Hobman JL, Brown NL (2008) "Evidence for direct interactions between the mercuric ion transporter (MerT) and mercuric reductase (MerA) from the Tn501 mer operon." *Biometals* 21:107-116.

Sedlmeier R, Altenbuchner J (1992) "Cloning and DNA sequence analysis of the mercury resistance genes of Streptomyces lividans." *Mol Gen Genet* 236:76-85.

Stanisich VA (1974) "Interaction between an R factor and an element conferring resistance to mercuric ions in Pseudomonas aeruginosa." *Molec Gen Genet* 128:201-212.

Stanisich VA, Bennett PM, Richmond MH (1977) "Characterization of a translocation unit encoding resistance to mercuric ions that occurs on a nonconjugative plasmid in Pseudomonas aeruginosa." *J Bacteriol* 129:1227-1233.

Summers AO (1986) "Organization, expression, and evolution of genes for mercury resistance." *Annu Rev Microbiol* 40:607-634.

Wang Y, Moore M, Levinson HS, Silver S, Walsh C, Mahler I (1989) "Nucleotide sequence of a chromosomal mercury resistance determinant from a Bacillus sp. with broad-spectrum mercury resistance." *J Bacteriol* 171:83-92.

Williams CH, Arscott LD, Muller S, Lennon BW, Ludwig ML, Wang PF, Veine DM, Becker K, Schirmer RH (2000) "Thioredoxin reductase two modes of catalysis have evolved." *Eur J Biochem* 267:6110-6117.

# CHAPTER 4

# The Linker Region of MerA aids Membrane Association Independent of MerT

This chapter includes unpublished results that build upon my work and associated publications presented in previous thesis chapters. Susan M. Miller was this project's principal investigator. I am grateful to Rachel E. Nauss for her assistance with the spectrophotometer.

## Project Background and Author's Contributions

As described in the Project Background and Author's Contributions section of Chapter 2, I first expressed Tn*21* MerA for co-crystallization experiments with MerT. Prior to my work it had been suggested that MerA's NmerA and linker region could interact with the cytoplasmic face of MerT (Schue et al. 2008). In developing the MerA purification protocol I chose to centrifuge the lysate of cells overexpressing MerA for 2 hrs at 42,000 × g to clarify the soluble fraction of the lysate from the membrane fraction and insoluble debris. The clarified soluble lysate is bright yellow in color due to the presence of MerA, as expected, that arises from the flavin adenine dinucleotide (FAD) chromophore bound to the MerA Core. To my surprise, I observed that the ultracentrifugation membrane pellets were also yellow in color (Figure 4). When

overexpressing proteins that lack a chromophore, such as MerT, the membrane pellets of *E. coli* generally appear light to dark brown. The yellow color of the membrane fractions, I hypothesized, was due to MerA associating with the cell membrane, and was the impetus for the experiments presented in this chapter. In independently deciding to pursue these studies it was my goal to determine if MerA could associate with the cell membrane and, if indeed it could, if membrane-localized MerA was catalytically active and which of MerA's three regions (NmerA, the ~26 residue linker that tethers NmerA to Core, and Core) promoted this association. For the work of this chapter I independently designed and executed all experiments, analyzed the data, and interpreted the results. Dr. Miller assisted with the editing of this chapter, and we have discussed the possibility of publishing this work as a short communication.

—Ian Harwood, 2012

I, Dr. Susan M. Miller, certify to the best of my knowledge that the above background and description of the chapter authors' contributions are accurate.

—Dr. Susan M. Miller, 2012

[Reprinted from a communication to Dr. Matthew Jacobs on August 30, 2012]

## Introduction

Isolates of Mercuric reductase (MerA), the central protein of mercury resistance encoded by *mer* loci, share a conserved catalytic core (Core) region tethered at its N-terminus to either zero (Sedlmeier and Altenbuchner 1992), one (Brown et al. 1983; Summers 1986) or two (Wang et al. 1989) tandem repeats of a metallochaperone-like domain NmerA. MerAs with a single NmerA domain represent the majority of identified sequences in GenBank (Barkay et al. 2003) and include the well-characterized MerA proteins originally obtained from *Shigella flexneri* (carried by the Tn*21* transposon of the plasmid NR1) (Nakahara et al. 1979; Johs et al. 2011), *Serratia marcescens* (of the plasmid pDU1358) (Griffin et al. 1987), and *Pseudomonas aeruginosa* (carried by the Tn*501* transposon of plasmid pVS1) (Stanisich 1974; Stanisich et al. 1977; Fox and Walsh 1983; Distefano et al. 1989; Miller et al. 1989; Moore and Walsh 1989; Distefano et al. 1990; Engst and Miller 1999; Ledwidge et al. 2005a; Ledwidge et al. 2005b; Hong et al. 2010; Ledwidge et al. 2010). Although the NmerAs and Cores of Tn*21* MerA, Tn*501* MerA, and pDU1358 MerA have been extensively studied, the structure and role of ~26 residue linker (~Phe70 to Asn/Gly/Ser95 in Tn*501*, pDU1358, and Tn*21* MerA, respectively) connecting the two MerA functional regions has not been well characterized (Figure 1). This lack of characterization has been due to difficulties in expressing full-length protein without proteolytic cleavage of the linker region *in vivo* and during protein purification (Fox and Walsh 1982; Moore and Walsh 1989).

Prior to a method for isolating intact MerA, analysis of the linker region was limited to secondary-structure predictions that suggested this region was unstructured.

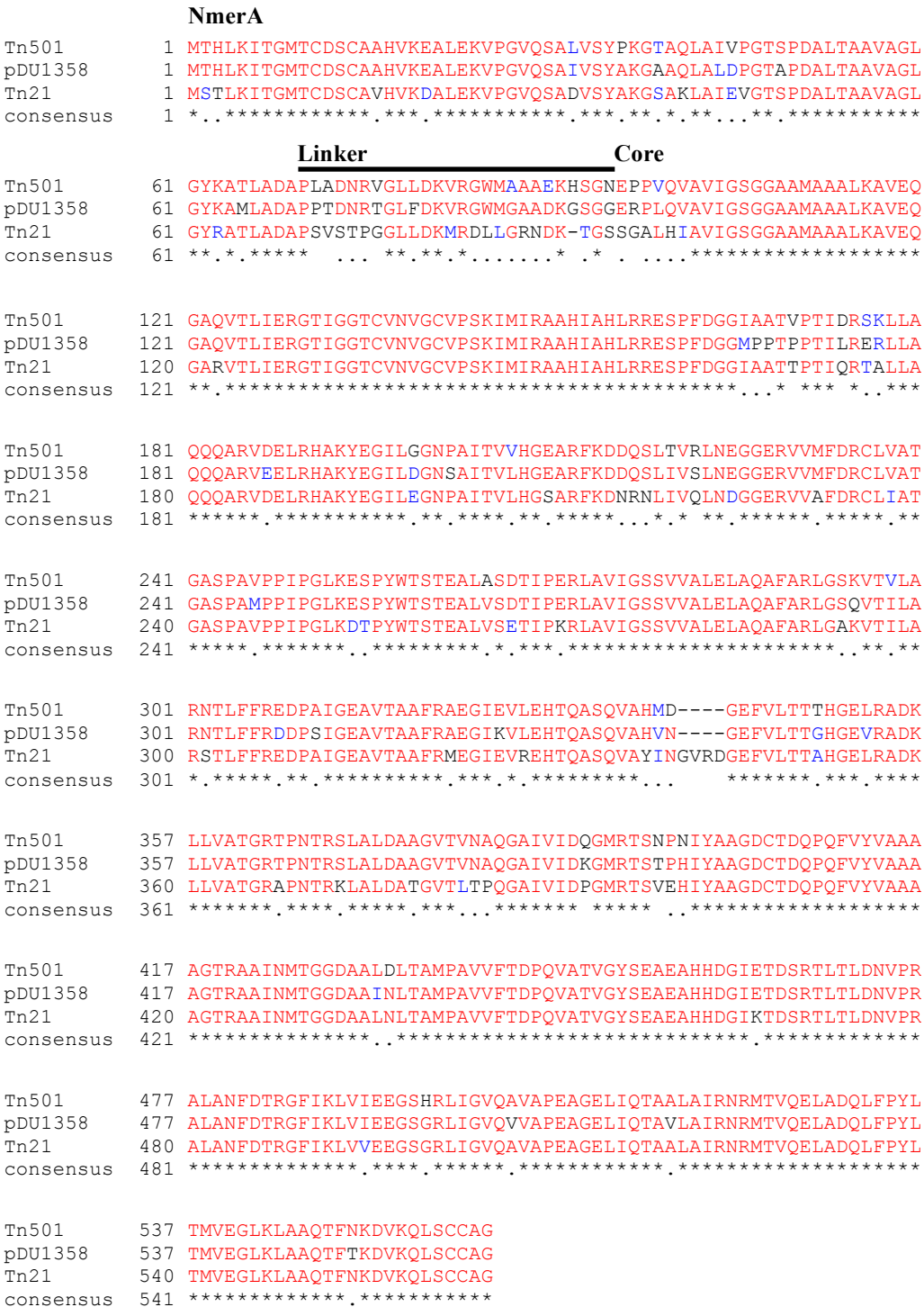


**Figure 1.** ClustalW alignment of MerA isolates from Tn*501* (*P. aeruginosa*), pDU1358 (*S. marcescens*), and Tn*21* (*S. flexneri*) (Thompson et al. 1994). The linker region, which tethers NmerA to Core region, is indicated by a black bar. Identity residues are in red; homologous residues are in blue.

We recently developed a novel strategy to prevent MerA linker cleavage during expression and purification, which allowed for the first chromatographic, small-angle X-ray (SAXS) and neutron (SANS) scattering, and molecular dynamics (MD) studies of intact Tn*21* MerA (Johs et al. 2011). These experiments showed that, in the absence of $Hg^{2+}$, NmerA is able to freely sample large volumes proximal to the Core dimer due to the observed flexibility of the linker. This flexible attachment of the two regions to one another is hypothesized to facilitate fast and efficient removal of $Hg^{2+}$ from substrates, including proteins upstream in the *mer* resistance pathway such as the integral membrane protein, MerT, and the organomercurial lyase, MerB. At the point of $Hg^{2+}$ exchange from the NmerA Cys11 to the Core C-terminal Cys562, the linker regions of each MerA monomer remain disordered and do not tightly pack against the Core.

In addition to facilitating MerA's acquisition of $Hg^{2+}$ from various substrates, the tethering of NmerA provides a kinetic advantage in $Hg^{2+}$ reduction. In our structural characterization of Tn*21* MerA, we showed the SAXS data is consistent with MerA being able to adopt an ensemble of multiple conformations as a result of flexibility in the linker regions. The most elongated of these confirmations showed NmerA is able to stray no more than ~80 Å from Core (Johs et al. 2011). This limited freedom enhances the efficiency of $Hg^{2+}$ reduction by enabling NmerA to deliver $Hg^{2+}$ to the Core more rapidly than untethered, freely diffusing NmerA. When presented with $Hg^{2+}$ liganded to the primary cellular reducing agent, glutathione [GSH], full-length Tn*501* MerA is ~2.6-fold more efficient than Tn*501* Core presented with $Hg^{2+}$ bound to untethered Tn*501* NmerA (Ledwidge et al. 2005a).

The linker region's flexibility, which allows NmerA to scavenge $Hg^{2+}$ from substrates within a large volume surrounding the Core, as well as inherently keeping NmerA close to the Core, which allows rapid delivery of $Hg^{2+}$ to the Core, directly enhances MerA's ability to acquire $Hg^{2+}$. Yet, is it possible that the linker region benefits $Hg^{2+}$ sequestration in a secondary manner? In other proteins featuring metallochaperone-domains tethered by flexible linkers, such as the yeast copper transporting ATPase (Ccc2) and the copper-binding Wilson and Menkes proteins, it has been suggested that the interdomain linkers may have additional roles in protein function, such as orchestrating the motions of the domains relative to one another or favoring tertiary structure interactions (Cobine et al. 2000; Arnesano et al. 2002).

To our knowledge, the only other observation concerning the linker region's function suggests such a secondary purpose. To examine interactions between MerT and regions of MerA *in vivo*, Schue et al. utilized a bacterial two-hybrid screen in which Tn*501* MerT, tethered to the T25 domain of adenylate cyclase (AC) at its cytosolic N-terminus, was co-expressed with MerA, Core, or an extended NmerA, tethered to the T18 domain of AC at each MerA construct's C-terminus, to screen for potential interactions with MerT. The extended NmerA consisted of NmerA (residues 1-69) (Ledwidge et al. 2010) and 19 subsequent residues of the linker region (~70% of the linker). The experiment suggested that the extended NmerA interacts transiently with MerT and the interaction is independent of the $Hg^{2+}$-binding cysteines on both proteins (Schue et al. 2007). In the same experiment, no interaction was detected between MerT and full-length MerA. The absence of a detectable interaction was suggested to be due to the previously

observed *in vivo* cleavage of the linker region, separating the Core and the C-terminally appended reporter from NmerA (Figure 2) (Fox and Walsh 1982; Moore and Walsh 1989). It may also be possible that T25 domain appended to MerT was sterically occluded from interacting with the T18 domain by the ~100 kDa Core dimer of full-length MerA or, independent of MerA linker cleavage, that MerT and MerA do not actually interact.

A $Hg^{2+}$-independent interaction between MerT and MerA may benefit the *mer* resistance mechanism (Brown 1985). In the absence of Tn*501* MerA, cells expressing Tn*501* MerT become hypersensitive to $Hg^{2+}$ and perish at lower $Hg^{2+}$ concentrations than cells harboring no *mer* loci (Nakahara et al. 1979). This observation suggests that MerT allows for the uptake of $Hg^{2+}$ faster than it can diffuse across the membrane into the cell as $HgCl_2$ independent of a dedicated transport system (Gutknecht 1981; Bienvenue et al. 1984). A localization of MerA to MerT, possibly by means of a protein-protein interaction, could increase resistance efficiency by minimalizing non-specific distribution of $Hg^{2+}$ to cellular constituents. This would also limit the distance MerA (and critically NmerA) could stray from MerT, paralleling the effect of the intramolecular localization of NmerA to Core. Such a protein-protein interaction would require MerA to interface with the two cytosolically accessible regions of MerT, the protein's ~6 residue N-terminus and/or a ~10 residue loop (which includes one of MerT's two $Hg^{2+}$-binding thiol pairs) that links the membrane protein's second and third transmembrane helicies. These ~16 MerT residues accessible to the cytoplasm may be sufficient for a protein-protein interaction (Jones and Thornton 1996; Tsai et al. 1996).

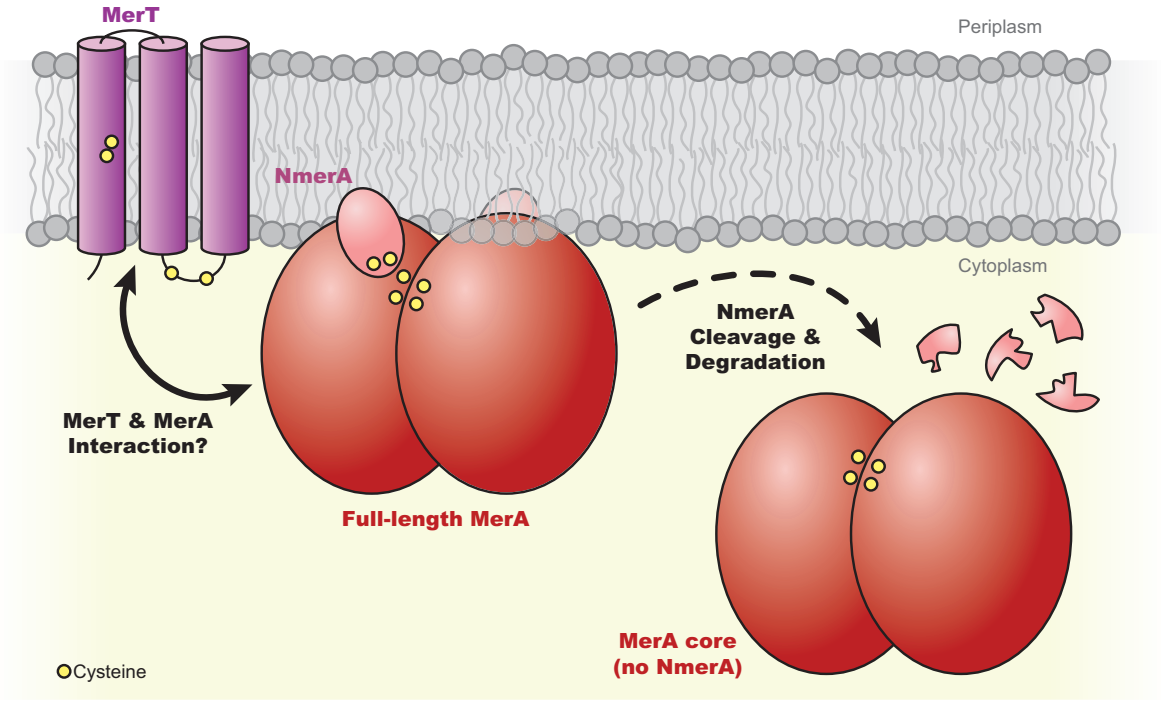


**Figure 2.** *in vivo* cleavage of MerA. Bacterial two-hybrid screens by Schue et al. did not detect an interaction between MerT (purple) and full-length MerA (red) when reporter tags were appended to the N- and C-termini of MerT and MerA respectively. (Schue et al. 2007). The authors of the study suggested such an interaction may not be able to be detected due to *in vivo* cleavage of the linker region (Fox and Walsh 1982; Moore and Walsh 1989).

Alternatively the interaction between MerT and MerA may only be at the point of $Hg^{2+}$ exchange from MerT to NmerA, but a localization of MerA to MerT independent of any direct protein-protein interaction would provide a similar benefit to cell viability. Here, we suggest that the MerA linker region may serve a secondary function of associating MerA to the membrane. We propose that the presence of the linker region in full-length MerA aids in anchoring it to the membrane proximal to MerT. To test this hypothesis we used electrophoretic and spectroscopic techniques to determine the localization of full-length MerA, Core, and NmerA in the soluble and washed membrane fractions from overexpression lysates grown at 17 °C. Additionally we co-expressed Tn*21* MerA and MerT to examine the membrane protein's effect on MerA localization and activity. Our preliminary results suggest that MerA, but not Core or NmerA lacking linker residues, can localize to the membrane, and that this localization is independent of MerT.

# Results

## Expression of Full-Length MerA at 17 °C Minimizes Linker Proteolysis

Previous attempts to express native full-length MerA have resulted in populations of homodimers of full-length MerA, homodimers of Core, and mixed heterodimers of Core and intact MerA (Schottel 1978; Fox and Walsh 1982; Distefano et al. 1989; Ledwidge et al. 2005a). These mixed protein ratios are believed to be due to the susceptibility of the MerA linker region, which tethers NmerA to Core, to *in vivo* proteolysis (Fox and Walsh 1982; Moore and Walsh 1989). In these cases, MerA was expressed at 32 °C to 37 °C. The first expression and purification of fully-intact Tn*21* MerA was accomplished by appending tandem $His_6$ and maltose binding protein (MBP) affinity purification tags to the protein's N-terminus and expressing the construct at 17 °C (Johs et al. 2011). Under these conditions no overexpression of Core monomers was observed, possibly due to the $His_6$-MBP tag protecting the linker region by steric occlusion. Here, we expressed native MerA in the absence of any affinity tags at 17 °C. SDS-PAGE analysis of the soluble fraction of cells expressing the full-length protein shows a band for full-length MerA (55 kDa) but no discernable band for Core (49 kDa) (Figure 3). The use of a lower-temperature for growth appears to minimize the proteolytic cleavage previously observed.

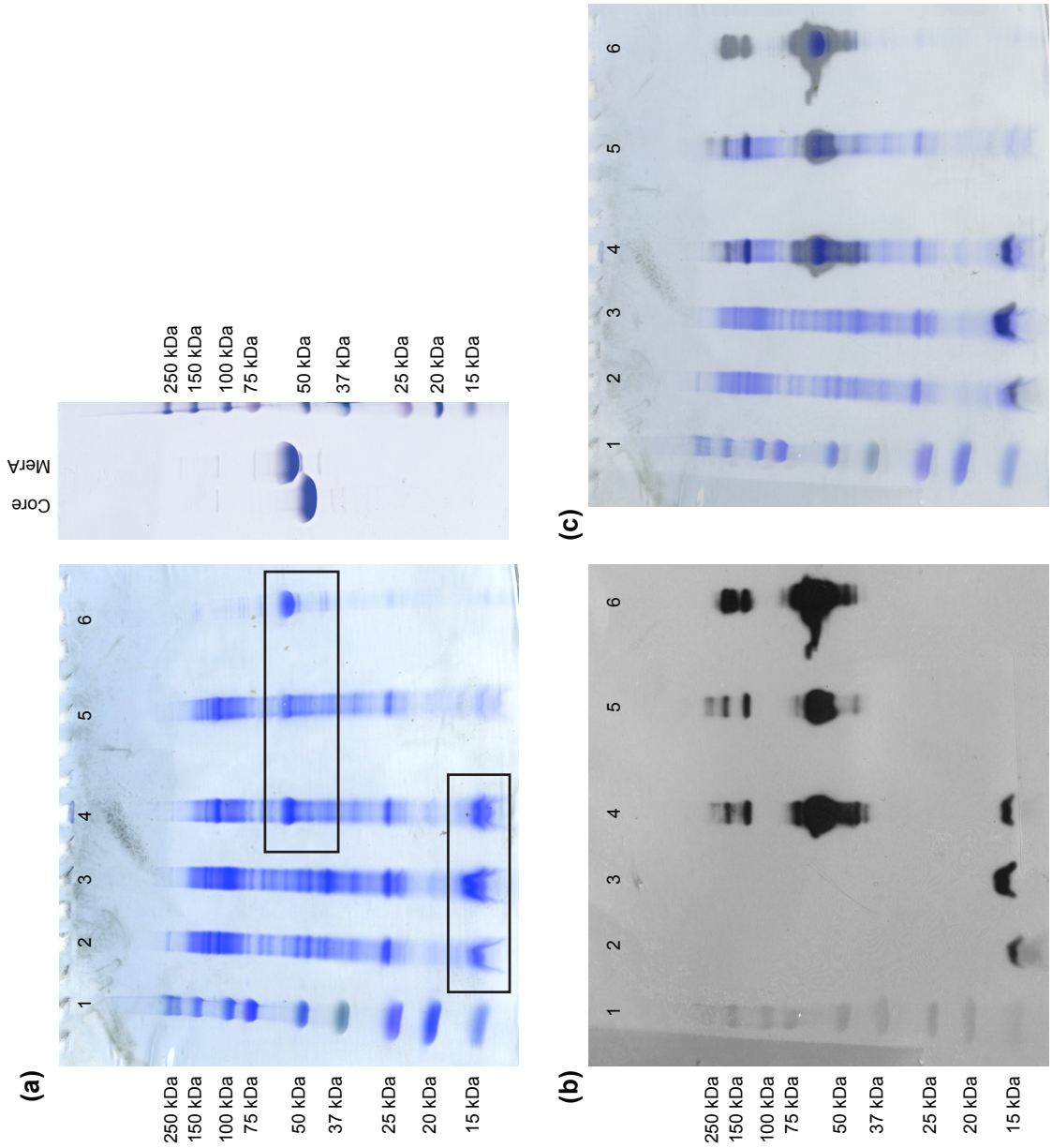


**Figure 3.** Characterization of MerT and full-length MerA localization. (a) SDS-PAGE with Coomassie Blue stain. Lower black box across lanes 2 through 4 highlights MerT. Upper black box across lines 4 through 6 highlights full-length MerA. Comparison with purified Core and full-length MerA (Johs et al. 2011) shows no Core monomers are present in the 17 °C growth lysate supernatants or washed membranes. (b) Western blot and (c) Merge of Coomassie and western detection. Lane 1: Precision Plus Protein™ Standards Kaleidoscope™ molecular mass standards (Bio-Rad Laboratories). Lane 2: Washed membranes of cells expressing MerT at 37 °C for 3 hrs. Lane 3: Washed membranes of cells expressing MerT at 17 °C for 18 hrs. Lane 4: Washed membranes of cells expressing MerT and MerA. Lane 5: Washed membranes of cells expressing MerA. Lane 6: 5-fold dilution of soluble cell lysate from cells expressing MerA.

## Full-Length MerA Localizes to both Soluble and Membrane Fractions

Western analysis of washed membranes from cells expressing MerT shows a band at the expected molecular weight (14 kDa) (Figure 3). This band is also present in washed membranes of cells expressing MerT+MerA. Both SDS-PAGE and western analysis confirm the presence of MerA in both the washed membranes of cells expressing MerT and MerA and, unexpectedly, those expressing MerA alone (Figure 3). Both washed membrane samples are intensely yellow, due to the FAD bound to Core (Figure 4), which is not observed in membrane preparations of other uncolored soluble or membrane proteins (Newby et al. 2009). Soluble fractions from cells expressing MerA or Core exhibit a similar coloring. This unexpected result suggests that full-length MerA can remain associated with the cell membrane after being washed in buffers of high ionic strength, aimed at weakening electrostatic attractions between proteins, and of high reducing potential, to minimize thiol crosslinking. As these results suggest MerA is able to independently associate with the membrane in the absence of MerT, it would be inappropriate to use this method to screen for MerT-MerA interactions.

Similar analyses of washed membranes from cells expressing Tn*501* Core or NmerA, which were successfully purified from the soluble lysis fraction to confirm expression, showed no association of either with the membrane (data not shown). The inability of either to remain with the membrane suggests that these regions alone are not accountable for full-length MerA membrane localization.

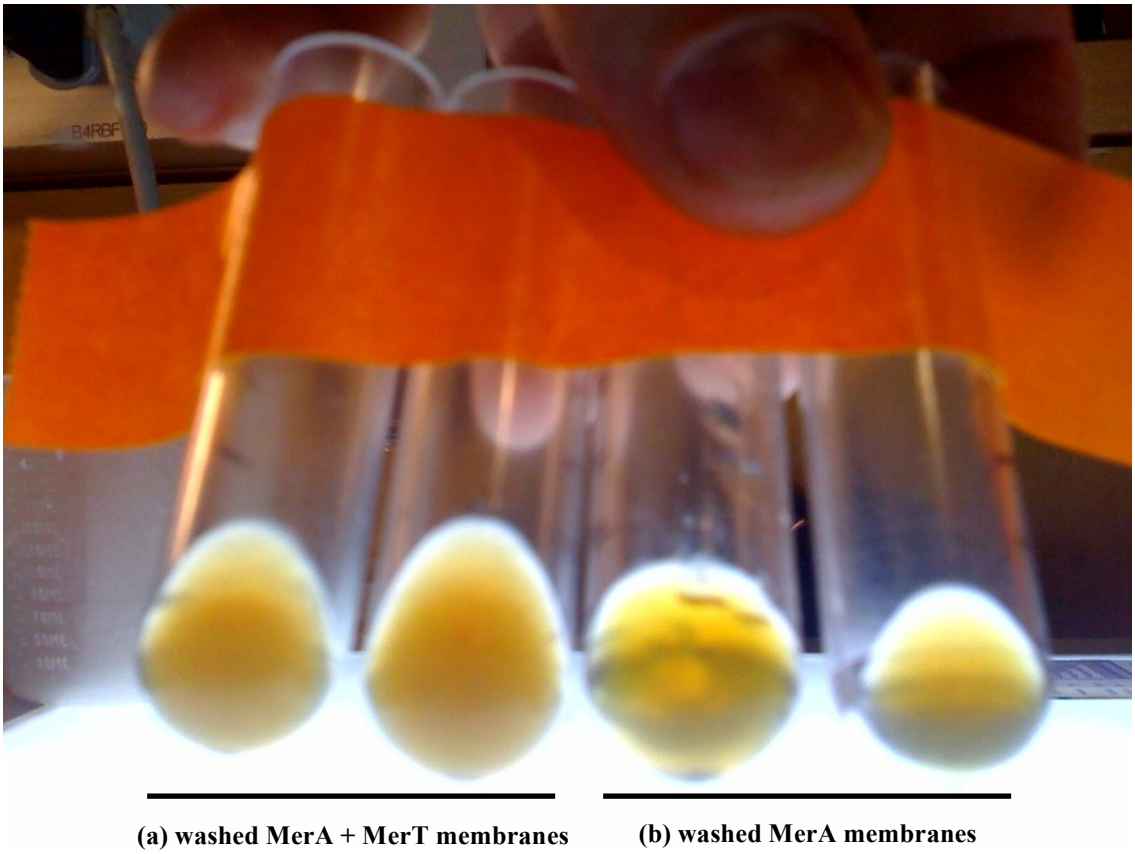


**Figure 4.** Washed membranes of cells expressing (a) MerT and MerA, and (b) MerA alone show intense yellow color from the presence of FAD bound to the MerA Core.

## Membrane-Associated MerA shows Reductase Activity

To test if full-length MerA is functional when associated with the membrane, we monitored the oxidation of NADPH by the loss of absorbance at 340 nm (Figure 5). Washed membranes were equilibrated with 50 μM NADPH in the presence of 1 mM cysteine, to which $HgBr_2$ at ~4.3 minutes was added to form $HgCys_2$. The use of excess thiol prevents $Hg^{2+}$ from binding nonspecifically to other ligands including NADPH, which leads to immediate loss of NADPH absorbance independent of MerA activity. Under these conditions the pronounced loss of signal due to NADPH consumption supports the presence of full-length MerA in washed membranes. The magnitude of reductase activity is comparable in the MerA and MerA+MerT samples. This suggests that association of MerA with the membrane is neither enhanced nor hampered by MerT expression. As we were unable to determine the exact concentration of MerA in either of these impure samples by spectroscopy, we could not determine the steady-state rate constants for MerA under these conditions, or quantitatively compare them to constants measured from pure samples (Johs et al. 2011). The small decrease in NADPH absorbance over the reaction period in assays of Core only membranes suggests the presence of a minimal amount of Tn*501* Core in the washed membranes, although neither SDS-PAGE nor western analyses showed Core associated with the membranes. The activity observed for Core is significantly less than that for the full-length samples and may be due to residual soluble protein not removed during membrane preparation.

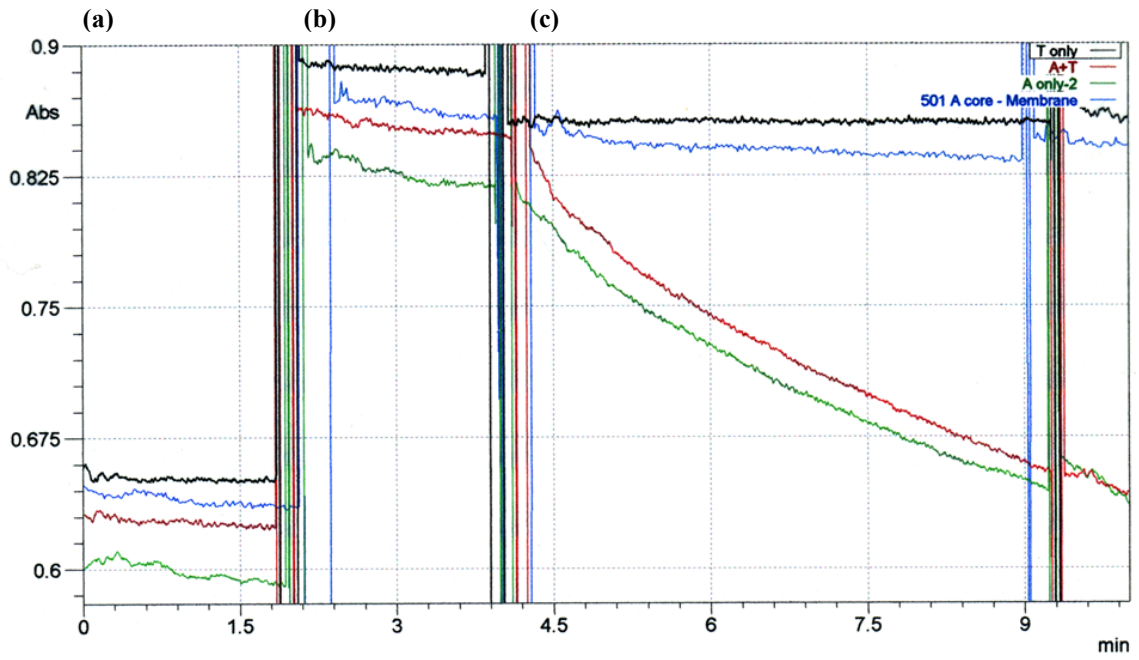


**Figure 5.** $Hg^{2+}$ reduction assayed by consumption of NADPH. Absorbance at 340 nm is shown. (a) Washed and normalized membranes resuspensions in 50 mM $KP_i$ pH 7.3, 1 mM cysteine at 25 °C. Membrane preparations were from cells expressing: MerT only (black; negative control); MerT+MerA (red); MerA only (green); and Tn*501* Core (blue). (b) Addition of NADPH to 50 µM final. (c) Addition of $HgBr_2$ to form 47 µM final $HgCys_2$ which, in the presence of MerA or Core, is reduced resulting in consumption of NADPH and loss of absorbance at 340 nm.

## Discussion

We have shown that full-length MerA can be expressed intact at 17 °C and, unlike NmerA or Core, independently associates with the cell membrane. This suggests that the MerA linker region may have a secondary role in recruiting MerA to the membrane in addition to its role in tethering NmerA. By positioning MerA at the "front line," the cell can defend against $Hg^{2+}$ entering by diffusion and, more critically, through a *mer* transporter (MerT or MerC) (Gutknecht 1981). Molecular dynamics simulations of the linker suggest a subsegment of the ~26 residues may form a one- or two-turn α-helix in solution (J. Parks, personal communication). This transient structure may partially insert into the membrane. Our results warrant further experimentation on the structure of the linker region in solution as well as in lipid and hydrophobic environments.

It remains unclear if MerA and MerT interact independent of $Hg^{2+}$. In our model NmerA directly receives $Hg^{2+}$ from the cytosolic thiols of MerT, and localization of MerA to the membrane in lieu of a direct protein-protein association enhances $Hg^{2+}$ trafficking efficiency while minimizing unfavorable binding to intracellular constituents. Our preliminary attempts to extract co-expressed MerT and MerA from the membrane using buffers containing either 20 mM n-Dodecyl-β-D-maltoside (DM) or 200 mM n-Octyl β-D-maltoside (OM), concentrations commonly used of each respective detergent for membrane protein extraction, result in precipitation of MerA (Newby et al. 2009). However the solubility and activity of MerA does not seem to be affected by 0.5 mM DM or 20 mM OM, detergent concentrations used to retain MerT in solution after extraction. Future *in vitro* studies of interactions between the two proteins may be possible with

these detergents if the periplasmic surface of MerT can be prevented from interacting with MerA, as would be the case *in vivo*. MerA may stabilize MerT sufficiently for structure determination and, in complex with MerT, provide solvent accessible surfaces for crystal contacts surpassing what may be accessible from MerT alone.

## Materials and Methods

Cloning and Mutagenesis: Plasmid pDG106, which codes for the Tn*21 mer* operon originally isolated from *Shigella flexneri*, was a generous gift from Dr. Anne O. Summers (Gambill and Summers 1985). Standard molecular biology protocols were used for PCR amplification, restriction digest, ligation, plasmid isolation, and transformation. The 1,692 bp coding sequence corresponding to the 564-residue MerA was PCR-amplified using a forward primer designed to introduce an NdeI site immediately upstream of the native start codon, and a reverse primer designed to introduce a BamH1 site 34 nucleotides downstream of the gene's native stop codon. The PCR product was ligated in between the NdeI and BamHI restriction sites of the ampicillin-resistant pET3a vector (Novagen, Madison, WI). This strategy results in expression of native protein without any appended affinity purification tags.

The 348 bp coding sequence corresponding to the 116-residue *Tn21* MerT was PCR-amplified using forward primer (5' CGCGCG**GGATCC**TCTGAACCACAAAAC// GGC 3') designed to introduce a BamHI site (in bold) at the beginning of the gene, and a reverse primer (5' GGCGCC**CTCGAG**ttattaAATAGAAAAATGGAACGACATAG 3') designed to introduce an XhoI site and two stop codons at the end of the gene (lower case). The PCR product was ligated at the BamHI and XhoI restriction sites of the kanamycin-resistant pET47sl vector, a modified pET47b(+) vector (Novagen) that codes for an N-terminal $His_6$ affinity purification tag followed by a 3C protease cleavage site (Alexandrov et al. 2001). After 3C cleavage, this strategy leaves only three protease

recognition site residues (GPG) upstream of the native Tn*21* MerT sequence, which begins at Ser2.

Following ligation, chemically-competent Top10 *Escherichia coli* (Invitrogen, Carlsbad, CA) were transformed with either the resulting pET3a:MerA and pET47sl:H-3C_MerT vectors and selected on LB/carbenicillin (50 μg/mL) and LB/kanamycin (30 μg/mL) plates, respectively. Plasmids were isolated by QIAprep Spin Miniprep (Qiagen, Valencia, CA). The MerT and MerA gene sequences and orientation were verified by DNA sequencing.

Protein Expression and Preparation: For expression of full-length MerA and MerT, *Escherichia coli* C43 cells (Miroux and Walker 1996), which we have found to give high expression of membrane proteins, were transformed with either (a) pET3a:MerA and plated on LB/carbenicillin (100 μg/mL) agar; (b) pET47sl:H-3C_MerT and plated on LB/kanamycin (15 μg/mL) agar; or (c) both pET3a:MerA and pET47sl:H-3C_MerT and plated on LB/carbenicillin (100 μg/mL)/ kanamycin (15 μg/mL) agar. In each case, a single colony was used to inoculate 10 L of LB with the same respective antibiotics used for each transformant and cells were grown in a 15 L Biostat-C fermentor (Sartorius Stedim Biotech, Concord, CA) stirred at 300 rpm, with the temperature and pH respectively maintained at 37 °C and 7.0. When the $OD_{600}$ reached ~0.4 the temperature was reduced to 17 °C. At $OD_{600}$ ~0.6, expression was induced with 1 mM isopropyl ß-D-thiogalactoside (IPTG) and growth was continued overnight (~18 hr). In all cases, cells were harvested by centrifugation at 6000 × g for 10 min. Harvested pellets,

corresponding to ~5 g per each liter of growth, were resuspended in 10 mL lysis buffer [20 mM $KP_i$ pH 8.0, 500 mM NaCl, 1 mM EDTA, 20 mM ß-mercaptoethanol (ßME)], and frozen for storage at -20 °C. Expression of Tn*501* Core and NmerA was performed as previously described (Ledwidge et al. 2005a).

All purification procedures were performed at 4 °C unless noted. Frozen cells from 2 L growth were thawed and incubated with one complete ULTRA protease inhibitor cocktail tablet (Roche Applied Science, Indianapolis, IN), 100 µM PMSF, and 20 mM fresh ßME. In preparing cells expressing either Tn*21* MerA, Tn*21* MerA and MerT, or Tn*501* MerA Core, flavin adenine dinucleotide (FAD) was additionally added to 100 µM. Suspended cells were homogenized and lysed by six passes through an Emulsiflex-C3 homogenizer (Avestin, Ottawa, Canada). To remove insoluble debris, lysates were centrifuged at 20,000 × g for 1 h. The soluble and membrane fractions of the lysates were separated by centriguation at 70,000 × g for 2 h. Following clarification, Tn*501* Core and Tn*21* MerA, expressed exclusively or alongside Tn*21* MerT, were purified from the soluble fraction as previously described (Ledwidge et al. 2005a). The membrane fractions of all cells (Tn*21* MerT, Tn*21* MerA, Tn*21* MerT+MerA, Tn*501* Core, and Tn*501* NmerA) were resuspended and diluted 10-fold by volume into fresh lysis buffer, and aliquoted as 150 µL samples into pre-weighed 1.5 mL Polyallomer Microcentrifuge tubes with snap-on caps (Beckman Coulter, Indianapolis, IN), which are compatible with a number of tabletop ultracentrifuge fixed-angle rotors. Membrane resuspensions were then flash frozen in liquid nitrogen and stored at -80 °C for later use.

Membrane Washing and Normalization: All membrane wash procedures were performed at 4 °C. Prior to experimentation, membranes were thawed on ice and centrifuged at 50,000 × g for 30 minutes. The ~150 µL of supernatant was removed by micropipette, and 1.2 mL of wash buffer [20 mM $KP_i$ pH 8.0, 500 mM NaCl, 4 mM ßME] was added prior to homogenization. Membranes were then washed (centrifuged, the supernatant removed, and resuspended into fresh wash buffer as before) two additional times. After the final round of centrifugation and removal of the wash supernatant, the masses of the resultant membrane pellets were calculated and resuspended in an appropriate volume of 50 mM $KP_i$ pH 7.3 to normalize membrane content. Following homogenization, the membrane samples were normalized to an $OD_{600}$ of 0.65 by addition of 50 mM $KP_i$ pH 7.3 and were used immediately.

Protein Detection and MerA Activity: SDS-PAGE analyses of samples were performed using Novex® 4-20% tris-glycine gels (Invitrogen), stained with Coomassie Blue with Precision Plus Protein™ Standards Kaleidoscope™ molecular mass standards (Bio-Rad Laboratories) used as a positive control. Samples separated by SDS-PAGE were analyzed by western blot as previously described (Newby et al. 2009) using His-Probe (H-3) (Santa Cruz Biotech, Santa Cruz, CA), a monoclonal α-$His_6$ conjugated to horseradish peroxidase (HRP), to detect the tagged MerT. MerA and NmerA were detected using polyclonal α-Core and α-NmerA, respectively, from clarified rabbit sera, a generous gift from Anne O. Summers, and monoclonal mouse α-rabbit IgG conjugated to HRP (Santa Cruz Biotech).

All activity assays were performed using a Uvikon XL spectrophotometer furnished with a thermostated cell holder connected to a constant temperature water bath set at 25 °C. Initial rates were monitored by the loss of absorbance at 340 nm due to NADPH oxidation ($\Delta\varepsilon_{340}$ = 6.2 $mM^{-1}$ $cm^{-1}$). The activity of Tn*21* MerA and Tn*501* Core purified from the soluble fractions was measured as previously described (Ledwidge et al. 2005a). To test for MerA activity in the washed membranes, samples that had been normalized to an $OD_{600}$ of 0.65 in 50 mM $KP_i$ PH 7.3 were equilibrated with added reduced nicotinamide adenine dinucleotide phosphate (NADPH) and cysteine at final concentrations of 50 μM and 1 mM, respectively, for ~2 minutes. $HgBr_2$ was then added to generate $HgCys_2$ at final concentration of 47 μM final; the use of excess thiol prevents nonspecific $Hg^{2+}$ binding to other biological constituents, as well as to NADPH which causes quenching of the NADPH signal. The solution was mixed by inversion, and consumption of NADPH from MerA activity was monitored for ~4 minutes.

## References


Alexandrov A, Dutta K, Pascal SM (2001) "MBP fusion protein with a viral protease cleavage site: one-step cleavage/purification of insoluble proteins." *Biotechniques* 30:1194-1198.

Arnesano F, Banci L, Bertini I, Ciofi-Baffoni S, Molteni E, Huffman DL, O'Halloran TV (2002) "Metallochaperones and metal-transporting ATPases: a comparative analysis of sequences and structures." *Genome Res* 12:255-271.

Barkay T, Miller SM, Summers AO (2003) "Bacterial mercury resistance from atoms to ecosystems." *FEMS Microbiol Rev* 27:355-384.

Bienvenue E, Boudou A, Desmazes JP, Gavach C, Georgescauld D, Sandeaux J, Seta P (1984) "Transport of mercury compounds across bimolecular lipid membranes: effect of lipid composition, pH and chloride concentration." *Chem Biol Interact* 48:91-101.

Brown NL (1985) "Bacterial resistance to mercury — reductio ad absurdum?" *Trends Biochem Sci* 10:400-403.

Brown NL, Ford SJ, Pridmore RD, Fritzinger DC (1983) "Nucleotide sequence of a gene from the Pseudomonas transposon Tn501 encoding mercuric reductase." *Biochemistry* 22:4089-4095.

Cobine PA, George GN, Winzor DJ, Harrison MD, Mogahaddas S, Dameron CT (2000) "Stoichiometry of Complex Formation between Copper(I) and the N-Terminal Domain of the Menkes Protein†." *Biochemistry* 39:6857-6863.

Distefano MD, Au KG, Walsh CT (1989) "Mutagenesis of the redox-active disulfide in mercuric ion reductase: catalysis by mutant enzymes restricted to flavin redox chemistry." *Biochemistry* 28:1168-1183.

Distefano MD, Moore MJ, Walsh CT (1990) "Active site of mercuric reductase resides at the subunit interface and requires Cys135 and Cys140 from one subunit and Cys558 and Cys559 from the adjacent subunit: evidence from in vivo and in vitro heterodimer formation." *Biochemistry* 29:2703-2713.

Engst S, Miller SM (1999) "Alternative routes for entry of HgX2 into the active site of mercuric ion reductase depend on the nature of the X ligands." *Biochemistry* 38:3519-3529.

Fox B, Walsh CT (1982) "Mercuric reductase. Purification and characterization of a transposon-encoded flavoprotein containing an oxidation-reduction-active disulfide." *J Biol Chem* 257:2498-2503.

Fox BS, Walsh CT (1983) "Mercuric reductase: homology to glutathione reductase and lipoamide dehydrogenase. Iodoacetamide alkylation and sequence of the active site peptide." *Biochemistry* 22:4082-4088.

Gambill BD, Summers AO (1985) "Versatile mercury-resistant cloning and expression vectors." *Gene* 39:293-297.

Griffin HG, Foster TJ, Silver S, Misra TK (1987) "Cloning and DNA sequence of the mercuric- and organomercurial-resistance determinants of plasmid pDU1358." *Proc Natl Acad Sci USA* 84:3112-3116.

Gutknecht J (1981) "Inorganic mercury (Hg2+) transport through lipid bilayer membranes." *J Membrane Bio* 61:61-66.

Hong B, Nauss R, Harwood IM, Miller SM (2010) "Direct measurement of mercury(II) removal from organomercurial lyase (MerB) by tryptophan fluorescence: NmerA domain of coevolved gamma-proteobacterial mercuric ion reductase (MerA) is more efficient than MerA catalytic core or glutathione." *Biochemistry* 49:8187-8196.

Johs A, Harwood IM, Parks JM, Nauss RE, Smith JC, Liang L, Miller SM (2011) "Structural characterization of intramolecular Hg(2+) transfer between flexibly linked domains of mercuric ion reductase." *J Mol Biol* 413:639-656.

Jones S, Thornton JM (1996) "Principles of protein-protein interactions." *Proc Natl Acad Sci USA* 93:13-20.

Ledwidge R, Hong B, Dötsch V, Miller SM (2010) "NmerA of Tn501 mercuric ion reductase: structural modulation of the pKa values of the metal binding cysteine thiols." *Biochemistry* 49:8988-8998.

Ledwidge R, Patel B, Dong A, Fiedler D, Falkowski M, Zelikova J, Summers AO, Pai EF, Miller SM (2005a) "NmerA, the metal binding domain of mercuric ion reductase, removes Hg2+ from proteins, delivers it to the catalytic core, and protects cells under glutathione-depleted conditions." *Biochemistry* 44:11402-11416.

Ledwidge R, Soinski R, Miller SM (2005b) "Direct monitoring of metal ion transfer between two trafficking proteins." *J Am Chem Soc* 127:10842-10843.

Miller SM, Moore MJ, Massey V, Williams CH, Jr., Distefano MD, Ballou DP, Walsh CT (1989) "Evidence for the participation of Cys558 and Cys559 at the active site of mercuric reductase." *Biochemistry* 28:1194-1205.

Miroux B, Walker JE (1996) "Over-production of proteins in Escherichia coli: mutant hosts that allow synthesis of some membrane proteins and globular proteins at high levels." *J Mol Biol* 260:289-298.

Moore MJ, Walsh CT (1989) "Mutagenesis of the N- and C-terminal cysteine pairs of Tn501 mercuric ion reductase: consequences for bacterial detoxification of mercurials." *Biochemistry* 28:1183-1194.

Nakahara H, Silver S, Miki T, Rownd RH (1979) "Hypersensitivity to Hg2+ and hyperbinding activity associated with cloned fragments of the mercurial resistance operon of plasmid NR1." *J Bacteriol* 140:161-166.

Newby ZER, O'Connell JD, Gruswitz F, Hays FA, Harries WEC, Harwood IM, Ho JD, Lee JK, Savage DF, Miercke LJW, Stroud RM (2009) "A general protocol for the crystallization of membrane proteins for X-ray structural investigation." *Nat Protocols* 4:619-637.

Schottel JL (1978) "The mercuric and organomercurial detoxifying enzymes from a plasmid-bearing strain of Escherichia coli." *J Biol Chem* 253:4341-4349.

Schue M, Glendinning KJ, Hobman JL, Brown NL (2007) "Evidence for direct interactions between the mercuric ion transporter (MerT) and mercuric reductase (MerA) from the Tn501 mer operon."

Schue M, Glendinning KJ, Hobman JL, Brown NL (2008) "Evidence for direct interactions between the mercuric ion transporter (MerT) and mercuric reductase (MerA) from the Tn501 mer operon." *Biometals* 21:107-116.

Sedlmeier R, Altenbuchner J (1992) "Cloning and DNA sequence analysis of the mercury resistance genes of Streptomyces lividans." *Mol Gen Genet* 236:76-85.

Stanisich VA (1974) "Interaction between an R factor and an element conferring resistance to mercuric ions in Pseudomonas aeruginosa." *Molec Gen Genet* 128:201-212.

Stanisich VA, Bennett PM, Richmond MH (1977) "Characterization of a translocation unit encoding resistance to mercuric ions that occurs on a nonconjugative plasmid in Pseudomonas aeruginosa." *J Bacteriol* 129:1227-1233.

Summers AO (1986) "Organization, expression, and evolution of genes for mercury resistance." *Annu Rev Microbiol* 40:607-634.

Thompson JD, Higgins DG, Gibson TJ (1994) "CLUSTAL W: improving the sensitivity of progressive multiple sequence alignment through sequence weighting, position-specific gap penalties and weight matrix choice." *Nucleic Acids Res* 22:4673-4680.

Tsai C-J, Lin SL, Wolfson HJ, Nussinov R (1996) "A Dataset of Protein–Protein Interfaces Generated with a Sequence-order-independent Comparison Technique." *J Mol Biol* 260:604-620.

Wang Y, Moore M, Levinson HS, Silver S, Walsh C, Mahler I (1989) "Nucleotide sequence of a chromosomal mercury resistance determinant from a Bacillus sp. with broad-spectrum mercury resistance." *J Bacteriol* 171:83-92.

**Publishing Agreement**

It is the policy of the University to encourage the distribution of all theses, dissertations, and manuscripts. Copies of all UCSF theses, dissertations, and manuscripts will be routed to the library via the Graduate Division. The library will make all theses, dissertations, and manuscripts accessible to the public and will preserve these to the best of their abilities, in perpetuity.

I hereby grant permission to the Graduate Division of the University of California, San Francisco to release copies of my thesis, dissertation, or manuscript to the Campus Library to provide access and preservation, in whole or in part, in perpetuity.

Author Signature

**8/30/2012**

Date